

DOUTORAMENTO EM CIÊNCIAS FARMACÊUTICAS
FITOQUÍMICA E FARMACOGNOSIA

Valorization of species from Thailand flora: phenolic characterization and antidiabetic properties

Ana Catarina Gomes Andrade

D

2022





Ana Catarina Gomes Andrade

**VALORIZATION OF SPECIES FROM THAILAND FLORA:
PHENOLIC CHARACTERIZATION AND ANTIDIABETIC PROPERTIES**

Thesis of Doctor Degree in Pharmaceutical Sciences

Phytochemistry and Pharmacognosy Specialty

Work performed under the supervision of

Professor Doctor Patrícia Carla Ribeiro Valentão

and co-supervision of

Professor Doctor Paula Cristina Branquinho de Andrade

Professor Doctor David Alexandre Micael Pereira

July 2022

THE REPRODUCTION OF THIS THESIS IT IS AUTHORIZED ONLY FOR RESEARCH PURPOSES, UNDER THE WRITTEN STATEMENT OF THE INTERESTED PARTY, COMMITTING ITSELF TO DO IT.

*“C'est le temps que tu as perdu pour ta rose
qui fait ta rose si importante”
- Antoine de Saint-Exupéry*

To my beloved family and endeared friends

This work was financially supported by Fundação para a Ciência e a Tecnologia (FCT) through the attribution of a Doctoral Grant (SFRH/BD/131431/2017) under the framework of POPH – QREN – Type 4.1. – Advanced Training, funded by the Fundo Social Europeu (FSE) and by National funds of Ministério da Ciência, Tecnologia e Ensino Superior (MCTES).



AUTHOR STATEMENT

The author declares to have afforded a major contribution to the technical execution, interpretation of the results and manuscript preparation of all works included on the current thesis, with the collaboration of the other co-authors.

PUBLICATIONS

The following publications resulted from the work describe in this thesis.

PUBLICATIONS IN INTERNATIONAL PEER-REVIEWED JOURNALS INDEXED AT THE JOURNAL CITATION REPORTS (JCR) OF THE ISI WEB OF KNOWLEDGE:

1. **Andrade C**, Ferreres F, Gomes NGM, Duangsrissai S, Srisombat N, Vajrodaya S, Pereira DM, Gil-Izquierdo A, Andrade PB, Valentão P. Phenolic profiling and biological potential of *Ficus curtipes* Corner leaves and stem bark: 5-lipoxygenase inhibition and interference with NO Levels in LPS-stimulated RAW 264.7 macrophages. **Biomolecules**. 2019 Aug; 9 (400): 1-17.
2. **Andrade C**, Gomes NGM, Duangsrissai S, Andrade PB, Pereira DM, Valentão P. Medicinal plants utilized in Thai Traditional Medicine for diabetes treatment: Ethnobotanical surveys, scientific evidence and phytochemicals. **J Ethnopharmacol**. 2020 Dec; 263 (113177):1-54.
3. **Andrade C**, Ferreres F, Gomes NGM, Gil-Izquierdo A, Bapia S, Duangsrissai S, Pereira DM, Andrade PB, Valentão P. *Gustavia gracillima* Miers. flowers effects on enzymatic targets underlying metabolic disorders and characterization of its polyphenolic content by HPLC-DAD-ESI/MSⁿ. **Food Res Int**. 2020 Nov; 137(109694): 1-10
4. Ferreres F, **Andrade C**, Gomes NGM, Andrade PB, Gil-Izquierdo A, Pereira DM, Suksungworn R, Duangsrissai S, Videira RA, Valentão P. Valorisation of kitul, an overlooked food plant: Phenolic profiling of fruits and inflorescences and assessment of their effects on diabetes-related targets. **Food Chem**. 2021 Apr; 342 (128323): 1-9
5. **Andrade C**, Ferreres F, Gomes NGM, Gil-Izquierdo A, Duangsrissai S, Pereira DM, Andrade PB, Valentão P. Valorisation of the industrial waste of *Chukrasia tabularis* A.Juss.: Characterization of the leaves phenolic constituents and antidiabetic-like effects. **Ind Crops Prod**. 2022 Oct; 185 (115100): 1–10.

ORAL COMMUNICATIONS

1. **Andrade C**, Gomes NGM, Ferreres F, Gil-Izquierdo A, Pereira DM, Suksungworn R, Duangsrissai S, Valentão P, Andrade PB. Characterization of the phenolic profile of *Caryota urens* L. - preliminary evidence on its antidiabetic properties. XXIV Luso-Galego Meeting of Chemistry. November 21-23, 2018. Porto (Portugal).
2. **Andrade C**, Gomes NGM, Andrade PB, Videira RA, Ferreres F, Duangsrissai S, Gil-Izquierdo A, Pereira DM, Valentão P. Antidiabetic screening of plant species from Thailand: Phenolic profile and *in vitro* antidiabetic activity of *Caryota urens* L. inflorescences. IberPhenol International Conference. November 4-5, 2020. Coimbra (Portugal).

POSTER COMMUNICATIONS

1. Mesquita J; **Andrade C**; Suksungworn R, Pereira DM, Andrade PB, Duangsrissai S, Valentão P, Gomes NMG. A multi-target approach towards diabetes based on the metabolic versatility of *Diospyros* spp. from Thailand. IJUP19 - 12th Meeting of Young Researchers of U. Porto. February 13-15, 2019. Porto (Portugal).
2. **Andrade C**, Gomes NGM, Pereira DM, Suksungworn R, Duangsrissai S, Valentão P, Andrade PB. Valorisation of *Gustavia gracillima* Miers: experimental evidence on its antidiabetic properties. 4th Meeting of Medicinal Biotechnology. May 17, 2019. Porto (Portugal).
3. **Andrade C**, Gomes NGM, Pereira DM, Suksungworn R, Duangsrissai S, Videira RA, Andrade PB, Valentão P. Valuing an overlooked food-plant: phenolic profiling fruits and inflorescences of kitul and assessing their effects on diabetes-related targets. 11th Symposium on Metabolism. October 30, 2019. Porto (Portugal).
4. **Andrade C**, Ferreres F, Gomes NGM, Duangsrissai S, Srisombat N, Vajrodaya S, Pereira DM, Gil-Izquierdo A, Andrade PB, Valentão P. Phenolic profiling of *Ficus curtipes* Corner leaves and stem bark and assessment of their anti-inflammatory potential. ICPH - 9th International Conference on Polyphenols and Health. November 28-December 1, 2019. Kobe (Japan).
5. Mesquita S, **Andrade C**, Suksungworn R, Duangsrissai S, Barbosa M, Valentão P, Andrade PB, Gomes NGM. Anti-inflammatory functionality of Karonda (*Carissa carandas* L.) and Djenkol (*Archidendron pauciflorum* (Benth.) I.C.Nielsen): *In*

vitro evidence and identification of bioactives. IJUP20 - 13th Meeting of Young Researchers of U. Porto. February 12-14, 2020. Porto (Portugal).

6. **Andrade C**, Ferreres F, Gomes NGM, Andrade PB, Gil-Izquierdo A, Pereira DM, Duangrisai S, Valentão P. Bioprospecting *Chukrasia tabularis* A. Juss. leaves: HPLC-DAD-ESI/MSⁿ profiling of phenolic bioactives and effects on inflammatory mediators and enzymatic targets engaged in metabolic disorders. Science Meeting'21. June 28-30, 2021. Lisbon (Portugal).

ACKNOWLEDGEMENTS

This journey could not be successfully accomplished without the support of several people and institutions to whom I would like to provide some grateful words:

To “Fundação para a Ciência e a Tecnologia” (FCT) for granting me a Doctoral scholarship (SFRH/BD/131431/2017) under the POPH – QREN – Type 4.1 – Advanced Training, funded by the European Social Fund (FSE) and by National funds from the “Ministério da Ciência, Tecnologia e Ensino Superior” (MCTES).

To my esteemed supervisor and friend, Prof. Doctor Patrícia Carla Ribeiro Valentão, for the knowledge shared and all the time and patience spent over the past four years. Her passion for teaching, learning and reinventing, have truly encouraged me to always renew my ideas and thoughts. All the support provided over these years, allied to her enormous scientific and problem-solving skills, were crucial for the final outcome of the current dissertation. Furthermore, her trust in my competence and judgment paved the way on the development of current autonomy and critical thinking. Finally, I would like also to thank her for the periods spend after work, that were many times revitalizing and fundamental on the overcome of many drawbacks. This path would have been, undoubtedly, a tougher and unpleasant task without her. Thank you!

To Professor Paula Cristina Branquinho de Andrade, co-supervisor of this thesis. First of all, for arousing my interest and curiosity in the research field, and for have me integrated, from earlier, in the Pharmacognosy family. Her charism and outstanding vision, have immediately draw my attention to the natural products area, at the first years of my Master degree. She always braced my scientific path and actively encourage me to pursue the PhD. Hence, this would have been an impossible mission from the start, without her support. As my co-supervisor, she was always aware and preoccupied to ensure that all the resources and investigation wherewithal were in line and available in proper time. She always encouraged me to want more and to look for more. I can't thank you enough for that.

To Prof. Doctor David Pereira, also co-supervisor of this thesis, I would like to acknowledge for the scientific support and for the inputs provided on the data analysis and on the critical discussion of the results.

To Prof. Doctor Sutsawat Duangrisai, from the Department of Botany of Faculty of Science of Kasetsart University (Bangkok, Thailand), for kindly providing the samples investigated at the current thesis and for her endless availability on the clarification of all the questions concerning Thai flora. This work would have not been design without your contribution from the beginning.

To Professor Federico Ferreres, from Centro de Edafología y Biología Aplicada del Segura (CEBAS), of Consejo Superior de Investigaciones Científicas (CSIC), Murcia, Spain, for his availability and crucial contribution on the identification of the samples phenolics constituents by HPLC-DAD-ESI/MSⁿ and UPLC-ESI-QTOF/MS. Part of this work would not have been accomplished without his kind and decisive contribution.

To Prof. Doctor Ángel Gil-Izquierdo, also from CEBAS-CSIC, for his assistance in conducting the HPLC-DAD-ESI/MSⁿ and UPLC-ESI-QTOF/MS analysis.

To Prof. Doctor Srunya Vajrodaya, from the Department of Botany of Faculty of Science of Kasetsart University (Bangkok, Thailand), for her availability and central help on the taxonomic identification and validation of the plant materials under study.

To Prof. Doctor Nelson Gomes my sincere thankfulness for the incessant support, for the important tips and for his constant presence at all stages of this journey. I am sure that the outcomes from the current work would have not been the same without your counselling and care.

To all the colleagues from the Laboratory of Pharmacognosy of the Faculty of Pharmacy of the University of Porto, for their camaraderie, for the motivating discussions and for contributing to the normal functioning of the lab. Special thanks to Doctor Mariana Barbosa and Doctor João Bernardo, for all the scientific and practical advises, all the jokes, all the laughs and mostly for the beyond boundaries friendship.

To my family and friends, for their care, support and patient.

Finally, to my beloved parents to whom I dedicate this doctoral thesis. I would like to express my deep gratitude for all the support, trust, love and care. Thank you for never giving up on me and for always guiding me and showing me the right path. Part of who I am now, I owe you, and I couldn't be prouder of that.

ABSTRACT

ABSTRACT

Diabetes mellitus is the deadliest metabolic disease of contemporaneous times and, therefore the research for new antidiabetic agents remains an urgent priority. Over the past 40 years, 65 new antidiabetic drugs were approved by FDA, approximately 54 % being derived from natural products. In fact, nature constitutes an important source of bioactive components and most of them still lack proper investigation. Peculiarly, the impressive Thai flora biodiversity, along with the conventional practices of Thai Traditional Medicine, place this world region at the forefront of many ethnomedicinal programs. Thus, in the current work 20 plant materials from Thailand were initially screened for their antidiabetic, anti-inflammatory and antioxidant properties. This preliminary screening allowed to select the more relevant species, namely *Caryota urens* L., *Ficus curtipes* Corner, *Chukrasia tabularis* A.Juss. and *Gustavia gracillima* Miers. The methanol extracts prepared from the selected species were subsequently studied in regards to their phenolic composition and antidiabetic-like properties.

Chromatographic analysis of the methanol extracts allowed the identification of a total of 72 phenolic compounds. In the methanol extracts prepared from *C. urens* (kitul) solely hydroxycinnamic acids derivatives were detected. The extract prepared from the leaves of *F. curtipes* displayed apigenin derivatives, while the one obtained from the stem bark additionally exhibited condensed tannins and hydroxycinnamic acids. In the leaves of *C. tabularis*, apart from condensed tannins, flavan-3-ols, flavonols and flavones were additionally detected. Finally, the extract obtained from the flowers of *G. gracillima* was predominantly constituted by kaempferol derivatives and ellagitannins. The phenolic content of each extract was estimated by HPLC-DAD and considerable amounts of polyphenols were quantified in the extracts obtained from the inflorescences of *C. urens* and from the flowers of *G. gracillima*.

All the extracts were capable of inhibiting yeast α -glucosidase activity in a concentration-dependent way, through a mixed or non-competitive mechanism. This constitutes an advantage over the conventional drug used in therapeutics, acarbose, once the inhibition elicited here is not limited by the intake of carbohydrates. The extracts obtained from the inflorescences of *C. urens* and from the flowers of *G. gracillima* displayed greater yeast α -glucosidase inhibitory activity, being significantly more active than acarbose. The α -glucosidase inhibition recorded is correlated to the concentrations of phenolics of the extracts. The noteworthy inhibitory activity displayed by *C. urens* and *G. gracillima* methanol extracts was also confirmed in α -glucosidase homogenates isolated from human intestinal cells. Relevantly, these extracts were also the only ones capable of

inhibiting pancreatic lipase activity through a mixed and competitive mechanism, respectively. However, only the extracts obtained from the inflorescences of *C. urens* and from the stem bark of *F. curtipes* were capable of inhibiting α -amylase. Moreover, all the extracts inhibited aldose reductase activity, the recorded effects being again correlated with the concentrations of polyphenols.

Specifically concerning the antiradical activity, all the extracts were capable of scavenging nitric oxide (\bullet NO) and superoxide anion ($O_2\bullet^-$) radicals, being particularly effective towards the latter. Furthermore, all the extracts lessened lipid peroxidation. Only the recorded $O_2\bullet^-$ scavenging activity was correlated with the concentrations of extract's phenolic constituents. Additionally, the extracts obtained from the inflorescences of *C. urens* and from the flowers of *G. gracillima* were capable of neutralizing glucose-induced reactive species overproduction in pancreatic cells (RIN-5F). Besides, in a cell-free system, *C. urens* and *G. gracillima* extracts were also capable of reducing protein glycation. Again, the effects reported are correlated with the concentrations of phenolics present at the samples.

In regards to the anti-inflammatory activity, the extracts obtained from the stem bark of *F. curtipes* and from the leaves of *C. tabularis* strongly inhibited 5-lipoxygenase (5-LOX) activity through an uncompetitive and mixed mechanism, respectively. Moreover, all the extracts were capable of damping NO and L-citrulline levels in lipopolysaccharide (LPS)-stimulated RAW macrophages, inhibiting inducible nitric oxide synthetases (iNOS) activity and/or expression. Relevantly, while all samples have lessened interleukin (IL)-6 levels, only the leaf extracts did not induce tumour necrosis factor- α (TNF- α) overexpression. However, and contrary to the former activities, the anti-inflammatory effects recorded on the cell model were not related with the concentrations of phenolic bioactives at the samples.

The outcomes of the current dissertation highlight the relevance of *C. urens* inflorescences and *G. gracillima* flowers, providing initial evidence of their antidiabetic-like potential. Also, *C. tabularis* and *F. curtipes* are here disclosed for their anti-inflammatory properties. The multi-target capacity displayed by the extracts, studied here, might inspire food industries and/or pharmaceutical companies to produce new functional products/foods. This work also highlights the urgent need for studies on the potential antidiabetic effects of food products derived from the inflorescences of *C. urens*, which are already widely marketed and consumed in Asian communities.

Keywords: Diabetes; Phenolic compounds; Thai traditional medicine; *C. urens*; *F. curtipes*; *C. tabularis*; *G. gracillima*.

RESUMO

RESUMO

A diabetes mellitus é a doença metabólica com maior mortalidade da atualidade, sendo a pesquisa de novos agentes antidiabéticos uma prioridade global emergente. Só nos últimos 40 anos, 65 novos medicamentos antidiabéticos foram aprovados pela FDA, sendo 54% destes derivados de produtos naturais. De facto, a natureza constitui uma fonte ilimitada de constituintes bioativos naturalmente selecionados, sendo muitos deles ainda pouco estudados. A impressionante biodiversidade da flora da Tailândia, associada às práticas convencionais inerentes à Medicina Tradicional Tailandesa, colocam esta região do globo na vanguarda de muitos programas de etnomedicina. Assim, neste trabalho foi feita uma triagem do potencial anti-inflamatório, antidiabético e antioxidante de 20 materiais vegetais da flora da Tailândia. Este *screening* preliminar permitiu selecionar as espécies com maior potencial terapêutico: *Caryota urens* L., *Ficus curtipes* Corner, *Chukrasia tabularis* A.Juss. e *Gustavia gracillima* Miers. A atividade antidiabética destes extratos foi posteriormente explorada, e a sua composição fenólica foi também elucidada.

A análise cromatográfica permitiu a identificação de um total de 72 compostos fenólicos. Na espécie *C. urens* (*kitul*) foram detetados apenas derivados de ácidos hidroxicinâmicos, enquanto nas restantes foi possível identificar também taninos. O extrato de folhas de *F. curtipes* apresentou na sua constituição apenas derivados da apigenina, enquanto o extrato preparado a partir das cascas do caule da mesma árvore continha, adicionalmente, taninos condensados e ácidos hidroxicinâmicos. Relativamente às folhas de *C. tabularis* foi possível identificar flavonóis, flavan-3-óis, flavonas e taninos condensados. Por fim, o extrato de flores de *G. gracillima* continha predominantemente derivados do campferol e elagitaninos. Os constituintes fenólicos foram posteriormente quantificados, tendo sido detetadas concentrações consideráveis de polifenóis nos extratos obtidos das inflorescências de *C. urens* e das flores de *G. gracillima*.

Todos os extratos inibiram a atividade da α -glucosidase de levedura, de forma dependente da dose, e por um mecanismo misto ou não competitivo, constituindo uma vantagem relativamente ao medicamento convencional usado na terapêutica (acarbose), uma vez que, neste caso, a inibição não é condicionada pela quantidade de hidratos de carbono ingerida. Os extratos obtidos a partir das inflorescências de *C. urens* e das flores de *G. gracillima* foram os que apresentaram maior atividade, tendo sido mais eficazes do que a acarbose. A inibição da α -glucosidase está correlacionada com a concentração de compostos fenólicos. Além disso, a atividade inibitória destes extratos foi também confirmada no sistema enzimático da α -glucosidase humana, isolado a partir de células intestinais. Estes extratos foram também capazes de inibir a atividade da lipase pancreática,

mitigando a absorção intestinal de lípidos. Relativamente à α -amílase, apenas os extratos obtidos a partir das inflorescências de *C. urens* e das cascas do caule de *F. curtipes* foram ativos. Todas as amostras inibiram a aldose redutase, estando a atividade inibitória novamente correlacionada com a concentração de constituintes fenólicos.

Relativamente à atividade anti-radicalar, todos os extratos foram capazes de neutralizar os radicais anião superóxido ($O_2^{\bullet-}$) e óxido nítrico ($\bullet NO$), tendo sido, particularmente eficazes no sequestro de $O_2^{\bullet-}$. Todos os extratos foram capazes de atenuar a peroxidação lipídica. Apenas o sequestro de $O_2^{\bullet-}$ pareceu estar relacionado com a concentração de compostos fenólicos das amostras. Adicionalmente, os extratos obtidos a partir das inflorescências de *C. urens* e das flores de *G. gracillima* foram capazes de neutralizar o aumento de produção de espécies reativas em células pancreáticas (RIN-5F) submetidas a condições de glucotoxicidade. Além disso, os dois extratos conseguiram também atenuar a glicação de proteínas ao longo do tempo num sistema não celular. Novamente, os efeitos estão correlacionados com as concentrações fenóis das amostras.

Considerando a atividade anti-inflamatória, os extratos obtidos a partir das cascas do caule de *F. curtipes* e das folhas de *C. tabularis* inibiram a atividade da 5-lipoxigenase (5-LOX) de forma não competitiva e mista, respetivamente. Adicionalmente, todos os extratos foram capazes de reduzir os níveis de NO e L-citrulina em macrófagos estimulados com lipopolissacarídeo (LPS). Todas as amostras diminuiram significativamente os níveis da citocina pro-inflamatória, interleukina-6 (IL-6). No entanto, apenas os extratos das folhas de *F. curtipes* e de *C. tabularis* não induziram um aumento nos níveis de fator de necrose tumoral- α (TNF- α). Contrariamente aos efeitos precedentes, a atividade anti-inflamatória registada nas células não está correlacionada com a concentração de fenóis dos extratos.

Os resultados da presente tese destacam a relevância das inflorescências de *C. urens* e das flores de *G. gracillima*, fornecendo evidências claras do seu potencial antidiabético. Paralelamente, as espécies *F. curtipes* e *C. tabularis* são também aqui salientados pelas suas propriedades anti-inflamatórias. A ação multialvo destes materiais vegetais, aqui demonstrada, poderá incentivar as indústrias alimentar e/ou farmacêutica para o desenvolvimento de novos produtos/alimentos funcionais. Este trabalho evidencia também a necessidade urgente de estudos sobre os potenciais efeitos antidiabético dos produtos alimentares derivados das inflorescências de *C. urens*, que são já amplamente comercializados e consumidos nas comunidades asiáticas.

Palavras-chave: Diabetes; Compostos fenólicos; Medicina tradicional tailandesa; *C. urens*; *F. curtipes*; *C. tabularis*; *G. gracillima*

TABLE OF CONTENTS

TABLE OF CONTENTS

ACKNOWLEDGEMENTS.....	XV
ABSTRACT.....	XIX
RESUMO	XXIII
LIST OF FIGURES.....	XXXV
LIST OF TABLES	XLIII
LIST OF ABBREVIATIONS	XLVII
THESIS OUTLINE	1
CHAPTER I: INTRODUCTION AND OBJECTIVES	
1. Introduction.....	5
1.1. Diabetes mellitus: overview.....	5
1.1.1. Physiopathology of type 2 diabetes	6
1.1.2. Pharmacological approaches and targets	12
1.2. Plants as sources of bioactive compounds.....	14
1.2.1. Phenolic compounds.....	15
1.2.1.1. Phenolic acids	16
1.2.1.1.1. Classification and biosynthesis	16
1.2.1.1.2. Biodiversity and chemistry.....	18
1.2.1.2. Flavonoids	20
1.2.1.2.1. Classification and biosynthesis	20
1.2.1.2.2. Biodiversity and chemistry.....	23
1.2.1.3. Tannins.....	24
1.2.1.3.1. Classification and biosynthesis	24
1.2.1.3.2. Biodiversity and chemistry.....	27
1.2.1.4. Extraction, purification and analysis of phenolics.....	27
1.2.1.5. Phenolics and the modulation of pathophysiological events underlying DM	30

1.3.	The role of Thai flora on the bioprospection of antidiabetic plants	34
1.3.1.	Selected species.....	37
1.3.1.1.	<i>Caryota urens</i> L.	37
1.3.1.2.	<i>Ficus curtipes</i> Corner	39
1.3.1.3.	<i>Gustavia gracillima</i> Miers	40
1.3.1.4.	<i>Chukrasia tabularis</i> A. Juss.....	41
2.	Objectives.....	44
CHAPTER II: EXPERIMENTAL SECTION		
3.	Experimental section	47
3.1.	General chemicals and standards.....	47
3.2.	Sample collection.....	48
3.3.	Extraction	48
3.4.	Preliminary screening of biological activities of plant species from Thailand	50
3.4.1.	α -Glucosidase inhibition.....	50
3.4.2.	5-LOX inhibition.....	51
3.4.3.	DPPH \cdot scavenging capacity.....	52
3.5.	Characterization of phenolic profiles of the selected species	53
3.5.1.	HPLC-DAD-ESI (Ion Trap)/MS ⁿ qualitative analysis.....	53
3.5.2.	UPLC-ESI-QTOF-MS qualitative analysis.....	54
3.5.3.	HPLC-DAD quantitative analysis	55
3.6.	Anti-diabetic-like activity	56
3.6.1.	Kinetic studies on yeast α -glucosidase inhibition	56
3.6.2.	α -Amylase inhibition	56
3.6.3.	Aldose reductase inhibition	57
3.6.4.	Pancreatic lipase inhibition	58
3.6.4.1.	Kinetic studies on pancreatic lipase inhibition	59
3.6.5.	Cellular assays.....	60

3.6.5.1.	Cell culture of intestinal Caco-2 cells and treatments.....	60
3.6.5.2.	Assessment of cell viability.....	60
3.6.5.3.	α -Glucosidase inhibition in Caco-2 cells homogenates	61
3.7.	Anti-radical activity	62
3.7.1.	Nitric oxide radical scavenging capacity.....	63
3.7.2.	Superoxide anion radical scavenging capacity	64
3.7.3.	Lipid peroxidation inhibition	65
3.7.4.	Protein glycation inhibition.....	67
3.7.5.	Cellular assays.....	68
3.7.5.1.	Culture of pancreatic RIN-5F cells and treatments	68
3.7.5.2.	Assessment of cell viability.....	69
3.7.5.3.	Determination of intracellular reactive species	70
3.8.	Anti-inflammatory-like activity	71
3.8.1.	Kinetic studies on 5-LOX inhibition.....	71
3.8.2.	Cellular assays.....	71
3.8.2.1.	Culture of RAW 264.7 macrophages and treatments.....	71
3.8.2.2.	Assessment of cell viability.....	72
3.8.2.1.	Determination of nitric oxide levels	73
3.8.2.2.	Determination of L-citrulline levels	73
3.8.2.3.	Determination of TNF- α and IL-6 levels.....	75
3.9.	Statistical analysis.....	75
CHAPTER III: RESULTS AND DISCUSSION		
4.	Results and discussion.....	79
4.1.	Preliminary screening of biological activities of plant species from Thailand	79
4.2.	Characterization of the phenolic profile of the selected species.....	85
4.2.1.	<i>C. urens</i>	85
4.2.1.1.	HPLC-DAD-ESI/MS ⁿ qualitative analysis	85
4.2.1.2.	HPLC-DAD quantitative analysis.....	88

4.2.2.	<i>F. curtipes</i>	90
4.2.2.1.	HPLC-DAD-ESI/MS ⁿ qualitative analysis	90
4.2.2.1.1.	Hydroxycinnamic acids	91
4.2.2.1.2.	Apigenin derivatives	92
4.2.2.1.3.	Flavan-3-ols	95
4.2.2.2.	HPLC-DAD quantitative analysis	97
4.2.3.	<i>C. tabularis</i>	98
4.2.3.1.	HPLC-DAD-ESI/MS ⁿ qualitative analysis	98
4.2.3.1.1.	Dimers and trimers	99
4.2.3.1.2.	Flavonoids	102
4.2.3.2.	HPLC-DAD quantitative analysis	104
4.2.4.	<i>G. gracillima</i>	105
4.2.4.1.	HPLC-DAD-ESI/MS ⁿ qualitative analysis	105
4.2.4.1.1.	Kaempferol derivatives	106
4.2.4.1.2.	Ellagic acid derivatives	110
4.2.4.2.	HPLC-DAD quantitative analysis	111
4.3.	Antidiabetic-like activity	112
4.3.1.	Inhibition of carbohydrates absorption enzymes	112
4.3.1.1.	Inhibition of carbohydrates absorption enzymes <i>vs</i> phenolic content	118
4.3.2.	Inhibition of lipids absorption enzyme	119
4.3.2.1.	Inhibition of lipids absorption enzyme <i>vs</i> phenolic content	121
4.3.3.	Aldose reductase inhibition	122
4.3.3.1.	Aldose reductase inhibition <i>vs</i> phenolic content	123
4.4.	Anti-radical activity	125
4.4.1.	Radical scavenging effects	125
4.4.1.1.	Antiradical activity <i>vs</i> phenolic content	128
4.4.2.	Modulation of reactive species in pancreatic cells	130

4.4.3.	Modulation AGEs formation	132
4.4.3.1.	Antiglycative effects <i>vs</i> phenolic content	136
4.5.	Anti-inflammatory-like activity	137
4.5.1.	Modulation of the arachidonic acid pathway	137
4.5.2.	Modulation of macrophages activation	139
4.5.2.1.	Anti-inflammatory effects <i>vs</i> phenolic content.....	145
CHAPTER IV: CONCLUSIONS		
5.	Conclusions.....	149
5.1.	Future perspectives.....	150
CHAPTER V: REFERENCES		
6.	References.....	155

LIST OF FIGURES

LIST OF FIGURES

Figure 1. Schematic representation of the main molecular pathways linking inflammation to insulin resistance	9
Figure 2. Schematic representation of the cross-linked relation between the polyol pathway and the production of AGEs	10
Figure 3. Schematic representation of the AGEs induced-inflammatory response.....	11
Figure 4. Conventional pharmacological approaches utilized in TD2 management and novel potential targets.	13
Figure 5. Schematic representation of biosynthetic pathway of phenylpropanoids (shikimate pathway).	18
Figure 6. Chemical structures of naturally occurring phenolic acids.	19
Figure 7. Core structure of flavonoids and numerating scheme.	20
Figure 8. Chemical structures of the main classes of flavonoids.	21
Figure 9. Schematic representation of flavonoids biosynthesis.....	22
Figure 10. Structures of the phenolic units of hydrolysable tannins and of two types of condensed tannins (proanthocyanidins).	25
Figure 11. Schematic representation of the biosynthesis of hydrolysable tannins..	26
Figure 12. Schematic representation on the antidiabetic effects of polyphenols.	31
Figure 13. <i>Caryota urens</i> tree (A) and its inflorescences (B) and fruits (C).....	37
Figure 14. <i>Ficus curtipes</i> tree (A) and the collected leaves (B)	40
Figure 15. <i>Gustavia gracillima</i> tree (A) and flowers (B and C).....	41
Figure 16. <i>Chukrasia tabularis</i> tree (A) and the collected leaves (B, C) and stem bark (B).	42
Figure 17. <i>p</i> -Nitrophenyl- α -glucopyranoside cleavage by α -glucosidase into α -D-glucose and <i>p</i> -nitrophenol.....	50
Figure 18. Oxidation of linoleic acid to 13-hydroxyoctadecadienoic acid catalysed by lipoxygenase (LOX).	51
Figure 19. Neutralization of the 2,2-diphenyl-1-picrylhydrazyl radical (DPPH \cdot) to 2,2-diphenyl-1-picrylhydrazine (DPPH-H) in the presence of antioxidant compounds (AH) able to donate a hydrogen atom.	52

Figure 20. Starch cleavage by α -amylase into reducing sugars that reduce 3,5-dinitrosalicylic acid (DNSA) to amino-5-nitrosalicylic acid.....	57
Figure 21. Reduction of DL-glyceraldehyde by aldose reductase and oxidation of the enzymatic co-factor (NADPH).....	58
Figure 22. <i>p</i> -Nitrophenyl butyrate cleavage by the pancreatic lipase.	59
Figure 23. Reduction of 3-(4,5-dimethylthiazol-2-yl)-2,5-diphenyltetrazolium bromide (MTT) to 5-(4,5-dimethylthiazol-2-yl)-1,3-diphenylformazan by mitochondrial dehydrogenases of metabolic active cells.	60
Figure 24. Schematic representation of the experiment conducted to assess the extracts inhibitory activity in the human α -glucosidase complex.	62
Figure 25. Determination of nitrites (NO_2^-) by the Griess method.	63
Figure 26. Formation of $\text{O}_2^{\cdot-}$ by the NADH/PMS system and reduction of NBT to a formazan blue dye.....	65
Figure 27. General reactions involved in the protocol utilized to study the effect of the extracts on lipid peroxidation.....	66
Figure 28. Schematic representation of bovine serum albumin (BSA) glycation and advanced glycation end products (AGEs) formation route from glucose and fructose.	68
Figure 29. Experimental design of the assays performed with pancreatic RIN-5F cells..	69
Figure 30. Cleavage of 2',7'-dichlorodihydrofluorescein diacetate (DCFH-DA) by cellular esterases into 2',7'-dichlorodihydrofluorescein (H_2DCF) and reaction with ROS, originating the fluorescent compound dichlorofluorescein (DCF).	70
Figure 31. Schematic representation of NO and L-citrulline production in LPS-stimulated RAW 264.7 macrophages and reactions used for their determination.	74
Figure 32. α -Glucosidase inhibition caused by the methanol extracts obtained from the inflorescences (TH01) and fruits (TH02) of <i>C. urens</i> (A), from the leaves (TH05) and stem bark (TH06) of <i>F. curtipes</i> (B), from the leaves (TH07) of <i>C. tabularis</i> (C) and from the flowers (TH19) of <i>G. gracillima</i> (D)	80
Figure 33. 5-LOX inhibition caused by the methanol extracts obtained from the inflorescences (TH01) and fruits (TH02) of <i>C. urens</i> (A), from the leaves (TH05) and stem bark (TH06) of <i>F. curtipes</i> (B), from the leaves (TH07) of <i>C. tabularis</i> (C) and from the flowers (TH19) of <i>G. gracillima</i> (D)..	82

Figure 34. DPPH [•] scavenging activity displayed by the methanol extracts obtained from the inflorescences (TH01) and fruits (TH02) of <i>C. urens</i> (A), from the leaves (TH05) and stem bark (TH06) of <i>F. curtipes</i> (B), from the leaves (TH07) of <i>C. tabularis</i> (C) and from the flowers (TH19) of <i>G. gracillima</i> (D)	83
Figure 35. HPLC-UV (320 nm) chromatogram of the methanol extracts prepared from the inflorescences (TH01) and fruits (TH02) of <i>C. urens</i>	85
Figure 36. MS fragmentation pattern of the <i>O</i> -caffeoylshikimic acid isomers identified in <i>C. urens</i> methanol extracts.	86
Figure 37. MS ² [(M-H)] ⁻ , MS ³ [(M-H)→(M-H-162)] ⁻ , MS ⁴ [(M-H)→(M-H-162)→(M-H-162-162)] ⁻ , and MS ⁵ [243] ⁻ analysis of caffeoyl-di-hexosyl-C ₁₁ H ₁₅ O ₆ (3) detected in the methanol extract obtained from <i>C. urens</i> fruits (TH02).....	87
Figure 38. HPLC-UV chromatograms of the methanol extracts obtained from the leaves (TH05, A) and from the stem bark (TH06, B) of <i>F. curtipes</i>	91
Figure 39. MS fragmentation pattern of some apigenin derivatives detected on the leaves (TH05) and stem bark (TH06) of <i>F. curtipes</i>	94
Figure 40. MS fragmentation pattern of some flavan-3-ols derivatives and the lignan aviculin (19) detected on the stem bark (TH06) of <i>F. curtipes</i>	96
Figure 41. HPLC-UV chromatogram of the methanol extract obtained from the leaves (TH07) of <i>C. tabularis</i>	99
Figure 42. MS fragmentation pattern of epiafzelechin-(4β-8)-catechin (A). Similar fragmentations were observed for the other detected dimers (B).....	101
Figure 43. MS fragmentation pattern of epifisetinidol-(4β-8)-epicatechin-(6-4β)-epifisetinidol (A). Similar fragmentations were observed for the other detected trimmers (B).	102
Figure 44. MS fragmentation pattern of 7,3'-dimethyl-quercetin-3- <i>O</i> -hexoside and 3',4'-dimethyl-quercetin-3- <i>O</i> -hexoside.	104
Figure 45. HPLC-UV chromatogram of the methanol extract obtained from the flowers of <i>G. gracillima</i> (TH19)	106
Figure 46. MS fragmentation pattern of some kaempferol diglycosides (A) and triglycosides (B).	108
Figure 47. MS fragmentation pattern of valoneic acid dilactone (2) and sanguisorbic acid dilactone (3).....	110

- Figure 48.** α -Amylase inhibition caused by the methanol extracts obtained from the inflorescences of *C. urens* (TH01) and from the stem bark of *F. curtipes* (TH06)113
- Figure 49.** Michaelis-Menten kinetics of α -glucosidase activity recorded in the absence and presence of increasing concentrations of the methanol extracts obtained from the inflorescences (A) and fruits (B) of *C. urens*, from the leaves (C) and stem bark (C) of *F. curtipes*, from the leaves of *C. tabularis* (E) and from the flowers of *G. gracillima* (F). ..115
- Figure 50.** Effects of the methanol extracts obtained from the inflorescences of *C. urens* (TH01) and from the flowers of *G. gracillima* (TH19) on Caco-2 cells viability (A) and human α -glucosidase activity (B)117
- Figure 51.** Pearson correlation between the content of phenolic compounds (g/kg of dry extract) of the extracts and the estimated IC_{50} values determined for the inhibition of α -glucosidase ($\mu\text{g/mL}$).119
- Figure 52.** (A) Pancreatic lipase inhibition caused by the methanol extracts obtained from the inflorescences of *C. urens* (TH01) and from the flowers of *G. gracillima* (TH19). (B) Michaelis-Menten kinetics of pancreatic lipase activity recorded in the absence and presence of the methanol extracts obtained from the inflorescences of *C. urens* (TH01) and from the flowers of *G. gracillima* (TH19)..... 120
- Figure 53.** Aldose reductase inhibition caused by the methanol extracts obtained from the inflorescences and fruits of *C. urens* (A), from the stem bark and leaves of *F. curtipes* (B), from the leaves of *C. tabularis* (C) and from the flowers of *G. gracillima* (D) 123
- Figure 54.** Pearson correlation between the content of phenolic compounds (g/kg of dry extract) of the extracts and the estimated IC_{50} value determined for the inhibition of aldose reductase ($\mu\text{g/mL}$). 124
- Figure 55.** $O_2\cdot^-$ (A) and $\cdot\text{NO}$ (B) scavenging activity displayed by the methanol extracts obtained from the inflorescences and fruits of *C. urens* (A1 and B1), from the stem bark and leaves of *F. curtipes* (A2 and B2), from the leaves of *C. tabularis* (A3 and B3) and from the flowers of *G. gracillima* (A4 and B4) 127
- Figure 56.** Inhibition of lipid peroxidation caused by the methanol extracts obtained from the inflorescences of *C. urens* (A), from the stem bark and leaves of *F. curtipes* (B), from the leaves of *C. tabularis* (C) and from the flowers of *G. gracillima* (D)..... 128
- Figure 57.** Pearson correlation between the content of phenolic compounds (g/kg of dry extract) of the extracts and the estimated IC_{50} value determined for the DPPH \cdot (A) and $O_2\cdot^-$ (B) scavenging activities ($\mu\text{g/mL}$). 129

Figure 58. Effects of the methanol extracts obtained from <i>C. urens</i> inflorescences (TH21) and from <i>G. gracillima</i> flowers (TH22) on RIN-5F cells' viability (A) and on intracellular species levels (B) under normal glucose conditions (11 mM glucose) and under glucotoxic conditions (33 mM glucose)	131
Figure 59. Inhibitory effects of <i>C. urens</i> (TH21) and <i>G. gracillima</i> methanol extracts on BSA glycation induced by methylglyoxal (A), glucose (B) and fructose (C), after 3, 7 and 14 days.	135
Figure 60. Pearson correlation between the content of phenolic compounds (g/kg of dry extract) of the extracts and the inhibition of BSA-methylglyoxal (A), BSA-glucose (B) and BSA-fructose (C) formation.	136
Figure 61. Michaelis-Menten kinetics of 5-LOX activity in the absence and presence of increasing concentrations of the methanol extracts obtained from the stem bark of <i>F. curtipes</i> (A), from the leaves of <i>C. tabularis</i> (B) and from the inflorescences of <i>C. urens</i> (C)	138
Figure 62. Effects of the methanol extracts obtained from the leaves (TH05, A) and stem bark (TH06, B) of <i>F. curtipes</i> , from the leaves of <i>C. tabularis</i> (TH07, C), from the inflorescences of <i>C. urens</i> (TH20, D) and from the flowers of <i>G. gracillima</i> (TH21, E) on the mitochondrial activity of RAW 264.7.	141
Figure 63. Effects of the methanol extracts obtained from the leaves (TH05, A) and stem bark (TH06, B) of <i>F. curtipes</i> , from the leaves of <i>C. tabularis</i> (TH07, C), from the inflorescences of <i>C. urens</i> (TH20, D) and from the flowers of <i>G. gracillima</i> (TH21, E) on the mitochondrial activity, NO levels and L-citrulline levels in LPS-stimulated RAW 264.7.	143
Figure 64. Effects of the treatment with the methanol extracts obtained from the leaves of <i>F. curtipes</i> (A), from the leaves of <i>C. tabularis</i> leaves (B), from the inflorescences of <i>C. urens</i> (C) and from the flowers of <i>G. gracillima</i> (D) on IL-6 and TNF- α levels in LPS-stimulated RAW 264.7 macrophages.....	145
Figure 65. Pearson correlation between the content of flavan-3-ols (g/kg of dry extract) of the extracts and the estimated IC ₅₀ value determined for the 5-LOX inhibition (μ g/mL).	146

LIST OF TABLES

LIST OF TABLES

Table 1. Epidemiological, clinical and pathological features of T1D and T2D.....	6
Table 2. Plant species found in Thailand that were prioritized for screening according to their medicinal value (score)	36
Table 3. Characterization of the panel of plant materials prioritized for screening.	49
Table 4. Chromatographic conditions used on the qualitative analysis of the selected methanolic extracts by HPLC-DAD-ESI (Ion Trap)/MS ⁿ	53
Table 5. Results on the biologic screening of the methanol extracts obtained from plant species collected in Thailand.	79
Table 6. Retention time (<i>Rt</i>), molecular formula (M), [M-H] ⁻ and MS ² [M-H] ⁻ data for the hydroxycinnamic acids detected on the methanol extracts obtained from the inflorescences (TH01) and from the fruits (TH02) of <i>C. urens</i> . ^a	89
Table 7. Content of phenolic compounds detected on the methanol extracts obtained from the inflorescences (TH01 - first collection, and TH21 - second collection) and from the fruits (TH02) of <i>C. urens</i> (mg/kg dry extract)	89
Table 8. Retention time (<i>Rt</i>), molecular formula (M) and MS [M-H] ⁻ and MS ² [M-H] ⁻ data for the apigenin derivatives detected in the methanol extract obtained from the leaves (TH05) and from the stem bark (TH06) of <i>F. curtipes</i> . ^a	93
Table 9. Retention time (<i>Rt</i>), molecular formula (M) and MS [M-H] ⁻ and MS ² [M-H] ⁻ data for the flavan-3-ols derivatives detected in the methanol extract obtained from the leaves (TH05) and from the stem bark (TH06) of <i>F. curtipes</i>	93
Table 10. Content of phenolic compounds detected on the methanol extracts obtained from the leaves (TH05) and from the stem bark (TH06) of <i>F. curtipes</i> (mg/kg dry extract).....	97
Table 11. Retention time (<i>Rt</i>), molecular formula (M) and MS [M-H] ⁻ and MS ² [M-H] ⁻ data for the proanthocyanidins detected in the methanol extract obtained from <i>C. tabularis</i> leaves (TH07). ^a	100
Table 12. Retention time (<i>Rt</i>), molecular formula (M) and MS [M-H] ⁻ and MS ² [M-H] ⁻ data for the flavonoids detected in the methanol extract obtained from <i>C. tabularis</i> leaves (TH07). ^a	103
Table 13. Content of phenolic compounds detected on the methanol extract obtained from the leaves of <i>C. tabularis</i> (TH07) (mg/kg dry extract).....	105

Table 14. Retention time (<i>Rt</i>), molecular formula (M) and MS [M-H] ⁻ and MS ² [M-H] ⁻ data for the kaempferol derivatives detected in the methanol extract obtained from <i>G. gracillima</i> flowers (TH19). ^a	107
Table 15. Retention time (<i>Rt</i>), molecular formula (M) and MS [M-H] ⁻ and MS ² [M-H] ⁻ data for the ellagic acid derivatives detected in the methanol extract obtained from <i>G. gracillima</i> flowers (TH19). ^a	107
Table 16. Content of phenolic compounds on the methanol extracts obtained from <i>G. gracillima</i> flowers (TH19 - first collection, TH22 - second collection) (mg/kg dry extract)	111
Table 17. Kinetic parameters for determining the type of α-glucosidase inhibition caused by the methanol extracts obtained from <i>C. urens</i> (TH01 and TH02), <i>F. curtipes</i> (TH05 and TH06), <i>C. tabularis</i> (TH07) and <i>G. gracillima</i> (TH19). ^a	114
Table 18. Kinetic parameters for determining the inhibition type of pancreatic lipase caused by the methanol extracts obtained from the inflorescences of <i>C. urens</i> (TH01) and from the flowers of <i>G. gracillima</i> (TH19). ^a	121
Table 19. Kinetic parameters for the inhibition of 5-LOX activity caused by the extracts obtained from <i>F. curtipes</i> stem bark (TH06), <i>C. tabularis</i> leaves (TH07) and <i>C. urens</i> inflorescences (TH21). ^a	139
Table 20. Estimated IC ₂₅ values for the methanol extracts on NO and L-citrulline levels in LPS-stimulated RAW 264.7 macrophages.	143

LIST OF ABBREVIATIONS

LIST OF ABBREVIATIONS

·NO	Nitric oxide radical
5-LOX	5-Lipoxygenase
AGEs	Advanced glycation end products
Akt	Protein kinase B
AMPK	AMP-activated protein kinase
APCI	Atmospheric pressure chemical ionization
API	Atmospheric pressure ionization
APPI	Atmospheric pressure photo-ionization
AS	Anthocyanidin synthetase
ATCC	American Type Culture Collection
ATP	Adenosine triphosphate
BHT	3,5-Di- <i>tert</i> -4-butylhydroxytoluene
BSA	Bovine serum albumin
CID	Collision-induced decomposition
DAD	Diode array detection
DAHPh	3-Deoxy-D-arabino-heptulosonate-7-phosphate
DCF	2',7'-Dichlorofluorescein
DCFH-DA	2',7'-dichlorodihydrofluorescein diacetate
DFR	Dehydroflavonol 4-reductase
DM	Diabetes mellitus
DMEM	Dulbecco's modified Eagle medium
DMSO	Dimethyl sulfoxide
DNA	Deoxyribonucleic acid
DNSA	3,5-Dinitrosalicylic acid
DPP-4	Dipeptidyl peptidase-4
DPPH·	Diphenyl-1-picrylhydrazyl radical
EMA	European Medicines Agency
ESI	Electrospray ionization
FBS	Fetal bovine serum
FDA	Food and Drug Administration
FFA	Free fatty acids
FS	Flavone synthase
GC	Gas chromatography
GK	Glucokinase

GLP-1	Glucagon-like peptide-1
GLUT	Glucose transporter
GS	Glycogen synthase
GSH	Glutathione reduced form
H ₂ DCF	2',7'-Dichlorodihydrofluorescein
HbA _{1c}	Glycated haemoglobin
HBSS	Hank's balanced salt solution
HPLC	High-pressure liquid chromatography
IC ₂₅	25% Inhibition concentration
IC ₅₀	50% inhibitory concentration
ICAM	Intercellular adhesion molecule
IDF	International Diabetes Federation
IFN- γ	Interferon- γ
IFR	Isoflavone synthetase
IKK	I κ B kinase
IL	Interleukin
iNOS	Inducible nitric oxide synthase
IR	Insulin resistance
IRS-1	Insulin receptor substrate 1
IUCN	International Union for Conservation of Nature
I κ B α	Inhibitor κ B- α
JNK	c-Jun- <i>N</i> -terminal kinases
K _m	Michaelis constant
LAR	Leucoanthocyanidin reductase
LC	Liquid chromatography
L-NAME	N-Nitro-L-arginine methyl ester hydrochloride
LOD	Limit of detection
LOQ	Limit of quantification
LPS	Lipopolysaccharide
LTB	Leukotrienes
MAPK	Mitogen-activated protein kinase
MCP	Monocyte chemoattractant protein
MS	Mass spectrometry
MTT	3-(4,5-Dimethylthiazol-2-yl)-2,5-diphenyltetrazolium bromide
NAC	<i>N</i> -acetylcysteine

NADH	Nicotinamide adenine dinucleotide reduced form
NADP ⁺	Nicotinamide adenine dinucleotide phosphate
NADPH	Nicotinamide adenine dinucleotide phosphate reduced form
NBT	Nitro blue tetrazolium
NF-κB	Nuclear factor-κB
NI	Negative ion
NWFP	Non-wood forest products
O ₂ ^{•-}	Superoxide anion radical
OAD	Oral antidiabetic drugs
PBS	Phosphate buffered saline
PEP	Phosphoenolpyruvate
PEPCK	Phosphoenolpyruvate carboxykinase
PI	Positive ion
PI3K	Phosphoinositide 3-kinase
PMS	Phenazine methosulfate
<i>p</i> -NGP	<i>p</i> -Nitrophenyl-α-glucopyranoside
<i>p</i> -NPB	<i>p</i> -Nitrophenyl butyrate
PPAR-γ	Peroxisome proliferator-activated receptor gamma
QTOF	Quadrupole time-of-flight
RAGEs	Receptors for advanced glycation end products
RDA	Retro-Diels-Alder reaction
RLTS	Red list of threatened species
ROS	Reactive oxygen species
RP	Reverse phase
RPMI	Roswell Park Memorial Institute
SLGT	Sodium-glucose transport proteins
SNP	Sodium nitroprusside
SPE	Solid phase extraction
T1D	Type 1 diabetes
T2D	Type 2 diabetes
TG	Triglycerides
TLC	Thin layer chromatography
TLR	Toll-like receptors
TNF-α	Tumor necrosis factor-α
TTM	Thai traditional medicine
UV	Ultraviolet

VCAM	Vascular cell adhesion protein
V_{\max}	Maximum velocity

THESIS OUTLINE

THESIS OUTLINE

The present thesis is divided into the following chapters:

CHAPTER I: INTRODUCTION AND OBJECTIVES

This chapter includes an overall contextualization of the main topics that will be covered throughout the current thesis, providing its underlying scientific rationale and allowing an intuitive follow up of the experimental work. The first part of the introductory section delivers a general overview on type 2 diabetes (T2D) pathophysiology, details current therapeutic approaches, also highlighting the role of plants as sources of bioactive phenolic compounds. The chemistry, biosynthesis, extraction, and analysis of phenolic compounds are addressed, including an overview on the biological effects with clinical relevance on diabetes management. The role of Thai Traditional Medicine and ethnomedical surveys on the prioritization of medicinal plants to be investigated on their potential antidiabetic properties is also included, providing the background underling the selected panel of plants from Thai flora. Previous knowledge on the species that were selected for an in-depth phenolic characterization and evaluation of biologic effects, namely *Caryota urens* L., *Ficus curtipes* Corner, *Chukrasia tabularis* A. Juss. And *Gustavia gracillima* Miers, is presented at the end of this section. The main objectives of the present thesis are stated at the end of this chapter.

CHAPTER II: EXPERIMENTAL SECTION

This chapter provides detailed information on sampling procedures, techniques, methodologies and experimental protocols used to achieve the objectives of this thesis.

CHAPTER III: RESULTS AND DISCUSSION

This chapter contains the scientific outcomes. Data gathered in the current thesis is presented, integrated and discussed under the light of the current knowledge.

CHAPTER IV: CONCLUSIONS

This chapter contains the main conclusions taken from this thesis, providing also future perspectives and challenges that remain to be overcome.

CHAPTER V: REFERENCES

All the bibliographic references used to support this thesis are listed in this chapter.

CHAPTER I

INTRODUCTION

OBJECTIVES

1. Introduction

1.1. Diabetes mellitus: overview

Diabetes mellitus (DM) is an emerging pandemic of the modern world, with high morbidity and mortality (1,2). According to the latest report of the Diabetes Atlas (10th edition), from the International Diabetes Federation (IDF), 537 million of people (1 in every 10 adults) worldwide are currently living with diabetes (1). The number of cases increased more than 60% over the past ten years and a global increase of 46% is estimated until 2045. This increase is strongly associated with the growing development of T2D in young people and adults, overweight and sedentarism being the main trigger factors (1). In fact, current dietary patterns, characterized by a generalized intake of processed and hypercaloric meals, along with sedentary daily habits and smoking are positively correlated with the risk of developing T2D (3). The situation is particularly dramatic in low and middle-income countries, where most cases (80.6%, 432.7 million of people) and diabetes-related deaths are recorded (1). In Europe, 61 million of people are diagnosed with diabetes (1 in every 11 adults), being estimated that over a third (36%) remain underdiagnosed and, therefore, at an extreme risk of developing irreversible complications, with unavoidable health and economics burdens (1). The management of diabetes and of its complications represents a massive economic burden for health care institutions and governmental entities, 19.6% of the European global health expenditure (USD \$189 billion) being spent (1). Furthermore, as evidenced at the IDF report, Turkey ranks first as the country with higher incidence of diabetes, followed by Spain, Andorra and Portugal, the latter with an incidence of 13.0 % in adults between 20 and 79 years. Hence, 1 in every 8 Portuguese adults have diabetes, resulting into an average cost for the Portuguese health entities of 2 293 USD *per patient* (1).

DM is a metabolic disorder characterized by a chronic hyperglycaemic state, deriving from defects on insulin production and/or action, leading to a generalized dysregulation of carbohydrates, lipids and proteins metabolism (4). Conventionally, this condition can be subdivided into two main types: type 1 diabetes (T1D), characterized by the autoimmune destruction of pancreatic β -cells, and T2D, characterized by a generalized resistance to insulin (5). Still, other forms of diabetes are also acknowledged, namely gestational diabetes, that develops in pregnant women with no prior medical diabetes history, and prediabetes, characterized by a blood glucose level higher than the normal, but with insufficient relevance to fall into diabetes category (4,5). T1D, often detected at younger ages, has an auto-immune background (islet cell antibodies present at diagnosis) and is

accompanied by a loss of pancreatic β -cells mass, with consequent absence of insulin production (4). In this case, insulin-therapy is mandatory. On the other hand, T2D is mostly associated with lifestyle and risk factors, such as hypertension, dyslipidaemia and obesity, therefore usually appearing at older ages (4). However, childhood obesity is dramatically changing this paradigm, strongly contributing for T2D development in younger adults (6,7). In T2D, the insulin released by pancreatic β -cells is unable to induce a proper response at the insulin-sensitive tissues, pressuring the pancreas to continuously produce more insulin (4). Glycaemic control in T2D patients can often be achieved with oral antidiabetic drugs (OAD), yet, in later stages of the disease, exogenous insulin therapy might also be required (4,8). The main clinical and pathological features of T1D and T2D are summarized in **Table 1**.

Table 1. Epidemiological, clinical and pathological features of T1D and T2D. Adapted from [(4)].

Characteristics	T1D	T2D
Prevalence	10 %	90 %
Background	Auto-immune	Potentiated by lifestyle
Onset age	< 30 years-old	> 30 years-old
Onset of symptoms	Abrupt	Gradual
Obesity association	No	Yes
Endogenous insulin in the plasma	Undetectable	Depend on the stage
Islet cells antibodies in the plasma	Yes	No
Oral antidiabetic drugs	No	Yes
Insulin therapy	Mandatory	It might be required
Development of complications	Yes	Yes

Commonly, *ca.* 90 % of diabetes cases correspond to T2D, this higher prevalence being related to some well-recognised risk factors, such as diet, sedentarism, age, smoking and obesity (4,9). Hence, considering the significant prevalence of TD2, this will be the metabolic disorder spotlighted in the current thesis.

1.1.1. Physiopathology of type 2 diabetes

T2D is often characterized by an impairment of insulin secretion and/or action, causing an abnormal rise of blood glucose levels (10). Insulin is an anabolic hormone that acts on insulin-sensitive tissues: in the liver it stimulates glucose uptake, glycogenesis (glycogen synthesis), glycolysis (metabolic oxidation of glucose) and the synthesis of free fatty acids (FFA) and proteins; in skeletal muscle it promotes glucose uptake, glycolysis, glycogenesis

and proteins synthesis; in the adipocytes it stimulates glucose and FFA uptake, glycolysis and triglycerides (TG) synthesis (4,11). Hence, impaired insulin secretion and/or action in the target tissues (insulin resistance, IR), causes a severe imbalance on carbohydrates, lipid and protein metabolism (4,11).

IR commonly occurs when insulin-sensitive cells fail to respond to the action of this plasmatic hormone (10). In this case, despite being produced and secreted by pancreatic cells, insulin is not able to induce a proper response and the already elevated blood glucose levels remain augmented. Considering that blood glucose levels are the main stimulus for the secretion of insulin, pancreatic β -cells are constantly triggered to produce and secrete more and more insulin. However, the released hormone is not capable of restoring the settled hyperglycaemic state, generating a vicious cycle that can ultimately lead to pancreatic cells dysfunction (10,11).

As above-stated, the worldwide increment of T2D cases has been particularly accelerated by the exponential growth of obesity (1,12). In fact, overweight, and the underlying chronic inflammatory state, are both involved on the development of IR and on the progressive dysfunction of pancreatic cells (13,14). Visceral fat accumulation promotes the release of adipokines and pro-inflammatory cytokines (tumor necrosis factor- α , TNF- α , and interleukin, IL-6) from the adipocytes, inducing the infiltration of resident macrophages in the adipose tissue, liver, skeletal muscle and pancreas (13). Thereafter, activated macrophages will be responsible for the abnormal secretion of pro-inflammatory cytokines (TNF- α , IL-1 β , IL-6 and monocyte chemoattractant protein, MCP), creating a generalized inflammatory microenvironment. This cascade of inflammatory cytokines activates the c-Jun-N-terminal kinases (JNK) in insulin-targeted tissues *via* toll-like receptors (TLR)2/4 recognition, blocking insulin signalling cascades and promoting IR (13,14). The molecular inflammatory pathways involved on β -cells dysfunction and on IR are schematized in **Figure 1**.

β -cell dysfunction is another key pathological event of T2D, being dramatically accelerated by the overproduction of inflammatory mediators and reactive oxygen species (ROS) (10,15). Pro-inflammatory cytokines (TNF- α , IL-1 β and interferon- γ , IFN- γ), released by activated macrophages, activate nuclear factor- κ B (NF- κ B), inducing the expression of the inducible nitric oxide synthase (iNOS) and the production of NO (16). In turn, NO overproduction induces the release of mitochondrial pro-apoptotic factors, including cytochrome *c*, which activates the cytosolic caspase cascade, ultimately leading to β -cells apoptosis (16) (**Figure 1**). In parallel, long-term exposure to glucose results in activation of the mitochondrial electron transport chain and exacerbates the polyol pathway, enhancing the formation of ROS and compromising cellular antioxidant systems

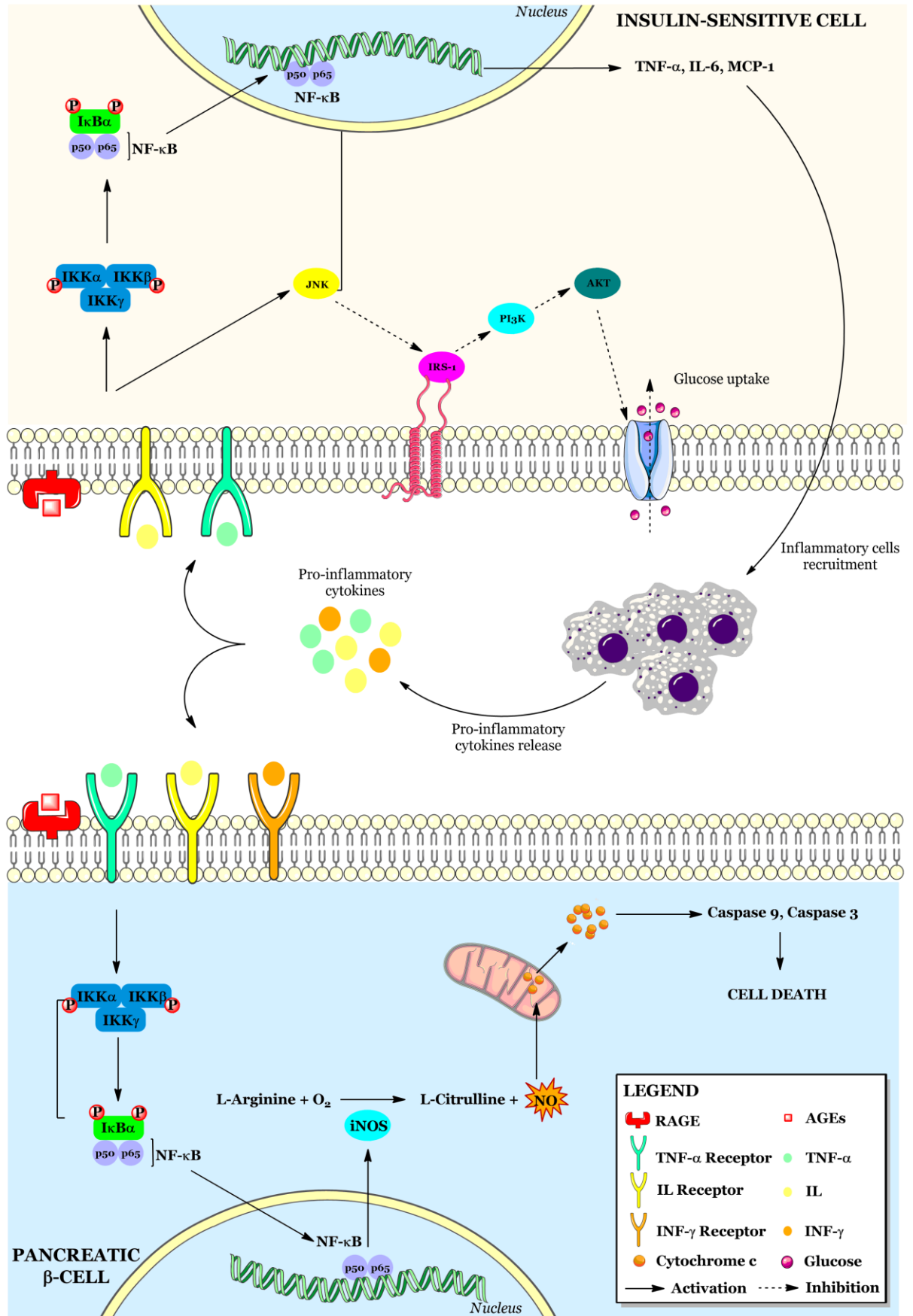


Figure 1. Schematic representation of the main molecular pathways linking inflammation to insulin resistance. AGEs, advanced glycation end products; Akt, protein kinase B; IFN- γ , interferon- γ ; IKK, I κ B kinase; IL, interleukin; iNOS, inducible nitric oxide synthase; IRS-1, insulin receptor substrate 1; I κ B α , inhibitor κ B- α ; JNK, c- Jun-*N*-terminal kinases; MCP-1, monocyte chemoattractant protein-1; NF- κ B, nuclear factor- κ B; PI3K, phosphoinositide 3-kinase; RAGEs, receptors for advanced glycation end products; TNF- α , tumor necrosis factor- α . [Adapted from (13,14,16)].

(17). Firstly, hyperglycaemia promotes the electron flux through the mitochondrial electron transport system by activation of uncouplers of oxidative phosphorylation, generating free radical species due to partial O₂ reduction (17). Secondly, high glucose levels exacerbate the polyol pathway, compromising cellular antioxidant systems. Through this metabolic route, glucose is reduced to sorbitol by the cytosolic nicotinamide adenine dinucleotide phosphate reduced form (NADPH)-dependent enzyme, aldose reductase (**Figure 2**) (17,18). The enzyme co-factor, NADPH, is essential for the generation of the intracellular antioxidant glutathione (GSH). Hence, under hyperglycaemic conditions there is depletion of NADPH due to an over-activity of the polyol pathway, which, in turn, will compromise cellular antioxidant systems (17,18). ROS can directly damage lipids, proteins and DNA, causing changes in protein expression and inducing β -cells apoptosis (15,17) (**Figure 2**). Moreover, ROS can induce JNK activation in pancreatic cells, reducing mTOR activation and contributing to the loss of β -cell mass (19). On the other hand, ROS overproduction can activate NF- κ B, inducing the release of pro-apoptotic factors, contributing also to the β -cells mass loss (19).

Besides its role on β -cell dysfunction, polyol pathway overexpression has also been implicated on the development and progression of diabetic complications (17,18). In this context, sorbitol, that results from glucose oxidation, cannot cross cellular membranes and therefore accumulates in cells, mostly in the eyes and kidneys, causing osmotic stress and compromising normal cellular function (17). Moreover, cells expressing high levels of glucose transporter (GLUT)-1 (vascular endothelial cells, renal cells and retinal cells) are particularly susceptible to hyperglycaemia-induced damage through non-enzymatic processes, conventionally known as glycation (20). In fact, protein glycation is one of the principal pathways underling the development and progression of diabetic-related complications including retinopathy, nephropathy, neuropathy and cardiomyopathy (20). This time-dependent process is generically subdivided into three main stages: early stage (occurs within hours), intermediate stage (occurs in days) and late stage (takes weeks/months). The early stage starts with the reaction between the carbonyl group of a reducing sugar and a free amino group of a protein, originating an unstable Schiff base that undergoes through rearrangement to form a reversible keto-amine, known as Amadori product (Maillard reaction) (**Figure 2**) (20). Their oxidation later leads to the formation of reactive dicarbonyl compounds, such as glyoxal, methylglyoxal and 2-deoxyglucosone

(intermediate stage). These highly-reactive compounds may react with free amino groups in proteins, originating irreversible compounds named advanced glycation end products (AGEs) (late stage) (**Figure 2**) (20). Pentosidine, *N*-carboxy-methyl-lysine and *N*-carboxy-ethyl-lysine are examples of known AGEs (20). Besides altering proteins conformation and, consequently, changing their function, AGEs can directly bind to specific surface receptors for advanced glycation end products (RAGEs), activating intracellular signalling pathways (**Figure 3**). RAGE activation by AGEs in macrophages activates the mitogen-activated protein kinase (MAPK) pathway, causing NF- κ B translocation into the nucleus; this will induce the transcription of inflammatory mediators, such as TNF- α and IL-6, and promote the expression of intercellular adhesion molecule (ICAM)-1 and vascular cell adhesion protein (VCAM)-1, also exacerbating ROS production (**Figure 3**) (20).

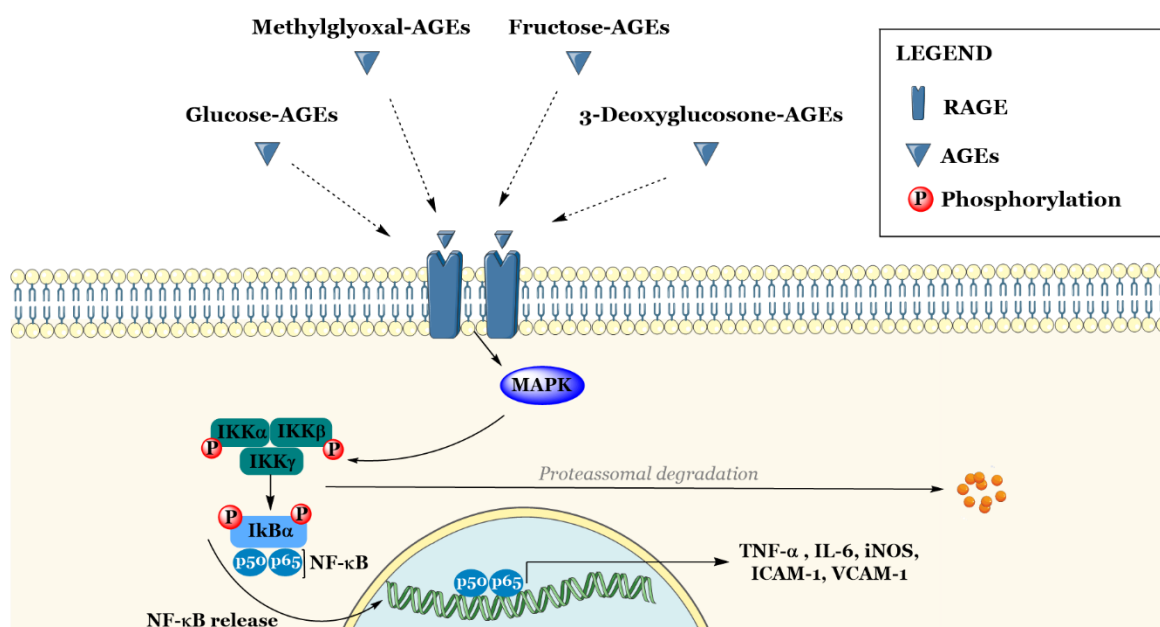


Figure 3. Schematic representation of the AGEs induced-inflammatory response. AGEs, advanced glycation end products; ICAM-1, intercellular adhesion molecule-1; IL-6, interleukin-6; I κ B α , inhibitor κ B- α ; IKK, I κ B kinase; MAPK, mitogen-activated protein kinase; NF- κ B, nuclear factor- κ B; RAGE, receptor for advanced glycation end products; ROS, reactive oxygen species; TNF- α , tumor necrosis factor- α ; VCAM-1, vascular cell adhesion protein-1.

Long-term exposure to hyperglycaemia promotes the polyol pathway overactivity and AGEs formation, being thereafter responsible for the development of both macrovascular (cerebrovascular disease, coronary artery disease and atherosclerosis) and microvascular (neuropathy, nephropathy, and retinopathy) complications in diabetic patients (17,20,21). While macrovascular complications are the main cause of premature death, microvascular lesions, mostly on the eyes, kidneys and nerves, are the principal causes of chronic kidney disease, irreversible blindness, and non-traumatic leg amputations, thus strongly

contributing to the disability caused by diabetes (21,22). The management of these complications represents a massive economic load for health institutions, resulting not only in significant and expensive hospitalizations, but also contributing to productivity loss due to chronic disabilities and premature deaths (2,23).

1.1.2. Pharmacological approaches and targets

In the light of the multifactorial etiology of the disease, therapeutic approaches to manage T2D are predominantly directed to the control of the metabolic parameters (glucose and lipid blood levels) as an attempt to prevent and/or delay the occurrence of associated complications (8,24,25). Glycaemic control in T2D can be achieved with OAD when pancreatic β -cells are not yet compromised and basal insulin production endures; otherwise, as for T1D, the use of exogenous insulin is mandatory (26). The treatment of T2D is personalized and optimized to the characteristics of each patient; even though the biguanide metformin remains the first-line treatment, other OAD can also be considered in combination therapy (24–26).

The principal classes of OAD include biguanides, sulfonylureas, glinides, thiazolidinediones, glucagon-like peptide-1 (GLP-1) agonists, dipeptidyl peptidase-4 (DPP-4) inhibitors, α -glucosidase inhibitors and, more recently, sodium-glucose transport proteins (SGLT) inhibitors (**Figure 4**) (8,27).

Biguanides (metformin) reduce hepatic gluconeogenesis and lipogenesis and increase insulin-mediated glucose uptake in muscles (**Figure 4**) (28). Sulfonylureas and glinides bind to specific receptors of pancreatic β -cells, activating adenosine triphosphate (ATP)-sensitive potassium channels, which alter the resting membrane potential of cells, promoting Ca^{2+} influx and insulin secretion (**Figure 4**) (29). Thiazolidinediones activate nuclear receptor peroxisome proliferator-activated receptor gamma (PPAR- γ), increasing insulin sensitivity by enhancing peripheral glucose uptake and adiponectin levels (**Figure 4**) (30). GLP-1 is an incretin secreted by intestinal cells with insulinotropic effects, being however quickly degraded by DPP-4 (**Figure 4**) (31). GLP-1 agonists mimic GLP-1 action, and are more resistant to DPP-4 hydrolysis, stimulating insulin secretion, suppressing glucagon release and decreasing gastric emptying (**Figure 4**) (31). DPP-4 inhibitors indirectly enhance GLP-1 levels, consequently displaying similar insulinotropic effects (32).

Dietary carbohydrates need to be metabolized into smaller monosaccharides, before being absorbed by enterocytes (26). α -Amylase, predominant in saliva and pancreatic juice,

hydrolyses the α -bounds of complex carbohydrates (starch and glycogen) into simple sugars (as maltotriose and maltose) (26). Afterwards, intestinal α -glucosidase cleaves maltose and saccharose α -(1-4) bonds, releasing glucose for further enterocyte uptake (26). Hence, α -glucosidase and α -amylase inhibitors hinder dietary carbohydrates digestion and absorption, lowering post-prandial glycaemia (**Figure 4**) (33). Lastly, SGLT-2 inhibitors inhibit renal glucose reabsorption, reducing blood glucose levels and inducing glucose excretion through the urine (**Figure 4**) (34).

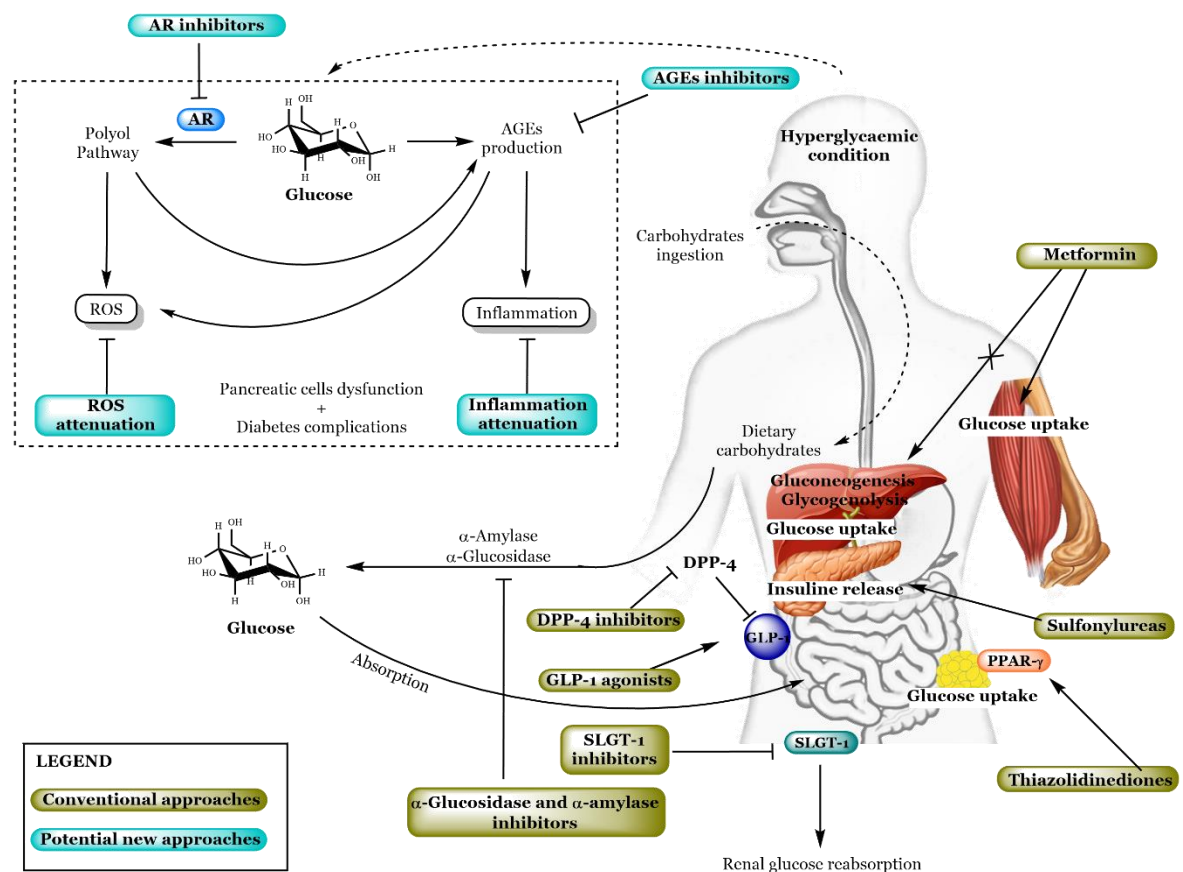


Figure 4. Conventional pharmacological approaches utilized in TD2 management and novel potential targets. AR, aldose reductase; AGEs, advanced glycation end products; DPP-4, dipeptidyl peptidase-4; GLP-1, glucagon-like peptide-1; PPAR- γ , peroxisome proliferator-activated receptor gamma; ROS, reactive oxygen species; SGLT-1, sodium-glucose transport protein-1. [Adapted from (26)].

Despite the current antidiabetic therapeutic arsenal, most medicines display side effects that may compromise adherence to therapy (8,27). For example, metformin is associated with gastrointestinal symptoms (nausea, vomiting, diarrhoea and abdominal discomfort) (35), thiazolidinediones are reported to cause oedema and hypoglycaemia (36) and α -glucosidase inhibitors often cause diarrhoea, flatulence and abdominal pain (37). As so, the call for new antidiabetic therapies, with higher selectivity, efficacy and fewer side effects

endures, 30 new drugs being approved by the European Medicines Agency (EMA) only over the last decade (38).

1.2. Plants as sources of bioactive compounds

Notwithstanding the general trend of combinatorial and synthetic chemistry in drug discovery programs, over the last decades, *ca.* 40% of the drugs approved by the Food and Drug Administration (FDA) were derived either directly or indirectly from natural products, while only 36% were considered fully synthetic (39). Specifically concerning the approved antidiabetic drugs, a total of 63 medicines were authorized between 1981 and 2019: 4 were fully synthetic, 16 have a natural product mimic structure, but were obtained by chemical synthesis, and 19 were derived from natural products or had their development inspired in a natural pharmacophore (39). Relevantly, the first line OAD, metformin (dimethylbiguanide), derives from guanidine, found on *Galega officinalis* L. seeds (traditionally utilized in medieval Europe to treat diabetes symptoms, as thirst and polyuria) (40). Also, the worldwide used acarbose is a natural-derived product, obtained from cultures of *Actinoplanes* sp. (41).

Besides paving the way for the development of new medicines, natural products represent also a valuable resource on the discovery and validation of new pharmacological targets (26). In this regard, the SGLT inhibitor phlorizin is a classic example: this dihydrochalcone, isolated in 1835 from the root bark of apple trees (*Malus pumila* Mill.), proved to markedly enhance urine glucose clearance and to lower blood glucose levels in diabetic patients; subsequent studies on phlorizin's mechanism of action elucidated the principal of renal glucose absorption, delivering initial evidence on the role of SGLT-2 inhibition on diabetes therapy (42).

In fact, Nature remains an inexhaustible source of bioactive molecules (43–45), which can be obtained from the most unexpected living beings, as insects, snakes, yeasts, lichens, marine organisms, or microorganisms, among others (43) Still, the *Plantae* Kingdom remains the main source of bioactive natural compounds (46). Curiously, despite of this "endless" offer, only *ca.* 15% of the known existing plant species were chemically characterized and solely 6% were investigated regarding their biological properties, a wide window of new opportunities remaining to be explored (45). Furthermore, genomic analysis allows estimating that plants can contain upwards of 200 000 different metabolites

(5 000 – 15 000 metabolites per species), many of which still lacking any pharmacological consideration (46).

Overall, plant metabolites fall into two distinct categories: primary metabolites that are involved on plants vital metabolic processes (photosynthesis and respiration) and cross, more or less, all living cells; secondary metabolites, obtained from the primary metabolism pathways, are required for plants environmental adaptation, playing an important role on plant's growth, innate immunity and on the defense response against pathogens, pests, and herbivores (47). The general classification of these secondary metabolites is based on their structure and biosynthetic pathway and includes families such as phenolics, terpenes and alkaloids, among others (48,49). Still, even when grouped, the structural diversity of plants secondary metabolites remains “uncountable”, as different molecules are discovered every new year (45). Among these vast range of constituents, phenolics, with numerous biological effects and promising therapeutic applications, have gained increased attention over the years (50–53). Considering their biologic relevance, as well as their ubiquitous distribution in plants, these secondary metabolites will be highlighted in the present dissertation.

1.2.1. Phenolic compounds

Phenolic compounds are widely distributed through the *Plantae* Kingdom, being one of the main secondary metabolites produced by higher plants (53,54). These ubiquitous compounds display several functions in nature, allowing the adaptation of plants to biotic and abiotic factors (54). They ensure protection against ultraviolet (UV) radiation and provide resistance against predators and pathogens, being also involved on the structural support of plant tissues and on the colouring of flowers, leaves and fruits (54). Apart from their importance on plants homeostasis, phenolic compounds have also several benefits for human health, mostly due to their antioxidant and anti-inflammatory properties (53,55). While some phenolics, such as chlorogenic acid, are broadly distributed in vascular plants, some are restricted and specific of certain genera or family and can work as taxonomic biomarkers, being used for quality control and authenticity of some species (56).

Structurally, all phenolic compounds have at least one benzoic ring with at least one hydroxyl group, which can be free or linked to other substituents through ether, ester or glycosidic bonds. Although phenolics can be found in free forms, they usually appear conjugated, with one or more sugar moieties attached by β -glycosidic bonds to a hydroxyl group (*O*-glycoside) or to a carbon (*C*-glycoside) (54,56). These sugar residues are generally

monosaccharides, as glucose, galactose, arabinose, rhamnose and glucuronic acid (54), though disaccharides and oligosaccharides can also be found (54).

The conventional definition of polyphenols, as secondary metabolites having at least one phenyl group, is not satisfactory enough to define this class of phytoconstituents, as the terminology may also include other structurally-related phytochemicals outcoming from distinct metabolic pathways, such as alkaloids and terpenes (57). Hence, Quideau et al. proposed a stricter definition, characterizing polyphenols as “secondary metabolites derived exclusively from the shikimate-derived phenylpropanoid and/or the polyketide pathway(s), featuring more than one phenolic ring and being devoid of any nitrogen-based functional group in their most basic structural expression” (57). These anabolic biosynthetic pathways will be next detailed, particularly in respect to hydroxycinnamic acids, flavonoids and tannins.

Even though the amino acids phenylalanine and tryptophan are considered to be essential for animals, plants have the metabolic tools required for their synthesis (48). They are produced through the shikimic acid pathway (the most frequent on phenolics aromatization), and their deamination originates benzoic acids, hydroxycinnamic acids, coumarins, lignans and neolignans (48,58). The other biosynthetic route refers to the polyketide pathway, which leads to the formation of poly- β -ketoesters of different dimensions, that cyclize through Claisen condensation or aldolic condensation, originating polycyclic metabolites, such as quinones, isocoumarins and chromones (48,58). Oftentimes, these two anabolic routes collide, originating a wide range of phenolics with a mixed biosynthetic origin, as flavonoids, stilbenes, xanthenes, etc (48,58). Phenolic acids, flavonoids and tannins, widely intaked through human diet, are the most common phenolic occurring in Nature (59).

1.2.1.1. Phenolic acids

1.2.1.1.1. Classification and biosynthesis

The term phenolic acids generically define compounds with a benzoic ring and a carboxylic function, deriving from the shikimate pathway (60). However, according to their structural features, two types of phenolic acids are distinguished: phenolic acids derived from benzoic acid (hydroxybenzoic acids, C6-C1) and phenolic acids derived from cinnamic acid, phenylpropanoids (hydroxycinnamic acids, C6-C3) (48,58).

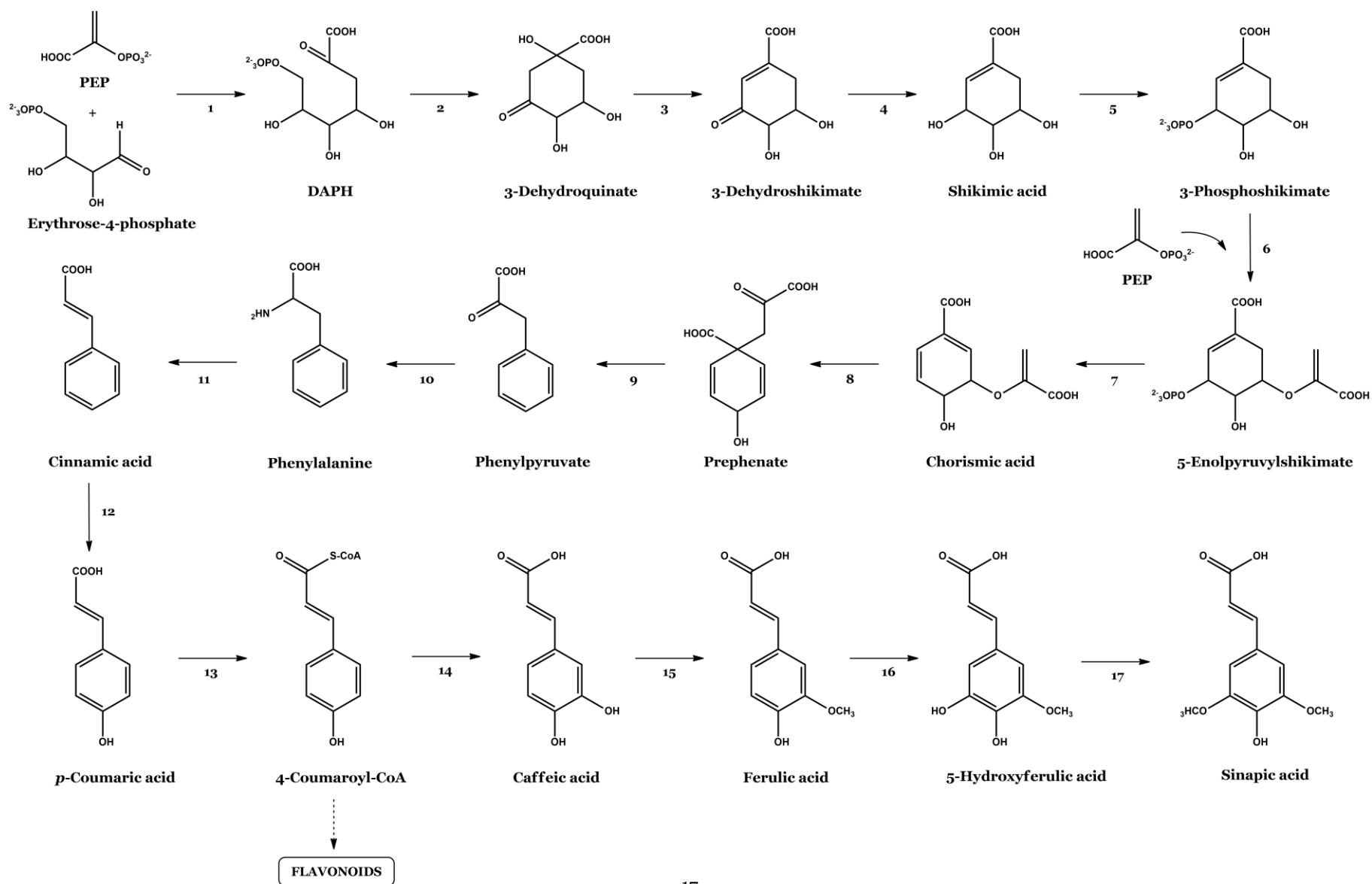


Figure 5. Schematic representation of biosynthetic pathway of phenylpropanoids (shikimate pathway). 1, DAHP synthetase; 2, Dehydroquinate synthase; 3, Dehydroquinase; 4, Shikimate dehydrogenase; 5, shikimate kinase; 6, 3-Phosphoshikimate 1-carboxyvinyltransferase; 7, Chorismate synthase; 8, Chorismate mutase; 9, Prephenate dehydratase; 10, Aromatic-amino-acid transaminase; 11, Phenylalanine ammonia lyase; 12, Cinnamate-4-hydroxylase; 13, Hydroxycinnamate coenzyme-A lyase; 14, *p*-Coumarate 3-hydroxylase; 15, Caffeate *O*-methyltransferase; 16, Ferulate 5-hydroxylase; 17, 5-hydroxyferulate *O*-methyltransferase. [Adapted from (48)].

The biosynthesis of these compounds occurs through the shikimate pathway, which starts with the condensation of an unit of phosphoenolpyruvate (PEP) with other unit of erythrose-4-phosphate, substrates derived from the primary metabolism (glycolysis and pentose-phosphate, respectively) (**Figure 5**) (60). The condensation of these two metabolites originates 3-deoxy-D-arabino-heptulosonate-7-phosphate (DAHP). Posteriorly, DAHP undergoes through an intramolecular aldolic condensation, with elimination of the phosphate group, originating a cyclic compound (3-dehydroquinate). 3-Dehydroquinate is dehydrated into 3-dehydroshikimate, which is after reduced to shikimate (48,58). Shikimate phosphorylation and subsequent condensation with other PEP molecule leads to an enolic ether (5-enolpiruvilshikimate) formation, that undergoes through an unusual 1,4-*trans*-elimination, originating chorismic acid (chorismate), which have a key role on this metabolic pathway (**Figure 5**) (48,58). The pericyclic regrouping of chorismate, catalysed by chorismate mutase, originates prephenate, the metabolic bioprecursor of L-phenylalanine, L-tyrosine and L-tryptophane. Prephenate hydroxylation and dehydration into iso-chorismic acid initiates the biosynthetic route of hydroxybenzoic acids (C6-C1) (48,58). On the other hand, the decarboxylation, aromatization and reducing deamination of prephenate originates L-phenylalanine and its further deamination leads to cinnamic acid formation, starting the biosynthetic pathway of hydroxycinnamic acids (C6-C3), also known as phenylpropanoids (**Figure 5**) (48,58). Cinnamic acid hydroxylation originates *p*-coumaric acid, that is further hydroxylated and *O*-methylated forming other hydroxycinnamic acid derivatives (48,58).

1.2.1.1.2. Biodiversity and chemistry

The structural diversity of the phenolic acids results from the number and the position of hydroxyl groups on the aromatic ring, and also from the possibility of conjugation with other naturally-occurring compounds (61). Among hydroxybenzoic acids, *p*-hydroxybenzoic acid, vanillic acid and protocatechuic acid are the most common, being frequently found in the glycosylated form. Gallic acid, despite of being abundant in Nature,

usually appears esterified with quinic acid or catechins, constituting the main structural block of tannins (53,62) (**Figure 6**). Regarding hydroxycinnamic acids, *p*-coumaric acid, caffeic acid and ferulic acid are the most recurrent, however they are rarely detected in free form (**Figure 6**) (62). As such, contrary to hydroxybenzoic acids, that often emerge on both free and conjugated forms (esters or heterosides), hydroxycinnamic acids usually appear esterified with quinic acid or bound to sugars (48). Hence, derivatives of the moncaffeoylquinic acids, as chlorogenic (5-*O*-caffeoylquinic acid) and neochlorogenic (3-*O*-caffeoylquinic acid) acids, are the most frequent hydroxycinnamates found in edible plants (**Figure 6**) (62). Relevantly, despite of both phenolic acids being intaken by humans, hydroxycinnamic acids are considerably more abundant than benzoic acids, fruits as apples, cherries, peaches, and citrus being the principal dietary sources of these compounds (53).

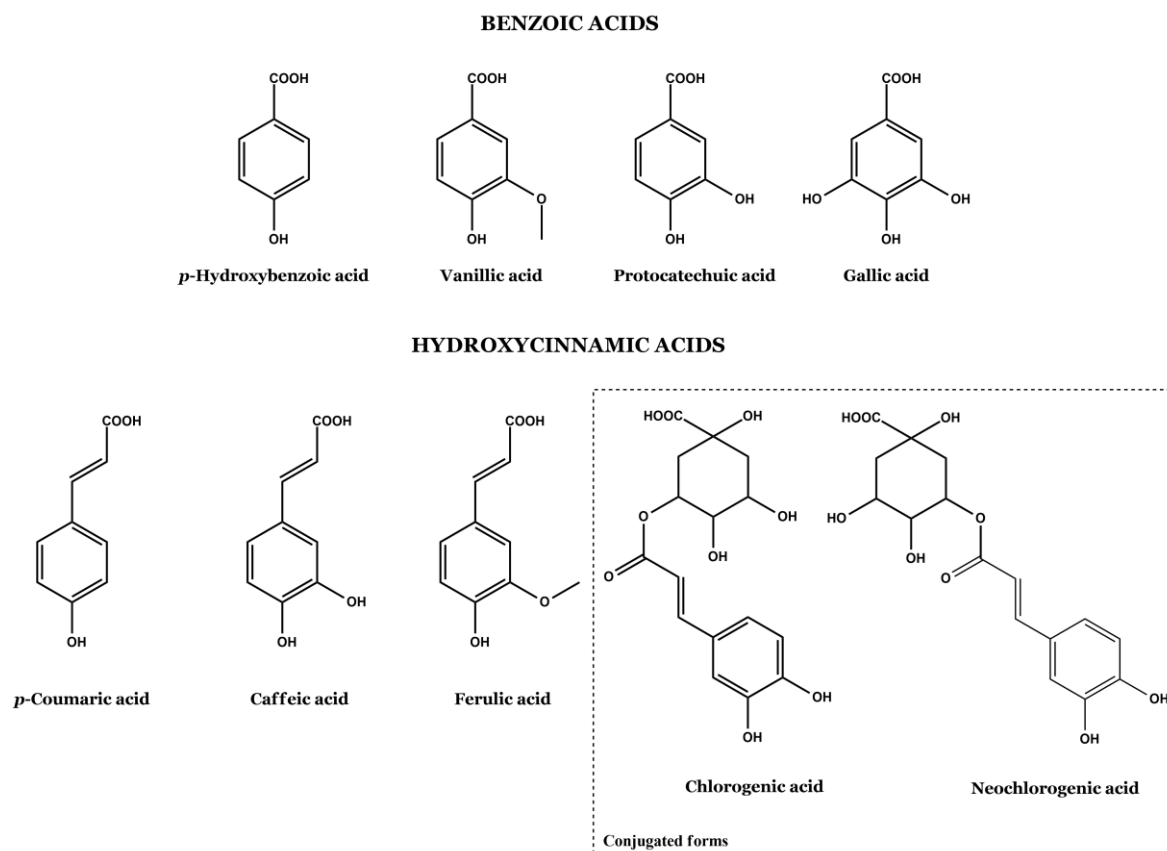


Figure 6. Chemical structures of naturally occurring phenolic acids.

Chemically, the presence of hydroxyl free groups favours the formation of hydrogen bonds, either intramolecular or/and intermolecular, explaining its interaction with some proteins (58). Some of these metabolites are fairly unstable, oxidating easily, mainly under alkaline conditions (48). Moreover, the double bound on the side chain of hydroxycinnamic acids allows the existence of two isomeric forms. The isomerization process is tendentially

accelerated in aqueous solutions, under UV light exposure (48). This explains the often detection of mixtures of isomers in vegetable extracts samples, when only *trans* isomers are found in Nature (61,62).

This type of compounds, as all phenolics, are weak acids, being consequently soluble in organic solvents under acidic conditions. However, conjugated forms (esters or heterosides) are also soluble in water and organic polar solvents, such as ethanol and methanol (48).

1.2.1.2. Flavonoids

1.2.1.2.1. Classification and biosynthesis

With around 6000 different structures documented, flavonoids represent the largest slice of naturally occurring polyphenols (63). These metabolites are abundantly found in fruits, vegetables and beverages, thus broadly consumed in plant-based diets, as the Mediterranean diet (characterized by a rich-daily intake of fruits, vegetables, virgin olive oil, herbs, spices and red wine) (64). Curiously, a daily intake of 428 ± 49 mg of flavonoids is estimated in Europe (*ca.* 4 times higher than observed in the U.S.A.), mainly outcoming from tea, vegetables and grains consumption (65,66).

Structurally, flavonoids are diphenylpropanes with a 15-carbon skeleton (C₆-C₃-C₆), displaying two aromatic rings linked by a chain of three carbons, that may create a third ring. The rings are named as A, B and C and the carbons numeration begins at the oxygen atom from the heterocycle, as presented on **Figure 7** (53).

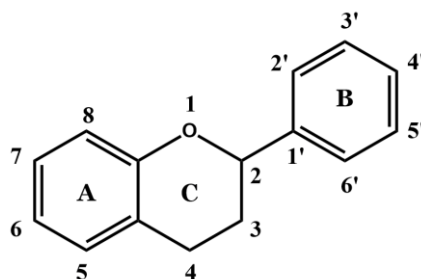


Figure 7. Core structure of flavonoids and numerating scheme.

According to the oxidation of the heterocycle (C ring) and the position of the B ring, flavonoids can be grouped into 9 main categories: chalcones, flavones, flavanones,

flavonols, dihydroflavonols, flavan-3,4-diols, flavan-3-ols, anthocyanins and isoflavones (**Figure 8**) (48).

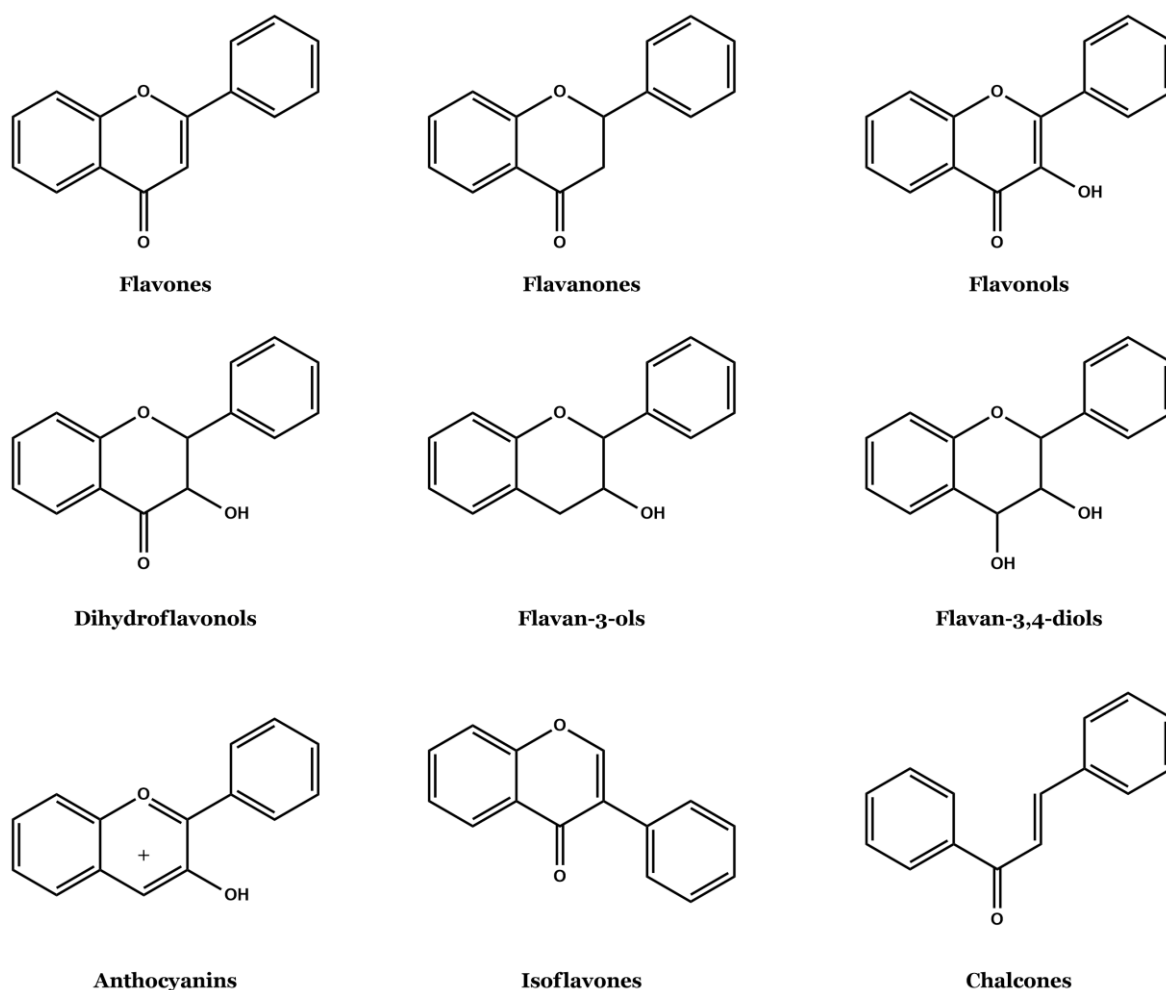


Figure 8. Chemical structures of the main classes of flavonoids.

The biosynthesis of flavonoids occurs through a mixed route, the A ring is formed through the polyketide pathway, while rings B and C rings are formed by the shikimate pathway (**Figure 9**) (48,58). This complex anabolic mechanism is initiated by the condensation of 3 molecules of malonyl-CoA with a unit of *p*-coumaroyl-CoA thioester (produced through the shikimate pathway), originating a chalcone (**Figure 9**) (48,58). The intramolecular cyclization of this chalcone originates 2*S*-naringenin, the biosynthetic precursor of all classes of flavonoids (**Figure 9**) (48,58). The oxidation of this flavanone at C3 originates dihydroflavonols. Dihydroflavonols can be reduced by dihydroflavonol 4-reductase (DFR) at C4 originating flavan-3,4-diols that can be further oxidated by anthocyanidin synthase (AS) into anthocyanins, or reduced at C4 by leucoanthocyanidin reductase (LAR) into flavan-3-ols (**Figure 9**) (48,58). On the other hand, dihydroflavonols reduction, catalysed by the flavonol synthetase (FLS), leads to the formation of flavonols

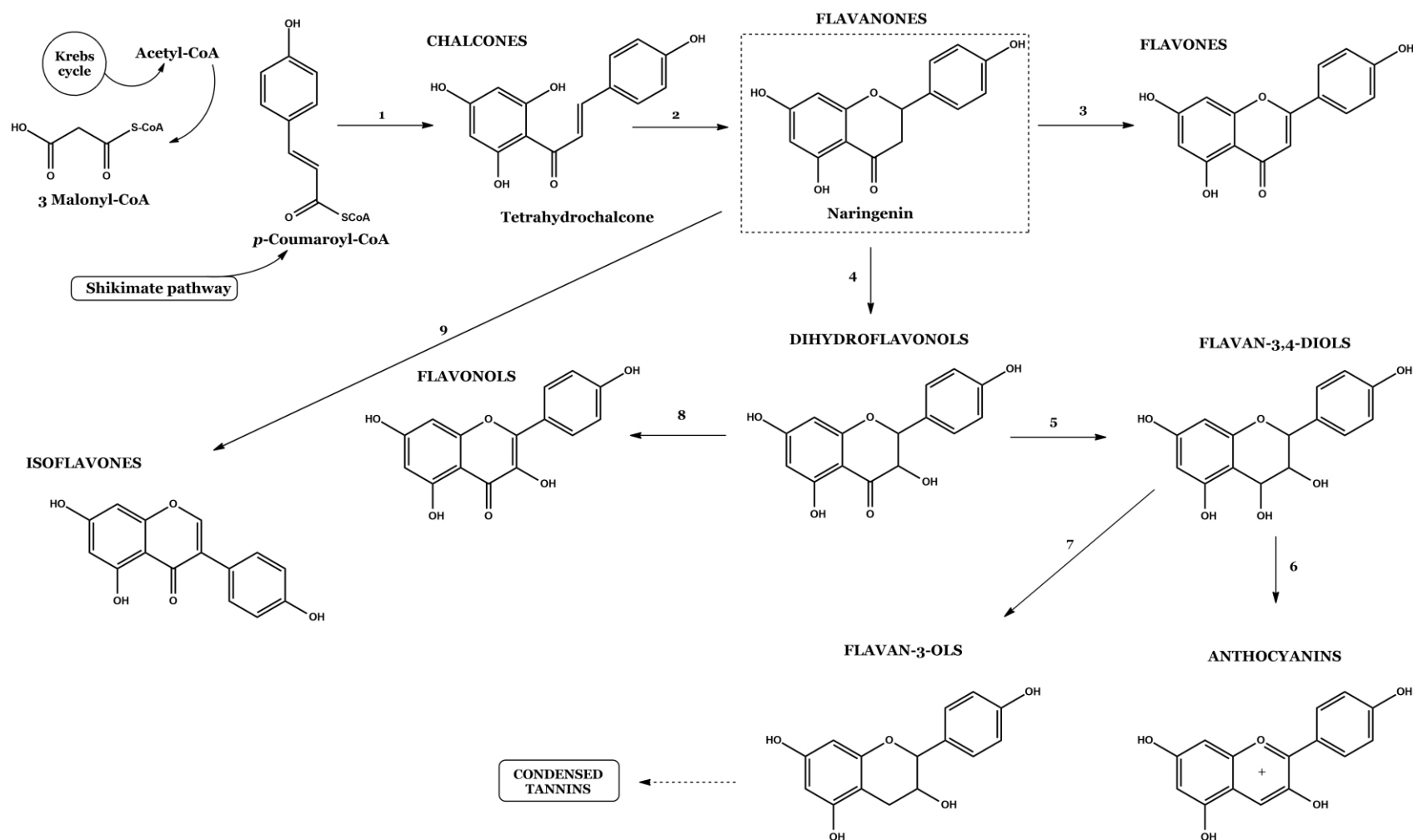


Figure 9. Schematic representation of flavonoids biosynthesis. [Adapted from (48)]. 1, Chalcone synthetase; 2, Chalcone isomerase; 3, Isoflavone synthetase; 4, Flavanone 3-hydroxylase; 5, Dehydroflavonol 4-reductase; 6, Anthocyanidin synthase; 7, Leucoanthocyanidin reductase; 8, Flavonol synthase; 9, Isoflavone synthase.

(with a 2*R*,3*R*-insaturation). Also, 2*S*-naringenin reduction by flavone synthetase (FS) originates flavones (C2, C3-insaturation). Alternatively, the stereospecific reduction of 2*S* naringenin, catalysed by the enzyme isoflavone synthetase (IFR), delivers the basis skeleton for the synthesis of isoflavones (**Figure 9**) (48,58).

1.2.1.2.2. Biodiversity and chemistry

As phenolic acids, also flavonoids are mainly found in Nature in their conjugated forms. Still, free forms are also often detected (48). Glycosylation is the foremost conjugation form, as it improves flavonoids water solubility and stability, enabling their storage on plants vacuoles (54,67). It can occur at oxygen (OH and COOH groups), carbon, nitrogen and sulfur atoms. The glycosidic moiety might differ regarding the number and sugar type, yet the monosaccharides glucose, rhamnose, xylose and arabinose are the most common (67). Disaccharides and oligosaccharides can also be found in association with flavonoids, being rutinose (6-*O*- α -L-rhamnosyl-D-glucose) and neohesperidose (2-*O*- α -L-rhamnosyl-D-glucose) the most common (67). Sugars are usually linked to aglycones on OH groups and/or directly to carbons groups (*O*-glycosides and *C*-glycosides, respectively) (54). Among these, *O*-glycosides are undoubtedly the most frequent (48). The substitution pattern is habitually the alternated hydroxylation at C5 and C7 of A ring and the hydroxylation at *para* (C4') in B ring; C3', C4'-dihydroxylation (catechol) and C3', C4', C5'-trihydroxylation at B ring are also frequent (48). Theoretically, *O*-glycosylation can occur at any of the available hydroxyl substituents, still it usually happens at the C7 hydroxyl group in flavones, flavanones and isoflavones, at the C3 and C5 hydroxyl groups in anthocyanins and at the C3 and C7 hydroxyl groups in flavonols and dihydroflavonols. *O*-Heterosides of flavonols (C3 and/or C7) and flavones (C7) are the most common in Nature (48,67). Regarding *C*-heterosides, glycosylation is usually found at C6 and C8 of the aglycone (48). While less frequent than glycosides, methylated flavonoids are also present in edible plants, *O*-methylation being again the more common (54). Methylation can occur at C6 and C8 (*C*-methylation) and on hydroxyls groups (C3', C4' or/and C5') of B ring (*O*-methylation) (48). The patterns of glycosylation, hydroxylation and methylation originate a wide variability of flavonoids within each subclass. The position, stereochemistry, type of substitutions and polymerization grade also contribute for the extensive structural diversity of flavonoids (48,58).

Analogously to other heterosides, also glycosylated flavonoids are preferentially soluble in aqueous solvents, alcoholic or hydroalcoholic mixtures. Still some glycosides as

rutinoside (quercetin-3-*O*-rutinoside) and hesperidin (hesperetin-7-*O*-rutinoside) have low water solubility. Aglycones are generally soluble in organic nonpolar solvents and, when displaying at least one free hydroxyl group, are also soluble in hydroxyl alkaline solution (48,58).

1.2.1.3. Tannins

1.2.1.3.1. Classification and biosynthesis

Tannins are water-soluble polyphenolic compounds with a molecular weight ranging from 500 to 30 000 Da. Specifically, these secondary metabolites have the particular ability to precipitate alkaloids, gelatin and other proteins (68).

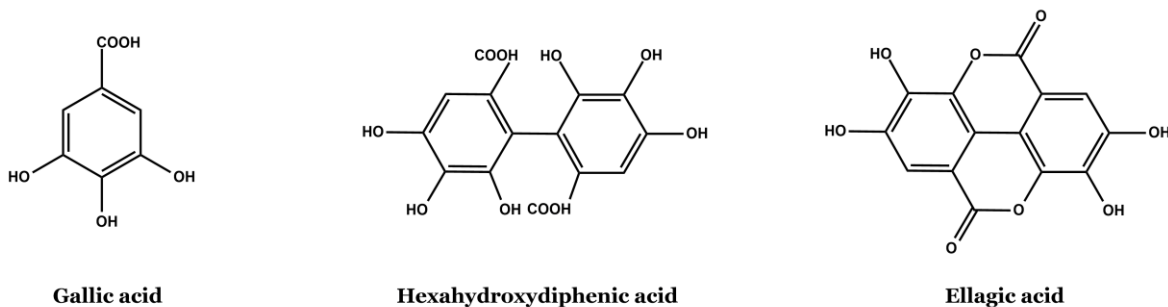
According to their resistance to hydrolysis, tannins are conventionally classified into two main groups: hydrolysable and non-hydrolysable, or condensed, tannins. The first are oligo-esters of a sugar (usually glucose) and a phenolic acid: gallic acid (gallotannins) or hexahydroxydiphenic acid (ellagitannins) (**Figure 10**). These compounds undergo through hydrolysis under acidic conditions (under heating), releasing, respectively, gallic acid and hexahydroxydiphenic acid (the later quickly lactonizes originating ellagic acid) (**Figure 10**). On the other hand, condensed tannins, also called proanthocyanidins, structurally are oligomers and polymers of flavan-3-ols, originating anthocyanidins under the same conditions (68) (**Figure 10**).

Hydrolysable tannins result from the shikimate pathway. Gallic acid, obtained from 3-dehydroshikimic acid dehydrogenation (**Figure 11**), is the biosynthetic precursor of both gallotannins and ellagitannins. This phenolic acid is initially esterified with a unit of glucose, originating 1-*O*-galloyl- β -D-glucose, the first key mediator on the biosynthesis of hydrolysable all tannins (**Figure 11**) (48,68). This molecule will be subsequently esterified with other units of gallic acid, originating 1,2,3,4,6-penta-*O*-galloyl- β -D-glucose. Thereafter, incorporation of galloyl moieties endures, yielding other hexa-, hepta-, octa-, etc.—galloyl glucose derivatives (gallotannins) (48,68). Alternatively, ellagitannins can also be formed by oxidative coupling of the C2-C2' of galloyl residues, originating hexahydroxydiphenoyl units (ellagitannins) (**Figure 11**) (48,68).

Condensed tannins, as flavan-3-ols derivatives, have a mixed biosynthetic origin, being formed both by the shikimic and the polyketide pathways. The monomeric catechins (flavan-3-ols) and leucoanthocyanidins (2,4-flavanodiols), resulting from dihydroflavonols

reduction (**Figure 9**), easily originate a carbocation at C4, that further reacts with the nucleophilic carbons at C6 or C8 of other flavon-3-ol. The repetition of this reaction leads to the formation of oligomers and polymers of flavan-3-ols (48,68).

PHENOLIC UNITS OF HYDROLYSABLE TANNINS



PHENOLIC UNITS OF CONDENSED TANNINS

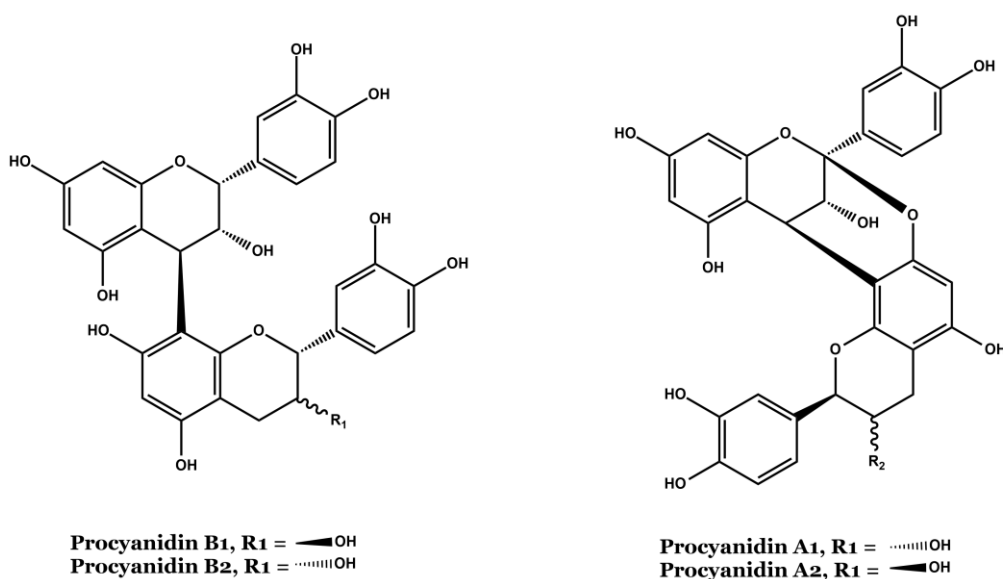


Figure 10. Structures of the phenolic units of hydrolysable tannins and of two types of condensed tannins (proanthocyanidins). [Adapted from (68)].

Condensed tannins are classified according to the number of flavonol moieties. Proanthocyanidins dimers, composed by two flavon-3-ols, are the simplest structures, followed by trimers and tetramers. Proanthocyanidins polymers can exhibit up to 50 units of flavan-3-ols (48). Condensation of the monomeric units results from interflavonoid links between the C4 of the superior subunit and the C8 of the inferior unit, or between the C4 of the superior subunit and the C6 of the inferior unit (less frequent). The dimers having a single interflavonoid link (C4-8 or C4-C6) are B-type proanthocyanidins, while those having

a double interflavonoid link (C4-8 and C2-O-C7) are A-type proanthocyanidins (48). Some examples are illustrated in **Figure 10**.

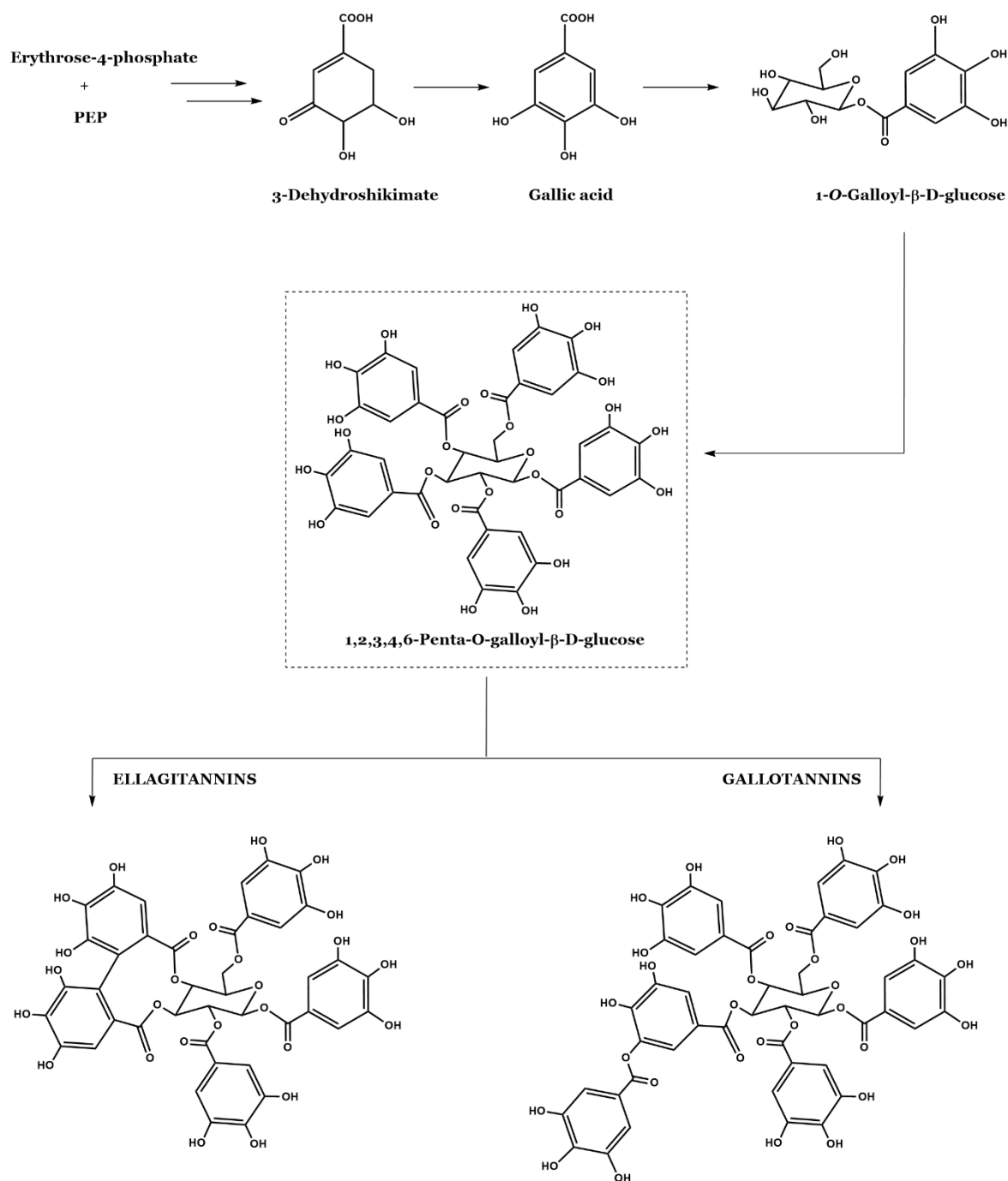


Figure 11. Schematic representation of the biosynthesis of hydrolysable tannins. [Adapted from (68)].

1.2.1.3.2. Biodiversity and chemistry

Tannins are water-soluble, their solubility being inversely related with the degree of polymerization. They are also soluble in alcohols and acetone and insoluble in ether, chloroform and ethyl acetate (48). They easily oxidize, principally in alkaline solutions, yielding yellow to brown solutions. Moreover, their stability in aqueous solutions depends on the type of tannin present, being regardless fairly low (48). Tannins precipitate aqueous solutions with aminated substances, such as proteins, alkaloids and gelatin, being this feature one classic characteristic of these compounds. Their high affinity for proteins is responsible for the astringency of some tannin-rich fruits, as persimmon (48). Therefore, the gelatin precipitation test is often used on the preliminary detection of tannins in vegetal samples.

Tannins chelate heavy metals, originating coloured complexes with ferric chloride: hydrolysable tannins originate blue complexes and condensed tannins originate green complexes (48). Besides, as above-mentioned, their behaviour under acidic conditions (under heating) also allows their selective differentiation: hydrolysed tannins break down, releasing ellagic acid and/or gallic acid (**Figure 10**), while condensed tannins originate anthocyanidins (48).

1.2.1.4. Extraction, purification and analysis of phenolics

Extracts containing phenolic compounds are usually prepared from dried or frozen plant materials, to guarantee that the target metabolites are not altered by enzymatic hydrolysis during the sample storage (69). Dried materials are most commonly used to prepare crude extracts, air-drying and freeze-drying being the most frequent drying procedures (70). Before extraction the dried plant material is usually milled and homogenized, to increase the contact surface as an attempt of enhancing the extraction yield (69). Even though several extraction technics are reported in the literature, solvent extraction is the most utilized because of its simplicity and efficiency (69,71,72). In this case extraction is affected by multiple factors, including the solubility of the compounds, the type of solvent, and the time and temperature of extraction (69). Despite solvents as methanol, ethanol, acetone, ethyl acetate, and their combinations with water being broadly used, there is not a universal extraction solvent, precisely because within the same sample the nature of the metabolites can vary tremendously, from simple phenolic acids to highly polymerized

tannins (72). Still, it is commonly accepted that polar solvents often lead to higher extraction yields of phenolics (72).

One of the principal drawbacks of solvent extraction relies on the coextraction of non-phenolic compounds, namely chlorophylls, peptides, proteins, sugars and organic acids (69). Thus, the obtained crude extracts are oftentimes fractionated by liquid-liquid partitioning and/or solid phase extraction (SPE). Liquid-liquid partitioning can be performed by simply extracting the crude extract with nonpolar solvents, as ether, hexane or chloroform to remove lipids (69). On the other hand, for SPE the extract is usually redissolved in water and preconditioned C18 columns are used. The column is washed with acidified water to remove sugars and water-soluble contaminants, while phenolic compounds remain attached to the stationary phase of the column by hydrophobic interactions and hydrogen bonds, being thereafter eluted with methanol or aqueous acetone (69,73). This technique can also be used on the fractionation of crude extracts, through the careful adjustment of the sample pH as a function of the polarity and pH of the eluents, to obtain several fractions with different “pools” of chemically related compounds (74).

Separation of compounds is usually achieved by chromatographic techniques, such as gas chromatography (GC), liquid chromatography (LC) or thin layer chromatography (TLC). Specifically concerning the separation of phenolics, reversed phase high-performance liquid chromatography (HPLC) is the most recurrent approach (69). HPLC systems can be further coupled to a wide range of detector systems (DAD, MS and UV/Vis), allowing the identification and quantification of the phenolics (69).

The presence of an aromatic ring, sometimes coupled to double conjugated systems, constitutes the main chromophore features of phenolic compounds, which have characteristic absorption spectrums in the UV-vis range (240-360 nm) (75,76). Thus, the UV detector is boardly used for the detection of this kind of metabolites. This detection technique is non-destructive and, consequently compatible with the use of other complementary detection methodologies, being also useful when isolation of compounds is further intended (75,77). Considering that each phenolic class has a characteristic UV spectrum, DAD detectors are widely used. Hence, the identification of phenolics is based on the mutual analysis of their retention time and spectral features (75,77).

Cinnamic acids absorb in two regions of the UV spectrum, having the first maximum at 225-235 nm, and other very close between 290-330 nm (78). The occurrence of two absorption bands at this region is related with the occurrence of *cis/trans* isomers (78). When cinnamic acids have a symmetric substitution pattern (*ca.* sinapic acid acid and *p*-

coumaric acid) it absorbs only in the second region of the spectrum (290-330 nm). On the other hand, benzoic acids absorb in a single region (235-325 nm) (78,79).

Flavonoids usually display two characteristic maximum absorption regions commonly known as band I (300-550 nm), related with the cinnamoyl group (rings B and C), and band II (240-285 nm), related with benzoyl group (ring A). The position and relative intensity of each of these peaks provide informative data, not only on the flavonoid subclass, but also on its substitution patterns. For example, on flavones and flavonols (devoid of substituents) band II is found between 250-280 nm, while band I appears at 310-350 nm and 350-385 nm, in flavones and flavonols respectively (80).

Increased oxygenation is recognized to lead to bathochromic shifts. Moreover, the presence of a second peak (sometimes an inflection) on band II of flavones and flavonols generally occurs due to an 3',4'-dihydroxyl system at B ring. On the other hand, methylation and glycosylation, particularly on the hydroxyl groups at C3, C5, C7 and C4' are known to cause hypsochromic shifts, especially in band II. When glycosylation occurs, the nature of the sugar has no further additional effect. Thus, the UV-vis spectra of flavonoids bearing the same aglycons are practically undistinguishable, the differentiation between di, tri and tetraglycosides being often made on the basis of retention time (for example, triglycosides have lower retention time than tetraglycosides) (80). In addition, the presence of an absorption maximum at 330 nm in a flavonoid may be due to the occurrence of cinnamic acids as acyl functions (80).

Even though identification based on UV/vis spectral data is extremely useful on the identification of many aglycones, it is usually insufficient to elucidate their derivatives, being in this case necessary to call on other detection systems as MS. Therefore, combination of HPLC separation with DAD and MS detection is often utilized on the characterization of the phenolic profile of plant extracts (76,81). MS allows the identification of compounds by producing specific ions (ionization) that are separated according to the mass (m)/charge (z) ratio and then detected (82). In fact, liquid chromatographic techniques, as HPLC, coupled to MS detection techniques are nowadays broadly utilized for the separation and identification of phenolic compounds. MS detectors enable the direct analysis of complex extracts, without purification, from small amounts of sample, being also highly sensible (82).

Conventional ionization techniques include electron impact and chemical ionization. However, these methods require the analyte to be vaporized, which in the case of polar, non-volatile and thermolabile phenolics implies a previous derivatization step (methylation, trimethylsilylation and acetylation) (82). "Soft" ionization techniques, as atmospheric

pressure ionization (API) allow the analysis of phenolics without a pre-derivatization, being particularly suitable for HPLC-MS systems. These ionization methods include electrospray ionization (ESI), atmospheric pressure chemical ionization (APCI), atmospheric pressure photo-ionization (APPI) and combinations of two types of sources. ESI is suitable for the analysis of compounds that are thermally unstable, with higher polarity and molecular weight, as phenolics (82). Hence, ESI, with good sensitivity for the structural analysis of heterosides, is one of the most used techniques for the elucidation of polyphenols. However, this soft ionization technique does not provide many fragments, which might hinder structural characterization. Still, the number of fragments can be enhanced by using a MS with a collision induced decomposition (CID), where the ion fragmentation is induced, originating different fragments of ions, useful for structural elucidation (82).

MS delivers information on the molecular weight, type of phenolic structure, the aglycone structure (hydroxylation profile, point of connection between rings B and C of flavonoids) and if there is any methylation, sulphuration or glycosylation. Regarding the glycosidic fraction, it allows to know the number of residues (mono, di, tri and tetrasaccharides) and type of sugars (hexoses, pentoses or deoxyhexoses) (83,84). Oftentimes, is also possible to obtain information on the stereochemistry of the terminal monosaccharide, the glycosidic sequence, the type of inter-glycosidic connections and also on the localization of the glycosidic fraction on the aglycone (83,84).

Phenolic compounds quantification is often performed by chromatographic hyphenated techniques, ideally through the comparison with a reference standard (85). However, based on absorption coefficients, standards structurally related with the analyte are often utilized for quantification purposes, when the demanded standard is not commercially available, or when the ratio cost/benefit does not justify (81). In addition, phenolics should be quantified at their maxima absorption, and therefore flavan-3-ol polymers are often quantified at 280 nm, hydroxycinnamic acids at 320 nm, flavonoids at 350 nm and anthocyanins at 520 nm (75).

1.2.1.5. Phenolics and the modulation of pathophysiological events underlying DM

The positive impact of phenolic compounds on human health has been extensively reported (86–89). The therapeutic potential of dietary polyphenols on diabetes management has also drawn the attention of the scientific community over past the years.

The observations obtained from the increasing number of *in vitro* studies and from animal experiments provided some clues on the general mode of action of these compounds (90–92). Overall, antidiabetic phenolics can act by multiple mechanisms, including protection of pancreatic islet β -cell, reduction of β -cell apoptosis, promotion of β -cell proliferation, attenuation of oxidative stress, activation of insulin signalling pathways, stimulation of insulin secretion and glucose uptake by peripheral tissues, inhibition of glucose absorption, and inhibition of AGEs formation (Figure 12). Besides, they can also attenuate diabetic complications through the direct modulation of AGEs formation, oxidative stress and inflammation (90–92).

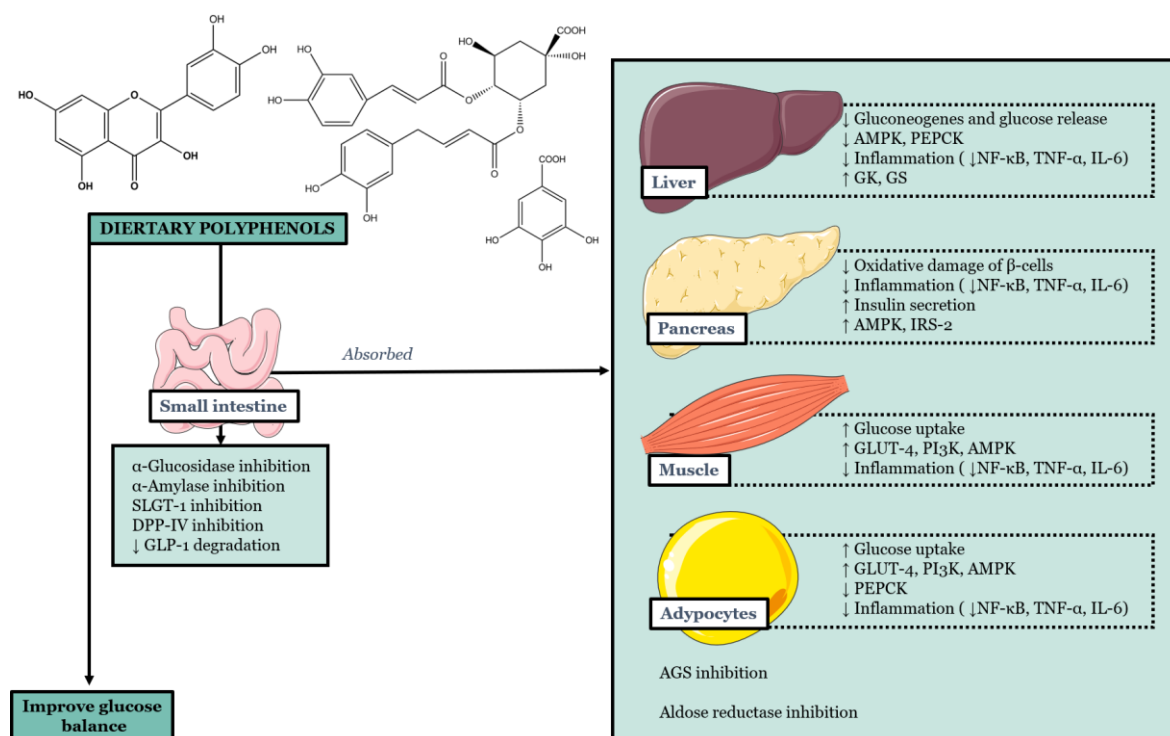


Figure 12. Schematic representation on the antidiabetic effects of polyphenols. AGEs, advanced glycation end-product; AMPK, adenosine monophosphate-activated protein kinase; DPP-IV, dipeptidyl peptidase-4; GK, glucokinase; GLP-1, glucagon-like peptide; GLUT-4, glucose transporter 4; GS, glycogen synthetase; IL-6, interleukin 6; IRS-2, insulin receptor substrate 2; NF- κ B, nuclear factor κ B; PEPCK, phosphoenolpyruvate carboxykinase; PI3K, phosphoinositide 3-kinase; SGLT-1, sodium-dependent glucose transporter; TNF- α , tumor necrosis factor α . [Adapted from (90–92)].

Dietary polyphenols might improve postprandial hyperglycaemia by reducing dietary carbohydrates absorption through the inhibition of carbohydrates digestive enzymes (α -amylase and α -glucosidase) and SGLT-1 transporters. The inhibition of these enzymes was observed with edible products as berries, legumes, vegetables, tea and beans, among others (93). Furthermore, evidence suggests that polyphenols might also inhibit DPP-IV in the small intestine, reducing GLP-1 degradation and consequently enhancing postprandial insulin secretion (Figure 12) (94). Likewise, phenolic compounds can also directly

stimulate the secretion of GLP-1 from L-cells, reinforcing the GLP1-insulin axis (94). Caffeoylquinic acids from sweet potatoes (95) and coffee (96) are examples of this.

Peripheral glucose uptake on insulin-sensitive tissues, as adipocyte tissue and muscle, may also be stimulated by phenolic compounds as result of GLUT-4 expression enhancement (90–92). Activation of the PI3K and AMPK signalling pathways appears to be the main underlying mechanism of black tea catechins (97) and other phenolics (92) (**Figure 12**).

Tea catechins, soybean isoflavones, grape polyphenols, and citrus flavonoids (naringenin and hesperidin) are also known to improve hepatic glucose metabolism (90,92). Suppression of glucose production, through the inhibition of glycogenolysis or gluconeogenesis, and stimulation of hepatic glycogen synthesis, through the activation of the glycogenesis pathway, are the principal reported mechanisms (90). Furthermore, some polyphenols inhibit the expression of phosphoenolpyruvate carboxykinase (PEPCK), a key enzyme involved on gluconeogenesis, and enhance the expression of glycogenesis enzymes as glucokinase (GK) and glycogen synthase (GS) (**Figure 12**) (90,92). Besides, reduction of hepatic lipid accumulation, through the stimulation of fatty acid β -oxidation, was also described, indirectly contributing for the amelioration of insulin resistance (92) (**Figure 12**).

Dietary polyphenols also appear to improve pancreatic β -cells function, mitigating chronic hyperglycaemia induced-cellular damage and endorsing insulin production and secretion (90,91). Oxidative stress and inflammation are pointed to be the principal boosters of β -cells dysfunction, and while the weight of each cause is not clearly understood yet, it is acknowledged that the overproduction of ROS and inflammatory mediators are involved in β -cells apoptosis (91). Besides, ROS disturb mitochondrial function, uncoupling ATP generation and consequently impairing insulin secretion (90). In fact, the mechanisms by which polyphenols preserve pancreatic β -cells survival might be related with the inhibition of NF- κ B signalling, inhibition of NO and ROS production and mitigation of cytokine-induced β -cell damage (**Figure 12**) (91). Moreover, these metabolites might also have direct insulinotropic effects, enhancing glucose-stimulated insulin secretion, by augmenting ATP production, GLUT-2 expression or AMPK activation (**Figure 12**)(91).

In parallel, some phenolic compounds, as well as phenolic-enriched extracts, appear to inhibit or regulate hyperactivated protein glycation pathways (52,91). As explained above, the formation and accumulation of AGEs alter proteins' conformation and promote oxidative stress and inflammation, strongly contributing for the progression of the disease and for the development of associated complications (**Figure 12**) (91). Therefore, glycation

inhibition can suppress inflammasome activation and reduce hyperglycaemia-induced inflammatory reactions and oxidative stress, slowing down the development of the disease. Relevantly, over the past years, several studies have demonstrated that polyphenols can suppress the glycation process by directly blocking RAGE and/or by delaying AGEs formation. (52). Also, as reviewed by Bouknana and colleagues, many phenolic compounds and phenolic-enriched extracts, have the capacity of blocking the polyol pathway through the inhibition of aldose reductase (**Figure 12**) (98) .

Most available data addressing the antidiabetic-like activity of polyphenols focus essentially on extracts obtained from vegetal materials, particularly from edible ones. It is worth to highlight soy (with high amounts of isoflavones) (99), tea (particularly rich in condensed tannins, catechins) (100), coffee (due to its phenolic acids content, mainly caffeic acid and chlorogenic acid) (101), grapes (essentially because of its resveratrol content) (102) and herbal spices (103). However, as already reviewed by others (26,51,104), the antidiabetic effects of isolated compounds, namely flavonoids and phenolic acids, have been also deeply investigated. Whilst data from clinical studies are still scarce, plenty of information on *in vitro* and *in vivo* studies is available (26,51,104). Most of the *in vitro* studies involve enzymatic inhibition assays against diabetes typical targets (α -glucosidase, α -amylase, aldose reductase, DPP-4) and cellular assays using cell lines of organ specific targets of the disease, as 3T3-L1 preadipocytes, L6 myotubes, HepG2 hepatic cells, RAW 264.7 macrophages and the pancreatic cells RIN-5F and INS-1 (26,51,104). On the other hand, most of the animal studies were performed with diabetic rats or mice, the disease being chemically and/or dietetically-induced. In this regard, alloxan and streptozotocin were the main diabetes chemical inducers, while high-fat and high-glucose diet constituted the principal dietetic inducers (26,51,104).

Considering all the above-stated bioactivities reported not only for isolated phenolic compounds but also for phenolic-rich extracts, a reasonable question ought to be made. Is it better to work with plant extracts or with isolated bioactive compounds? The truth is, there is no right or wrong answer to this paradigmatic question, as it all depends on the objectives of the investigation and on its applications. Pharmaceutical companies and industries, attempting to attain the utopian magic bullet, usually work with bioassayed-guided fractionation and isolation, to obtain bioactive lead compounds that may be structurally modified. However, this process is extremely time-consuming, expensive, and often unsuccessful. Alternatively, working with plant extracts may be considered an appealing task, as generally herbal medicines are preferred by patients, either as primary treatment or as adjunctive, mostly due to their affordability and to the ancestral claims on their effectiveness (105). Moreover, and notwithstanding the reported antidiabetic effects

of bioactive phenolics (26,51,104), evidence shows that crude extracts often display greater activity than the isolated bioactive phytochemicals (106–108). This might occur due to synergic and/or additive pharmacodynamic interactions between the components of crude extracts that cannot occur when the presumed bioactive constituent is assessed individually. Moreover, the constituents occurring at crude extracts might also interact in a synergic pharmacokinetic way, enhancing the bioavailability of bioactive components (105,109). In fact, traditional healers empirically know that specific combinations of medicinal plants are more effective on the treatment of certain illnesses, therefore taking advantage of the cumulative and/or synergic interactions of phytochemicals (110). Particularly concerning diabetes multifactorial physiopathology, and the diverse range of known pharmacological targets, potentiation and additive effects leading to multimodal activities could be extremely useful for the management of the disease (111). In fact, this has provided the rationale of the current work, justifying the fact of polyphenolic extracts being selected as the object of study, rather than isolated compounds.

1.3. The role of Thai flora on the bioprospection of antidiabetic plants

The peculiar phytogeographical characteristics of Thailand strongly contributes to its impressive biodiversity, mostly due to the genetic isolation of some populations and their speciation. So far, over 10 000 plant species have been described, 2 187 of them being used for their medicinal properties based in more than 16 700 ethnomedicinal use records (112).

In Thailand, the primary health care system includes 74 herbal medicinal products to treat a variety of diseases and associated symptomatology (113). Despite the recent revitalization of Thai Traditional Medicine (TTM) in modern healthcare, particularly in rural areas, practitioners recommending the use of medicinal plants are mainly traditional (or folk) healers (114). Specifically concerning diabetes, traditional healers perform their clinical assessment through the evaluation of physical symptoms, such as internal body heat, increased urine volume, weight loss and body weakness. Also, detection of glycosuria is oftentimes performed through the “ants hill test”. Briefly, patients are asked to urinate beside an ant hill, and if ants gathered around the urinated area, one is detected positive for diabetes (115). In fact, several Thai ethnic groups still rely on medicinal plants in their primary healthcare needs, not only due to economic and cultural considerations, but also due to an abundant floral biodiversity further contributing to an easy access. Furthermore, despite the remarkable progress on Health primary care, many rural communities still have a limited access to medical resources. While sharing some common medicinal practices with

neighbouring countries, specific cultural forces led to the development of a unique Traditional Medicine system in Thailand, encompassing a long tradition of empirical clinical practice (116). The revitalization of TTM has been supported by the Thai government, with many provincial Ministries of Public Health having active departments dedicated to the cataloguing of herbal drugs (116). Therefore, as an attempt to revitalize TTM at a similar extent as the one observed with Traditional Chinese Medicine, the use of herbal remedies has been increasingly documented in recent years. The traditional Thai/Lanna Medicinal Plants/Recipe Database “MANOSROI II” contains an impressive number of 50 000 traditional recipes, 7 467 medicinal plants being described to treat 3 613 diseases/symptoms (115). Just to mention a few, polyherbal preparations used in diabetes treatment include the Mor Porn’s recipe (with 14 medicinal plants) and the Ya-Rak-Sa-Bao-Wan (composed of 11 species) (117). While the antidiabetic activity of some of these Thai folk remedies has been already investigated and validated, as reviewed by Andrade et al., many medicinal plants used by local healers on diabetes management still lack sustained evidence on their claimed antidiabetic properties (ca. 30%) (117).

Relevantly, and even though ethnomedicinal studies have not been carried out in all Thai villages yet, the proportion of medicinal plants used in TTM (22%, relatively to the number of plants described in Thailand) overcomes by far the world average (8%) (112). The selection of medicinal plants by local healers is often based on criteria including tradition, efficacy, abundance, accessibility, and taxonomic affiliation (112,118). Based on this, it is evident that the medicinal importance of different plant families is not entirely overlapping in distinct world regions (118).

Phumthum et al. reviewed the available ethnobotanical knowledge on medicinal plants in Thailand and estimated that among the diverse Thai flora, 2 187 species, belonging to 206 families, were or still are utilized in TTM (112). Moreover, based on the number of use reports and on the number of interviewed informants, the medicinal value of each family, ranging 0.008-11 (1 report of use-1420 reports of use), was estimated by the authors (112). Fabaceae, Asteraceae, Euphorbiaceae, Lamiaceae, Zingiberaceae, Rubiaceae, Acanthaceae, and Apocynaceae were the families ranked with higher medicinal value (112). This systematic survey was the basis for the selection of the plant materials investigated in the current dissertation, as follows.

A screening of the antidiabetic capacity of a panel of plant materials obtained in Thailand was performed. A total of 20 materials from 12 plant species were collected (**Table 2**). The species’ medicinal value was taken as a starting point to select some poorly investigated species. Only species belonging to families with a recorded medicinal value higher than 0.3 were included. Moreover, all the selected species, excluding *Ficus curtipes*

Table 2. Plant species found in Thailand that were prioritized for screening according to their medicinal value (score). The scores presented were reported by Phumthum et al. (112) and represent the medicinal value of each species and each family.

Family/ Species	Score	Thai ethnomedicinal utilization	References
Acanthaceae	4.603		
<i>Justicia gendarussa</i> Burm.f.	0.149	Viral infections	(119)
Arecaceae	0.818		
<i>Caryota urens</i> L.	0.008	Liver disease, heart symptoms	(112)
Capparaceae	0.959		
<i>Crateva adansonii</i> DC.	0.099	Broken bones, spastic paralysis	(120,121)
Moraceae	2.289		
<i>Ficus curtipes</i> Corner	-	Not reported	
Ebenaceae	0.752		
<i>Diospyros decandra</i> Lour.	0.025	Fever, hypertension	(122,123)
Hypericaceae	0.380		
<i>Cratoxylum formosum</i> subsp. <i>pruniflorum</i> (Kurz) Gogelein	0.298	Stomach ache, mouth ulcers, urinary tract infections, laxative, skin disease, healing wounds and bruises	(124)
Leguminosae	11.736		
<i>Sindora siamensis</i> Miq.	0.066	Skin disease, healing wounds, haemorrhoids, fever, appetizer	(125)
<i>Azelia xylocarpa</i> (Kurz) Craib	0.099	Skin disease, healing wounds, body aching, bruises, laxative and snake bites	(120,125)
Lecythidaceae	0.388		
<i>Careya arborea</i> Roxb.	0.207	Healing wounds, cough and for recover after childbirth	(120,126)
<i>Gustavia gracillima</i> Miers	-	Not reported	
Meliaceae	0.711	Coryza, headache, fever, skin diseases and vomiting	
<i>Chukrasia tabularis</i> A.Juss.	0.025	Astringent and antipyretic	(124)
Rubiaceae	5.025		
<i>Hymenodictyon orixense</i> (Roxb.) Mabb.	0.331	Haemorrhoids	(124)

Corner and *Gustavia gracilima* Miers, had evidenced of being utilized in TTM, the estimated medicinal value of each species being presented at **Table 2** (112). Worth referring that *Ficus* species reported to have a high medicinal value were not available for collection, and therefore throughout a chemotaxonomic criterion, the species *F. curtipes* was also included in the initial panel of plants. On the other hand, materials of *G. gracillima* were collected due to its wide abundance all over Thai territory and also due to the lack of records on its biologic potential and chemical profile.

1.3.1. Selected species

1.3.1.1. *Caryota urens* L.

Caryota urens L., also known as kitul, is a palm tree native to tropical Asia rain forests, being widely found in Thailand, Myanmar, India, Sri Lanka, Malaysia and Nepal (127–129). Within the palm family (Areaceae), the genus *Caryota*, with 13 plant species, is the only being characterized by bipinnate leaf. The term “Caryota” comes from the Greek word, *karyotes*, which means “nutlike”, as reference to the characteristic small-size fruits of those palms. On the other hand, the denomination “urens” reassembles to the word “burning”, due to the presence of irritating needle-like crystals on the outer shell of this palm tree fruits (**Figure 13**) (128).



Figure 13. *Caryota urens* tree (A) and its inflorescences (B) and fruits (C). Photographs by Dr. Nelson Gomes.

The palm tree, also known as fishtail, toddy, jaggery (130) or wine palm (131), can grow up to 20 m tall and is topped by a rosette of large drooping leaves, that can reach 6 meters

long (130). Flowering begins after 10-15 years old and endures for 5 years or more. The inflorescences (3 metres long) emerge at each leaf node producing pendant clusters of white, unisexual flowers, and once the last fruit on the bottom inflorescence matures, the plant dies (128,130).

In famine times, the sago extracted from the inflorescences is used by local natives as starch source in Bangladesh (132). Also, the inflorescences sap is often fermented into an alcoholic drink (palm wine or toddy) or boiled down to make syrup or sugar (jaggery) (128,130). The stem apex is also edible and can be eaten raw or cooked (130). Despite of the presence of irritant calcium oxalate crystals on the outer shell of the fishtail palm fruits (133), shellless fruits are eaten raw in Bangladesh (132).

Apart from its ornamental and alimentary features, kitul has been widely utilized for medicinal proposes by native Asian tribes, mostly in India and Sri Lanka (128,133). The decoction of the root is used by nursing mothers as galactagogue (134) and the juice made from the inflorescences is used on asthma management and as a laxative (133). Also, the toddy prepared from the sap is reported to heal urinary problems and the ashes obtained from burned old leaves are used on tympanites (inflammation of middle ear) (132). The roots are used for tooth ailments (128) and the flowers are reported to heal gastric ulcer, migraine headaches, snake bite poisoning and rheumatic swellings (133). Besides, in Thailand *C. urens* is particulary used in tradicional practices to treat liver diseases and to alleviate heart symptoms (112).

In addition to its medicinal value, kitul is widely utilized in Asian food industries, and therefore was included on the list of the most important Non-Wood Forest Products (NWFP) in several Asian countries (135). Commercialized kitul food products include flour, treacle, jaggery, toddy and vinegar (136). While the treacle and jaggery obtained from kitul sap are extracted from the inflorescences of the plant (136), the flour is obtained from the internal pith of the fishtail palm, being widely use on the production of foodstuffs like noodles, sauces, dry mixes, flakes, snacks and baby foods (137). Beyond of the above-mentioned health effects, genuine kitul products are reported to be suitable for diabetic patients. In fact, Senavirathna et al. demonstrated that roti and porridge made with flour obtained from *C. urens* have a low and middle glycaemic index, respectively, when comparing with other mainstream flours (138). Additionally, kitul pith was reported to have amylase inhibitors and, consequently, low *in vitro* starch digestibility (136). However, details on the species antidiabetic mechanism remain to be investigated.

Unexpectedly, despite of its broad utilization, systematic studies on the biologic properties of kitul are limited. The leaves and fruits have antimicrobial activity (139) and

also exhibit significant antioxidant properties, mostly due to the presence of phenolic compounds (131,140,141). Besides, anti-inflammatory effects on lipopolysaccharide (LPS)-stimulated macrophages were also noted with a leaf hydroalcoholic extract and with the two previously detected phenolics, rutin and umbelliferone (142). Worth to mention that on this study the crude extract was considerably more active than the isolated compounds, suggesting that synergic effects contributed for the observed outcomes (142). Relevantly, Sujitha and colleagues found a positive association between rutin content and the antioxidant activity of the leaves (131). This flavonoid was also detected on the fruits of the plant (133). In addition, other phenolic constituents have been identified on the species. LC-ESI- quadrupole time-of-flight (QTOF)/MS characterization of a hydroalcoholic extract obtained from ripened fruits allowed the identification of 51 phenolics, flavonoids and phenolic acids being identified as predominant; quercetin-3-*O*-glucoside followed by quercetin and 5-*O*-caffeoylquinic acid were the most abundant phenolic components on the extract (129). In agreement, Ma and colleagues observed that phenolic acids and flavonoids were the main metabolites of a hydroalcoholic extract obtained from the leaves, being also detected in the fruits (143). Also, flavonol-*O*-sophorosides, namely quercetin-*O*-sophoroside, kaempferol-*O*-hexosylpentoside and kaempferol-*O*-sophoroside, were detected on the leaves (143). Though authors claimed that these flavonoids could serve as chemotaxonomic markers of the species (143), this theory still lacks phylogenetic confirmation.

Considering the widespread use of kitul as a traditional food in Asian countries, its economic impact, medicinal utilization on traditional practices and also the lack of evidence on its antidiabetic effects, the fruits and the inflorescences of the palm tree were selected and investigated in detail.

1.3.1.2. *Ficus curtipes* Corner

F. curtipes (synonym: *Ficus obtusifolia* Roxb.) is a large free standing fig tree, belonging to the large and economically relevant *Ficus* genus (144). This monoecious tree is epiphytic when young, but after developing can reach up to 5-10 m tall (**Figure 14**) (145).

The tree produces figs throughout the year and typically develop as well-synchronized crops, with individual trees producing syconia (preceding figs) at different times of the year (145). The mature figs are usually dark red to purplish red and measure 15.52 ± 0.75 mm in diameter (144). This species is widely distributed through tropical forests, namely in China,

India, Malaysia and Thailand (146). In Southeast Asia it is also cultivated in cities and villages as an ornamental tree (147).

Even though no reports are recorded on the use of *F. curtipes* in TTM, in Mexico, the decoction of the plant fresh latex is orally given to heal toothache and headache (148).

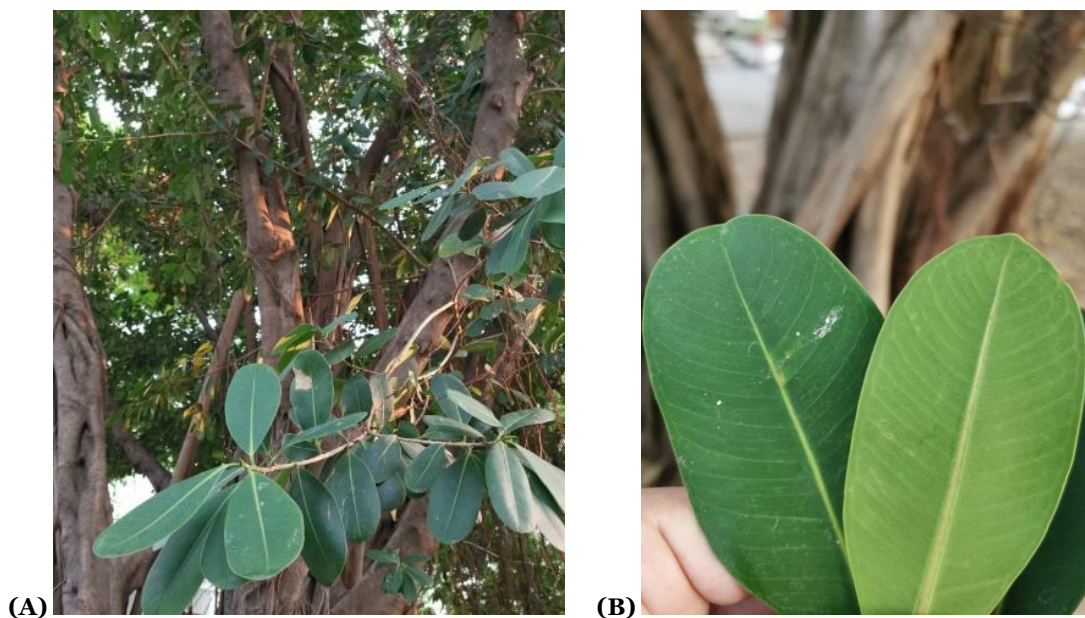


Figure 14. *Ficus curtipes* tree (A) and the collected leaves (B). Photographs by Dr. Nelson Gomes.

With a global distribution of approximately 800 species, the therapeutic and economic value of *Ficus* genus has been gaining increased attention. Scientific reports support its therapeutic potential, with several biologically active compounds being also reported (148). However, unlike other valued *Ficus* species, *F. curtipes* remains to be investigated, particularly concerning the potential pharmacological effects and chemical composition. Hence, notwithstanding the absence of records on *F. curtipes* utilization in TTM, the leaves and the stem bark of this tree were investigated.

1.3.1.3. *Gustavia gracillima* Miers

G. gracillima (synonym: *Japarandiba gracillima* (Miers) Nied.) is a small slender tree with leaf-bearing branches of 5-7 mm in diameter and with pink actinomorphic flowers (10 cm in diameter) (**Figure 15**) (149). Despite of recently being included in the Red List of Threatened Species (RLTS) in Colombia (150), this plant is widely found in Thailand, being one of the species that attracts more pollinator individuals per flower (151).

As far as we are aware, there are no available records on *G. gracillima* ethnomedicinal utilization. However, the widespread distribution of this plant through all Thai territory, along with the lack of information on its biologic potential and chemical composition constituted a criterion of inclusion of *G. gracillima* in the current dissertation. Still, worth mentioning that on a screening of ethanol extracts prepared from 44 Thai plants, *G. gracillima* featured as the most active on α -amylase inhibition, originating a 44% decrease of the enzyme activity at 100 $\mu\text{g}/\text{mL}$ (152).

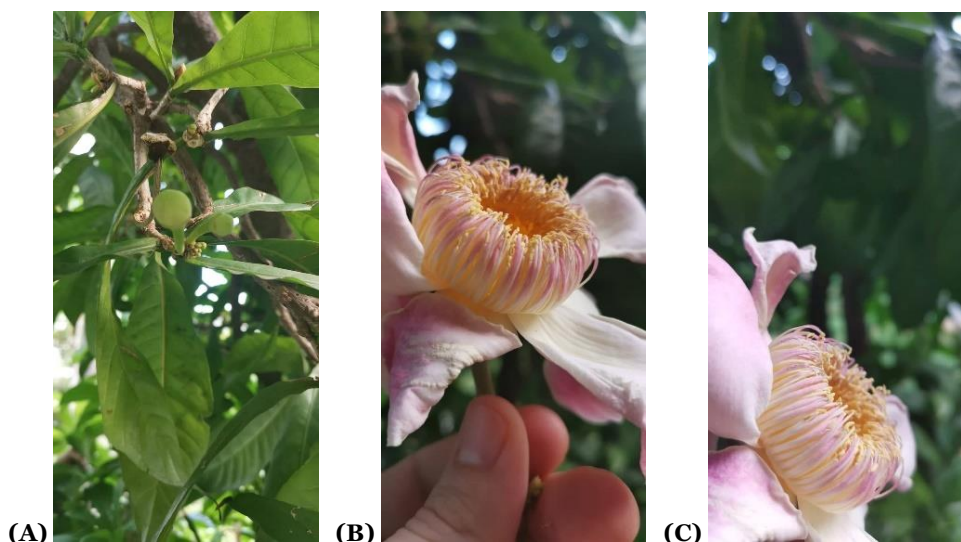


Figure 15. *Gustavia gracillima* tree (A) and flowers (B and C). Photographs by Dr. Nelson Gomes.

Hence, taking into consideration this pilot study on the antidiabetic potential of the species, and also bearing in mind its wide distribution and reasonable easy access through Thai communities, the flowers of *G. gracillima* were also included in the panel of plant materials to be screened.

1.3.1.4. *Chukrasia tabularis* A. Juss.

Chukrasia tabularis A. Juss is a tree species broadly distributed through South and South East Asia, being commonly found in India, Nepal, Cambodia, Thailand, Laos, Myanmar, Bangladesh, Sri Lanka, and Malaysia. The plant can also be encountered in Cameroon, Costa Rica, Nigeria, Puerto Rico, South Africa and United States of America (153). Considering its widespread distribution, the plant has several vernacular names, as hittagong wood, Burmese almondwood, white cedar, bastard wood, Red Indian wood (Eng.), repoh, sutnag puteh (Malay), yinma (Burmese), siat-ka, yom-hin (Thai), Hulan hik, hiri kita, and kaloti (Sri Lanka) (153).

The tree can grow up until 40 m tall, is branchless until 25 – 28 m and has a large convex buttresses at the top (**Figure 16**) (153). The green paripinnate leaves are about 30 - 50 cm long, have dentate margins and usually a smooth surface (**Figure 16**). When the tree is young, its bark is usually smooth, but gets rusty brown with deep vertical fissures with age. The species has red coloured leaflets at the top, being this feature the principal morphological identifier of the plant (153). Notwithstanding its widespread distribution in the Asian territory, *C. tabularis* has been recently included on the RLTS of the International Union for Conservation of Nature (IUCN), mostly due to its overexploitation by wood industry (26).

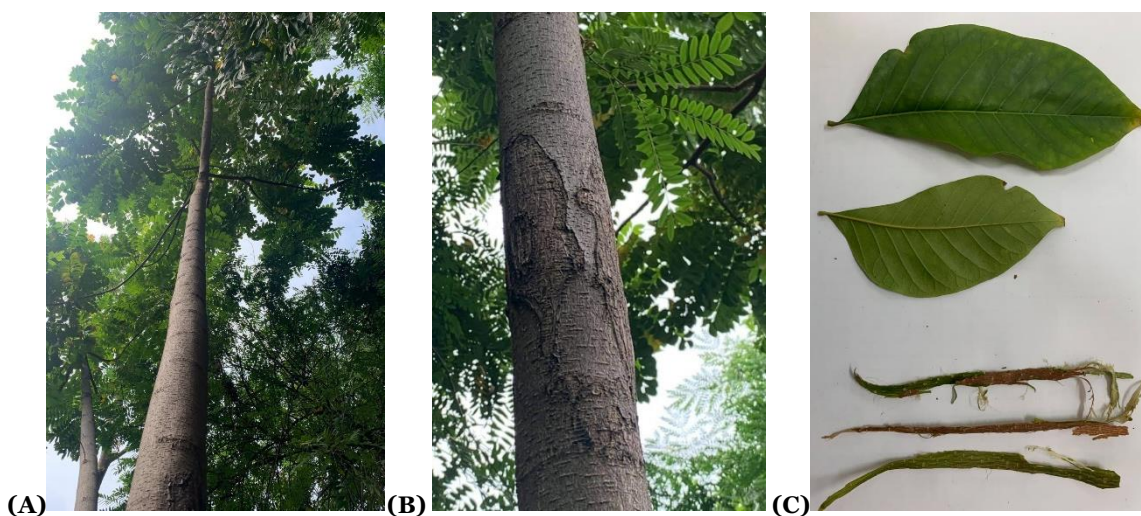


Figure 16. *Chukrasia tabularis* tree (A) and the collected leaves (B, C) and stem bark (B). Photographs by Dr. Nelson Gomes.

In TTM *C. tabularis* has been used for its astringent and antipyretic properties, being also utilized as an antidiarrheal and anti-influenza agent in China and India (154,155). The leaves display antifungal and antibacterial activities (156), and appear to have also anti-inflammatory effects (157). In addition, antiradical effects have also been experimented with different phenolic-rich fractions obtained from the leaves (158–160).

Previous studies evidenced that *C. tabularis* is particularly rich in limonoids (155,161–164). This particular class of tetranortriterpenes (155,161–164) has been mainly detected on the wood and on the bark of the plant, with many showing relevant biological/pharmacological properties. For example, the phragmalin-type limonoids tabularisin S and T, obtained from the stems, displayed significant inhibitory activity against yeast α -glucosidase (161). Structurally related phragmalin-type limonoids were found to inhibit NF- κ B activation (162) and to reduce NO levels in LPS-stimulated RAW 264.7 macrophages (165). Indeed, most studies on *C. tabularis* deal with the structural

diversity and biological properties of terpenes (155,161–164). However, while tabularin (166), gallic acid, catechin, epicatechin, quercetin and 3-*O*-glycosylated derivatives, tannic acid, and 7-hydroxycoumarin (153,160) have been detected on the leaves, phenolic composition of the species remains poorly investigated.

Hereupon, taking into consideration *C. tabularis* medicinal value (0.025, **Table 2**) and also aiming the valorisation of the waste, resulting from the wood industry, the leaves were selected for screening.

1.4. Objectives

The main objectives of the current thesis are the following:

- 1.** Screening of plant materials from species from Thai flora based on their antidiabetic-like, antioxidant and anti-inflammatory properties;
- 2.** Characterization of the phenolic constituents present at the most active extracts;
- 3.** Elucidation of the biologic effects of the most active extracts by detailing the *in vitro* anti-diabetic and anti-inflammatory-like activity;
- 4.** Evaluation of the antioxidant properties of the most active extracts;
- 5.** Investigation of the relationships between the observed bioactivities and phenolic compounds quantities.

CHAPTER II
EXPERIMENTAL SECTION

2. Experimental section

2.1. General chemicals and standards

3-, 4- and 5-*O*-caffeoylquinic acids and 4-*O*-caffeoylshikimic acid were obtained from Biopurify Phytochemicals Ltd. (Chengdu, China). Epicatechin, catechin, vitexin, isovitexin, isorhamnetin-3-*O*-glucoside, kaempferol-3-*O*-glucoside, luteolin-7-*O*-glucoside, quercetin-3-*O*-rhamnoside, ellagic acid, kaempferol-3-*O*-rutinoside, kaempferol-3-*O*-glucoside and kaempferol-3-*O*-rutinoside-7-*O*-rhamnoside were purchased from Extrasynthese S.A. (Genay, France) and vicenin-2 was from HWI Analytik GMBH (Rülzheim, Germany).

The water was treated in a Milli-Q purification system (Millipore, Bedford, US).

Formic acid was acquired from Labkem (Barcelona, Spain). *N*-(1-Naphthyl)ethylenediamine dihydrochloride, H₃PO₄, methanol and acetonitrile were obtained from Merck (Darmstadt, Germany).

α -Glucosidase (from *Saccharomyces cerevisiae*), *p*-nitrophenyl- α -glucopyranoside (*p*-NPG), KH₂PO₄, 5-lipoxygenase from *Glycine max* (Type V; 5-LOX), linoleic acid, ethanol, Na₂HPO₄·2H₂O, 2,2-diphenyl-1-picrylhydrazyl radical (DPPH·), α -amylase (from porcine pancreas), 3,5-dinitrosalicylic acid (DNSA), NaOH, potassium sodium tartrate tetrahydrate, starch, Na₃PO₄, NaCl, (NH₄)₂SO₄, β -mercaptoethanol, DL-glyceraldehyde, porcine pancreatic lipase, *p*-nitrophenyl butyrate (*p*-NPB), CaCl₂, tris-HCl, dimethyl sulfoxide (DMSO), sodium nitroprusside dihydrate (SNP), sulfanilamide, β -nicotinamide adenine dinucleotide reduced form (NADH), nitroblue tetrazolium chloride (NBT), phenazine methosulfate (PMS), FeSO₄·7H₂O, ascorbic acid, ether, bovine serum albumin (BSA), glucose, fructose, methylglyoxal, NaN₃, L-arginine monohydrochloride, diacetyl monoxime, antipyrine E, H₂SO₄, L-glutamic acid monosodium salt monohydrate, 3-(4,5-dimethylthiazolyl-2)-2,5-diphenyltetrazolium bromide (MTT), LPS from *Escherichia coli*, trypan blue, 2',7'-dichlorofluorescein diacetate (DCFH-DA), propano-2-ol, and protease inhibitor cocktail were purchased from Sigma-Aldrich (St. Louis, US). Standards used as positive controls, namely acarbose, quercetin, rutin hydrate, orlistat, 3,5-di-*tert*-4-butylhydroxytoluene (BHT), aminoguanidine hydrochloride, *N*-nitro-L-arginine methyl ester hydrochloride (L-NAME) and *N*-acetylcysteine (NAC) were acquired from Sigma-Aldrich (St. Louis, US).

Dulbecco's Modified Eagle Medium (DMEM), Roswell Park Memorial Institute (RPMI) medium, penicillin-streptomycin solution (penicillin 5000 units/mL and streptomycin 5000 mg/mL) and foetal bovine serum (FBS) were acquired from GIBCO, Invitrogen™

(Grand Island, NY, US). NADPH and human aldose reductase were obtained from Pozomix (Haltwhistle, UK). Mouse IL-6 ELISA MAXTM Deluxe and Mouse TNF- α ELISA MAXTM Deluxe kits were purchased from BioLegend Inc. (San Diego, CA, US). RAW 264.7 macrophages, intestinal Caco-2 cells, and pancreatic RIN-5F cells were obtained from the American Type Culture Collection (ATCC) (LGC Standards S.L.U., Spain).

2.2. Sample collection

All the plant materials prioritized for screening, excluding *C. formosum* (TH12 and TH13), *C. arborea* (TH16 and TH17), *J. gendarussa* (TH18) and *H. orixense* (TH20), were collected in January 2015 at Kasetart University Campus (Bangkok, Thailand). The leaves of *J. gendarussa* (TH18) were collected at the Kho Hin Son Herb Garden in Bangkok (Thailand), while the remaining plant materials (TH12, TH13, TH16, TH17 and TH20) were collected in Wang Man, Chai Nat province (Thailand). Once the initial amounts of the extracts prepared from the inflorescences of *C. urens* and from the flowers of *G. gracillima* were not sufficient to perform all the intended assays, second samples of these plant materials were later obtained (in April 2019) from the same trees as before and new fresh extracts were prepared (TH20 and TH21, **Table 3**). Taxonomic identification of the plants was carried out by Dr. Srunya Vajrodaya (Faculty of Science, Kasetart University). The voucher specimens (**Table 3**) were deposited at the Phyto-Chemodiversity and Ecology Research Unit of Faculty of Science (Kasetart University).

2.3. Extraction

After being collected, plant materials were milled to fine powder (particle size $\leq 910 \mu\text{m}$). The powdered materials (**Table 3**) were macerated in 1 L of methanol for 7 days. After this period, the resulting methanol extracts, were filtered through a Büchner funnel and dried under reduced pressure in a Rotavapor[®] R-210 (Büchi, Mumbai, India). Thereafter, the dried extracts (**Table 3**) were sent to the Laboratory of Pharmacognosy of the Faculty of Pharmacy (University of Oporto) and stored at room temperature, in the dark, until analysis. The extracts prepared from samples collected in January 2015 arrived to Faculty of Pharmacy (University of Oporto) in January 2018 and the ones posteriorly prepared (April 2019) arrived at June 2019.

Table 3. Characterization of the panel of plant materials prioritized for screening.

ID	Plant species	Voucher specimens	Plant material	Vegetal powder (g)	Dry extract (g)
Collected in January 2015					
TH01	<i>C. urens</i>	PCERU_CU10005	Inflorescences	19.20	1.64
TH02		PCERU_CU20005	Fruits	50.20	11.20
TH03	<i>C. adansonii</i>	PCERU_CA0003	Leaves	42.2	3.20
TH04		PCERU_CA0004	Stem bark	30.4	1.10
TH05	<i>F. curtipes</i>	PCERU_FC0005	Leaves	51.10	4.80
TH06		PCERU_FC0006	Stem bark	71.80	4.00
TH07	<i>C. tabularis</i>	PCERU_CT0007	Leaves	39.10	2.30
TH08	<i>D. decandra</i>	PCERU_DD0008	Leaves	22.6	1.80
TH09		PCERU_DD0009	Stem bark	37.1	1.80
TH10	<i>S. siamensi</i>	PCERU_SS00010	Leaves	31.8	2.90
TH11		PCERU_SS00011	Stem bark	57.1	3.60
TH12	<i>C. formosum</i>	PCERU_CF00012	Leaves	121.9	4.80
TH13		PCERU_CF00013	Stem bark	308.4	5.60
TH14	<i>A. xylocarpa</i>	PCERU_AX00014	Leaves	18.2	1.40
TH15		PCERU_AX00015	Stem bark	22.9	0.80
TH16	<i>C. arborea</i>	PCERU_CA00016	Leaves	211.3	6.00
TH17		PCERU_CA00017	Wood	393.5	5.00
TH18	<i>J. gendarussa</i>	PCERU_JG00018	Leaves	12.6	2.44
TH19	<i>G. gracillima</i>	PCERU-GG00019	Flowers	15.70	0.99
TH20	<i>H. orixense</i>	PCERU_HO00020	Stem bark	102.6	8.00
Collected in April 2019					
TH21	<i>C. urens</i>	PCERU_CU00021	Inflorescences	50.0	3.93
TH22	<i>G. gracillima</i>	PCERU-GG00022	Fruits	50.0	2.46

2.4. Preliminary screening of biological activities of plant species from Thailand

In order to select the most active plant materials, 20 methanol extracts were screened on their antidiabetic-like, anti-inflammatory-like and antiradical activities. For this purpose, extracts were investigated on the ability to inhibit the activity of α -glucosidase and 5-LOX, and to scavenge the synthetic DPPH \cdot , as described below. The maximum concentration tested was 1000 $\mu\text{g/mL}$ of dry extract.

2.4.1. α -Glucosidase inhibition

The inhibitory effects on α -glucosidase (*Saccharomyces cerevisiae*) activity were assessed by following *p*-nitrophenol release, according to a procedure described before (167). This assay is based on the ability of α -glucosidase to selectively cleave the α -(1-4) bonds of the *p*-NGP, releasing α -D-glucose and *p*-nitrophenol (yellow colour), which can be estimated spectrophotometrically at 450 nm (**Figure 17**).

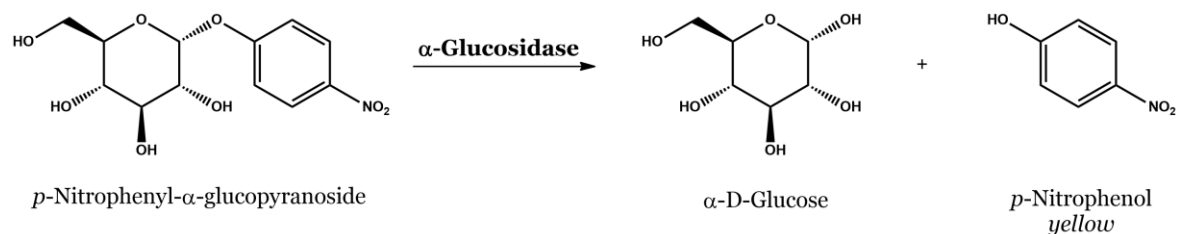


Figure 17. *p*-Nitrophenyl- α -glucopyranoside cleavage by α -glucosidase into α -D-glucose and *p*-nitrophenol.

Different concentrations of the extracts (50 μL) were pre-incubated (2 min, at 37 $^{\circ}\text{C}$) with 180 μL of potassium phosphate buffer (KH_2PO_4 , 100 mM, pH 7.0) and 20 μL of yeast α -glucosidase (0.35 U/mL). The reaction was initiated by the addition of 100 μL *p*-NGP (2.5 mM), and the *p*-nitrophenol formation was followed every 20 s, along 10 min, at 405 nm, in a Multiskan GO plate reader (Thermo Fisher Scientific; Waltham, MA, US). All reagents and samples were prepared in potassium phosphate buffer (KH_2PO_4 , 100 mM, pH 7.0). The maximum non-interfering DMSO concentration (5 %, v/v) was used to facilitate the solubilization of buffer insoluble extracts. α -Glucosidase inhibition was determined according to the following equation: α -Glucosidase inhibitory activity (%) = $[1 - (\text{V of sample} / \text{V of negative control})] \times 100$, where V corresponds to the mean velocity of the

reaction in the well. To determine the half maximal inhibitory concentration (IC_{50}) values, the different concentrations of the extract were plotted against the respective percentage of α -glucosidase inhibitory activity. When α -glucosidase inhibitory activity did not reach 70% the 25% inhibition concentration (IC_{25}) was determined. The commercial drug acarbose was used as positive control. Three independent experiments were performed, each in triplicate.

2.4.2. 5-LOX inhibition

Lipoxygenases obtained from soybean are a broadly employed model to assess lipoxygenase inhibition (168), once they display a high homology with the catalytic domain of mammalian lipoxygenases (169). Thus, the inhibitory effects on 5-LOX (*Glycine max* – Type V) activity were assessed by following the formation of the conjugated diene, 13-hydroperoxylinolenic acid, that results from linoleic acid oxidation (**Figure 18**) (169).

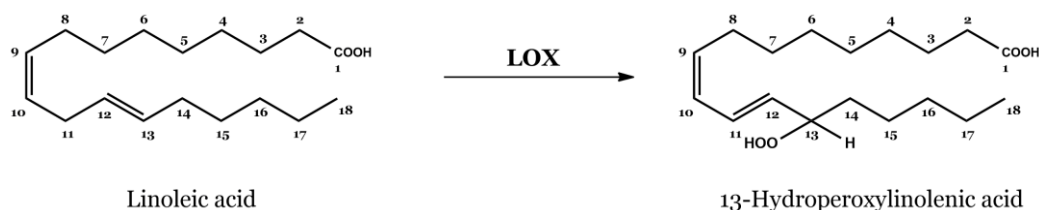


Figure 18. Oxidation of linoleic acid to 13-hydroxyoctadecadienoic acid catalysed by lipoxygenase (LOX).

Equal volumes (20 μ L) of different concentrations of the methanol extracts and 5-LOX (100 U), prepared in phosphate buffer ($Na_2HPO_4 \cdot 2H_2O$, 0.1 M, pH 9.0), were pre-incubated with 200 μ L of the same phosphate buffer for 5 min, at 37°C. The reaction was initiated by the addition of 20 μ L of linolenic acid (4.18 mM, prepared in ethanol), and the formation of the resulting oxidation product (13-hydroxyoctadecadienoic acid) was monitored every 20 s, for 3 min, at 234 nm, in a Multiskan GO plate reader (Thermo Fisher Scientific; Waltham, MA, USA). The maximum non-interfering DMSO concentration (0.5 %, v/v) was used to facilitate the solubilization of insoluble extracts. 5-LOX inhibition was determined according to the following equation: 5-LOX inhibitory activity (%) = $[1 - (V \text{ of sample} / V \text{ of negative control})] \times 100$, where V corresponds to the mean velocity of the reaction at the well. To determine the IC_{50} values, the different concentrations of the extracts were plotted against the respective percentage of 5-LOX inhibitory activity. When 5-LOX inhibitory activity did not reach 70%, IC_{25} values were determined. Quercetin was used as positive control. Three independent experiments were performed, each in triplicate.

2.4.3. DPPH• scavenging capacity

The antiradical-like activity was investigated by the DPPH• assay, routinely used to screen the antiradical capacity of vegetable samples (170). DPPH• is a free radical with a deep violet colour, stabilized by resonance. In the presence of compounds able to donate a hydrogen atom, DPPH• is reduced to a yellow-coloured non-radical compound, 2,2-diphenyl-1-picrylhydrazine, that can be estimated at 515 nm (**Figure 19**).

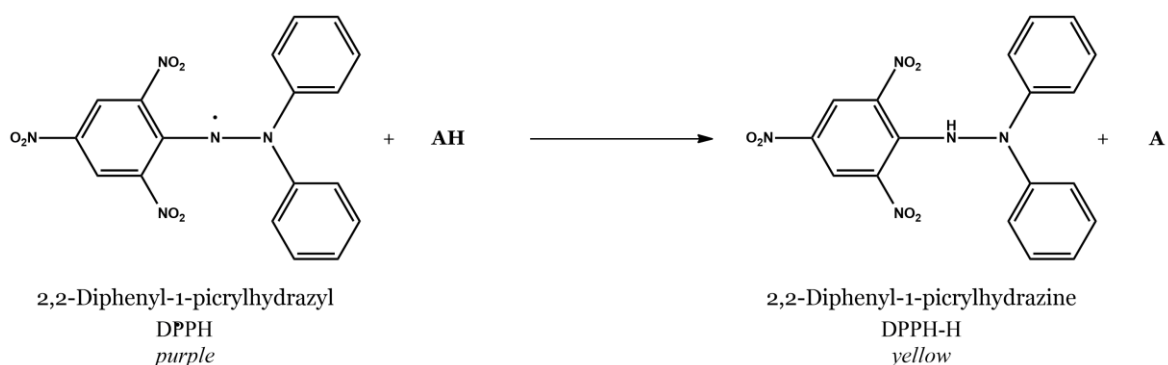


Figure 19. Neutralization of the 2,2-diphenyl-1-picrylhydrazyl radical (DPPH•) to 2,2-diphenyl-1-picrylhydrazine (DPPH-H) in the presence of antioxidant compounds (AH) able to donate a hydrogen atom.

Briefly, 25 μ L of different concentrations of the methanol extracts, prepared in methanol, were incubated with 200 μ L of DPPH• solution (150 μ M, in methanol), at room temperature for 30 min, in the dark. Afterwards, the absorbance was measured at 515 nm against a blank (methanol instead of DPPH• solution) in a Multiskan GO plate reader (Thermo Fisher Scientific; Waltham, MA, USA). The absorption of the blank was discounted and the DPPH• scavenging capacity was determined according to the following equation: DPPH• scavenging (%) = [1 – (absorbance of sample / absorbance of negative control)] x 100. To determine the IC₅₀ values, the different concentrations of the extract were plotted against to the respective DPPH• scavenging capacity. When the inhibition did not reach 70%, IC₂₅ values were calculated instead. Ascorbic acid was used as positive control. Three independent experiments were performed, each in triplicate.

2.5. Characterization of phenolic profiles of the selected species

Identification of the phenolic constituents was performed by HPLC-DAD-ESI/MSⁿ and UPLC-ESI-QTOF/MS, under the conditions detailed below. Quantitate analysis was carried out by HPLC-DAD.

2.5.1. HPLC-DAD-ESI (Ion Trap)/MSⁿ qualitative analysis

Chromatographic separation was carried out on a Kinetex column (5 μm, C18, 100 Å, 150 × 4.6 mm; Phenomenex, Macclesfield, UK). The mobile phase consisted of two solvents, acidified water (0.1% formic acid) (A) and acetonitrile (B), even though distinct gradients and flow rates were used for the analysis of the different methanolic extracts (**Table 4**). The injection volume was 20 μL. Spectral data from all peaks were accumulated in the range of 240–400 nm and chromatograms were recorded at distinct wavelengths, according to the phenolics composition (**Table 4**).

Table 4. Chromatographic conditions used on the qualitative analysis of the selected methanolic extracts by HPLC-DAD-ESI (Ion Trap)/MSⁿ.

Species	Gradient ^a	Flow rate (mL/min)	Detection λ (nm)
<i>C. urens</i>	0 min: 90% of A + 10% of B	0.7	320
	20 min: 70 % of A + 30 % of B		
	25 min: 40 % of A + 60 % of B		
<i>F. curtipes</i>	0 min: 95% of A + 5% of B	0.8	280 and 340
	20 min: 70 % of A + 30 % of B		
	30 min: 50 % of A + 50 % of B		
<i>C. tabularis</i>	0 min: 95% of A + 5% of B	0.7	280
	30 min: 75 % of A + 25 % of B		
	35 min: 30 % of A + 70 % of B		
<i>G. gracillima</i>	0 min: 95% of A + 5% of B	0.8	255 and 350
	20 min: 70 % of A + 30 % of B		
	30 min: 50 % of A + 50 % of B		

^a A, acidified water (0.1% formic acid); B, acetonitrile.

Analyses were performed in an Agilent HPLC 1200 series equipped with a DAD and MS detector in series (Agilent Technologies, Waldbronn, Germany). The HPLC had a binary pump (model G1376A), an autosampler (model G1377A) refrigerated at 4 °C (G1330B), a degasser (model G1379B), and a DAD (model G1315D). The HPLC system was controlled by the ChemStation software (Agilent, v. B.01.03-SR2). The MS detector was a Bruker ion trap

spectrometer (model HCT Ultra) equipped with an electrospray ionisation interface and was controlled by LCMSD software (Agilent, v. 6.1). The ionisation conditions were adjusted at 350 °C for capillary temperature and at 4.0 kV for voltage. The nebulizer pressure and flow rate of nitrogen were 65.0 psi and 11 L/min, correspondingly. The full scan mass covered the range from m/z 100 up to m/z 1500. Collision-induced fragmentation experiments were performed in the ion trap using helium as the collision gas, with voltage ramping cycles from 0.3 up to 2 V. Data were acquired in the negative ionisation mode. MS² was carried out in the automatic mode on the more abundant fragment ion in MS.

2.5.2. UPLC-ESI-QTOF-MS qualitative analysis

UPLC-ESI-QTOF-MS is a resourceful technique for the metabolic profiling of complex samples, providing high selectivity, sensitivity and mass accuracies (171). Determination of the exact mass was achieved using an Agilent 1290 Infinity LC System coupled to a 6550 Accurate-mass QTOF (Agilent Technologies, Waldbronn, Germany) with an electrospray interface (Jet Stream Technology). Extracts (2 µL) were injected onto a RP-Kinetex column (1.7 µm, C18, 100 Å, 50 × 2.1 mm; Phenomenex, Macclesfield, UK) with a SecurityGuard ULTRA cartridge of the same material, operating at 30 °C and a flow rate of 0.5 mL/min. The mobile phase consisted of two solvents, acidified water (0.1% formic acid) (Phase A) and acidified acetonitrile (0.1% formic acid) (Phase B), however different gradients were applied to each extract. Compounds from *C. urens* methanol extracts were separated using the following gradient conditions: 5% B at 0 min to obtain 20% B at 12 min and 50% B at 15 min. Compounds from *F. curtipes* and *G. gracillima* methanol extracts were separated using a gradient starting with 5% B, to obtain 30% B at 12 min and 50% B at 15 min. For the separation of *C. tabularis* phenolics the gradient started with 5% B, obtaining 40% B at 12 min and 70% B at 15 min.

The optimal conditions for the electrospray interface were as follows: gas temperature 280 °C, drying gas 11 L/min, nebulizer pressure 45 psi, sheath gas temperature 400 °C, sheath gas flow 12 L/min. The MS system was operated in negative ion mode with the mass range set at m/z 50–1500 in full scan resolution mode. To prevent carry-over effects, methanol was injected every five samples as a blank run. Moreover, the MS analysis external calibration of the instrument was performed at the beginning of the batch by using a mixture of reference compounds (Tuning Mix), to assure mass accuracy (171). Data were processed using the Mass Hunter Qualitative Analysis software (version B.06.00 Agilent Technologies).

2.5.3. HPLC-DAD quantitative analysis

Quantification of the identified phenolics was performed on an HPLC unit (Gilson Medical Electronics, Villers le Bel, France), using a RP-Kinetex C18 column (150 x 4.6 mm, 5 μm particle size, 100 \AA pore size) (Phenomenex, USA). The elution was performed as described above for the qualitative analysis (*subsection 2.5.1.*). Extracts were redissolved in methanol, filtered through a 0.45 μm pore size membrane and injected (20 μL) at final concentrations of 10 $\mu\text{g}/\text{mL}$ (*C. urens*), 150 $\mu\text{g}/\text{mL}$ and 70 $\mu\text{g}/\text{mL}$ (*F. curtipes* stem bark and leaves, respectively), 50 $\mu\text{g}/\text{mL}$ (*C. tabularis*) and 20 $\mu\text{g}/\text{mL}$ (*G. gracillima*). Detection was attained with an Agilent 1260 series DAD. Spectral data were collected in the range of 200–700 nm and chromatograms were recorded at 320 nm (*C. urens*), 280 and 340 nm (*F. curtipes*), 280 nm (*C. tabularis*), and at 255 and 350 nm (*G. gracillima*). Data were processed on Clarity software system, version 5.04.158 (DataApex, Ltd., Prague, Czech Republic).

Serial dilutions of external standards were injected under the same chromatographic conditions as those used for the chemical characterization of the extracts, absorbances recorded being utilized to build the calibration curves (concentration *vs* absorbance). The concentration of each phenolic compound was then determined by graphic interpolation, considering the individual absorbances. Linearity of the standards curves was determined from the coefficients of determination (R^2) and limits of detection (LOD) and quantification (LOQ) were calculated from the residual standard deviation (σ) of the regression curves and the slopes (S), according to the following equations: $\text{LOD} = 3.3\sigma/S$ and $\text{LOQ} = 10\sigma/S$. Compounds with commercial standards available were quantified as themselves, the remaining were quantitated using structurally related compounds. For the *C. urens* inflorescences and fruits (TH01 and TH02, **Table 3**) first collected, 3-, 4- and 5-*O*-caffeoylquinic acids were used to quantify the respective caffeoylshikimic acids derivatives. As 4-*O*-caffeoylshikimic acid was acquired afterwards it was utilized on the quantification of the caffeoylshikimic acids derivatives from the methanol extract obtained from the second collection of *C. urens* (TH21, **Table 3**). The caffeoylquinic acids from *F. curtipes* (TH05 and TH06, **Table 3**) were quantified as 5-*O*-caffeoylquinic acid, the proanthocyanidins as epicatechin, the catechin derivatives as catechin, the apigenin derivatives as vicenin-2 and the flavonolignans as epigallocatechin. On *C. tabularis* methanol extract (TH07, **Table 3**) proanthocyanidins were quantified as epicatechin, kaempferol derivatives as kaempferol-3-*O*-glucoside, luteolin derivative as luteolin-7-*O*-glucoside and quercetin derivatives as isorhamnetin-3-*O*-glucoside. Ellagic acid derivatives from *G. gracillima* (TH19 and TH22, **Table 3**) were quantified as ellagic acid, while the tri-

glycosylated and the di-glycosylated kaempferol derivatives were quantified as robinin and as kaempferol-3-*O*-rutinoside, respectively. Finally, flavan-3-ols derivatives were quantified at 280 nm, hydroxycinnamic acids at 320 and flavonoids at 350 nm.

2.6. Anti-diabetic-like activity

Anti-diabetic-like activity of the plant materials selected from the initial biological screening was evaluated through enzymatic assays, according to the protocols detailed below. The inhibitory activity of the two more active extracts was further assessed on human α -glucosidase enzymatic system.

2.6.1. Kinetic studies on yeast α -glucosidase inhibition

The study of the type of inhibition (competitive, uncompetitive or mixed) was performed using the nonlinear regression Michaelis–Menten enzyme kinetics.

To characterize the kinetic inhibition elicited by the selected methanol extracts, α -glucosidase activity was recorded, in the absence and in the presence of three different concentrations of the extracts. The assay was performed as outlined above (*subsection 2.4.1.*), using now eight concentrations of *p*-NPG (0.017–1.67 mM). Data were fitted into a Michaelis–Menten kinetic model, and the kinetic parameters (maximum velocity, V_{\max} and Michaelis constant, K_m) were determined using the GraphPad Prism Software 6.0. Kinetic study of the commercial drug acarbose was also performed. Three independent experiments were performed, each in triplicate.

2.6.2. α -Amylase inhibition

The inhibitory effects on α -amylase activity were assessed using a colorimetric method based on the reduction of DNSA (172). Briefly, α -amylase selectively hydrolyses α -(1,4) glycosidic bounds of starch, originating smaller reducing sugars, as maltotriose and maltose, that reduce DNSA (orange-red colour) to 3-amino-5-nitrosalicylic acid (yellow colour) (**Figure 20**).

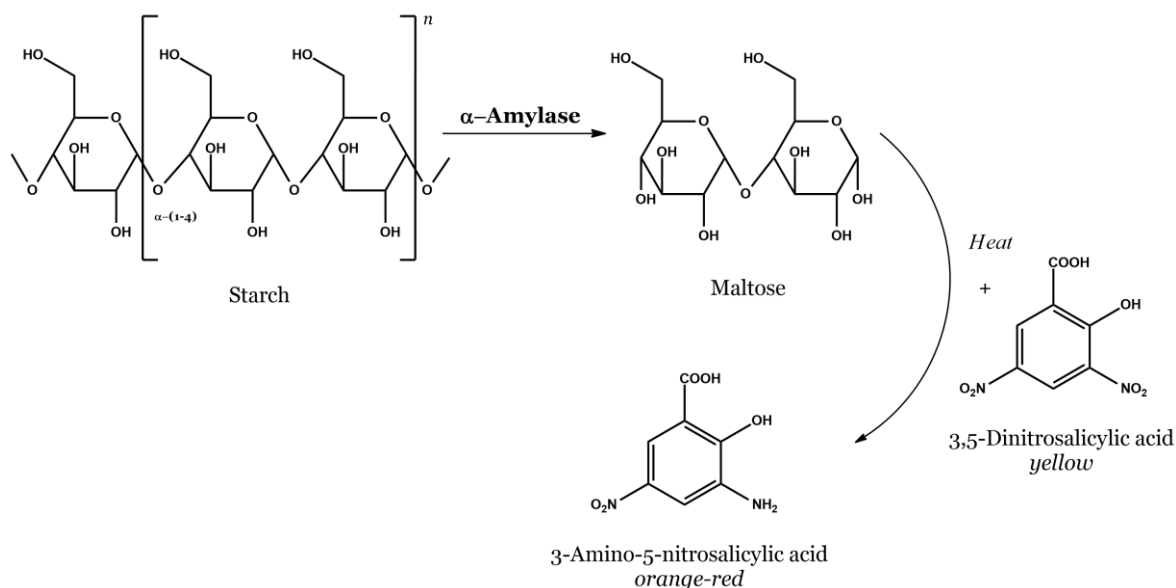


Figure 20. Starch cleavage by α -amylase into reducing sugars that reduce 3,5-dinitrosalicylic acid (DNSA) to amino-5-nitrosalicylic acid.

Equal volumes (100 μL) of different concentrations of the extracts and starch (1%), prepared in 20 mM Na_3PO_4 (with 6 mM NaCl, pH 6.9), were pre-incubated for 10 min, at room temperature. Thereafter, 100 μL of porcine α -amylase (7.5 U/mL) were added to the reactional mixture for another 10 min. The reaction was started by the addition of 400 μL of DNSA and tubes were incubated at 100 $^\circ\text{C}$, for 5 min. After cooling down, 50 μL of the reactional mixture were transferred to a 96-well plate and diluted with 200 μL of water, absorbance being then recorded at 540 nm in a Multiskan GO plate reader (Thermo Fisher Scientific; Waltham, MA, USA). The absorption of the blank (buffer instead of enzyme) was discounted and α -amylase inhibition was determined according to the following equation: α -Amylase inhibitory activity (%) = $[1 - (\text{absorbance of sample} / \text{absorbance of negative control})] \times 100$. To determine the IC_{50} values, the different concentrations of the extract were plotted against the respective percentage of α -amylase inhibitory activity. The commercial drug acarbose was used as positive control. Three independent experiments were performed, each in triplicate.

2.6.3. Aldose reductase inhibition

The inhibitory effects on aldose reductase activity were investigated by measuring the decay on the absorption of the enzyme co-factor (NADPH) at 340 nm, according to a previously reported method with some modifications (173). The cytosolic oxidoreductase, aldose reductase, catalyses the reduction of a vast array of aldehydes and carbonyls, namely

of the selected substrate, DL-glyceraldehyde. This reaction requires the oxidation of NADPH into nicotinamide adenine dinucleotide (NADP⁺) (**Figure 21**). NADPH has maximum absorption at 340 nm and, therefore, its consumption rate can be measured at this wavelength.

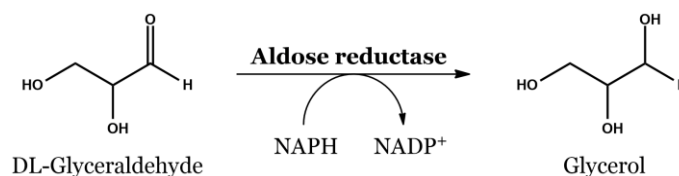


Figure 21. Reduction of DL-glyceraldehyde by aldose reductase and oxidation of the enzymatic co-factor (NADPH).

In a 96-well UV plate 40 μ L of different concentrations of the extracts were pre-incubated with 40 μ L of DL-glyceraldehyde (10 mM) and 40 μ L of the human-recombinant aldose reductase (0.052 U/mL) for 2 min, at 37°C. Posteriorly, the reaction was initiated by the addition of 80 μ L of NADPH (0.5 mM), and the absorbance was recorded at time 0 and after 20 min, at 340 nm in a Multiskan GO plate reader (Thermo Fisher Scientific; Waltham, MA, USA). All the reagents and samples were prepared in 0.1 M phosphate buffer (containing 0.2 mM (NH₄)₂SO₄ and 5 mM β -mercaptoethanol, pH 6.2). Absorbance at time 20 was subtracted from the absorbance at time 0 (Δ) and aldose reductase inhibition was determined according to the following equation: Aldose reductase inhibitory activity (%) = $[1 - (\Delta \text{ absorbance of sample} / \Delta \text{ absorbance of negative control})] \times 100$, where Δ corresponds to the absorbance difference between time 20 and time 0. To determine the IC₅₀ values, the different concentrations of the extract were plotted against the respective percentage of aldose reductase inhibitory activity. Rutin was used as positive control. Three independent experiments were performed, each in triplicate.

2.6.4. Pancreatic lipase inhibition

The inhibitory effects on porcine pancreatic lipase activity were assessed through a colorimetric assay based on *p*-nitrophenol release (174). Basically, pancreatic lipase cleaves the ester link of the substrate, *p*-NPB, releasing butyric acid and *p*-nitrophenol (yellow colour). The rate of the resulting chromophore formation is thereafter spectrophotometrically measured at 405 nm (**Figure 22**).

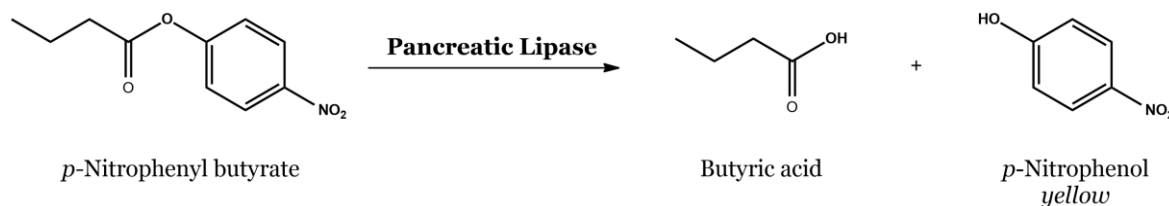


Figure 22. *p*-Nitrophenyl butyrate cleavage by the pancreatic lipase.

In microtubes, 100 μL of different concentrations of the extracts, prepared in tris-HCl buffer (100 mM, pH 7.0), were pre-incubated with 850 μL of 100 mM tris-HCl buffer (containing 5 mM of CaCl_2 , pH 7.0) and 30 μL of lipase solution (80 μg of protein/mL). The reaction was initiated by the addition of *p*-NPB (40 mM, prepared in DMSO), and the *p*-nitrophenol release was followed for 10 min (37 $^\circ\text{C}$), at 410 nm, in a Multiskan GO plate reader (Thermo Fisher Scientific; Waltham, MA, USA). The final DMSO concentration on the reactional mixture did not exceed 2%. Pancreatic lipase inhibition was determined according to the following equation: Pancreatic lipase inhibitory activity (%) = $[1 - (V \text{ of sample} / V \text{ of negative control})] \times 100$, where V corresponds to the mean velocity of the reaction at the well. To determine the IC_{50} values, the different concentrations of the extract were plotted against the respective percentage of pancreatic lipase inhibitory activity. The commercial drug orlistat was used as positive control. Three independent experiments were performed, each in triplicate.

2.6.4.1. Kinetic studies on pancreatic lipase inhibition

The study of the type of inhibition (competitive, uncompetitive or mixed) was performed using the nonlinear regression Michaelis–Menten enzyme kinetics.

To characterize the kinetic inhibition, pancreatic lipase activity was recorded in the absence and the presence of two extract concentrations, according to the above-mentioned procedure, using now eight concentrations of *p*-NPB (0.02–0.8 mM). Data were fitted into a Michaelis–Menten kinetic model, and the kinetic parameters (V_{max} and K_{m}) were determined using the GraphPad Prism Software 6.0. Three independent experiments were performed, each in triplicate.

2.6.5. Cellular assays

2.6.5.1. Cell culture of intestinal Caco-2 cells and treatments

Caco-2 cells (passages 66-80) were cultured in DMEM + GlutaMAX medium, supplemented with 10% of FBS and 1% penicillin/streptomycin. Cells were maintained in 75 cm³ flasks, at 37 °C, under a humidified atmosphere (5% CO₂). After reaching 80–90% confluence, cells were washed with Hank's balanced salt solution (HBSS), trypsinized, counted and sub-cultured for the cellular assays, as described below.

The extract solutions were prepared in culture medium and sterilized through a 0.22 µm pore size membrane. To determine the effect of the extracts on the viability of Caco-2 cells, serial dilutions, ranging from 15.63 to 250 µg/mL, were prepared.

2.6.5.2. Assessment of cell viability

Cytotoxic effects on Caco-2 cells were determined by assessing the mitochondrial activity, through the MTT reduction assay. This colorimetric method is often used to screen cell viability (175). Briefly, the soluble yellow tetrazolium dye, MTT, is reduced by the mitochondrial dehydrogenases of metabolic active cells, originating an insoluble purple formazan crystal, 5-(4,5-dimethylthiazol-2-yl)-1,3-diphenylformazan, which, after solubilized in isopropanol/DMSO, is spectrophotometrically determined at 560 nm (**Figure 23**) (175).

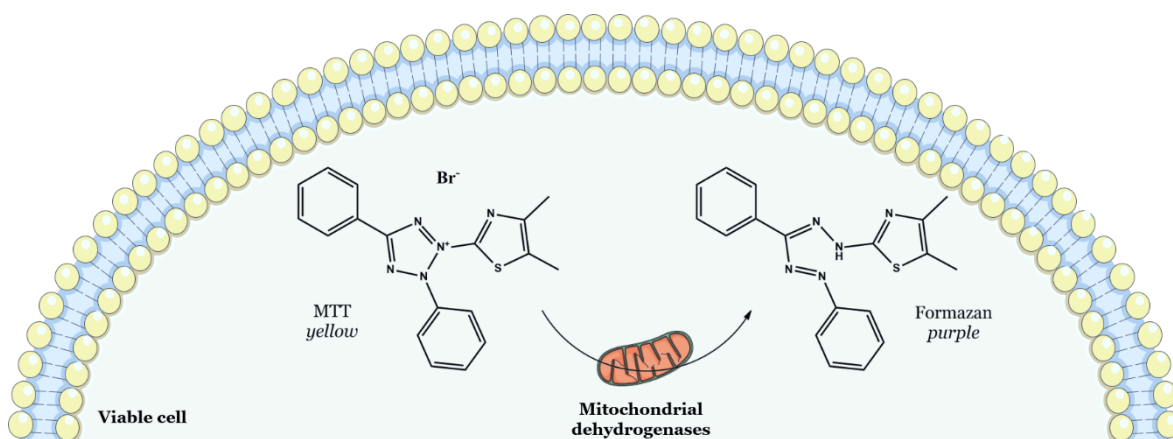


Figure 23. Reduction of 3-(4,5-dimethylthiazol-2-yl)-2,5-diphenyltetrazolium bromide (MTT) to 5-(4,5-dimethylthiazol-2-yl)-1,3-diphenylformazan by mitochondrial dehydrogenases of metabolic active cells.

Caco-2 cells were seeded in a 96-well plate, at a density of 20,000 cells/well, and allowed to attach for 24 h. After this period, cells were pre-incubated with the extracts, prepared as above-mentioned (*subsection 2.6.5.1.*), for another 24 h. Posteriorly, the medium was removed and cells were incubated with MTT (final concentration 0.5 mg/mL) for 1 h. The resulting formazan crystals were solubilized in a mixture of DMSO:isopropanol (3:1, *v/v*) and spectrophotometrically quantified at 560 nm in a Multiskan GO plate reader (Thermo Fisher Scientific; Waltham, MA, USA). Caco-2 cells viability was expressed in percentage, by comparing treated cells with the negative control (untreated cells), according to the following equation: Caco-2 viability (%) = (absorbance of treatment / absorbance of untreated cells) x 100. At least three independent experiments were performed, each in triplicate.

2.6.5.3. α -Glucosidase inhibition in Caco-2 cells homogenates

At late confluency and in culture, Caco-2 cells express most of the morphological and functional human intestinal epithelium characteristics, including the dimeric intestinal enzyme sucrase-isomaltase system, in apical membrane (mucosal α -glucosidase complex) (176). Hence, this cell line is commonly used to study human α -glucosidase activity (176). To evaluate the inhibitory activity of the extracts on the human α -glucosidase complex, enzyme-enriched cell supernatants were obtained from homogenates of human Caco-2 cells, as described below (**Figure 24**).

Caco-2 cells were seeded in 75 cm³ flasks and, after achieving full confluence, the cells were washed with 2.5 mL of cold phosphate buffered saline (PBS) solution and scraped with rubber cell scrapers. Thereafter, cells were homogenized in ice-cooled maleate buffer (100 mM, containing 1% of protease inhibitors cocktail, pH 6.0) using a glass/Teflon Potter Elvehjem. The obtained cell homogenates were centrifuged for 20 min, at 16,000 *g*, to collect the supernatant, containing the plasma membrane vesicles with the intestinal enzyme sucrase-isomaltase system. The remaining pellet, containing cell nucleus, mitochondria and other heavy organelles, was discharged. The protein content on the supernatants was estimated by the Bradford method, using BSA as standard (0-50 μ g/mL) and the purified supernatants were stored at -4 °C.

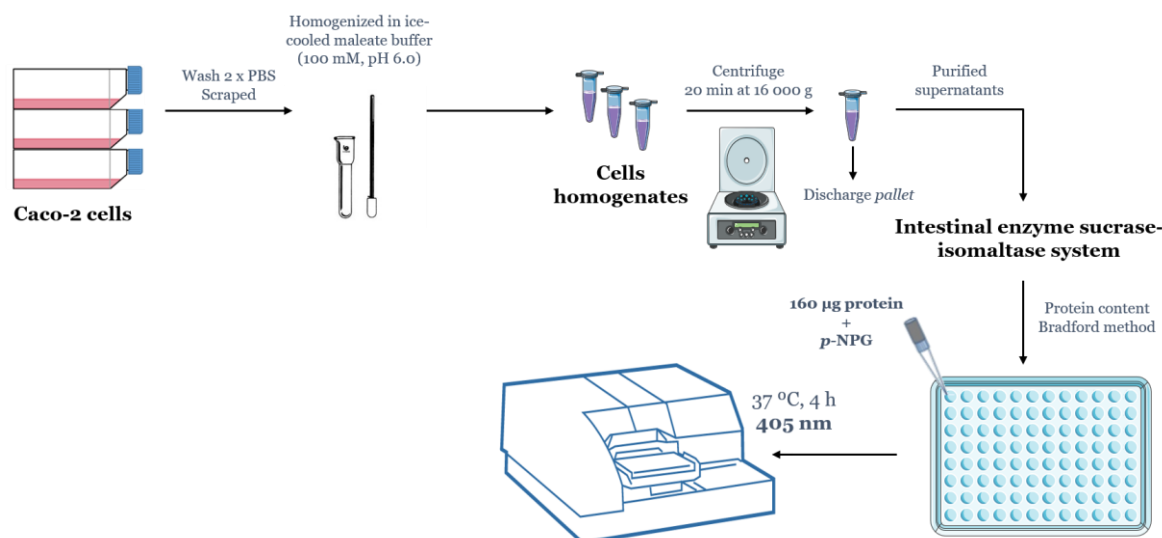


Figure 24. Schematic representation of the experiment conducted to assess the extracts inhibitory activity in the human α -glucosidase complex.

Posteriorly, the enzyme activity was assessed with 160 μg of purified cellular supernatant, in the absence and presence of increasing concentrations of the methanolic extracts, at 37 $^{\circ}\text{C}$, monitoring the *p*-nitrophenol release from *p*-NGP (1.67 mM), for 4 h (37 $^{\circ}\text{C}$), at 405 nm, in a Multiskan GO plate reader (Thermo Fisher Scientific; Waltham, MA, USA). Only non-cytotoxic concentrations of the extracts were tested. The general α -glucosidase activity (abs/h/mg protein), obtained by the linear range of the plot absorption *versus* time, in the absence and presence of extract, was used to determine enzyme inhibition. The effect was determined according to the following equation: Human α -glucosidase inhibitory activity (%) = $[1 - (V \text{ of sample} / V \text{ of negative control})] \times 100$, where V corresponds to the mean velocity of the reaction at the well. To determine the IC_{50} values, the different concentrations of the extract were plotted against the respective percentage of human α -glucosidase inhibitory activity. The commercial drug acarbose was used as positive control and tested at 400 $\mu\text{g}/\text{mL}$. Five independent assays were performed, using five different α -glucosidase homogenates obtained from different cells passages.

2.7. Anti-radical activity

The antiradical activity of the plant materials selected from the initial biological screening was investigated through non-cellular assays, according to the following protocols. For the two extracts that displayed greater antidiabetic potential, the ability to

prevent protein glycation in a cell-free system and to reduce intracellular reactive species overproduction in pancreatic cells was also assessed.

2.7.1. Nitric oxide radical scavenging capacity

The ability to scavenge nitric oxide radicals ($\cdot\text{NO}$) was initially evaluated in a cell-free system, using SNP as a NO donor (170). Generated $\cdot\text{NO}$ radicals interact with oxygen, originating NO_2^- ions, which are thereafter quantified by the Griess method (**Figure 25**). Briefly, NO_2^- reacts with sulfanilamide to produce a diazonium ion, that couples with *N*-(1-naphthyl)ethylenediamine, originating a diazonium product with a pink colour, which is spectrophotometrically measured at 560 nm (**Figure 25**).

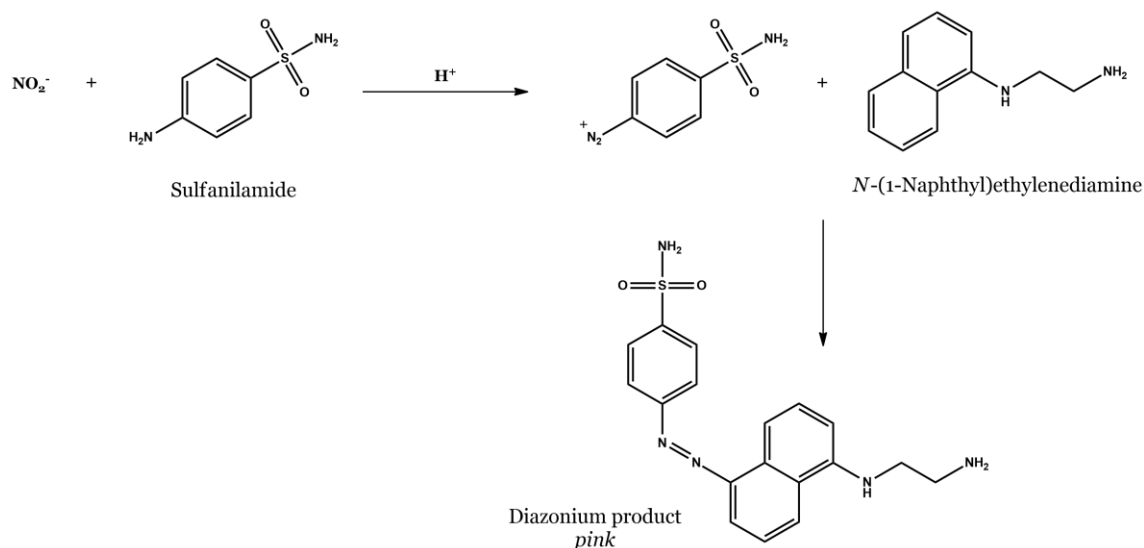


Figure 25. Determination of nitrites (NO_2^-) by the Griess method.

Different concentrations of the extracts (100 μL), prepared in potassium phosphate buffer (KH_2PO_4 , 100 mM, pH 7.4), were pre-incubated in a 96-well plate with 100 μL of SNP solution (20 mM, prepared in phosphate buffer), at room temperature, under light, to generate the $\cdot\text{NO}$ radicals. After 1h, 100 μL of Griess reagent (1% sulphanilamide and 0.1% *N*-(1-naphyl)ethylenediamine in 2% H_3PO_4) were added to each well and the plate was incubated in the dark, for 10 min. Posteriorly, the resulting diazonium pink product was spectrophotometrically measured at 560 nm, against a blank (2% H_3PO_4 instead of Griess reagent), in a Multiskan GO plate reader (Thermo Fisher Scientific; Waltham, MA, USA). The absorption of the blank was discounted and the $\cdot\text{NO}$ scavenging capacity was determined according to the following equation: $\cdot\text{NO}$ scavenging activity (%) = $[1 -$

(absorbance of sample / absorbance of negative control)] x 100. To determine the IC₅₀ values, different concentrations of each extract were plotted against the respective percentage of ·NO scavenging activity. Quercetin was used as positive control. Three independent experiments were performed, each in triplicate.

2.7.2. Superoxide anion radical scavenging capacity

The capacity to scavenge superoxide anion radicals (O₂^{·-}) was evaluated according to a previously published protocol, using the NADH/PMS system (170). Briefly, NADH reduces PMS, releasing O₂^{·-} radicals; thereafter, the generated radicals reduce NBT, originating a formazan blue dye, that is spectrophotometrically measured at 560 nm (**Figure 26**).

Different concentrations of the methanolic extracts (50 µL), prepared in potassium phosphate buffer (KH₂PO₄, 19.2 mM, pH 7.4), were incubated in a 96-well plate with 150 µL of NBT (43 µM, prepared in phosphate buffer) and 50 µL of NADH solution (166 µM, prepared in phosphate buffer). The reaction was initiated by the addition of 50 µL of PMS solution (2.7 µM, prepared in phosphate buffer) and the blue formazan formation was spectrophotometrically followed for 2 min, at 560 nm in a Multiskan GO plate reader (Thermo Fisher Scientific; Waltham, MA, USA). The effect was determined according to the following equation: O₂^{·-} scavenging activity (%) = [1 - (V of sample / V of negative control)] x 100, where V corresponds to the mean velocity of the reaction at the well. To determine the IC₅₀ values, different concentrations of each extract were plotted against the respective percentage of O₂^{·-} scavenging activity. Quercetin was used as positive control. Three independent experiments were performed, each in triplicate.

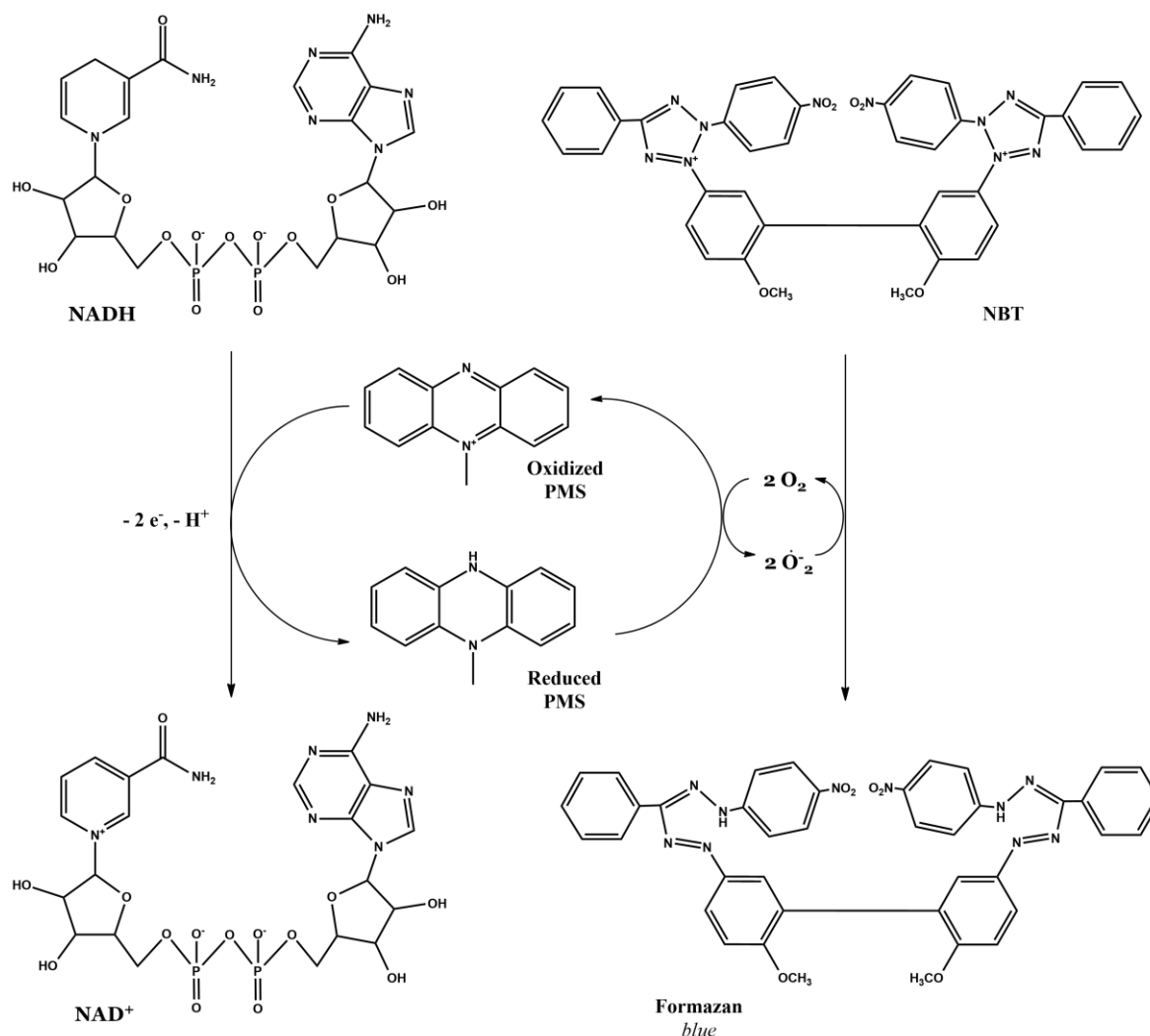


Figure 26. Formation of O₂⁻ by the NADH/PMS system and reduction of NBT to a formazan blue dye.

2.7.3. Lipid peroxidation inhibition

The ability of the extracts to reduce the oxidative degradation of lipids was evaluated according to a reported protocol, with minor modifications (**Figure 27**) (177). This free radical chain reaction begins with the abstraction of a hydrogen atom from an unsaturated lipid, leading to the formation and propagation of lipid radicals, that undergo through rearrangements, originating conjugated dienes, as the 13-hydroxyoctadecadienoic acid, with a characteristic absorption at 233 nm (**Figure 27**) (177). The lipid peroxidation chain can be stopped by antioxidant molecules, as ascorbic acid, that neutralize the lipid peroxy radicals and/or the lipid radicals (**Figure 27**) (177).

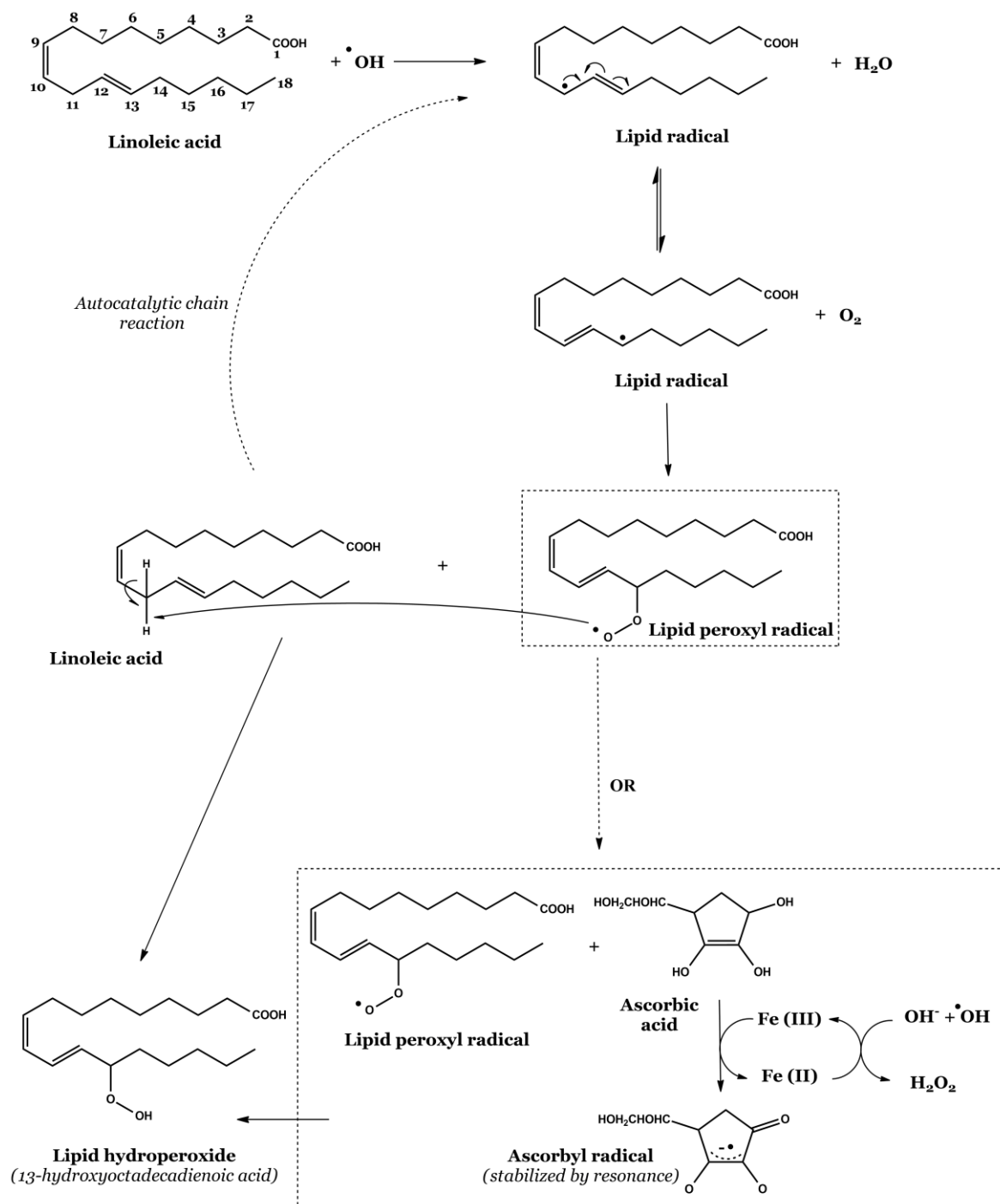


Figure 27. General reactions involved in the protocol utilized to study the effect of the extracts on lipid peroxidation.

The reactional mixture, containing 25 μL of different extract dilutions, 75 μL of Tris-HCl solution (100 mM, pH 7.5), 125 μL of linoleic acid (20 mM, in ethanol), 25 μL of $\text{FeSO}_4 \cdot 7\text{H}_2\text{O}$ (4 mM, in distilled H_2O) and 25 μL of ascorbic acid (5 mM, in distilled H_2O), was incubated for 1 h, at 37 $^\circ\text{C}$. The reaction was then stopped by the addition (725 μL) of an ethanol:ether (3:1, v/v) solution, which allowed the rearrangement of the double bonds, resulting in the

formation of conjugated dienes (lipid hydroperoxides). Those dienes were posteriorly estimated at 233 nm in a UNICAM Helios α UV/vis spectrophotometer (Thermo Fisher Scientific; Waltham, MA, USA), against a blank (ethanol instead of linoleic acid). The absorption of the blank was discounted and the percentage of lipid hydroperoxides formation was determined according to the following equation: Lipid peroxidation (%) = (absorbance of sample/absorbance of negative control) \times 100%. BHT was the positive control. Three independent experiments were performed, each in duplicate.

2.7.4. Protein glycation inhibition

Inhibition of protein glycation was assessed by following the formation of AGEs resulting from BSA glycation, according to a previously described procedure (178). Fructose, glucose and methylglyoxal induce BSA glycation, leading to the irreversible formation of fluorescent AGEs (as 1-alkyl-2-formyl-3, 4-glycosyl pyrrole, 2-(2-fluoril)-4, 5-furanyl-imidazole-1 and pentosidine), detectable at λ_{exc} 360 nm and λ_{em} 435 nm. While the BSA-fructose and BSA-glucose system cover the effects on protein glycation at all glycation stages, BSA-methylglyoxal assesses the protein glycation in a middle stage (**Figure 28**).

All the reagents and extract dilutions were prepared in 0.2 M sodium phosphate buffer ($\text{Na}_2\text{HPO}_4 \cdot 2\text{H}_2\text{O}$, containing NaN_3 0.2 mg/mL, pH 7.4). Briefly, 25 μL of several concentrations of the extracts were incubated with 75 μL of BSA (50 mg/mL), 150 μL of 0.2 M sodium phosphate buffer and 125 μL of glycation inducer (glucose at 800 mM, fructose at 300 mM or methylglyoxal at 15 mM). The test tubes were maintained at 37 $^\circ\text{C}$ during all the experiment. The fluorescent AGEs were quantified in aliquots (200 μL) of each reaction mixture, at four time-points (0, 3, 7 and 14 days) in a spectrofluorometer (λ_{exc} 360 nm; λ_{em} 435 nm) (SynergyTM HT, Biotek Instruments Winooski, USA) operated by Gen5 Software. Data were expressed as fold increase between each time-point (day 3, 7 or 14) and the basal fluorescent signal (day 0). BSA-inductor inhibition was estimated at the end of the experiment (day 14), according to the following equation: BSA-glucose/BSA-fructose/BSA-methylglyoxal inhibitory activity (%) = [1 - (fold change of sample / fold change of negative control)] \times 100%. The experimental drug aminoguanidine was used as positive control. Three independent experiments were performed, each in triplicate.

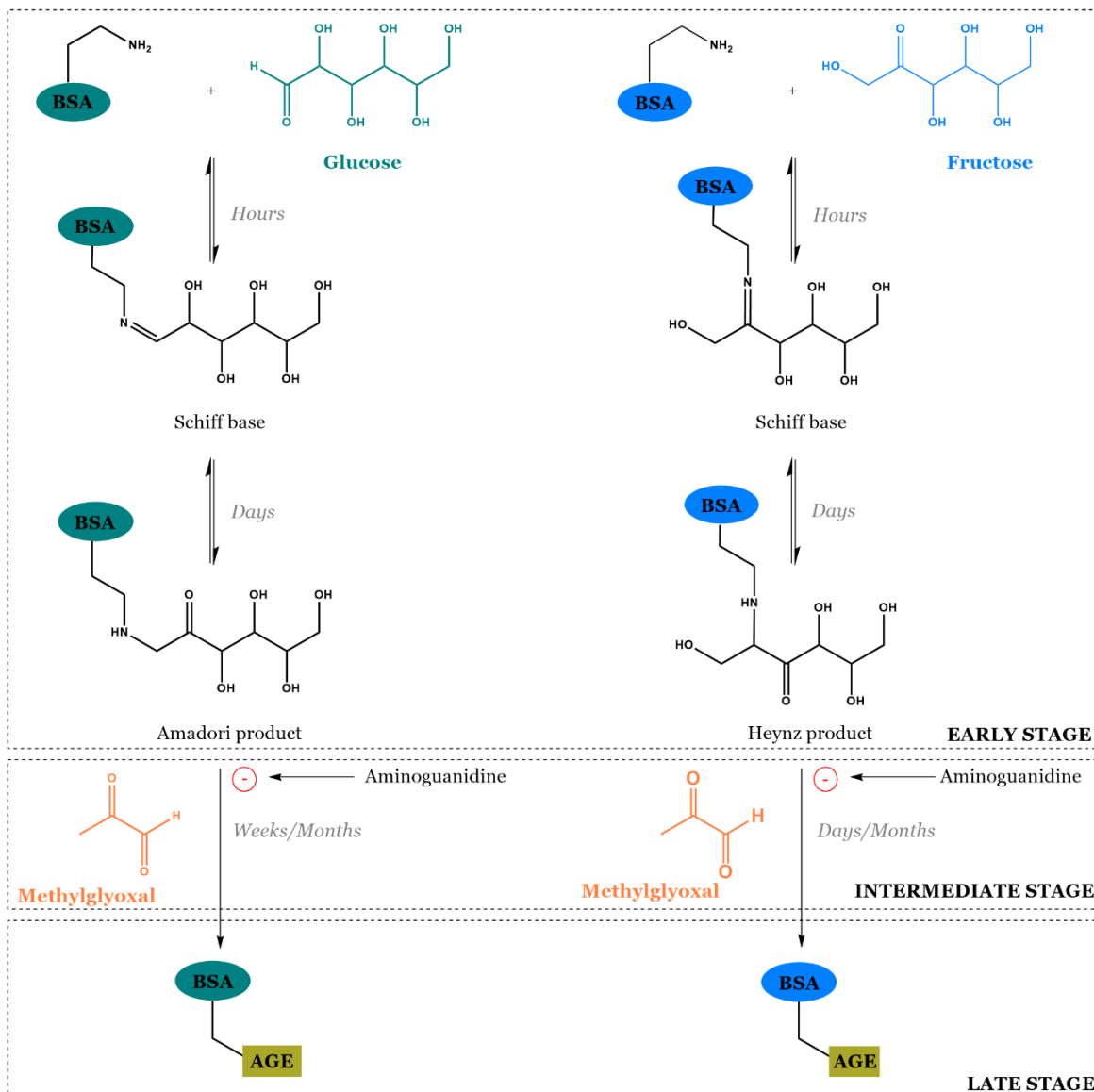


Figure 28. Schematic representation of bovine serum albumin (BSA) glycation and advanced glycation end products (AGEs) formation route from glucose and fructose.

2.7.5. Cellular assays

2.7.5.1. Culture of pancreatic RIN-5F cells and treatments

RIN-5F cells (passages 7-25) were cultured in RPMI-1640 medium, supplemented with 10% of FBS and 1% penicillin/streptomycin. Cells were maintained in 75 cm³ flasks, at 37 °C, under a humidified atmosphere (5% CO₂). The medium was renewed every two days.

After reaching 80–90% confluence, cells were washed with HBSS, trypsinized, counted and sub-cultured for the cellular assays, as described next.

The extract solutions were prepared in culture medium and sterilized by crossing a 0.22 μm pore size membrane. To determine the effect of the extracts on cells viability and intracellular reactive species production, serial extracts dilutions were prepared in the range of 15.63 to 500 $\mu\text{g}/\text{mL}$. Cells were treated under two different conditions: Normal conditions, where extracts were incubated in normal glucose conditions (using the maintaining RPMI medium with 11 mM of glucose) *vs* glucotoxic conditions, where extracts were incubated in high concentrations of glucose (using RPMI medium with 33 mM of glucose) (**Figure 29**).

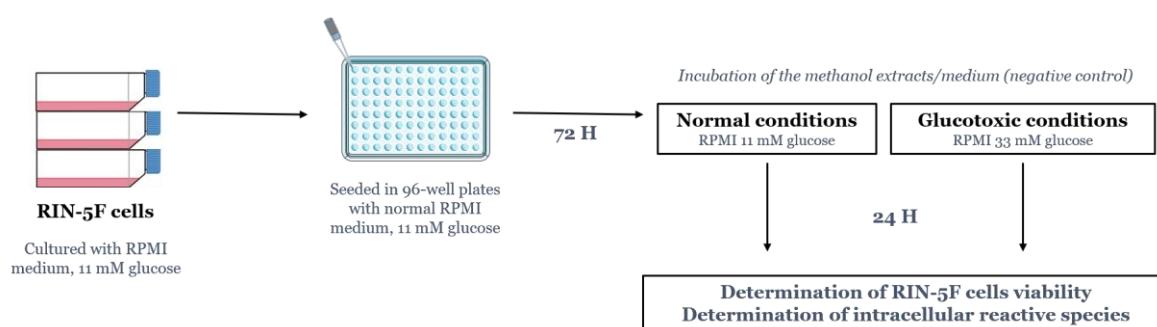


Figure 29. Experimental design of the assays performed with pancreatic RIN-5F cells.

2.7.5.2. Assessment of cell viability

Effects on the viability of RIN-5F cells were determined by assessing the mitochondrial activity, through the MTT reduction assay, as explained above (**Figure 23**).

RIN-5F cells were seeded in a 96-well plate at a density of 20,000 cells/well and allowed to attach. After 3 days, the medium was removed, and cells were pre-incubated with the extracts, under normal and glucotoxic conditions, for 24 h. Afterwards, the medium was removed and cells were incubated with MTT (final concentration 0.5 mg/mL) for 4 h. The resulting formazan crystals were solubilized in a mixture of DMSO:isopropanol (3:1, *v/v*) and spectrophotometrically quantified at 560 nm in a Multiskan GO plate reader (Thermo Fisher Scientific; Waltham, MA, USA). RIN-5F cell viability is expressed in percentage, by comparing treated cells with the negative control (untreated cells), according to the following equation: RIN-5F viability (%) = (absorbance of treatment / absorbance of untreated cells) x 100. At least three independent experiments were performed, each in triplicate.

2.7.5.3. Determination of intracellular reactive species

The ability of the extracts to reduce reactive intracellular species in pancreatic RIN-5F cells was investigated according to a slightly modified protocol, using the 2',7'-dichlorodihydrofluorescein diacetate (DCFH-DA) probe (179). DCFH-DA passively diffuses into cells membranes and is quickly deacetylated by cellular esterases into 2',7'-dichlorodihydrofluorescein (H_2DCF). This product is, thereafter, oxidised by intracellular reactive species originating a high fluorescent carboxylate anion, 2',7'-dichlorofluorescein (DCF) (**Figure 30**).

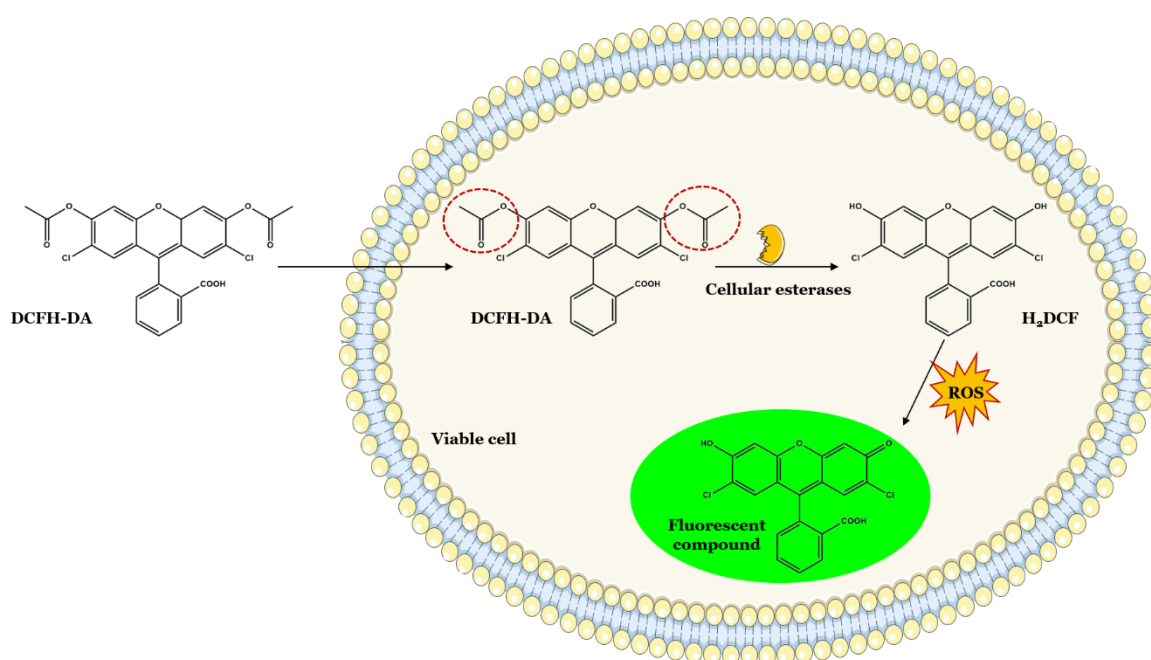


Figure 30. Cleavage of 2',7'-dichlorodihydrofluorescein diacetate (DCFH-DA) by cellular esterases into 2',7'-dichlorodihydrofluorescein (H_2DCF) and reaction with ROS, originating the fluorescent compound dichlorofluorescein (DCF).

RIN-5F cells were seeded in a dark 96-well plate at a density of 20,000 cells/well and allowed to attach. After 3 days, the medium was removed, and cells were pre-incubated with the extracts, under normal and glucotoxic conditions, for 24 h. Culture medium was then removed, as cells were washed two times with HBSS and incubated with the DCFH-DA probe (20 μ M, prepared in methanol) for 30 min, at 37 °C. Fluorescence was then determined at 485 nm excitation and 520 nm emission using a spectrofluorimeter (SynergyTM HT, Biotek Instruments Winooski, USA) operated by Gen5 Software. The intracellular reactive species recorded are expressed in absolute fluorescence values. The

antioxidant NAC was used as positive control. At least three independent experiments were performed, each in triplicate.

2.8. Anti-inflammatory-like activity

The anti-inflammatory-like activity of the plant materials was also deeper investigated. Initially, kinetic studies regarding 5-LOX inhibition were performed, in order to understand the type of inhibition caused by the most active extracts. Additionally, the effects upon inflammatory mediators, namely NO, IL-6 and TNF- α , were evaluated in LPS-stimulated RAW 264.7 macrophages.

2.8.1. Kinetic studies on 5-LOX inhibition

The study of the 5-LOX inhibition type was performed using the nonlinear regression Michaelis–Menten enzyme kinetics.

5-LOX activity was recorded in the presence and absence of two different extracts concentrations, using increasing concentrations of linolenic acid (1-600 μM), according to the procedure described above (*subsection 2.4.2.*). Afterwards, data was fitted into a Michaelis-Menten kinetic equation to obtain V_{max} and K_{m} values. Kinetic parameters were obtained for the different extract concentrations as a function of increasing concentrations of linolenic acid (1-600 μM). Data were analysed by nonlinear regression fit models on GraphPad Prism 6.0 Software (San Diego, US), and the best models were employed according to the R^2 values. Three independent experiments were performed, each in triplicate.

2.8.2. Cellular assays

2.8.2.1. Culture of RAW 264.7 macrophages and treatments

RAW 264.7 macrophages (passages 7-60) were cultured using DMEM + GlutaMAX medium, supplemented with 10% of FBS and 1% penicillin/streptomycin. Cells were maintained in 25 cm^3 flasks, at 37 $^{\circ}\text{C}$ in a humidified atmosphere (5% CO_2). After reaching

80–90% confluence, cells were washed with fresh medium, scraped, counted and sub-cultured for the cellular assays.

The extract solutions were prepared in culture medium and sterilized by crossing a 0.22 µm pore size membrane. To determine the effect on RAW 264.7 macrophages viability and on the inflammatory mediators' levels, serial extracts dilutions were prepared in the range of 15.63 to 1000 µg/mL. LPS from *Escherichia coli* (prepared in HBSS) was used to induce an inflammatory phenotype.

2.8.2.2. Assessment of cell viability

Effects on RAW 264.7 macrophages viability was determined by assessing the mitochondrial activity of the cells, using the MTT reduction assay (**Figure 23**).

First, interference with RAW 264.7 macrophages viability was investigated in LPS-unstimulated cells. For this propose, cells were cultured in 96-well plates (25,000 cells/well) and allowed to attach for 24 h. Afterwards, cells were incubated with increasing concentrations of the extracts for 24 h. The medium was then removed and MTT (final concentration 0.5 mg/mL) was added to each well, cells being incubated for 90 min at 37 °C. The resulting formazan crystals were solubilized in a mixture of DMSO: isopropanol (3:1, *v/v*) and spectrophotometrically quantified at 560 nm in a Multiskan GO plate reader (Thermo Fisher Scientific; Waltham, MA, USA). Thereafter, the extracts interference with RAW 264.7 macrophages viability was also investigated in the experimental inflammatory model (LPS-stimulated cells). In this case, the cells were cultured in 96-well plates (35,000 cells/well) and allowed to attach for 24 h, being posteriorly exposed to increasing concentrations of the extracts. After the treatment with the extracts (2 h), a solution of LPS, at a final concentration of 1 µg/mL, was added to each well and plates were incubated for further 22 h. After this period, the medium was removed and cells were incubated with MTT solution (final concentration 0.5 mg/mL), as described above (*subsection 2.8.2.1*).

RAW 264.7 macrophages viability was expressed in percentage, by comparing treated cells with the negative control (untreated cells), according to the following equation: Cell viability (%) = (absorbance of treatment / absorbance of untreated cells) x 100. At least three independent experiments were performed, each in triplicate. Non-cytotoxic concentrations of extracts were selected for the following determinations.

2.8.2.1. Determination of nitric oxide levels

To investigate the effects of the methanolic extracts on the NO levels in LPS-stimulated RAW 264.7 macrophages, cells were cultured in 96-well plates (35,000 cells/well) for 24 h, and exposed to increasing concentrations of the extracts. After 2 h, cells were co-stimulated with LPS (1 $\mu\text{g}/\text{mL}$, final concentration) for another 22 h. The NO_2^- formed by the conversion of NO in the culture medium was spectrophotometrically quantified at 540 nm in a microplate reader (Multiskan ASCENT, Massachusetts, MA, USA). For this purpose, equal volumes (75 μL) of cell culture supernatants and Griess reagent (1% sulfanilamide and 0.1 % *N*-(1-naphthyl)-ethylenediamine in 2% H_3PO_4) were incubated for 10 min, in the dark, at room temperature. Under acidic conditions, cellular NO converts into NO_2^- . The diazonium product resulting from the reaction of the anion with sulphanilamide and *N*-(1-naphthyl)-ethylenediamine was measured at 540 nm (**Figure 31**). NO levels of LPS-stimulated RAW 264.7 macrophages were expressed in percentage, by comparing treated cells with the negative control (untreated cells), according to the following equation: NO levels (%) = (absorbance of treatment / absorbance of untreated cells) x 100. *N*-methyl-L-arginine (25 μM) was used as positive control. At least three independent experiments were performed, each in triplicate.

2.8.2.2. Determination of L-citrulline levels

The ability to modulate iNOS (activity and/or expression) was determined by following the formation of L-citrulline, a bioproduct resulting from L-arginine oxidative deamination (**Figure 31**).

L-citrulline levels in RAW 264.7 cellular supernatants were determined according to a former described procedure, with some modifications (180). Briefly, cells were cultured in 48-well plates (90 000 cells/well) for 24 h, and exposed to increasing concentrations of the extracts. After 2 h, cells were co-stimulated with LPS (1 $\mu\text{g}/\text{mL}$, final concentration) for another 22 h at 37 $^\circ\text{C}$, in a humidified atmosphere of 5% CO_2 . After this period, the medium was removed, the cells were washed with HBSS and the substrate of iNOS, L-arginine (50 μM , prepared in HBSS), was added to each well. The reaction was allowed to occur for 2 h, and L-citrulline levels were thereafter determined on the cells supernatants. For this, 250 μL of cell culture supernatants were added to 100 μL of a mixture containing 79 mM diacetyl monoxime (prepared in 83 mM CH_3COOH), 47.8 mM antipyrine E (prepared in H_2O) and

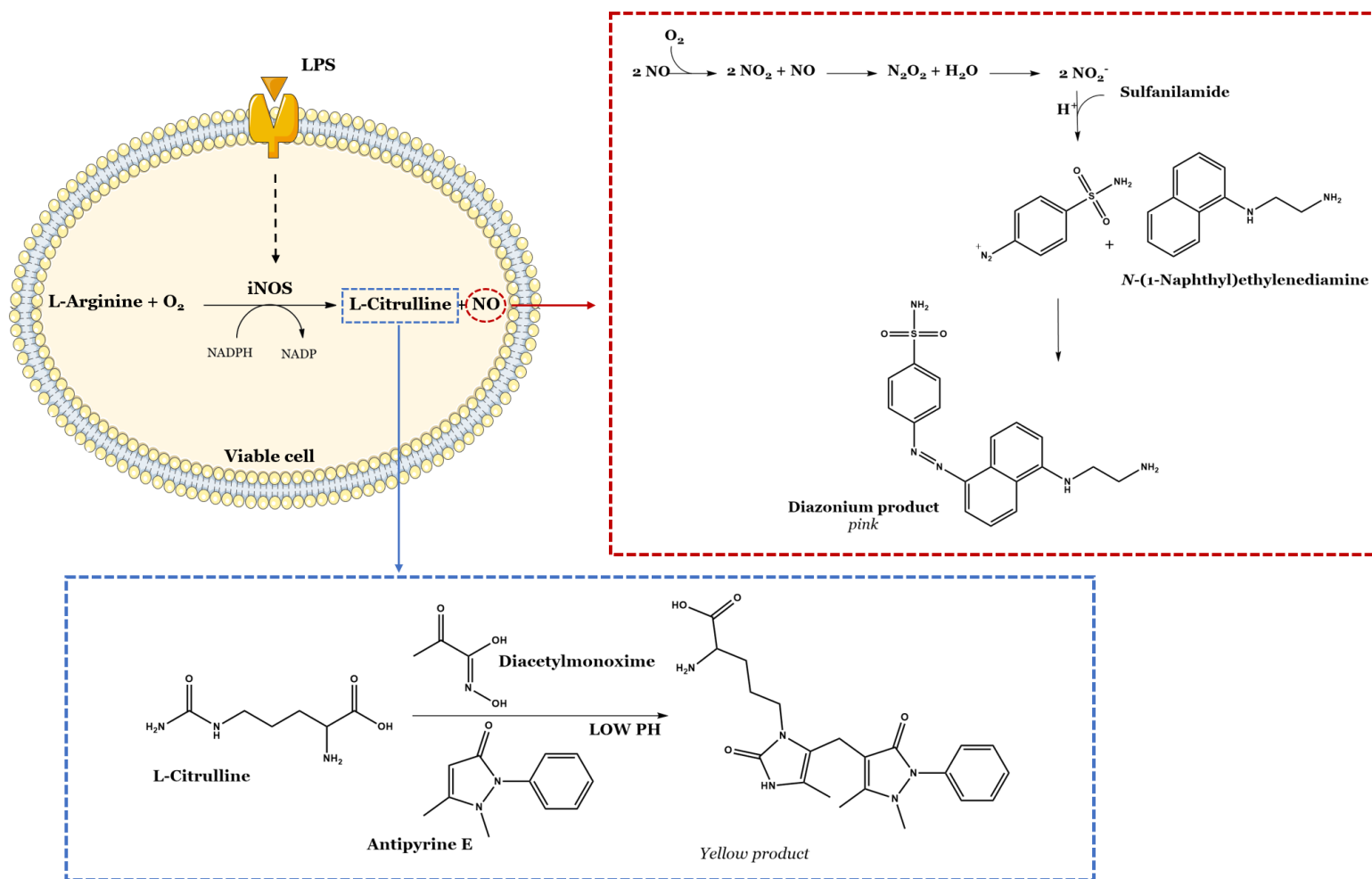


Figure 31. Schematic representation of NO and L-citrulline production in LPS-stimulated RAW 264.7 macrophages and reactions used for their determination.

7.5 M H₂SO₄. The reaction mixture was incubated at 96 °C and the reaction was allowed to occur for 25 min. L-citrulline reacts with diacetyl monoxime and antipyrine E, originating a stable compound, with a maximum absorbance at 460 nm (**Figure 31**). Posteriorly, the solution was cooled down to room temperature and the resulting yellow product was spectrophotometrically quantified at 460 nm in a microplate reader (Multiskan ASCENT, Massachusetts, MA, USA). L-Citrulline levels are expressed in percentage, by comparing treated cells with the negative control (untreated cells), according to the following equation: L-Citrulline levels (%) = (absorbance of treatment / absorbance of untreated cells) x 100. N-methyl-L-arginine (25 µM) was used as positive control. Five independent experiments were performed, each in duplicate.

2.8.2.3. Determination of TNF-α and IL-6 levels

The capacity of the extracts to downregulate pro-inflammatory cytokines (TNF-α and IL-6) levels was investigated, using the treatment doses that significantly reduced NO cellular levels. Cells were treated as described in section 8.2.3., TNF-α and IL-6 levels being quantified in the cellular supernatants. After 22 h of LPS co-stimulation (1 µg/mL), the cellular supernatants, containing TNF-α and IL-6, were collected and frozen at -80 °C until analysis. The attached cells were lysed with RIPA buffer (containing 150 mM NaCl, 1.0 % Triton X-100, 0.5% sodium deoxycholate, 0.1% SDS, 50 mM Tris HCl and 1% protease inhibitor cocktail, pH 8.0), collected and frozen at -80 °C until further determination of the protein content. TNF-α and IL-6 levels on RAW 264.7 cellular supernatants were determined using an ELISA kit (ELISA MAX™, BioLegend), according to the protocol provided by the manufacturer. The total protein content of the cell lysates was estimated by the Bradford method, BSA being used as a standard to build the calibration curve. Cytokines amounts were normalized to the protein content and TNF-α and IL-6 levels were expressed as a percentage of the control (untreated cells). At least three assays were performed, each in duplicate.

2.9. Statistical analysis

The statistical analysis was performed on GraphPad Prism 6.0 Software (San Diego, US). A Grubbs' test was applied to cellular assays results, to identify significant outliers. Posteriorly, to ensure that all data followed a normal distribution, normality was checked

through D'Agostino-Pearson normality test. Afterwards, One-way analysis of variance (ANOVA) with Dunnett as *post hoc* test was used to compare each experimental condition with the respective control (untreated cells), except in RIN-5F cells, where an unpaired T-test was used to compare the intracellular species levels of the control under normal glucose conditions with the control under glucotoxic conditions. In the same way, significant differences between the kinetic parameters were determined with a One-way ANOVA with Dunnett as *post hoc* test, after normality validation by the D'Agostino-Pearson normality test. Differences at $p < 0.05$ were considered significant.

Pearson correlations between the total amounts of phenolic compounds in each targeted extract and the IC_{50} values of the bioassays were also calculated on GraphPad Prism 6.0 Software.

CHAPTER III
RESULTS AND DISCUSSION

3. Results and discussion

3.1. Preliminary screening of biological activities of plant species from Thailand

Considering the multi-factorial aetiology of diabetes, and also having into account the role of inflammation, oxidative stress and postprandial hyperglycaemia on the development and progression of the disease, the collected medicinal species were first assessed on their ability to inhibit the enzymatic activity of 5-LOX and α -glucosidase, and also on the capacity to scavenge DPPH \cdot . In fact, yeast α -glucosidase (181) and soybean 5-LOX (168) have been broadly used to screen antidiabetic-like and anti-inflammatory-like activities. Assessments on the scavenging activity towards the synthetic radical DPPH \cdot can also provide some clues on the antiradical capacity (182). Therefore, these cell-free systems were chosen to preliminary screen the biologic potential of the collected vegetable samples (**Table 3**).

Table 5. Results on the biologic screening of the methanol extracts obtained from plant species collected in Thailand.

ID	IC ₅₀ (μ g/mL)		
	α -Glucosidase inhibition	5-LOX inhibition	DPPH \cdot scavenging
TH01	1.526	164.419	23.807
TH02	108.089	53.680 ^a	373.356
TH03	n.d.	n.d.	212.983
TH04	n.d.	n.d.	n.d.
TH05	146.628	200.080	542.120
TH06	9.261	10.750	14.658
TH07	21.124	13.118	24.231
TH08	90.304	666.918	795.383
TH09	n.d.	477.402	288.622
TH10	n.d.	n.d.	708.343
TH11	48.023	23.723	5.872
TH12	17.833	109.584	129.848
TH13	43.665	63.960	18.687
TH14	n.d.	150.198	668.301
TH15	n.d.	402.058	230.534
TH16	16.121	33.139	48.994
TH17	129.264 ^a	383.558	77.829
TH18	n.d.	251.999 ^a	485.791
TH19	4.719	258.939	44.958
TH20	6.555	28.915	47.942

^aIC₂₅; nd. Not determined

The extract obtained from *C. urens* inflorescences (TH01) was the most effective in inhibiting yeast α -glucosidase activity ($IC_{50} = 1.526 \mu\text{g/mL}$), followed by the extracts obtained from the flowers of *G. gracillima* (TH19, $IC_{50} = 4.719 \mu\text{g/mL}$) and from the stem bark of *F. curtipes* (TH06, $IC_{50} = 9.261 \mu\text{g/mL}$) (**Table 5, Figure 32**).

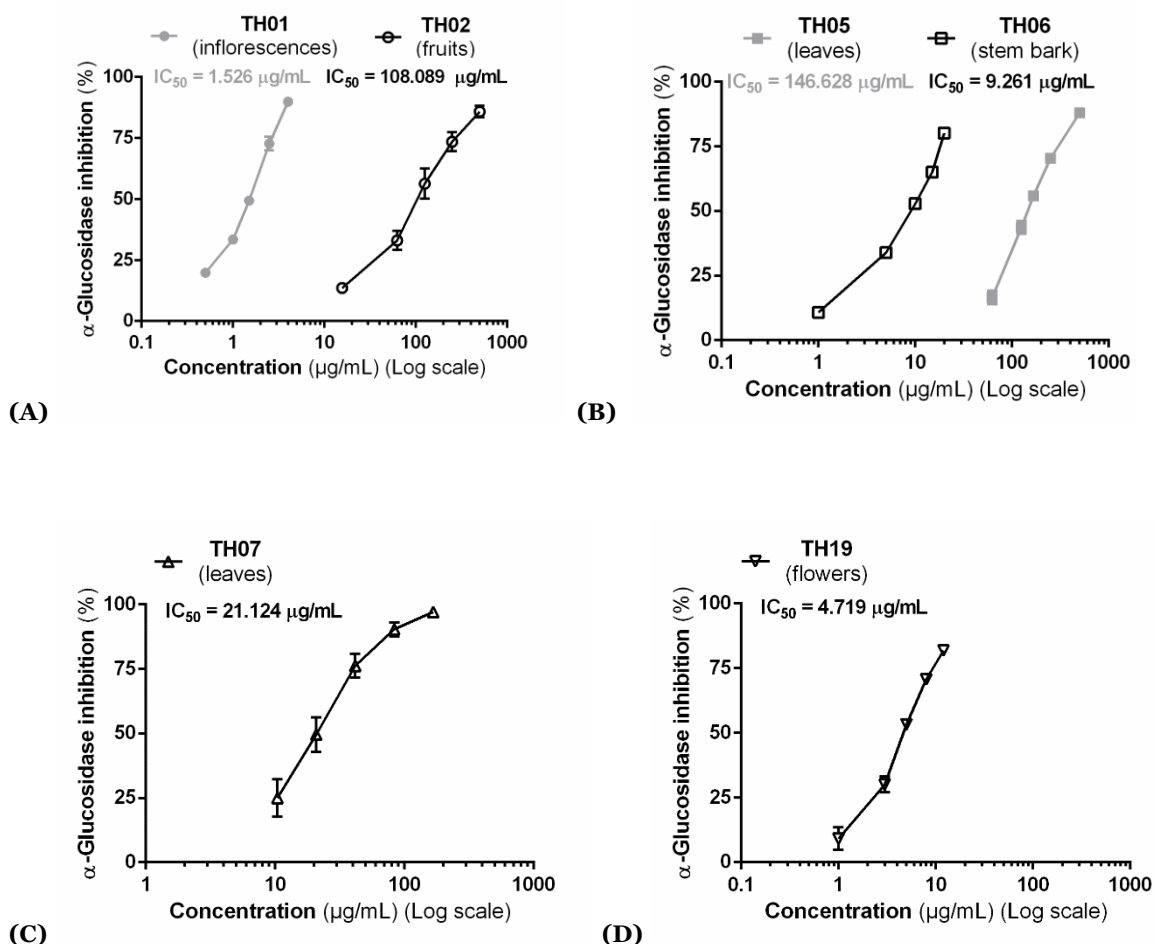


Figure 32. α -Glucosidase inhibition caused by the methanol extracts obtained from the inflorescences (TH01) and fruits (TH02) of *C. urens* (A), from the leaves (TH05) and stem bark (TH06) of *F. curtipes* (B), from the leaves (TH07) of *C. tabularis* (C) and from the flowers (TH19) of *G. gracillima* (D). Results represent the mean \pm SEM of three experiments, each performed in triplicate.

The extracts obtained from the leaves of *C. tabularis* (TH07), the leaves (TH11) and stem bark (TH12) of *S. siamensis*, the stem bark of *C. formosum* (TH13), the leaves of *C. arborea* (TH16) and the stem bark of *H. orixense* (TH20), along with extracts TH01, TH06 and TH19 were significantly ($p < 0.0001$) more effective in inhibiting α -glucosidase than the reference drug acarbose ($IC_{50} = 113.430 \mu\text{g/mL}$). As evidenced on **Table 5**, neglectable effects on the activity of the enzyme were recorded with the methanol extracts obtained from the leaves (TH03) and stem bark (TH04) of *C. adansonii*, from the stem bark of *D. decandra* (TH09),

from the leaves of *S. siamensis* (TH10), from the leaves (TH14) and stem bark (TH15) of *A. xylocarpa* and from the leaves of *J. gendarussa* (TH18) (less than 40% inhibition at the highest tested concentration). Furthermore, the extract obtained from the wood of *C. arborea* (TH17, estimated IC_{25} value of 129.264 $\mu\text{g/mL}$), only originated a 50.143 ± 6.062 % inhibition at the highest tested concentration (**Table 5**). Apart from those, the remaining extracts were capable of inhibiting α -glucosidase activity in a concentration-dependent manner. Worth to highlight that the extracts obtained from the leaves appeared to be more active than the ones collected from other plant materials, except in the case of *F. curtipes* and *S. siamensis* (**Table 5**). Also, the two more active extracts were obtained either from inflorescences (TH01) or flowers (TH19) (**Table 5, Figure 32**).

Regarding the anti-inflammatory potential, the most active extracts were the ones obtained from the stem bark of *F. curtipes* (TH06, $IC_{50} = 10.750$ $\mu\text{g/mL}$), from the leaves of *C. tabularis* (TH07, $IC_{50} = 13.118$ $\mu\text{g/mL}$) and from the stem bark of *S. siamensis* (TH11, $IC_{50} = 23.723$ $\mu\text{g/mL}$) (**Table 5, Figure 33**). Still, none of those extracts was more effective than the positive control quercetin ($IC_{50} = 2.532$ $\mu\text{g/mL}$).

Once again, all the extracts, except TH03, TH04 and TH10, inhibited the activity of the enzyme in a concentration-dependent manner (**Table 5, Figure 33**). Additionally, at the highest concentration tested, TH02 elicited around 48 % inhibition of 5-LOX, enabling to determine the IC_{25} value (53.680 $\mu\text{g/mL}$) (**Table 5**). In the same way, the methanol extract prepared from the leaves of *J. gendarussa* (TH18), displayed an IC_{25} value of 251.999 $\mu\text{g/mL}$. Contrary to what was observed on α -glucosidase activity, the extracts obtained from stem bark samples appear to be more active than those obtained from the leaves, except in the case of *A. xylocarpa* (TH15 and TH16), which leaf extract scored higher (**Table 5**). Relevantly, comparing with α -glucosidase, the extracts obtained from the inflorescences (TH01) and flowers (TH19) caused a less accentuated 5-LOX inhibition (IC_{50} value of 164.419 $\mu\text{g/mL}$ and 258.939 $\mu\text{g/mL}$, respectively), suggesting their greater selectivity for the former enzyme (**Table 5, Figure 33**).

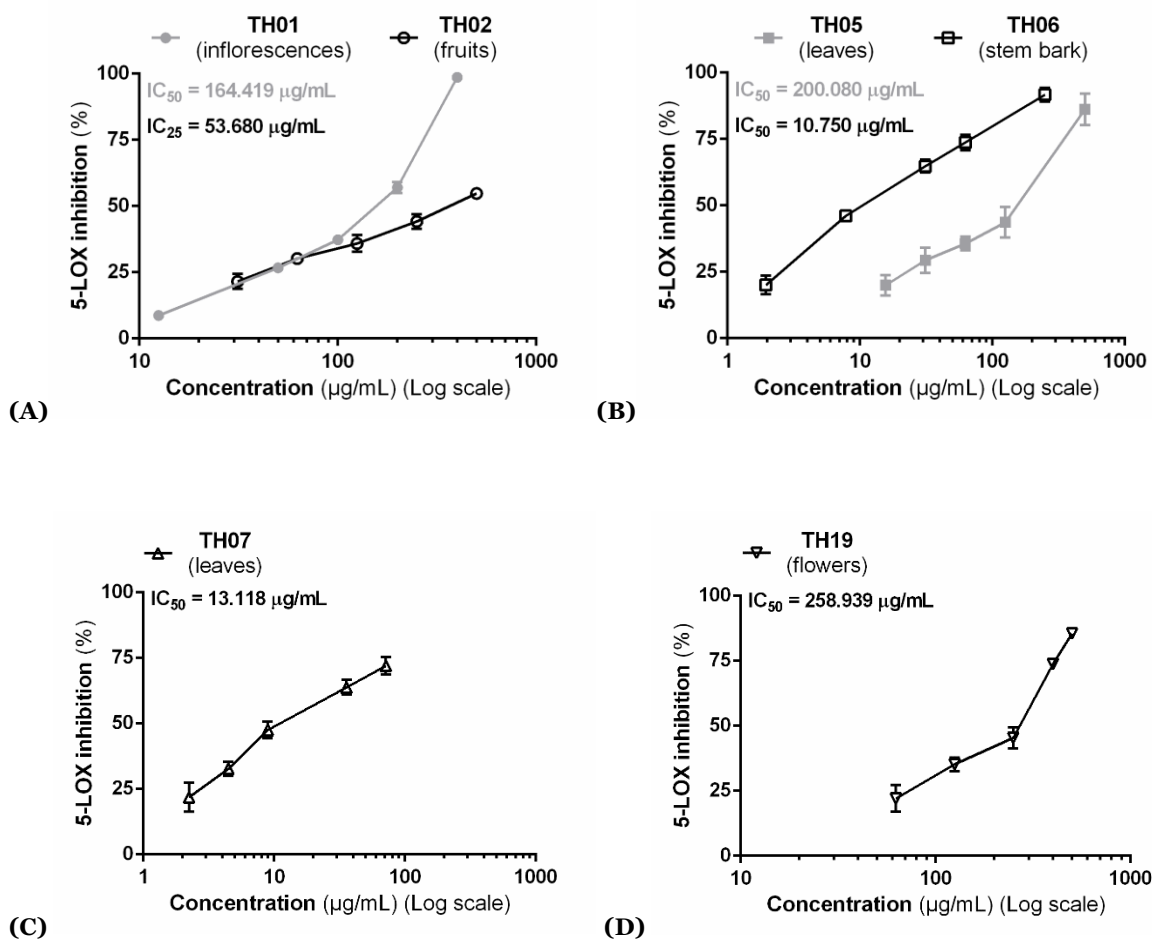


Figure 33. 5-LOX inhibition caused by the methanol extracts obtained from the inflorescences (TH01) and fruits (TH02) of *C. urens* (A), from the leaves (TH05) and stem bark (TH06) of *F. curtipes* (B), from the leaves (TH07) of *C. tabularis* (C) and from the flowers (TH19) of *G. gracillima* (D). Results represent the mean \pm SEM of three experiments, each performed in triplicate.

Finally, the analysis of the antiradical potential of the medicinal species revealed that a higher DPPH \cdot scavenging activity was recorded with the methanol extracts obtained from the stem barks, *S. siamensis* (TH11, IC₅₀ = 5.872 µg/mL) being the most active plant, followed by *F. curtipes* (TH06, IC₅₀ value of 14.658 µg/mL) and *C. formosum* (TH13, IC₅₀ = 18.687 µg/mL) (Table 5, Figure 34). Nevertheless, the recorded DPPH \cdot scavenging activity was not significantly higher than the one displayed by the reference antioxidant compound, ascorbic acid (IC₅₀ = 6.678 µg/mL). Relevantly, the extracts obtained from the leaves were more active than those obtained from the stem bark only for *C. adansonii* and *C. tabularis* (Table 5). Furthermore, the radical scavenging activity was concentration-dependent for all samples, with the exception of extract TH04, which maximum scavenging activity recorded was ca. 15% (Table 5).

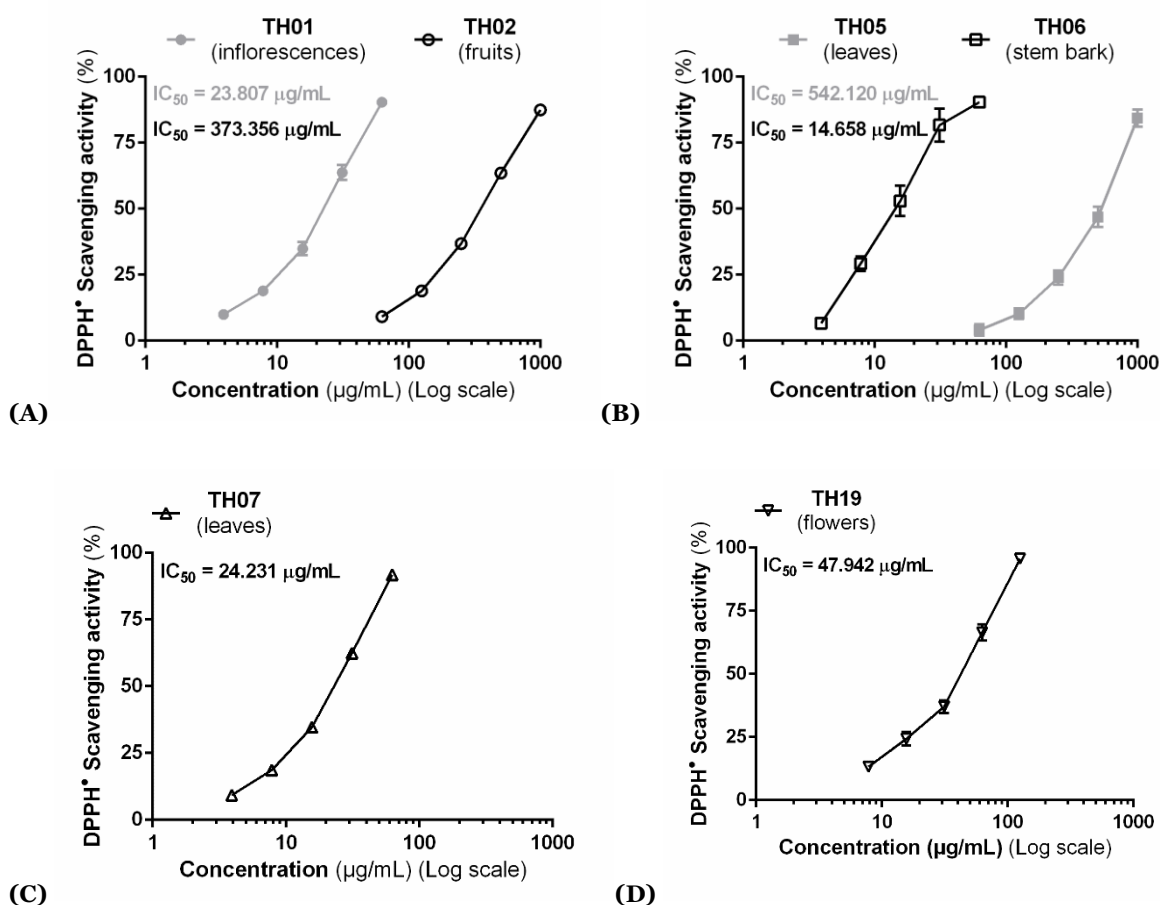


Figure 34. DPPH• scavenging activity displayed by the methanol extracts obtained from the inflorescences (TH01) and fruits (TH02) of *C. urens* (A), from the leaves (TH05) and stem bark (TH06) of *F. curtipes* (B), from the leaves (TH07) of *C. tabularis* (C) and from the flowers (TH19) of *G. gracillima* (D). Results represent the mean \pm SEM of three experiments, each performed in triplicate.

While reported by Rathinavel and colleagues that methanol and chloroform extracts prepared from *C. adansonii* leaves exhibited a potent α -glucosidase inhibitory activity (IC_{50} values of 112.25 and 87.96 $\mu\text{g/mL}$, respectively) (183), this effect was not observed with our sample, not even at the highest tested concentration (500 $\mu\text{g/mL}$) (**Table 5**). Besides, and even though not detected by us, significant DPPH• scavenging effects are reported ($IC_{50} = 72.50 \mu\text{g/mL}$) (184). Such differences may be related with phytogeographic conditions. In addition, and in agreement with our findings, Arsakit and co-workers also evidenced significant α -glucosidase inhibitory effects with extracts obtained from the leaves ($IC_{50} = 45.0 \mu\text{g/mL}$) and from the stems ($IC_{50} = 31.10 \mu\text{g/mL}$) of *C. formentosum* (185). In the same way, pronounced DPPH• scavenging effects were previously recorded with an aqueous extract obtained from the leaves ($IC_{50} = 3.63 \mu\text{g/mL}$) (186). Even though the anti-inflammatory effects *C. formosum* have already being investigated in LPS-stimulated macrophages (186,187), 5-LOX inhibitory capacity (**Table 5**) remained to be investigated.

On *C. arborea* most available studies deal with extracts obtained from the bark, evidencing its anti-inflammatory (187), antioxidant (188), antimicrobial (188) and antidiarrhoeal (189) properties. However, investigations on the biologic effects of the leaves and wood are seldom found. Still, in agreement with our results (**Table 5**), previously a leaf extract moderately inhibited α -glucosidase activity ($IC_{50} = 210 \mu\text{g/mL}$) (190) and exhibited significant DPPH \cdot scavenging effects ($IC_{50} = 78.10 \mu\text{g/mL}$) (191). DPPH \cdot scavenging effects have also been earlier reported for *C. urens* (131), *C. tabularis* (159), *J. gendarussa* (192) and *H. oxirens* (193). Nonetheless, for the remaining species, namely *F. curtipes*, *C. tabularis*, *D. decandra*, *S. siamensis*, *A. xylocarpa*, and *G. gracillima*, this is, as far as we know, the first study dealing with their bioactive effects.

Having now an overview on the biological potential of the plant materials, some criteria were employed to tune and prioritize samples for further studies. Therefore, based on the preliminary screening, the two plant materials with greater α -glucosidase inhibitory capacity (the inflorescences of *C. urens*, TH01, and the flowers of *G. gracillima*, TH19) were studied in more detail (**Figure 32**). These plant materials also displayed a significant DPPH \cdot scavenging capacity (IC_{50} values of $23.807 \mu\text{g/mL}$ and $44.958 \mu\text{g/mL}$, respectively) and a moderate 5-LOX inhibitory activity (IC_{50} values of $164.419 \mu\text{g/mL}$ and $258.939 \mu\text{g/mL}$, respectively) (**Table 5**). Moreover, another selection criterion, based on 5-LOX inhibitory activity, was also applied. In this regard, the methanol extracts obtained from the stem bark of *F. curtipes* (TH06, $IC_{50} = 10.750 \mu\text{g/mL}$) and from the leaves of *C. tabularis* (TH07, $IC_{50} = 13.118 \mu\text{g/mL}$) were also selected for additional studies (**Table 5, Figure 33**). Both extracts also exhibited a noteworthy α -glucosidase inhibitory activity ($IC_{50} = 9.261 \mu\text{g/mL}$ and $21.124 \mu\text{g/mL}$, respectively) and DPPH \cdot scavenging capacity (IC_{50} values of $14.658 \mu\text{g/mL}$ and $24.231 \mu\text{g/mL}$, respectively) (**Table 5**). Finally, the fruits of *C. urens* (TH02) and the leaves of *F. curtipes* (TH05), despite of appearing biologically less promising, were also considered due to chemotaxonomic criteria.

To sum up, the extracts obtained from the inflorescences (TH01) and fruits (TH02) of *C. urens*, from the leaves (TH05) and stem bark (TH06) of *F. curtipes*, from the leaves of *C. tabularis* (TH07) and from the flowers of *G. gracillima* (TH19) were selected for the next metabolic and biologic studies in current dissertation (**Figures 32, 33 and 34**). Their phenolic profile was characterized and their antidiabetic, anti-inflammatory and antioxidant properties were investigated in cell-free and cell-based *in vitro* models.

3.2. Characterization of the phenolic profile of the selected species

One of the primary objectives of the current work was to disclose the phenolic profile of the selected plant materials, to provide a chemical fingerprint of the extracts that may be applied on their future authentication and quality control. Additionally, the characterization of the phenolic constituents was performed also aiming to identify some possible bioactives that may have a role on the biological effects studied. Hence, the selected extracts (TH01, TH02, TH04, TH05, TH06, TH07 and TH19) were analysed by HPLC-DAD-ESI/MSⁿ and UPLC-ESI-QTOF/MS. Quantitative analysis was carried out by HPLC-DAD.

3.2.1. *C. urens*

3.2.1.1. HPLC-DAD-ESI/MSⁿ qualitative analysis

HPLC-DAD-ESI/MSⁿ analysis of the methanol extracts obtained from inflorescences (TH01) and fruits (TH02) allowed the structural elucidation of the phenolic constituents. As evidenced on the HPLC-UV chromatogram (**Figure 35**), six peaks were detected on the inflorescences and nine on the fruits, all sharing a similar UV spectrum (~ 300 sh, 324 nm) characteristic of hydroxycinnamic acids.

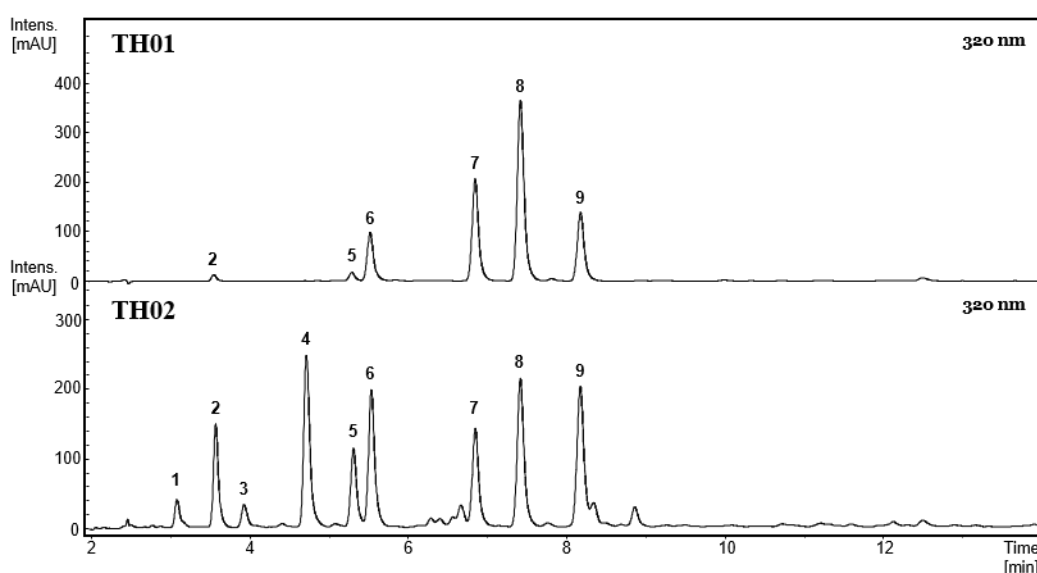


Figure 35. HPLC-UV (320 nm) chromatogram of the methanol extracts prepared from the inflorescences (TH01) and fruits (TH02) of *C. urens*. Peaks: (1) caffeoyl-di-hexosyl-C₁₁H₁₅O₆ isomer, (2) 3-*O*-caffeoylquinic acid, (3) caffeoyl-di-hexosyl-C₁₁H₁₅O₆ isomer, (4) caffeoyl-hexosyl-C₁₁H₁₅O₆, (5) 4-*O*-caffeoylquinic acid, (6) 5-*O*-caffeoylquinic acid, (7) 3-*O*-caffeoylshikimic acid, (8) 4-*O*-caffeoylshikimic acid, (9) 5-*O*-caffeoylshikimic acid.

Analysis of the MS spectra revealed that compounds **2**, **5** and **6** have the same deprotonated molecular ion at m/z 353.0873 (molecular formula $C_{16}H_{18}O_9$) and MS fragmentation characteristic of caffeoylquinic acids, with ions at m/z 191 [quinic acid - H]⁻, 179 [caffeic acid - H]⁻ and 173 [quinic acid - H-18]⁻ (**Table 6**). These structural isomers can be easily distinguished by their fragmentation patterns. According to Clifford et al., the relative abundance of the ions from the MS fragmentation indicates that **2**, having the ion at m/z 191 as base peak and another ion at m/z 179 (30%), corresponds to 3-*O*-caffeoylquinic acid, while **6**, with the same base peak, though minor abundance of the ion at m/z 179 (2%), is 5-*O*-caffeoylquinic acid, and **5**, with the base peak at m/z 173, is 4-*O*-caffeoylquinic acid (**Table 6**) (194). Comparison with authentic standards unequivocally confirmed the identity of **2**, **5** and **6**.

Compounds **7-9** exhibited deprotonated molecular ions (m/z 335.0772) 18 amu lower than the previous caffeoylquinic acid derivatives and, therefore, their molecular formula is $C_{16}H_{16}O_8$. In their MS fragmentations ions deriving from caffeic acid (m/z 179 and 135) were found, suggesting that these compounds correspond to esters of caffeic acid, in this case with shikimic acid. Hence, compounds **7-9** are caffeoylshikimic acid isomers, probably derivatives of the caffeoylquinic acids above described; according to their reverse phase mobility they could tentatively be labelled as 3-*O*-caffeoylshikimic acid (**7**), 4-*O*-caffeoylshikimic acid (**8**) and 5-*O*-caffeoylshikimic acid (**9**) (**Figure 36**). Comparison with an authentic standard unequivocally confirmed the identity of **8** as 4-*O*-caffeoylshikimic acid.

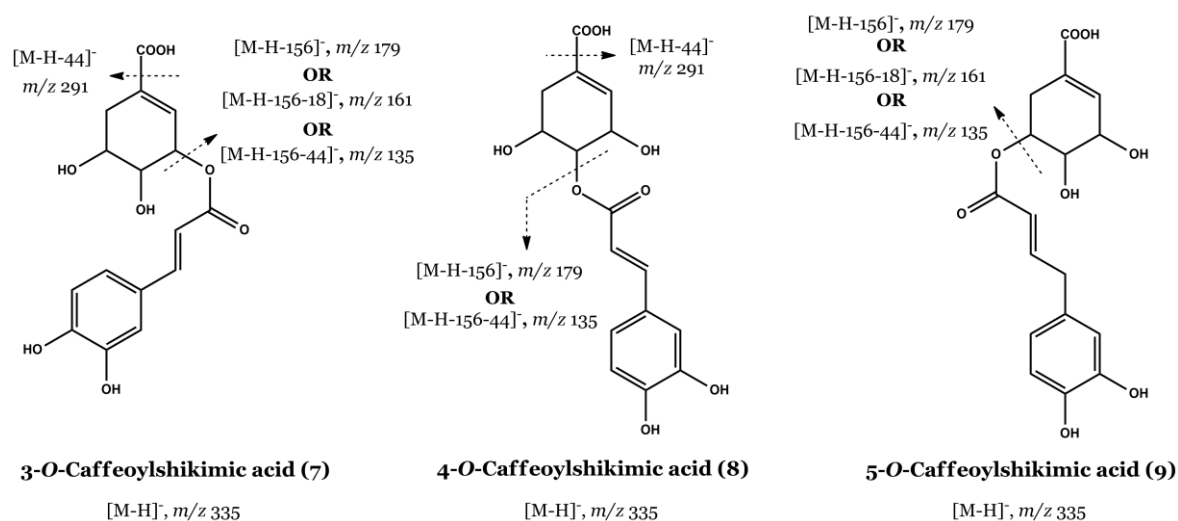


Figure 36. MS fragmentation pattern of the *O*-caffeoylshikimic acid isomers identified in *C. urens* methanol extracts.

Compounds **1**, **3** and **4** were detected just in the extract obtained from the fruits (TH02). Their MS fragmentation shows sequential losses of fragments of 162 amu until obtaining an ion at m/z 243 amu (**Table 6**, **Figure 35**). Compound **4** presents the deprotonated molecular ion at m/z 567.1710 (molecular formula $C_{26}H_{32}O_{14}$) and losses of two fragments of 162 amu. According to its UV spectrum (~ 300 sh, 324 nm) (**Table 6**), one of those fragments must correspond to a caffeoyl radical, while the other is likely to be a glycosyl (hexosyl) radical because of its reverse phase mobility. The deprotonated molecular ions of **1** and **3** (m/z 729.2252) are 162 amu higher than that of compound **4** and their reverse phase mobility, as well as their molecular formula, indicate the presence of an additional hexose. In the MS^n ($n=2-4$) fragmentation of **1** and **3** (data from **Table 6**), as well as in the MS analysis of **3** (**Figure 37**), the sequential losses of the 162 amu fragments indicated above are observed. Therefore, **1**, **3** and **4** are caffeoyl-hexosyl derivatives of a compound with deprotonated molecular ion at m/z 243 (molecular formula $C_{11}H_{16}O_6$), which MS fragmentation (MS^5 [243] $^-$; **Figure 37**) does not present any characteristic ion allowing their identification. As so, these compounds were labelled as caffeoyl-di-hexosyl- $C_{11}H_{15}O_6$ isomers (**1** and **3**) and caffeoyl-hexosyl- $C_{11}H_{15}O_6$ (**4**).

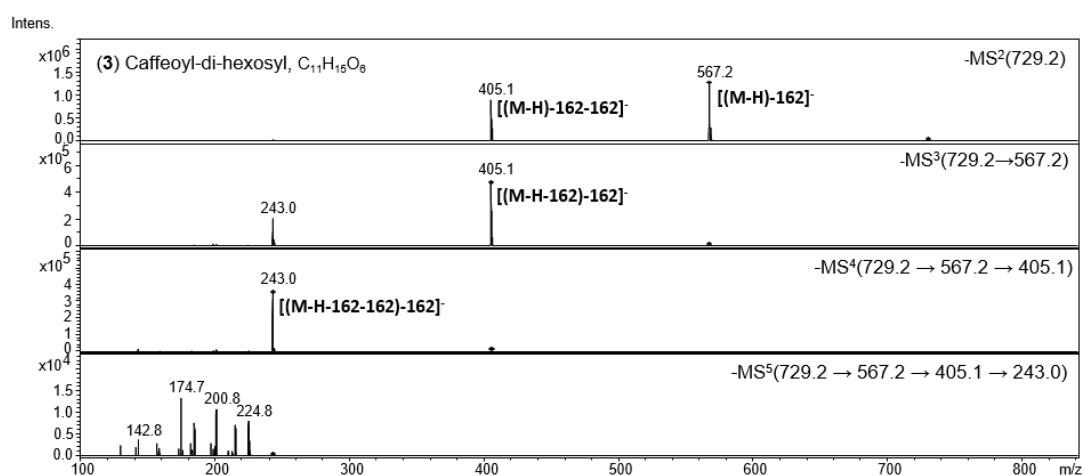


Figure 37. MS^2 [(M-H)] $^-$, MS^3 [(M-H)→(M-H-162)] $^-$, MS^4 [(M-H)→(M-H-162)→(M-H-162-162)] $^-$, and MS^5 [243] $^-$ analysis of caffeoyl-di-hexosyl- $C_{11}H_{15}O_6$ (**3**) detected in the methanol extract obtained from *C. urens* fruits (TH02).

Considering that the initial extract obtained from the inflorescences of *C. urens* (TH01) was not enough to perform all the assays intended, additional inflorescences samples were obtained, from the same tree, four years after (April 2019). A second methanol extract was posteriorly prepared from the new fresh material (TH21) and the identity of the phenolic compounds was confirmed by HPLC-DAD through comparison with the spectral data of the former sample (TH01). Regardless the peaks intensity, the chromatogram overlapped the

previous one and, as before, the same hydroxycinnamic acid derivatives (compounds **4**, **5**, **6**, **7**, **8** and **9**) were detected on the methanol extract labelled as TH21.

3.2.1.2. HPLC-DAD quantitative analysis

Calibration curves were used for the quantitation of six and nine phenolic compounds on the methanol extracts obtained from the inflorescences (TH01 and TH02) and from the fruits (TH02) of *C. urens*, respectively (**Table 7**). While qualitatively poorer, the extract prepared from the inflorescences, was 3-fold (first collection, TH01) and 19-fold (second collection, TH21) richer in phenolics than the one prepared from the fruits (TH02) (**Table 7**). Also, and despite of the qualitative similarity, the extracts obtained from the inflorescences of kitul, TH01 and TH21, unveiled marked quantitative differences, extract TH21 being 6 times richer in phenolic constituents than TH01 (**Table 7**). Worth recalling that the inflorescences were collected not only in distinct years (2018 for TH01 and 2019 for TH21), but also in distinct seasons (winter for TH01 and spring for TH21) (**Table 3**), which might justify the different quantities of phenolics detected here. In fact, it is known that abiotic environmental conditions, such as temperature, humidity and radiation, which differ over the years and seasons, can affect plants metabolic pathways, influencing their metabolic profiles (195). Moreover, as previously demonstrated by others (196,197), the phenolic content can also vary according to the maturation stage of the plant, which might also account for the quantitative discrepancies observed. Still, even considering the distinct environmental conditions and maturation stages noticed at the time of collection, the phenolic profile of *C. urens* inflorescences did not exhibit a marked variation in terms of phenolic profile.

The caffeoylshikimic acid derivatives (**7**, **8** and **9**) represented the major fraction of phenolic compounds detected on the inflorescences (*ca.* 88% and 73% of the total quantifiable phenolics on TH01 and TH21, respectively), while the proportion of caffeoylshikimic acid derivatives and caffeoylquinic acid derivatives (**1**, **2**, **3**, **4**, **5** and **6**) was identical in the fruits (**Table 7**). 4-*O*-Caffeoylshikimic acid (**8**) was the main hydroxycinnamic acid present in all samples, being detected at growing concentrations in extracts TH02 ($2\,027.80 \pm 60.30$ mg/kg of dry extract), TH01 ($17\,783.22 \pm 608.30$ mg/kg of dry extract) and TH21 ($88\,384.71 \pm 1\,063.28$ mg/kg of dry extract) (**Table 7**). 3-*O*-Caffeoylshikimic acid (**7**) was the second major phenolic found in TH01 ($7\,462.53 \pm 127.13$ mg/kg of dry extract), its isomer, 5-*O*-caffeoylshikimic acid (**9**), being the second component in extract TH21 ($41\,904.30 \pm 1\,702.123$ mg/kg of dry extract) (**Table 7**). Also,

Table 6. Retention time (*Rt*), molecular formula (M), [M-H]⁻ and MS²[M-H]⁻ data for the hydroxycinnamic acids detected on the methanol extracts obtained from the inflorescences (TH01) and from the fruits (TH02) of *C. urens*.^a

	Compounds	<i>Rt</i> (min)	Formula (M)	[M-H] ⁻ , <i>m/z</i>	MS ² [M-H] ⁻ , <i>m/z</i> (%)
1	Caffeoyl-di-hexosyl-C ₁₁ H ₁₅ O ₆ isom.	3.1	C ₃₂ H ₄₂ O ₁₉	729.2257	567(70), 405(100) ^b , 243(30)
3	Caffeoyl-di-hexosyl-C ₁₁ H ₁₅ O ₆ isom.	3.9	C ₃₂ H ₄₂ O ₁₉	729.2252	567(100) ^c , 405(65)
4	Caffeoyl-hexosyl-C ₁₁ H ₁₅ O ₆	4.7	C ₂₆ H ₃₂ O ₁₄	567.1710	405(100) ^b , 243(30)
2	3- <i>O</i> -Caffeoylquinic acid	3.5	C ₁₆ H ₁₈ O ₉	353.0871	191(100), 179(30), 135(6)
5	4- <i>O</i> -Caffeoylquinic acid	5.3	C ₁₆ H ₁₈ O ₉	353.0875	191(7), 179(27), 173(100), 135(7)
6	5- <i>O</i> -Caffeoylquinic acid	5.5	C ₁₆ H ₁₈ O ₉	353.0873	191(100), 179(2)
7	3- <i>O</i> -Caffeoylshikimic acid	6.8	C ₁₆ H ₁₆ O ₈	335.0772	291(25), 179(100), 161(70), 135(45)
8	4- <i>O</i> -Caffeoylshikimic acid	7.4	C ₁₆ H ₁₆ O ₈	335.0774	291(20), 179(100), 135(25)
9	5- <i>O</i> -Caffeoylshikimic acid	8.2	C ₁₆ H ₁₆ O ₈	335.0771	179(100), 161(6), 135(20)

^a Main observed fragments; other ions were detected, but they were not included because they were not significant. Isom: isomer.

^b **1** MS³(729→405): 243(100); **4** MS³(567→405): 243(100).

^c **3** MS³(729→567): 405(100), 243(45); MS⁴(729→567→405): 243(100).

Table 7. Content of phenolic compounds detected on the methanol extracts obtained from the inflorescences (TH01 - first collection, and TH21 - second collection) and from the fruits (TH02) of *C. urens* (mg/kg dry extract). Results correspond to mean ± SD (n = 3).

	Compounds	TH01	TH02	TH21
1	Caffeoyl-di-hexosyl-C ₁₁ H ₁₅ O ₆ isom.	Not detected	83.58 ± 14.95	Not detected
3	Caffeoyl-di-hexosyl-C ₁₁ H ₁₅ O ₆ isom.	Not detected	96.34 ± 8.55	Not detected
4	Caffeoyl-hexosyl-C ₁₁ H ₁₅ O ₆	Not detected	2 090.15 ± 58.51	Not detected
2	3- <i>O</i> -Caffeoylquinic acid	594.20 ± 30.01	1 209.93 ± 18.04	2 452.87 ± 89.18
5	4- <i>O</i> -Caffeoylquinic acid	1051.44 ± 89.46	954.60 ± 25.84	31 375.46 ± 619.97
6	5- <i>O</i> -Caffeoylquinic acid	2 657.44 ± 220.82	1 808.53 ± 107.93	24 062.73 ± 1 363.44
7	3- <i>O</i> -Caffeoylshikimic acid	7 462.53 ± 127.13	1 229.07 ± 41.74	29 312.15 ± 1 438.794
8	4- <i>O</i> -Caffeoylshikimic acid	17 783.22 ± 608.30	2 027.80 ± 60.30	88 384.71 ± 1 063.28
9	5- <i>O</i> -Caffeoylshikimic acid	5 990.04 ± 535.10	1 591.57 ± 92.35	41 904.30 ± 1 702.123
	TOTAL	35 538.9 ± 1 610.82	11 091.57 ± 4 82.21	217 492.22 ± 6 276.79

the amount of 5-*O*-caffeoylquinic acid (**5**) ($31\,375.46 \pm 619.97$ mg/kg of dry extract) was higher on the second collection of *C. urens* inflorescences (TH21), this hydroxycinnamic acid being the third more abundant phenolic (**Table 7**). Finally, it should be noted that, considerable amounts of caffeoyl-hexosyl derivatives (non-detected on the methanol extracts obtained from the inflorescences, TH01 and TH21) were quantitated on the fruits (TH021, 2270.07 ± 82.01 mg/Kg dry extract), corresponding to 20.5% of the total phenolic content (**Table 7**).

In agreement with the current observations, El-Akad and colleagues detected a series of phenolic acids, including caffeoylquinic acid and caffeoylshikimic acid isomers, in the leaves and fruits of *C. urens*, collected in the Egypt (143). However, those authors have also encountered several flavonoids, particularly flavonols-*O*-sophorosides, which were not detected in none of our samples. Additionally, Ma and colleagues reported the occurrence of a series of phenolic constituents on the fruits of the plant (collected in Australia), namely ferulic acid, protocatechuic acid, 4-hydroxybenzoic acid, quercetin, quercetin-3-*O*-glucoside and kaempferol-3-*O*-glucoside. Yet, these constituent were also not present on our samples (129). In fact, as above mentioned, such discrepancies might be related with the different phytogeographic conditions of the samples, which are known to affect the phenolic profile (195). Even though several phenolic constituents have been already identified on kitul leaves and fruits, this is, as far as we are aware, the first work disclosing the phenolic fingerprint of the edible inflorescences.

3.2.2. *F. curtipes*

3.2.2.1. HPLC-DAD-ESI/MSⁿ qualitative analysis

HPLC–DAD–ESI/MSⁿ analysis of the methanol extracts obtained from the leaves (TH05) and from the stem bark (TH06) of *F. curtipes* allowed the identification of three and twenty-one compounds, respectively (**Figure 38**). While only apigenin derivatives were found on the methanol extract obtained from the leaves (TH05) (**Figure 38A**), the extract obtained from the stem bark (TH06) was also characterized by the occurrence of cinnamic acid derivatives and polymeric flavan-3-ols (**Figure 38B**).

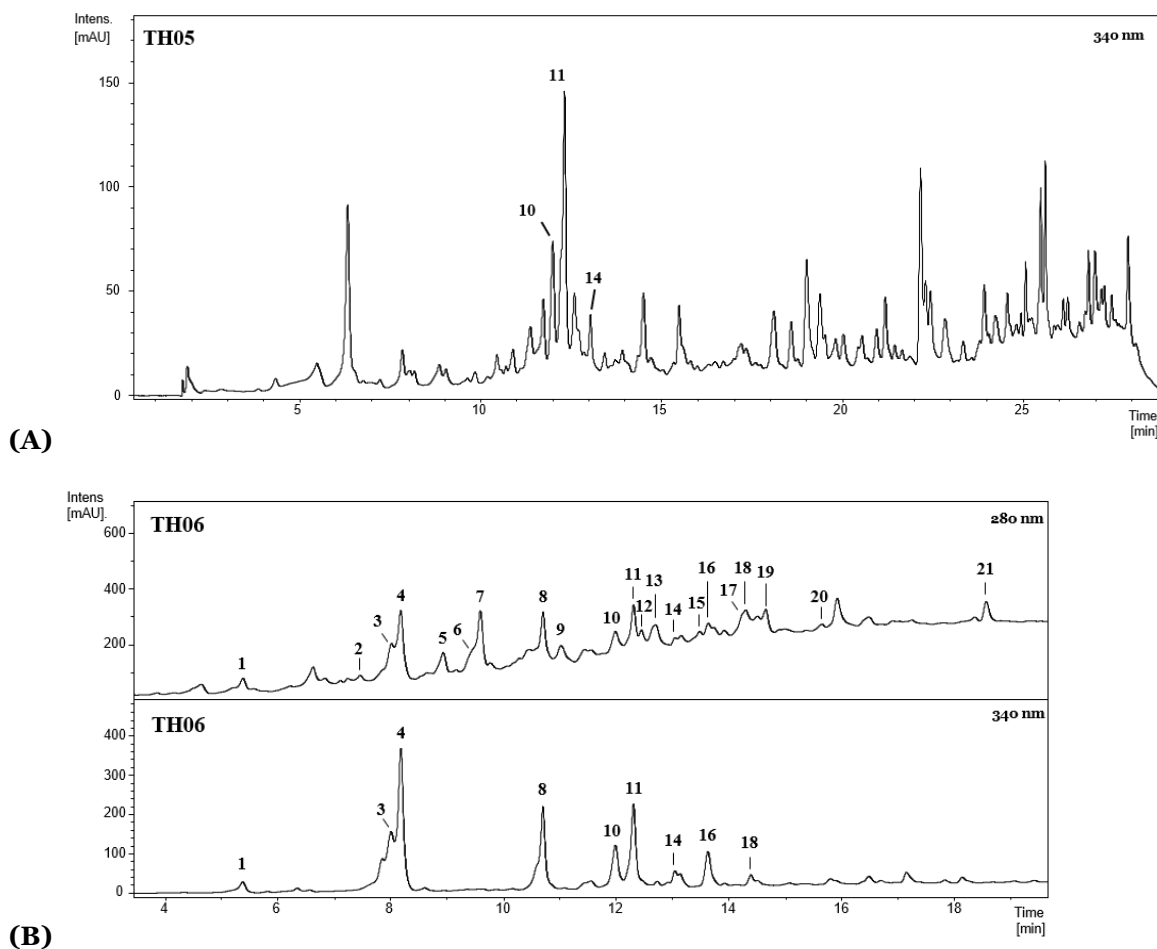


Figure 38. HPLC-UV chromatograms of the methanol extracts obtained from the leaves (TH05, A) and from the stem bark (TH06, B) of *F. curtipes*. Peaks: (1) 3-*O*-caffeoylquinic acid, (2) catechin, (3) 5-*O*-caffeoylquinic acid isomer, (4) 5-*O*-caffeoylquinic acid, (5) procyanidin type B, (6) catechin/epicatechin derivative, (7) epicatechin, (8) vicenin-2, (9) procyanidin type C, (10) apigenin-7-*O*-hexoside-6/8-*C*-hexoside, (11) apigenin-6-*C*-pentoside-8-*C*-hexoside, (12) cinchonain type II, (13) cinchonain type II, (14) apigenin-6-*C*-hexoside-8-*C*-pentoside, (15) cinchonain type I, (16) vitexin, (17) procyanidin type B, (18) isovitexin, (19) aviculin, (20) cinchonain type I, (21) cinchonain type I.

3.2.2.1.1. Hydroxycinnamic acids

Compounds **1**, **3** and **4** here detected have a characteristic UV spectrum of caffeoylquinic acids (300 sh, 326 nm) and have all the same deprotonated molecular ion at m/z 353.0878 ($C_{16}H_{18}O_9$) (**Figure 38B**). MS fragmentation of these compounds revealed a base peak at m/z 191; however, while in compounds **3** and **4** the ion at m/z 179 was weak or undetectable, a high relative abundance (50%) of this ion was observed in **1**. Thus, according to Clifford et al., compound **3** can be labelled as a chlorogenic acid isomer (194), while compounds **1**

and **4**, chromatographically matching with the authentic standards, can be unequivocally identified as 3-*O*-caffeoylquinic acid and 5-*O*-caffeoylquinic acid, respectively.

3.2.2.1.2. Apigenin derivatives

According to the MS analysis, compounds **8**, **10**, **11**, **14**, **16** and **18** (**Figure 38**) exhibit an UV spectrum of apigenin derivatives (272, 336 nm) with 6' and/or 8' substitutions, corresponding to *C*-glycosyl derivatives. Compounds **16** and **18** exhibited a deprotonated molecular ion at m/z 431.0977 and their MS fragmentations revealed mono-*C*-glycosylflavones with characteristic ions at m/z 341 ($X^{0.3}$) (aglycone+71) and 311 ($X^{0.2}$) (aglycone+41) (**Table 8**, **Figure 38**), matching their apigenin aglycone, thus allowing to identify these compounds as apigenin-6/8-*C*-hexosides (198). The higher reverse phase mobility (**Table 8**) and relative abundance of the ion m/z 341 in compound **18**, comparing to **16** (30% *vs* 3%), as well as the occurrence of the $[(M-H)-18]^-$ ion in **18** and its absence in **16** (data not shown), indicates that the *C*-glycosylation in compound **16** occurs at position 8, while in **18** it occurs at position 6. Thus, considering that the hexose corresponds to glucose, these compounds can be labelled as apigenin-8-*C*-glucoside (vitexin) (**16**) and apigenin-6-*C*-glucoside (isovitexin) (**18**) (**Figure 39**). Comparison with commercial standards confirmed the previous structure elucidation, allowing to unequivocally identify **16** and **18** as vitexin and isovitexin, correspondingly.

The $[M-H]^-$ of compound **10** at m/z 593.1506 is characteristic of a diglycoside. As previously mentioned, ions 341 and 311, observed in MS fragmentation, are typical of apigenin-mono-*C*-glycosides, ions observed at m/z 503 $[(M-H)-90]^-$ and 473 $[(M-H)-120]^-$ being both representative of a *C*-hexoside MS fragmentation. Additionally, the loss of a 162 amu fragment and the absence of -180 (**Table 8**) indicate the presence of another hexoside, now linked to a phenolic hydroxyl (199). Consequently, compound **10** can certainly correspond to an apigenin-*O*-hexoside-*C*-hexoside. While *O*-glycosylation generally occurs at position 7, *C*-glycosylation can appear either at position 6 or 8; thus, compound **10** can be labelled as apigenin-7-*O*-hexoside-6/8-*C*-hexoside, corresponding, in the case of glucose being the hexose, to apigenin-7-*O*-glucoside-6/8-*C*-glucoside (isovitexin-7-*O*-glucoside or vitexin-7-*O*-glucoside) (**Figure 39**).

Unlike the previously described apigenin derivatives, which were only detected on the methanol extract from the stem bark (TH06), compound **10** was detected in both extracts (TH05 and TH06) (**Figure 38**). Despite having the same $[M-H]^-$ as **10**, compound **8** did not exhibit representative ions of mono-*C*-glycosyl flavonoids (aglycone +71/+41),

Table 8. Retention time (*Rt*), molecular formula (M) and MS [M-H]⁻ and MS²[M-H]⁻ data for the apigenin derivatives detected in the methanol extract obtained from the leaves (TH05) and from the stem bark (TH06) of *F. curtipes*.^a

Compounds	<i>Rt</i> (min)	Formula (M)	[M-H] ⁻ <i>m/z</i>	MS ³ [M-H] ⁻ , <i>m/z</i> (%)							
				-60	-90	-120	-162	Agl ^b +113	Agl ^b +83	Agl ^b +71	Agl ^b +41
8	10.7	C ₂₇ H ₃₀ O ₁₅	593.1508	533(2)	503(30)	473(100)		383(45)	353(80)		
10	12.0	C ₂₇ H ₃₀ O ₁₅	593.1506		503(2)	473(30)	431(60)			341(15)	311(100)
11	12.3	C ₂₆ H ₂₈ O ₁₄	563.1396	503(15)	473(80)	443(100)		383(65)	353(90)		
14	13.0	C ₂₆ H ₂₈ O ₁₄	563.1402	503(7)	473(85)	443(50)		383(75)	353(100)		
16	13.6	C ₂₁ H ₂₀ O ₁₀	431.0980							341(3)	311(100)
18	14.3	C ₂₁ H ₂₀ O ₁₀	431.0974							341(30)	311(100)

^aMain observed fragments. ^bAgl, aglycone.

Table 9. Retention time (*Rt*), molecular formula (M) and MS [M-H]⁻ and MS²[M-H]⁻ data for the flavan-3-ols derivatives detected in the methanol extract obtained from the leaves (TH05) and from the stem bark (TH06) of *F. curtipes*.

Compounds	<i>Rt</i> (min)	Formula (M)	[M-H] ⁻ <i>m/z</i>	MS ³ [M-H] ⁻ <i>m/z</i> (%)
2	7.4	C ₁₅ H ₁₄ O ₆	289.0717	245(100), 205(50)
5	8.9	C ₃₀ H ₂₆ O ₁₂	577.1345	425(100), 407(80), 289(25)
6	9.4	C ₁₅ H ₁₄ O ₆	289.0714	245(100), 205(35)
7	9.6	C ₁₅ H ₁₄ O ₆	289.0714	245(100), 205(30)
9	11.0	C ₄₅ H ₃₈ O ₁₈	865.1988	695(100), 577(90), 425(60), 407(60), 287(30)
12	12.4	C ₃₉ H ₃₂ O ₁₅	739.1651	587(100), 569(25), 435(65), 417(40), 339(30), 289(20)
13	12.6	C ₃₉ H ₃₂ O ₁₅	739.1678	587(100), 569(30), 435(50), 417(10), 339(30), 289(15)
15	13.4	C ₂₄ H ₂₀ O ₉	451.1020	341(10)
17	14.3	C ₃₀ H ₂₆ O ₁₂	577.1347	425(100), 407(70), 289(30)
20	15.6	C ₂₄ H ₂₀ O ₉	451.1026	341(100)
21	18.5	C ₂₄ H ₂₀ O ₉	451.1024	341(10)

displaying instead ions of aglycone +113/83 (m/z 383/353), typically found in di-*C*-glycosylflavones (198). Ions from *C*-hexoside fragmentation (-60/-90/-120) were also found, suggesting that **8** corresponds to an apigenin-6,8-di-*C*-hexoside. Comparison with an authentic standard allowed to unambiguously identify compound **8** as apigenin-6,8-di-*C*-glucoside (vicenin-2) (**Figure 39**).

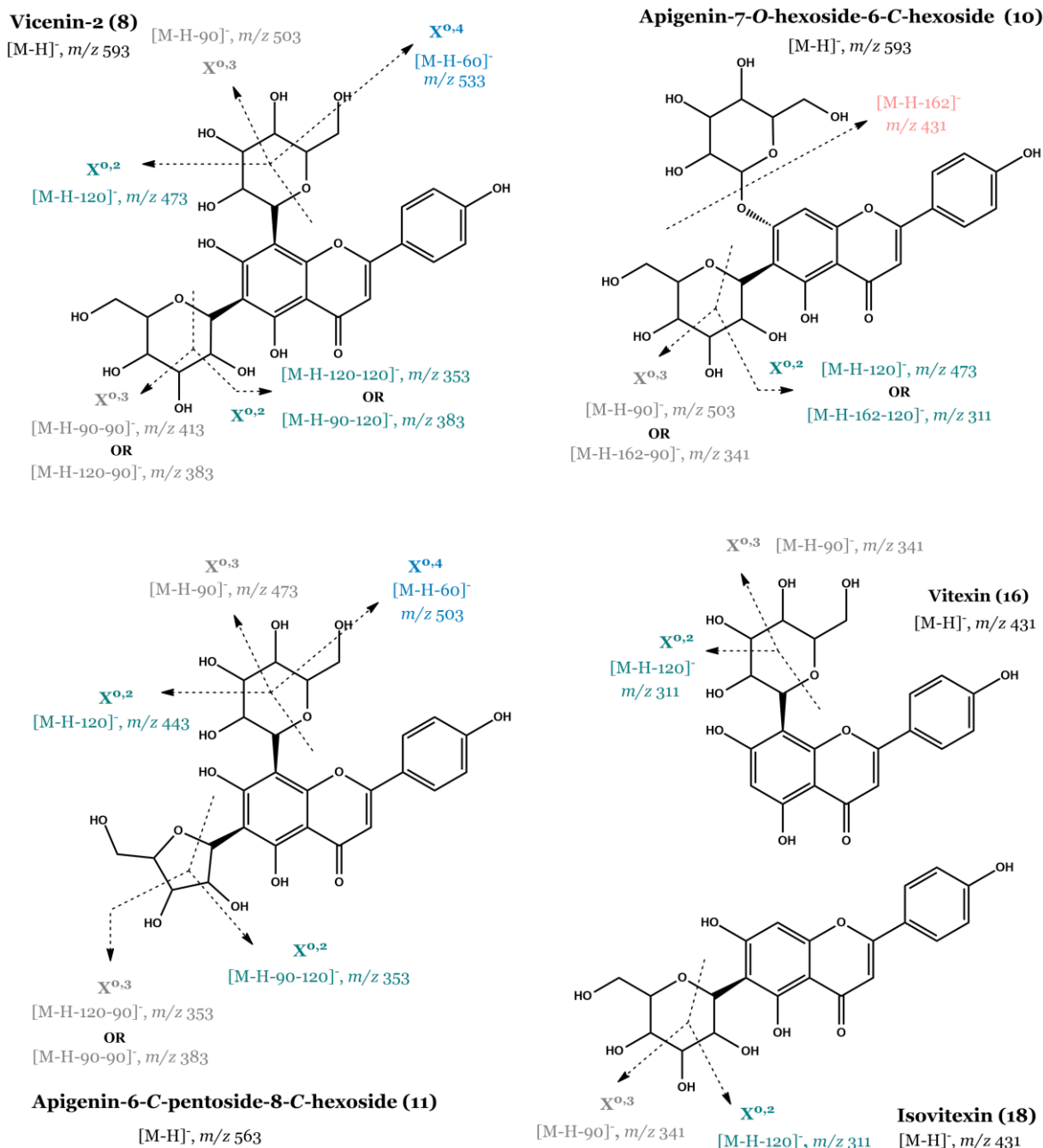


Figure 39. MS fragmentation pattern of some apigenin derivatives detected on the leaves (TH05) and stem bark (TH06) of *F. curtipes*.

Compounds **11** and **14**, sharing the same ions at m/z 383/353 as **8** and having the deprotonated molecular ion (~ 563.1400), correspond to apigenin-di-*C*-glycosides with both hexose and pentose as sugar moieties. In both compounds, the relative abundance of the ion $[(M-H)-60]^-$ is higher than the one found in compound **8**, ion abundance (15%) in compound **11** being higher than in **14** (7%), which discloses the preferential fragmentation position at position 6 in compound **11** (**Figure 39**). Since in reverse phase the elution order of asymmetric di-*C*-glycosylflavones indicates that the 6-*C*-pentosyl-8-*C*-hexosyl elutes before the isomeric 6-*C*-hexosyl-8-*C*-pentosyl (198), **11** can be labelled as apigenin-6-*C*-pentoside-8-*C*-hexoside and **14** as apigenin-6-*C*-hexoside-8-*C*-pentoside. Not only **10**, but also compounds **14** and **11** were detected in the two methanol extracts obtained from *F. curtipes* (TH05 and TH06), while the remaining compounds were solely identified on the extract obtained from the stem bark (TH06).

3.2.2.1.3. Flavan-3-ols

In addition to apigenin derivatives, the extract obtained from the stem bark of *F. curtipes* (TH06) is also characterized by the occurrence of eleven compounds (**2**, **5-7**, **9**, **12**, **13**, **15**, **17**, **20** and **21**) structurally related with flavan-3-ols, with characteristic UV spectrum (λ_{\max} 280 nm). The fragmentation products of their deprotonated molecular ions indicate that these compounds must correspond to monomers, dimers and trimers.

With a $[M-H]^-$ at m/z 289.0714 ($C_{15}H_{14}O_6$), compounds **2**, **6** and **7** have the same MS fragmentation pattern, characteristic of the most common naturally occurring monomers, catechin and epicatechin (**Table 9**). Comparison with authentic standards allowed the unequivocal identification of **2** and **7** as catechin and epicatechin, respectively (**Figure 40**).

Compounds **15**, **20** and **21** ($C_{24}H_{20}O_9$), displaying the same MS fragmentation, are substituted monomers coinciding with cinchonain Ib (a phenylpropanoid linked through a carbon-carbon linkage to the C-8 A-ring of epicatechin) (**Figure 40**). Having the same deprotonated molecular ion ($C_{30}H_{26}O_{12}$) and the same MS fragmentation, compounds **5** and **17** correspond to catechin/epicatechin dimers, being known as type B procyanidins (**Table 9**). Compounds **12** and **13** ($C_{39}H_{32}O_{15}$) share the same MS fragmentation pattern, corresponding to cinchonain II type compounds, structurally related with procyanidin B but having a cinchonain I type similar substitution (a phenylpropanoid moiety on the C-8 position of the flavan superior unit). Furthermore, a catechin/epicatechin trimer ($C_{45}H_{38}O_{18}$) was also identified, procyanidin type C (**9**) (**Figure 40**). Compound **19** (Rt: 14.6

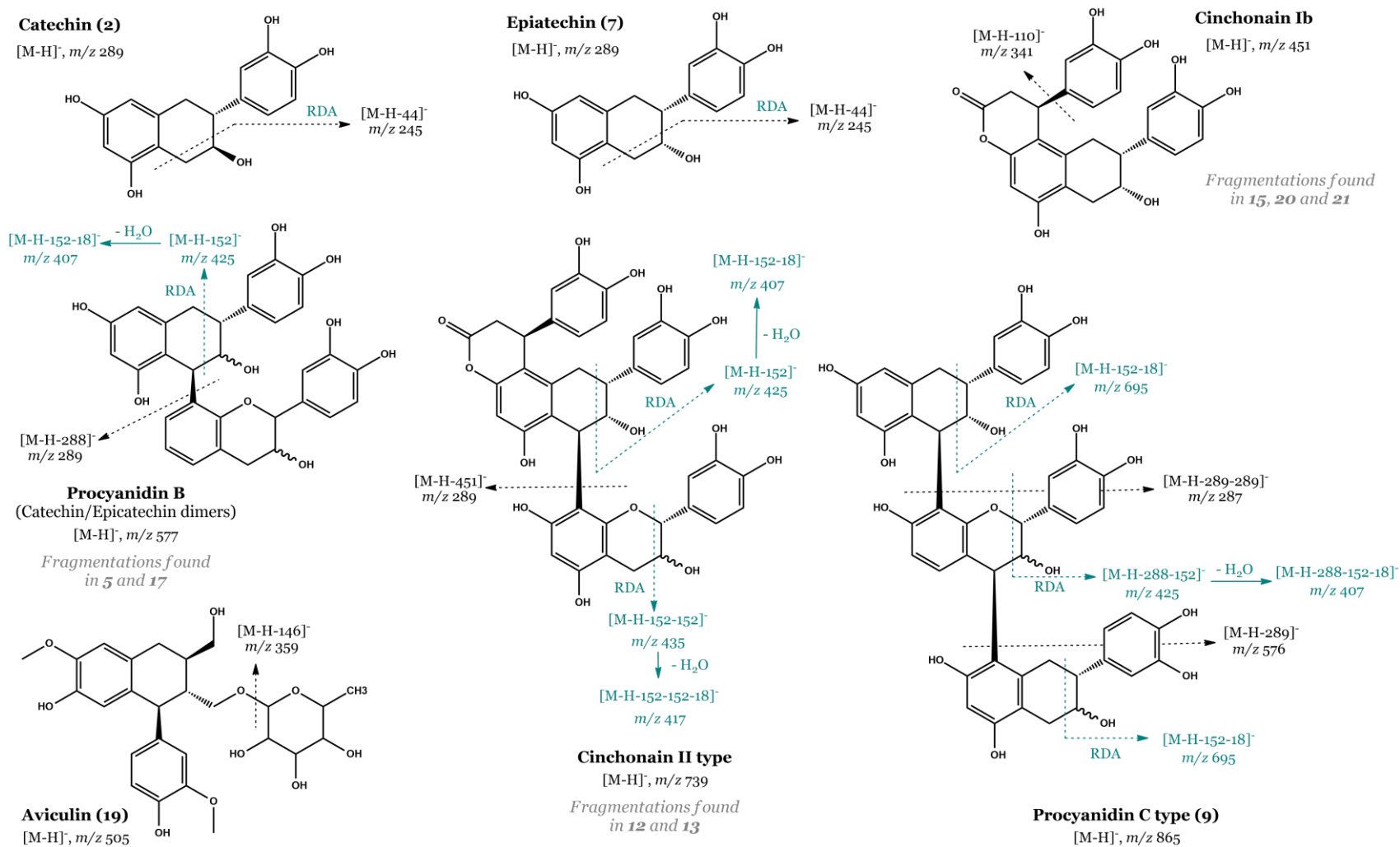


Figure 40. MS fragmentation pattern of some flavan-3-ols derivatives and the lignan aviculin (**19**) detected on the stem bark (TH06) of *F. curtipes*. RDA, Retro-Diels-Alder reaction

min; UV: 282nm; MS, [M-H]⁻: 505.2072, MS²: 359 (100%, -146)) shares the same UV spectrum (C₂₆H₃₄O₁₀) as the previous compounds. In its MS fragmentation it was observed a base peak at *m/z* 359 due to the loss of a rhamnosyl radical (146 amu fragment) (**Figure 40**). This compound matches the structure of aviculin (isolariciresinol rhamnopyranoside), a rhamnoside lignan reported for the first time in *Polygonum aviculare* L. (200).

3.2.2.2. HPLC-DAD quantitative analysis

HPLC-DAD quantitative analysis of the methanol extracts obtained from the leaves (TH05) and stem bark (TH06) was attained using calibration curves, allowing the quantitation of seventeen flavonoids (**2**, **5-18**, **20**, **21**), three hydroxycinnamic acids (**1**, **3**, **4**) and aviculin (**19**) (**Table 10**).

Table 10. Content of phenolic compounds detected on the methanol extracts obtained from the leaves (TH05) and from the stem bark (TH06) of *F. curtipes* (mg/kg dry extract). Results correspond to mean ± SD (n=3).

	Compound	TH05	TH06
Hydroxycinnamic acids			
1	3- <i>O</i> -Caffeoylquinic acid	Not detected	33.79 ± 2.45
3	Chlorogenic acid isomer	Not detected	33.78 ± 2.29
4	5- <i>O</i> -Caffeoylquinic acid	Not detected	201.23 ± 6.88
Apigenin derivatives			
8	Vicenin-2	Not detected	218.23 ± 11.41
10	Apigenin-7- <i>O</i> -hexoside-6/8- <i>C</i> -hexoside	152.17 ± 2.83	96.99 ± 6.59
11	Apigenin-6- <i>C</i> -pentoside-8- <i>C</i> -hexoside	381.20 ± 10.58	204.19 ± 9.89
14	Apigenin-6- <i>C</i> -hexoside-8- <i>C</i> -pentoside	78.27 ± 16.40	8.46 ± 1.13
16	Vitexin	Not detected	72.73 ± 4.29
18	Isovitexin	Not detected	18.08 ± 2.96
Flavan-3-ols derivatives			
2	Catechin	Not detected	10.17 ± 2.64
5	Procyanidin type B	Not detected	52.17 ± 1.10
6	Catechin/Epicatechin derivative	Not detected	129.38 ± 19.16
7	Epicatechin	Not detected	377.51 ± 21.29
9	Procyanidin type C	Not detected	27.44 ± 0.82
12	Cinchonain type II	Not detected	280.94 ± 56.52
13	Cinchonain type II	Not detected	727.65 ± 67.62
15	Cinchonain type I	Not detected	293.45 ± 113.90
17	Procyanidin type B	Not detected	8.81 ± 1.69
20	Cinchonain type I	Not detected	77.30 ± 11.35
21	Cinchonain type I	Not detected	1 478.00 ± 18.67
Lignans			
19	Aviculin	Not detected	1 024.17 ± 81.73
TOTAL		611.5 ± 29.81	53 74.15 ± 436.61

The extract obtained from the stem bark (TH06) was richer (*ca.* 9 times) in polyphenolic compounds (**Table 10**). Even though only apigenin derivatives were detected on the leaves (TH05), the total amount of apigenin derivatives was similar in the two extracts (TH05: 611.65 ± 29.81 mg/Kg dry extract; TH06: 618.67 ± 36.26 mg/Kg dry extract) (**Table 10**). However, while vicenin-2 (**8**) was the apigenin derivative identified in higher amounts in the stem bark extract (TH06), the main apigenin derivative, and simultaneously the major phenolic constituent present in the extract obtained from the leaves (TH05), was apigenin-6-*C*-pentoside-8-*C*-hexoside (**11**) (**Table 11**).

On the extract obtained from the stem bark (TH06) the main constituents were cinchonain type I (**15**, **20** and **21**) and type II (**12** and **13**) derivatives, corresponding to *ca.* 34 and 19% of the total quantifiable phenolic content, respectively (**Table 10**). As seen on **Table 10**, the cinchonain type I derivative **21** is the main component ($1\,478.00 \pm 18.67$ mg/Kg dry extract), the stem bark extract being also characterized by significant amounts of the lignan aviculin (**19**; $1\,024.17 \pm 81.73$ mg/Kg dry extract). Worth also to note that hydroxycinnamic acids were only detected in trace amounts, corresponding to 5% of the quantifiable phenolic content (**Table 10**).

Contrary to other *Ficus* species that have already been deeply investigated on their metabolic composition, this is the first time that the phenolic constituents of *F. curtipes* are reported.

3.2.3. *C. tabularis*

3.2.3.1. HPLC-DAD-ESI/MSⁿ qualitative analysis

HPLC–DAD–ESI/MSⁿ analysis of the methanol extract obtained from *C. tabularis* leaves allowed the identification of twenty-five phenolic compounds (**Table 11** and **12**, **Figure 41**). Even though compounds **13**, **16**, **18**, **21** and **23-25** display UV spectra of flavonoids, most peaks (**1-12**, **14**, **15**, **17**, **19**, **20** and **22**) detected in the UV chromatogram (280 nm) (**Figure 41**) exhibit spectral features of flavan-3-ols (280 nm) (**Table 11**). While compound **2** exhibits a deprotonated molecular ion at *m/z* 289 and co-chromatographically matches epicatechin, all other flavan-3-ols exhibit MS data indicating that they are dimers and trimers of flavan-3-ols (proanthocyanidins).

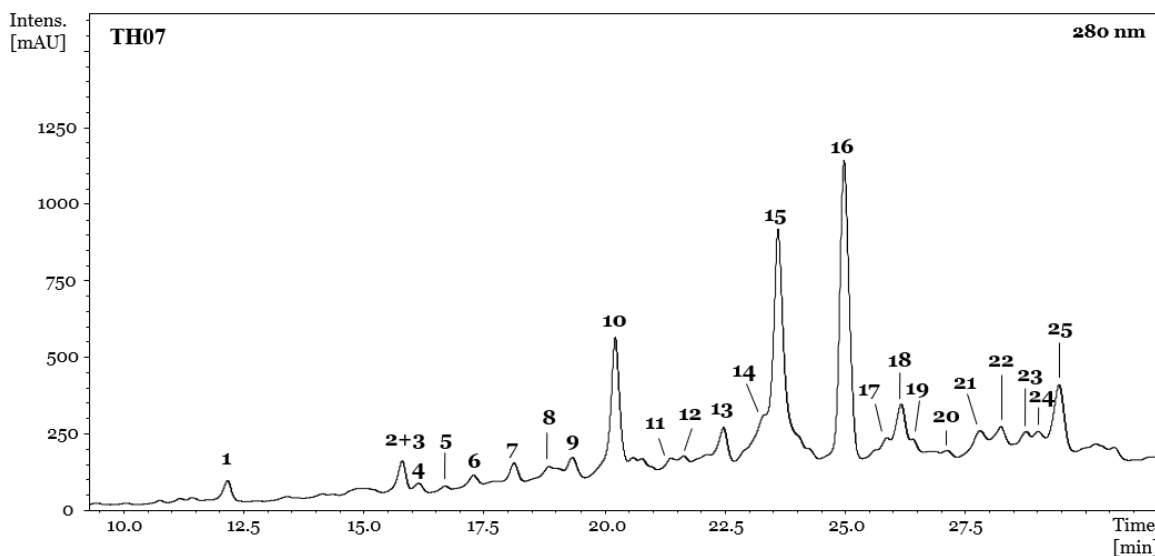


Figure 41. HPLC-UV chromatogram of the methanol extract obtained from the leaves (TH07) of *C. tabularis*. Peaks: (1, 3-6, 8) proanthocyanidins dimers, (2) epicatechin, (7, 9-12, 14, 15, 17, 19, 20, 22) proanthocyanidins trimers, (13) kaempferol-3-*O*-hexoside, (16) quercetin-3-*O*-rhamnoside, (18) luteolin-7-*O*-hexoside, (21) 7,3'-dimethyl-quercetin-3-*O*-hexoside, (23) kaempferol-3-*O*-rhamnoside, (24) isorhamnetin-3-*O*-hexoside, (25) 3',4'-dimethyl-quercetin-3-*O*-hexoside.

3.2.3.1.1. Dimers and trimers

Compounds **1**, **3-6** and **8**, with the same deprotonated molecular ion at $m/z \sim 561.1406$ and a similar MS fragmentation, solely differ in the relative abundances of their ions. The ion at $m/z 289$ is the most abundant fragment being detected in these compounds, often corresponding to the base peak (**Table 11**, **Figure 42A** (MS² QTOF(561): 289.0717, [C₁₅H₁₃O₆]⁻, pentahydroxyflavan) that coincides with the deprotonated ion of catechin/epicatechin. A series of flavan-3-ol derivatives complying with these characteristics (UV and molecular formula C₃₀H₂₆O₁₁) have been detected, most of them corresponding to dimers with a total of nine hydroxyls, including gambiriin C (epiafzelechin-(4β-8)-catechin), fisetinidol-(4β-8)-catechin, fisetinidol-(4α-8)-catechin, and catechin-(4α-8)-epiafzelechin (**Figure 42B**). Therefore, current data suggests that constituents **1**, **3-6** and **8** might correspond to dimers of catechin/epicatechin and epiafzelechin or fisetinidol.

Table 11. Retention time (*Rt*), molecular formula (M) and MS [M-H]⁻ and MS²[M-H]⁻ data for the proanthocyanidins detected in the methanol extract obtained from *C. tabularis* leaves (TH07).^a

Compounds		<i>Rt</i> (min)	UV (nm)	Formula (M)	[M-H] ⁻ , <i>m/z</i>	MS ² [M-H] ⁻ , <i>m/z</i> (%)
Dimers 561						
1	Dimer 1	12.2	280	C ₃₀ H ₂₆ O ₁₁	561.1402	409(60), 391(50), 289(100)
3	Dimer 2	15.8	280	C ₃₀ H ₂₆ O ₁₁	561.1401	409(100), 391(40), 289(50)
4	Dimer 3	16.1	280	C ₃₀ H ₂₆ O ₁₁	561.1406	409(35), 391(50), 289(100)
5	Dimer 4	16.8	280	C ₃₀ H ₂₆ O ₁₁	561.1405	409(100), 391(35), 289(65)
6	Dimer 5	17.2	280	C ₃₀ H ₂₆ O ₁₁	561.1412	409(100), 391(55), 289(70)
8	Dimer 6	18.8	280	C ₃₀ H ₂₆ O ₁₁	561.1408	409(70), 391(60), 289(100)
Trimers 833						
7	Trimer 1	18.1	280	C ₄₅ H ₃₈ O ₁₆	833.2090	681(50), 663(100), 561(90), 529(80), 409(40), 391(75), 289(50)
9	Trimer 2	19.2	280	C ₄₅ H ₃₈ O ₁₆	833.2092	681(30), 663(50), 561(100), 529(70), 409(35), 391(50), 289(20)
10	Trimer 3	20.2	280	C ₄₅ H ₃₈ O ₁₆	833.2089	681(45), 663(60), 561(100), 529(77), 409(40), 391(40), 289(35)
11	Trimer 4	21.4	280	C ₄₅ H ₃₈ O ₁₆	833.2093	681(40), 663(55), 561(55), 529(100), 409(45), 391(15), 289(15)
12	Trimer 5	21.7	280	C ₄₅ H ₃₈ O ₁₆	833.2089	681(45), 663(55), 561(100), 529(95), 409(35), 391(60), 289(40)
15	Trimer 6	23.6	280	C ₄₅ H ₃₈ O ₁₆	833.2092	681(45), 663(60), 561(100), 529(80), 409(40), 391(40), 289(30)
Trimers 817						
14	Trimer 7	22.9	---	C ₄₅ H ₃₈ O ₁₅	817.2138	665(20), 647(20), 561(100), 529(35), 409(35), 391(40), 289(40)
17	Trimer 8	25.8	280	C ₄₅ H ₃₈ O ₁₅	817.2140	665(30), 647(20), 561(100), 529(20), 409(35), 391(50), 289(50)
19	Trimer 9	26.5	---	C ₄₅ H ₃₈ O ₁₅	817.2135	665(35), 647(15), 561(100), 529(10), 409(35), 391(50), 289(50)
20	Trimer 10	27.1	---	C ₄₅ H ₃₈ O ₁₅	817.2137	665(10), 647(20), 561(100), 529(45), 409(55), 391(25), 289(20)
22	Trimer 11	28.3	280	C ₄₅ H ₃₈ O ₁₅	817.2137	665(5), 647(20), 561(100), 529(45), 409(50), 391(20), 289(20)

^a Main observed fragments. Other ions have been detected but were not significant. MS ions and their relative abundance were obtained by ESI(Ion Trap), except [M-H]⁻, which was obtained by ESI-QTOF. Data from other MS²QTOF ions is presented in the main text.

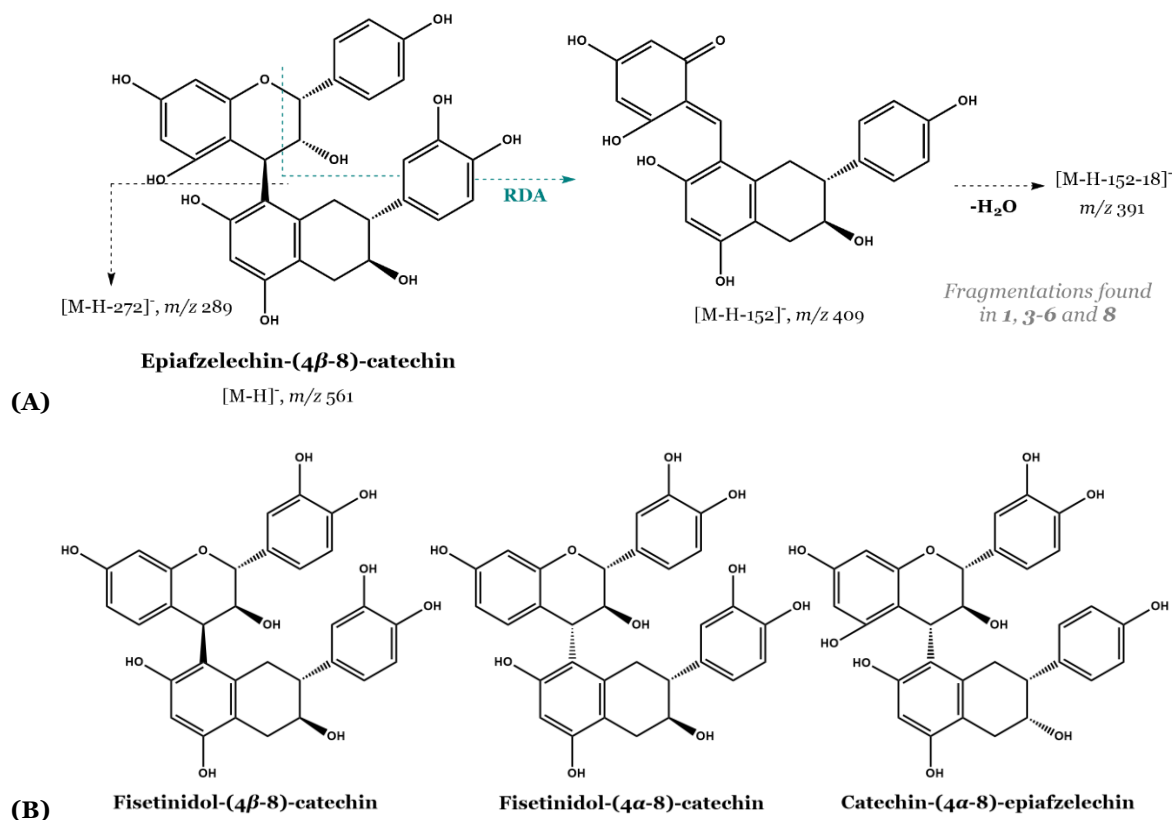


Figure 42. MS fragmentation pattern of epiafzelechin-(4 β -8)-catechin (A). Similar fragmentations were observed for the other detected dimers (B). RDA, Retro-Diels-Alder reaction.

Compounds **7**, **9-12** and **15**, sharing a deprotonated molecular ion at $m/z \sim 833.2092$, can be labelled as trimers with a total of thirteen hydroxyl groups. The ion at m/z 561 is very abundant, and sometimes the base peak, in their MS² fragmentations, displaying also the same fragmentations ions of the dimers **2-6** and **8** (Table 11). In the MS³ (833 \rightarrow 561) the base peak is the ion at m/z 289 (data not indicated in Table 12), the ion 289.0717 being also observed in MS²(QTOF). This indicates that these trimers are derived from the previous ones, being characterized by an additional tetrahydroxyflavan moiety. In this matter, they might possibly correspond to those previously reported by Steynberg et al. (201): epifisetinidol-(4 β -8)-epicatechin-(6-4 β)-epifisetinidol, *ent*-fisetinidol-(4 β -8)-catechin-(6-4 β)-*ent*-fisetinidol and *ent*-fisetinidol-(4 β -8)-catechin-(6-4 α)-*ent*-fisetinidol (Figure 43).

Compounds **14**, **17**, **19**, **20** and **22**, with a deprotonated molecular ion at $m/z \sim 817.2135$, must be trimers exhibiting one hydroxyl group less than the preceding ones, their base peak being the ion at m/z 561. Additional ions are the same as those observed in the MS fragmentation of compounds **7**, **9-12** and **15**, except for some ions that are displaced by 16 amu. Likewise, the base peak in the MS³(817 \rightarrow 561) is the ion at m/z 289 (data not indicated in Table 11), while the ion 289.0717 is detected in MS²(QTOF). Based on the above, the possible presence of catechin/epicatechin and the base peak at m/z 561 suggest

that these compounds derive from the previously described dimers and exhibit an additional trihydroxyflavan, possibly guibourtinidol (3,7,4'-trihydroxyflavan).

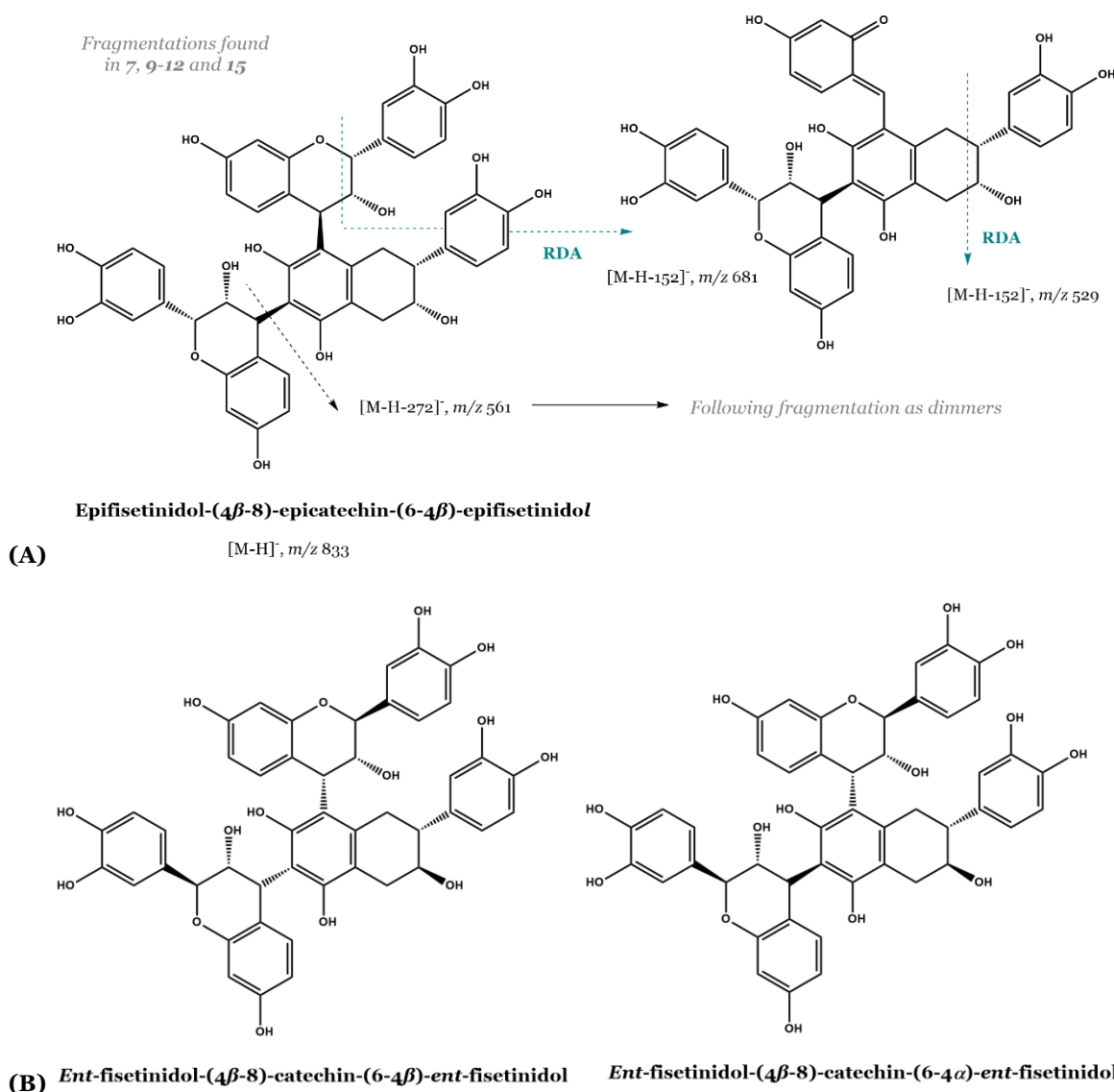


Figure 43. MS fragmentation pattern of epifisetinidol-(4 β -8)-epicatechin-(6-4 β)-epifisetinidol (A). Similar fragmentations were observed for the other detected trimmers (B). RDA, Retro-Diels-Alder reaction.

3.2.3.1.2. Flavonoids

Compounds **13**, **16**, **18**, **21** and **23-25** have an UV spectrum of flavonoids and exhibit deprotonated molecular ions of monoglycosides (**Table 12**). Excepting compound **21**, the other flavonols detected in *C. tabularis* extract have a MS fragmentation that is

characterized by the occurrence of a base peak ion corresponding to their deprotonated aglycons: kaempferol (**13** and **23**), quercetin (**16**), luteolin (**18**), and isorhamnetin (**24**).

Table 12. Retention time (*Rt*), molecular formula (M) and MS [M-H]⁻ and MS²[M-H]⁻ data for the flavonoids detected in the methanol extract obtained from *C. tabularis* leaves (TH07).^a

Compounds ^b		<i>Rt</i> (min)	UV (nm)	Formula (M)	[M-H] ⁻ , <i>m/z</i>	MS ² [M-H] ⁻ , <i>m/z</i> (%)
13	Kaempferol-Hx	22.5	267, 298sh, 348	C ₂₁ H ₂₀ O ₁₁	447.0933	285(100)
16	Quercetin-Rh	24.9	255, 266sh, 288sh, 350	C ₂₁ H ₂₀ O ₁₁	447.0940	301(100)
18	Luteolin-Hx	26.2	255sh, 268, 340	C ₂₁ H ₂₀ O ₁₁	447.0937	285(100)
21	Dimethylquercetin-Hx	27.8	250, 268sh, 296, 352	C ₂₃ H ₂₄ O ₁₂	491.1195	476(100), 329(90)
23	Kaempferol-Rh	28.8	266, 296sh, 348	C ₂₁ H ₂₀ O ₁₀	431.0996	285(100)
24	Isorhamnetin-Hx	29.0	---- ^c	C ₂₂ H ₂₂ O ₁₂	477.1059	315(100)
25	Dimethylquercetin-Hx	29.4	---- ^c	C ₂₃ H ₂₄ O ₁₂	491.1197	329(100)

^a Main observed fragments. Other ions have been detected, but were not significant. MS ions and their relative abundance were obtained by ESI(Ion Trap), except [M-H]⁻, which was obtained by ESI-QTOF. Data from other MS²QTOF ions is presented in the main text.

^b Rh, rhamnoside; Hx, hexoside.

^c Coelutes with other compounds and its UV spectrum could not be well observed;

The UV spectral data of the flavonol derivatives **13**, **16** and **23** indicate that the glycosylation occurs in position 3, pointing that they correspond to kaempferol-3-*O*-hexoside (**13**), quercetin-3-*O*-rhamnoside (**16**) and kaempferol-3-*O*-rhamnoside (**23**). Comparison with authentic standards allowed to unequivocally label compounds **13**, **18**, **16** and **24** as kaempferol-3-*O*-glucoside, luteolin-7-*O*-glucoside, quercetin-3-*O*-rhamnoside and isorhamnetin-3-*O*-glucoside, respectively. Compounds **21** and **25**, with a deprotonated molecular ion at *m/z* 491.1195 (molecular formula, C₂₃H₂₄O₁₂) and a deprotonated aglycon at *m/z* 329.0665, correspond to trihydroxy-dimethoxyflavon-hexoside isomers. The occurrence of 3-*O*-glycosylated derivatives of quercetin (**16**) and isorhamnetin (**24**) on the extract suggests that **21** and **25** can be labelled as dimethylquercetin (methylisorhamnetin) derivatives. In fact, considering the abundance of the ion (base peak) at *m/z* 476 [(M-H)-15]⁻ in compound **21** and its absence in **25**, compound **21** can tentatively be identified as 7,3'-dimethyl-quercetin-3-*O*-hexoside and **25** as 3',4'-dimethyl-quercetin-3-*O*-hexoside (**Figure 44**).

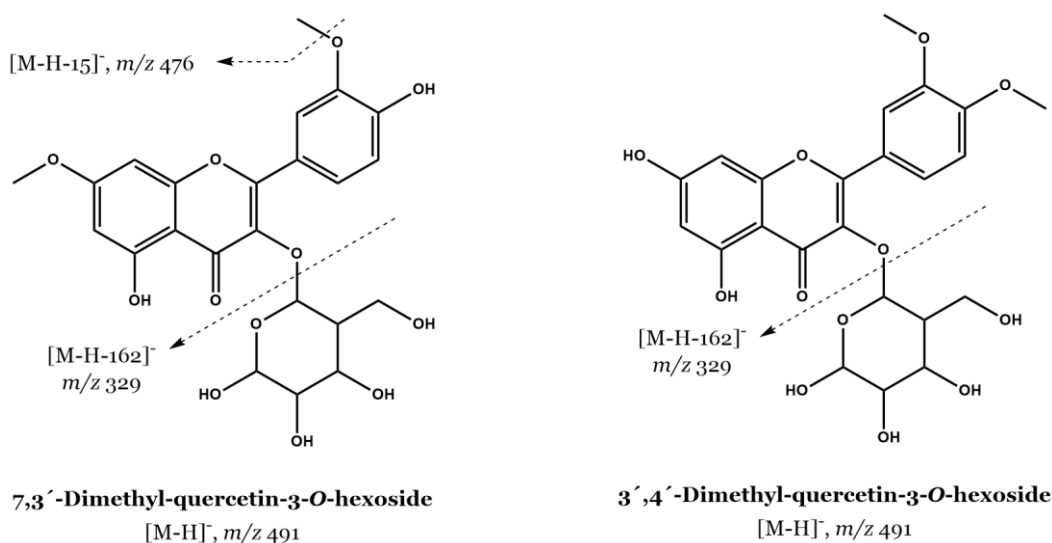


Figure 44. MS fragmentation pattern of 7,3'-dimethyl-quercetin-3-O-hexoside and 3',4'-dimethyl-quercetin-3-O-hexoside.

3.2.3.2. HPLC-DAD quantitative analysis

The results obtained from the HPLC-DAD quantitation of the phenolic compounds identified in the extract obtained from *C. tabularis* leaves (TH07) are displayed in **Table 13**. Data collected evidenced that proanthocyanidins ($29\,796.41 \pm 1\,441.45$ mg/kg of dry extract) are the main metabolites, corresponding to ca. 70 % of the total quantified phenolics ($41\,899.95 \pm 1\,768.87$ mg/kg of dry extract). Worth to note that trimers ($26\,402.61 \pm 1\,150.90$ mg/kg of dry extract) represent ca. 90% of the proanthocyanidins, trimers 6 (**15**) ($12\,839.08 \pm 570.51$ mg/kg of dry extract) and trimers 3 (**10**) ($8\,279.20 \pm 229.65$ mg/kg of dry extract) being the main flavan-3-ol derivatives. Considerable quantities of quercetin-3-O-rhamnoside (quercitrin; **16**) were also detected ($10\,021.22 \pm 231.01$ mg/kg of dry extract), being the second most abundant phenolic compound present in the extract.

First report on the phenolic composition of *C. tabularis* leaves deals with the isolation of the flavone tabularin (166). Since then, a few phenolic constituents have been described, namely gallic acid, catechin, quercetin, quercetin-3-O-rutinoside, tannic acid (160), and the coumarins 7-hydroxycoumarin and scopoletin (202). Our MS-based qualitative analysis did not allow the identification of the previously reported constituents, which might be explained by the different phytogeographical parameters and seasonal variations. However, as identified by Kaur and co-workers (160), epicatechin (**2**) was also present in the current sample, along with high valued condensed tannins (proanthocyanidins),

sustaining the plant commercial utilization on tanning industry (153). This is, as far as we know, the first time that these constituents are reported on the leaves of the plant.

Table 13. Content of phenolic compounds detected on the methanol extract obtained from the leaves of *C. tabularis* (TH07) (mg/kg dry extract). Results correspond to mean \pm SD (n=3).

Compound		TH07
Dimmers 561		
1	Dimer 1	358.03 \pm 31.00
3	Dimer 2	2 308.67 \pm 184.84 ^a
4	Dimer 3	221.81 \pm 19.77
5	Dimer 4	109.18 \pm 20.56
6	Dimer 5	223.00 \pm 12.90
8	Dimer 6	173.09 \pm 21.46
Trimmers 833		
7	Trimer 1	2 045.13 \pm 100.94
9	Trimer 2	1 631.73 \pm 55.02
10	Trimer 3	8 279.20 \pm 229.65
11	Trimer 4	197.39 \pm 31.07
12	Trimer 5	193.276 \pm 25.69
15	Trimer 6	12 839.08 \pm 570.51
Trimmers 817		
14	Trimer 7	153.77 \pm 14.51
17	Trimer 8	217.69 \pm 23.69
19	Trimer 9	120.63 \pm 26.15
20	Trimer 10	125.63 \pm 8.47
22	Trimer 11	599.08 \pm 65.53
Flavonoids		
13	Kaempferol-3- <i>O</i> -hexoside	580.92 \pm 18.17
16	Quercetin-3- <i>O</i> -rhamnoside	10 021.22 \pm 231.01
18	Luteolin-7- <i>O</i> -hexoside	498.50 \pm 15.43
21	Dimethylquercetin-3- <i>O</i> -hexoside	152.22 \pm 8.82
23	Kaempferol-3- <i>O</i> -rhamnoside	63.43 \pm 6.81
24	Ishoramnetin-3- <i>O</i> -hexoside	67.18 \pm 7.58
25	Dimethylquercetin-3- <i>O</i> -hexoside	720.08 \pm 39.06
TOTAL		41 899.95 \pm 1 768.87

^aQuantified with compound **2** (epicatechin).

3.2.4. *G. gracillima*

3.2.4.1. HPLC-DAD-ESI/MSⁿ qualitative analysis

HPLC-DAD-ESI/MSⁿ analysis of the methanol extract obtained from *G. gracillima* flowers (TH19) allowed the identification of twenty-one polyphenolic constituents (**Table 14** and **15**). A series of peaks exhibiting UV spectra characteristic of ellagic acid and kaempferol derivatives were observed in the UV chromatogram (**Figure 45**).

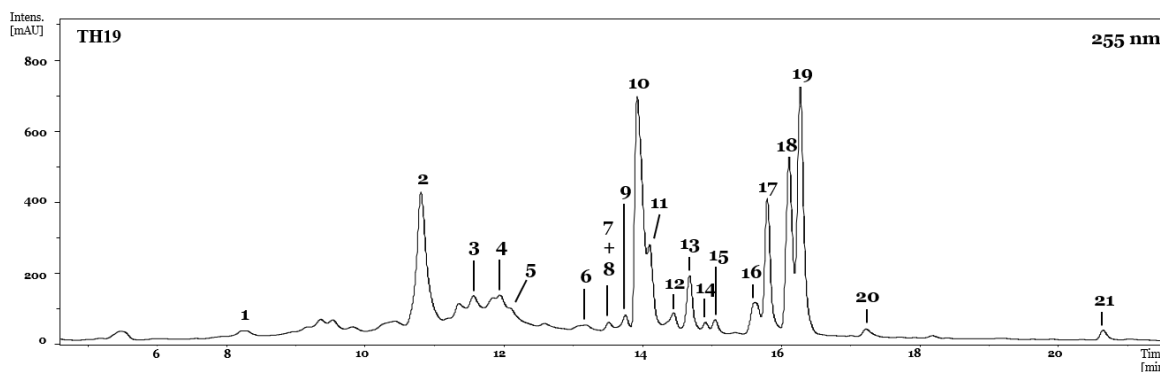


Figure 45. HPLC-UV chromatogram of the methanol extract obtained from the flowers of *G. gracillima* (TH19). Peaks: (1) punicalin + 2H, (2) valoneic acid dilactone, (3) sanguisorbic acid dilactone, (4) unknown, (5) kaempferol-3-*O*-(2-rhamnosyl-6-hexosyl)hexoside (6) kaempferol-*O*-(2-rhamnosyl-3/4-pentosyl)hexoside (7) kaempferol-3-*O*-(3,6-di-rhamnosyl)hexoside (8) kaempferol-3-*O*-(2-hexosyl)hexoside (9) kaempferol-3-*O*-(3/4,6-di-rhamnosyl)hexoside (10) ellagic acid (11) kaempferol-3-*O*-(6-hexosyl)hexoside (12) kaempferol-3-*O*-(2-rhamnosyl-3-hexosyl)hexoside (13) kaempferol-3-*O*-(2-rhamnosyl)hexoside (14) kaempferol-3-*O*-(6-pentosyl)hexoside (15) kaempferol-3-*O*-(6-rhamnosyl)hexoside (16) **2** or **3** + CH₃ (17) kaempferol-3-*O*-rutinoside (18) **2** or **3** + CH₃ (19) kaempferol-3-*O*-glucoside (20) **2** or **3** - CO₂ (21) **2** or **3** + CH₃.

3.2.4.1.1. Kaempferol derivatives

Compounds **5-9**, **11-15**, **17** and **19** (Figure 45) have UV spectra characteristic of kaempferol derivatives (~266, 302sh, 348 nm), with a hydroxyl group at position 3, their MS fragmentations exhibiting ions at m/z 285.0405 ([C₁₅H₉O₆]⁻), corresponding to the deprotonated ion of kaempferol. Their deprotonated molecular ions indicate distinct degrees of glycosylation (mono- to triglycosides). With a deprotonated molecular ion at m/z 447.0929 ([C₂₁H₁₉O₁₁]⁻) (kaempferol-3-*O*-hexoside), compound **19** chromatographically matches with authentic standard of kaempferol-3-*O*-glucoside (Table 14).

Compounds **8**, **11**, **13-15** and **17** presented deprotonated molecular ions of diglycosides at m/z ~593.1465 (**13**, **15** and **17**, kaempferol-rhamnosyl-hexosides), 579.1353 (**14**, kaempferol-pentosyl-hexoside), and ~609.1440 (**8** and **11**, kaempferol-dihexosides) (Table 14). The kaempferol deprotonated ion can be observed in the MS fragmentations of **11**, **14**, **15** and **17**, but no ions have been detected evidencing an interglycosidic linkage rupture (Table 14). The diglycosidic linkage should be 1→6, considering that its fragmentation is very difficult to achieve. As such, compound **11** could be labelled as kaempferol-3-*O*-hexosyl(1→6)hexoside, **14** as kaempferol-3-*O*-pentosyl(1→6)hexoside, and **15** and **17** as kaempferol-3-*O*-rhamnosyl(1→6)hexoside isomers. According to their chromatographic mobility, **15** and **17** could correspond to kaempferol-3-*O*-rhamnosyl(1→6)galactoside and kaempferol-3-*O*-rhamnosyl(1→6)glucoside, respectively (Figure 46A).

Table 14. Retention time (*Rt*), molecular formula (M) and MS [M-H]⁻ and MS²[M-H]⁻ data for the kaempferol derivatives detected in the methanol extract obtained from *G. gracillima* flowers (TH19).^a

Compounds ^b	<i>Rt</i> (min)	Formula (M)	[M-H] ⁻ , <i>m/z</i>	MS ² [M-H] ⁻ , <i>m/z</i> (%)								
				-132	-146	-150	-162	-164	-180	-266 ^c	-282 ^c	[Agl-H/2H] ⁻
5 K-3-(2Rh-6-Hx)Hx	12.1	C ₃₃ H ₄₀ O ₂₀	755.2038		609(10)			591(90)			473(10)	285(100)
6 K-3-(2Rh-3-Pt)Hx	13.2	C ₃₂ H ₃₈ O ₁₉	725.1926	593(10)	579(7)	575(5)		561(100)				284(95)
7 K-3-(3Rh-6-Rh)Hx	13.4	C ₃₃ H ₄₀ O ₁₉	739.2097		593(15)			575(75)		473(10)		285(100)
8 K-3-(2-Hx)Hx	13.5	C ₂₇ H ₃₀ O ₁₆	609.1430				447(10)		429(5)			285(100)
9 K-3-(2Rh-6-Rh)Hx	13.7	C ₃₃ H ₄₀ O ₁₉	739.2072		593(20)			575(100)		473(10)		285(75)
11 K-3-(6-Hx)Hx	14.1	C ₂₇ H ₃₀ O ₁₆	609.1450									285(100)
12 K-3-(2-Rh-3-Hx)Hx	14.4	C ₃₃ H ₄₀ O ₂₀	755.1989		609(85)		593(100) ^d			575(60)		285(85)
13 K-3-(2-Rh)Hx	14.7	C ₂₇ H ₃₀ O ₁₅	593.1460		447(15)			429(30)				284(100)
14 K-3-(6-Pt)Hx	14.9	C ₂₆ H ₂₈ O ₁₅	579.1353									285(100)
15 K-3-(6-Rh)Hx	15.0	C ₂₇ H ₃₀ O ₁₅	593.1467									285(100)
17 K-3-(6-Rh)Hx	15.8	C ₂₇ H ₃₀ O ₁₅	593.1465									285(100)
19 K-3-Hx	16.3	C ₂₁ H ₂₀ O ₁₁	447.0929									284(100)

^a Main observed fragments.^b K, kaempferol; Rh, rhamnose; Hx, hexose; Pt, pentose.^c 266 (146+120); 282 (162+120).^d MS³(755→593): 447(15, -146), 429(15, -164), 284(100).**Table 15.** Retention time (*Rt*), molecular formula (M) and MS [M-H]⁻ and MS²[M-H]⁻ data for the ellagic acid derivatives detected in the methanol extract obtained from *G. gracillima* flowers (TH19).^a

Compounds	<i>Rt</i> (min)	Formula (M)	[M-H] ⁻ , <i>m/z</i>	MS ² [M-H] ⁻ , <i>m/z</i> (%)	MS ³ [(M-H)→(base peak)] ⁻
1 Punicalin + 2H	8.3	C ₃₄ H ₂₄ O ₂₂	783.0693	481(100), 301(50)	301(100)
2 Valoneic acid dilactone	10.2	C ₂₁ H ₁₀ O ₁₃	469.0030	425(100), 301(10)	301(100)
3 Sanguisorbic acid dilactone	10.8	C ₂₁ H ₁₀ O ₁₃	469.0022	425(100), 301(15)	301(100)
4 Unknown	11.9	C ₄₃ H ₂₄ O ₂₀	859.0752	765(30), 301(100)	
10 Ellagic acid	13.9	C ₁₄ H ₆ O ₈	300.9980		
16 2 or 3 + CH ₃	15.6	C ₂₂ H ₁₂ O ₁₃	483.0203	451(100), 407(45), 301(60)	301(100)
18 2 or 3 + CH ₃	16.1	C ₂₂ H ₁₂ O ₁₃	483.0169	301(100)	
20 2 or 3 - CO ₂	17.2	C ₂₀ H ₁₀ O ₁₁	425.0153	301(100)	
21 2 or 3 + CH ₃	20.6	C ₂₂ H ₁₂ O ₁₃	483.0189	451(100), 301(15)	301(100)

^a Main observed fragments.

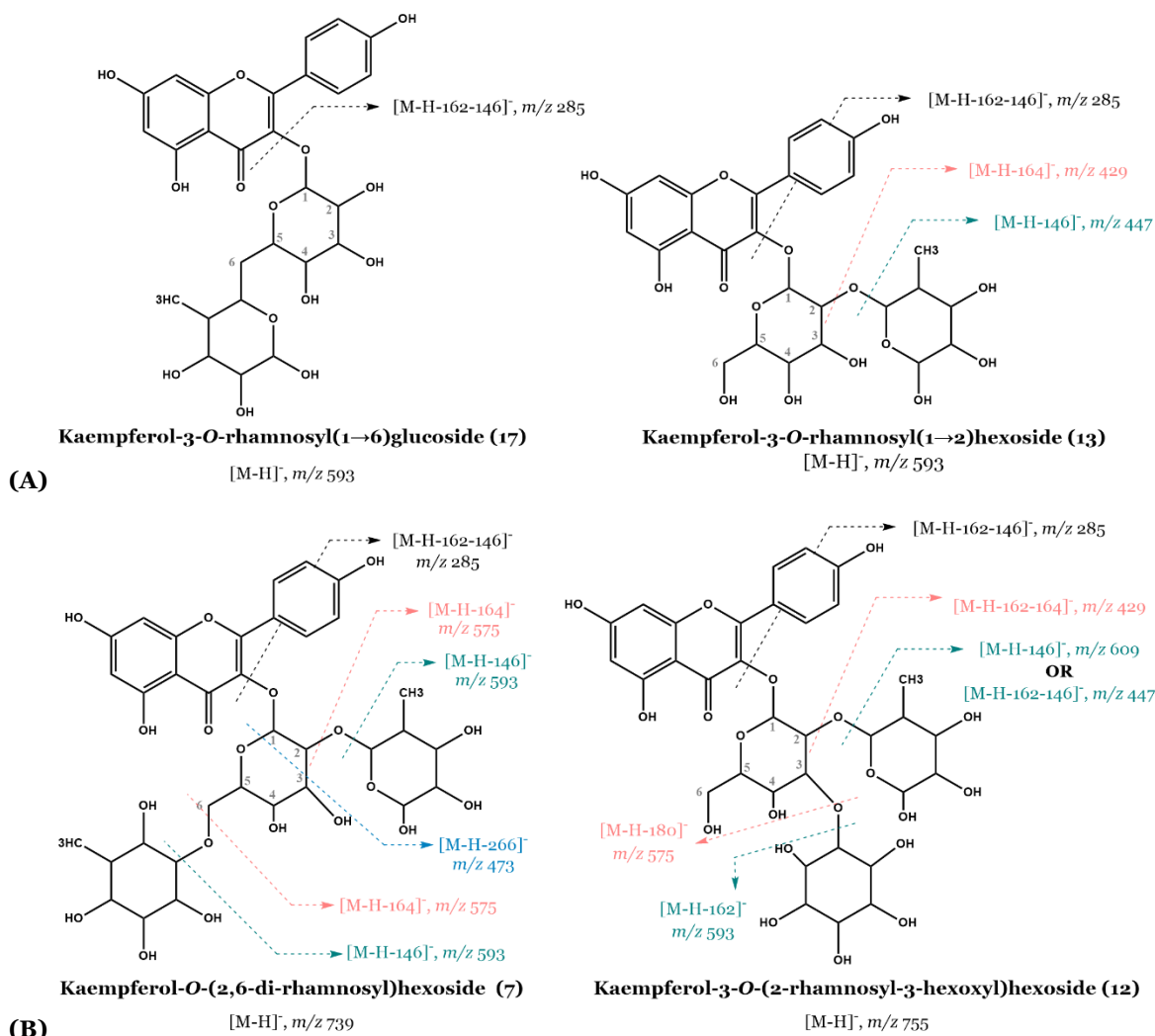


Figure 46. MS fragmentation pattern of some kaempferol diglycosides (A) and triglycosides (B).

Ions at *m/z* 447/429 are observed in the MS fragmentation of compounds **8** and **13**, due to the losses of 162/180 (**8**) and 146/164 (**13**) amu deriving from the rupture of the interglycosidic linkages hexosyl-hexoside (**8**) and rhamnosyl-hexoside (**13**) (Figure 46A). Therefore, **8** and **13** were tentatively identified as kaempferol-3-*O*-hexosyl(1→2)hexoside and kaempferol-3-*O*-rhamnosyl(1→2)hexoside, respectively.

Compounds **5-7**, **9** and **12** exhibit masses of triglycosides (Table 14). Deprotonated molecular ions of **5** and **12**, at *m/z* ~755.2000, indicate that they correspond to kaempferol derivatives with two hexoses and one rhamnose. In addition to the deprotonated ion of kaempferol (*m/z* 285, base peak), MS fragmentation of **5** evidences also the loss of a fragment of 282 amu (162+120), which implies a global loss of one hexose in position 6", and also a fraction of the hexose moiety attached directly to the aglycone and that contains

the carbons 6''-3''. Losses of 146 and 164 amu (146+18) are also observed, suggesting a rhamnose linked to a non-phenolic hydroxyl that, discharging 6''-3'' positions, should be linked in 2''. Hence, this compound corresponds to a kaempferol-3-*O*-(2-rhamnosyl-6-hexoxyl)hexoside and could be considered as a derivative of **11**, with one additional rhamnosylation at 2''.

The losses of 162 and 180 amu (162+18) fragments are detected in the MS of isomer **12**, which characterize a hexose linked to a non-phenolic hydroxyl, the ion at *m/z* 609 (with a great abundance) pointing to the loss of a rhamnosyl radical (-146). That, together with the absence of the ion [(M-H)-(146+18)]⁻ could indicate that the rhamnose is linked to a phenolic hydroxyl (**Table 14**). However, MS³ fragmentation of the ion at *m/z* 593 (kaempferol-rhamnohexosyl, generated after the loss of -162), (data indicated at the bottom of **Table 14**) results in ions 447 (-146) and 429 (-164), indicating that the rhamnose is not linked to a phenolic hydroxyl. Thus, compound **12** could be tentatively ascribed as a derivative of **8** or **13**, bearing an additional rhamnosylation or hexosylation, respectively. As **13** is more abundant than **8** (**Figure 45**), compound **12** can be labelled as kaempferol-3-*O*-(2-rhamnosyl-3-hexoxyl)hexoside (**Figure 46B**).

The deprotonated molecular ion of **6** ([M-H]⁻, *m/z* 725.1926) indicates that it corresponds to a kaempferol with one hexose, one rhamnose and one pentose substitution, its MS fragmentation showing losses of -132/-150 and -146/-164 (pentosyl and rhamnosyl, respectively, linked to a non-phenolic hydroxyl), different than the 6'' position, as previously discussed. Therefore, compound **6** could be considered a derivative of **13** with an additional pentose at position 3'' or 4'', and tentatively identified as a kaempferol-*O*-(2-rhamnosyl-3/4-pentosyl)hexoside.

Compounds **7** and **9**, with the same mass of di-rhamnosylated kaempferol-hexoside ([M-H]⁻, *m/z*~739.2080), exhibit the same MS fragmentation, where the loss of two fragments of -146 and -164 amu can be observed and, as previously mentioned, the fragments indicate the presence of a rhamnosylation on a non-phenolic hydroxyl. On the other hand, ion at *m/z* 473, resulting from the loss of the fragment of 266 amu (146+120) (**Table 14**), indicates that the other rhamnose occurs on the hydroxyl present at the position 6'' from the hexose, as in compound **5**. Compounds **7** and **9** could be derivatives of **17**, bearing an additional rhamnose for one of them on the 2'' hydroxyl, and for the other on 3'' or 4'' hydroxyl, thus corresponding to kaempferol-*O*-(2,6-di-rhamnosyl)hexoside (**7**) (**Figure 46B**) and kaempferol-*O*-(3/4,6-di-rhamnosyl)hexoside (**9**).

3.2.4.1.2. Ellagic acid derivatives

The chromatogram of the methanol extract obtained from *G. gracillima* flowers shows an abundant peak (compound **10**) at 13.9 min (**Figure 45**). This compound has an UV spectrum characteristic of ellagic acid (254, 300sh, 350sh, 370 nm). Its MS exhibits a deprotonated molecular ion at m/z 300.9980 ($[M-H]^-$, $C_{14}H_5O_8$), chromatographic comparison with an authentic standard allowing to unequivocally identify it as ellagic acid. Other compounds (**1-4**, **16**, **18**, **20** and **21**) (**Table 15**) with similar UV spectral characteristics have been also detected. Their MS fragmentations exhibit an ion with the same exact mass as deprotonated ellagic acid.

Compound **2** with deprotonated molecular ion at m/z 469.0030, and other in trace amounts with a similar mass (**3**) (**Table 15**), are also observed in the chromatogram, their molecular formulas ($C_{21}H_{10}O_{13}$) corresponding to the isomers valoneic acid dilactone and sanguisorbic acid dilactone. According to their elution order in reverse phase, the most abundant isomer should be valoneic acid dilactone (**2**) (**Figure 47**) (203). Compounds **16**, **18** and **21** have a molecular formula ($C_{22}H_{12}O_{13}$) similar to that of the previous ones, but with one additional methyl group, thus corresponding to **2** and/or **3** methyl derivatives. Similarly, compound **20** appears to be a decarboxylated derivative of **2** or **3**, due to the loss of a CO_2 group, as indicated by the molecular formula ($C_{20}H_{10}O_{11}$). Compound **1** displays a deprotonated molecular ion at m/z 783.0693 ($C_{34}H_{23}O_{22}$), with two additional protons in comparison with punicalin, possibly derived from a ring opening. Based on the characteristic UV spectrum, compound **4** might also be tentatively ascribed as an ellagic acid derivative, as further suggested by the deprotonated molecular ion at m/z 859.0752 ($C_{43}H_{23}O_{20}$), and the deprotonated ellagic acid ion observed in the MS fragmentation. However, structural elucidation of **4** could not be fully achieved.

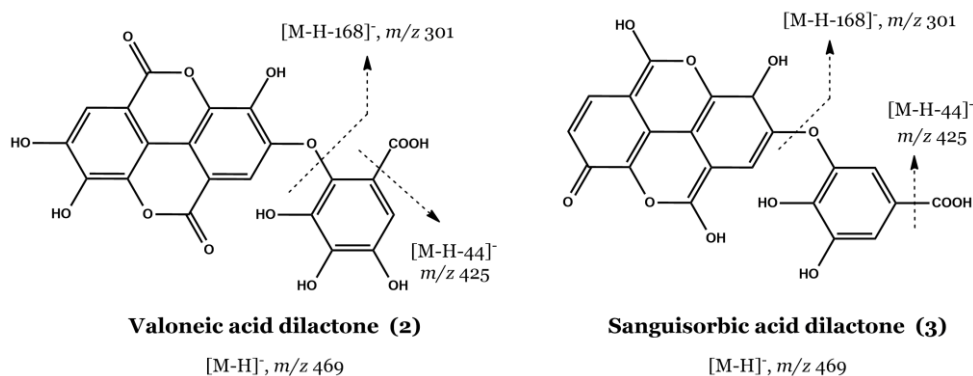


Figure 47. MS fragmentation pattern of valoneic acid dilactone (**2**) and sanguisorbic acid dilactone (**3**).

A second sample of *G. gracillima* flowers was collected from the same tree four years later (April 2019), a new methanol extract being prepared from this dry plant material (TH22). The identity of the phenolic compounds in the second methanol extract (TH22) was confirmed by HPLC-DAD through comparison with the spectral data and chromatographic behaviour of the former sample. The phenolic compounds above described and detected in the first sample (TH19) were also found in TH22, except the kaempferol derivative, kaempferol-3-*O*-rhamnosyl(1→6)galactoside (**15**).

3.2.4.2. HPLC-DAD quantitative analysis

Both extracts obtained from the flowers of *G. gracillima* were quantified by HPLC-DAD using calibration curves, a total of twenty-one and twenty phenolics being quantified in the first (TH19) and in the second (TH22) extracts, respectively (**Table 16**).

Table 16. Content of phenolic compounds on the methanol extracts obtained from *G. gracillima* flowers (TH19 - first collection, TH22 - second collection) (mg/kg dry extract). Results correspond to mean \pm SD (n = 3).

	Compounds ^a	TH19	TH22
1	Punicalin + 2H	215.60 \pm 45.24	260.32 \pm 8.51
2	Valoneic acid dilactone	2 182.83 \pm 50.02	1 827.01 \pm 12.43
3	Sanguisorbic acid dilactone	1 136.26 \pm 11.61	1 127.28 \pm 29.83
4	Unknown	1 834.89 \pm 54.97	677.32 \pm 18.65
5	K-3-(2Rh-6-Hx)Hx	1 083.98 \pm 48.55	512.64 \pm 52.10
6	K-3-(2Rh-3-Pt)Hx	2 364.60 \pm 77.99	608.91 \pm 41.82
7 + 8	K-3-(3Rh-6-Rh)Hx + K-3-(2-Hx)Hx	1 985.31 \pm 126.92	842.71 \pm 25.23
9	K-3-(2Rh-6-Rh)Hx	3 013.50 \pm 162.05	3 514.06 \pm 192.86
10	Ellagic acid	3 631.83 \pm 94.85	4 584.56 \pm 110.06
11	K-3-(6-Hx)Hx	2 923.60 \pm 118.39	7 781.12 \pm 91.92
12	K-3-(2-Rh-3-Hx)Hx	2 598.26 \pm 39.14	1 094.51 \pm 19.72
13	K-3-(2-Rh)Hx	1 548.24 \pm 62.69	2 227.76 \pm 7.11
14	K-3-(6-Pt)Hx	856.86 \pm 125.10	1 472.08 \pm 83.27
15	K-3-(6-Rh)Hx	723.39 \pm 104.99	Not detected
16	2 or 3 + CH ₃	290.57 \pm 30.17	240.59 \pm 7.94
17	K-3- <i>O</i> -rutinoside	4 659.71 \pm 28.27	20 397.43 \pm 498.38
18	2 or 3 + CH ₃	1 507.03 \pm 36.17	455.94 \pm 8.92
19	K-3- <i>O</i> -glucoside	12 998.91 \pm 585.02	23 360.75 \pm 920.33
20	2 or 3 - CO ₂	82.09 \pm 8.09	239.48 \pm 31.42
21	2 or 3 + CH ₃	152.20 \pm 6.19	189.10 \pm 16.64
TOTAL		45 889.66 \pm 1816.43	71 413.55 \pm 2177.13

^a Hex, hexoside; Isom, isomer; Pent, pentoside.

As observed in *C. urens* extracts (TH01 and TH21, **Table 7**), also the methanol extract obtained from the second collection of *G. gracillima* flowers (TH22) was richer in phenolic constituents (**Table 16**). Considering the time between collection of the samples (195), and also having into account the stage of maturation of both plant materials (196,197), the increment on the phenolics concentration noted, is somehow expected.

Despite of the noted quantitative discrepancies, the phenolic profile of the two extracts was very similar. Both extracts were predominantly characterized by the presence of kaempferol derivatives, constituting ca. 75.7% (TH19) and 86.6% (TH22) of the total quantifiable polyphenolic content (**Table 16**). The main constituent being detected in both extracts was kaempferol-3-*O*-glucoside (**19**) (12 998.91 ± 585.02 mg/kg dry extract on TH19 and 23 360.75 ± 920.33 mg/kg dry on TH22), followed by kaempferol-3-*O*-rutinoside (**17**) (4659.71 ± 28.27 mg/kg dry extract on TH19 and 20 397.43 ± 498.38 mg/kg dry extract on TH22) (**Table 16**). However, compound **17** was found in considerable higher amounts on the last extract (TH22) (**Table 16**). Furthermore, kaempferol-3-*O*-(2-rhamnosyl-6-hexoxyl)hexoside (**11**) was also present at appreciable concentrations on the second extract (TH22, 7 781.12 ± 91.92 mg/kg dry extract). Ellagic acid (**10**) was also detected at considerable amounts in the two extracts (3 631.83 ± 94.85 and 4 584.56 ± 110.06 mg/kg dry extract on TH19 and TH22, respectively) (**Table 16**).

So far, reports on the occurrence of kaempferol and ellagic acid derivatives in *Gustavia* spp. are limited to a single study by Souza and colleagues, where ellagic acid was identified in an ethanol extract obtained from the stem bark of *G. augusta* (204). Anyway, this is the first time that this metabolite and the above-reported ellagitannins and kaempferol derivatives are detected in *G. gracillima*.

3.3. Antidiabetic-like activity

3.3.1. Inhibition of carbohydrates absorption enzymes

The capacity of the selected extracts to inhibit the activity of the carbohydrates absorption enzymes and to improve postprandial hyperglycaemia was detailed. As above noted (*subsection 3.1.*), all the extracts were capable of inhibiting yeast α -glucosidase activity in a concentration-dependent way (**Figure 32**). The extracts obtained from the inflorescences of *C. urens* (TH01) and from the flowers of *G. gracillima* (TH19) were the most effective ((IC₅₀ value of 1.526 μ g/mL and 6.55 μ g/mL, respectively, **Table 5**), being significantly more active than the commercial drug acarbose (IC₅₀ value of 113.430 μ g/mL).

However, practically all samples, up until 1 000 $\mu\text{g}/\text{mL}$ concentration, displayed neglectable effects on α -amylase activity. In fact, only the extracts obtained from the inflorescences of *C. urens* (TH01) and from the stem bark of *F. curtipes* (TH06) were able to inhibit α -amylase activity in a concentration-dependent manner ($\text{IC}_{50} = 44.748$ and 109.802 $\mu\text{g}/\text{mL}$, respectively), yet in lesser extent than acarbose ($\text{IC}_{50} = 16.638$ $\mu\text{g}/\text{mL}$) (**Figure 48**).

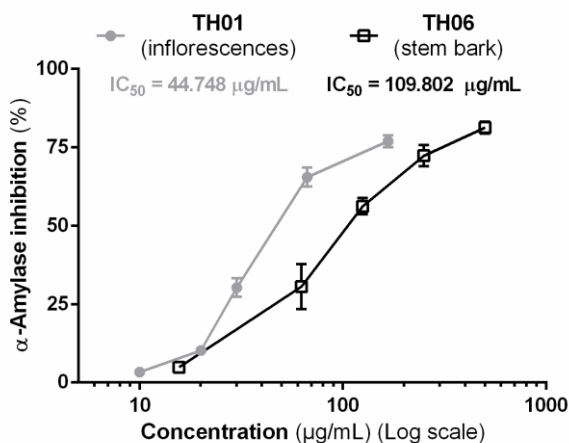


Figure 48. α -Amylase inhibition caused by the methanol extracts obtained from the inflorescences of *C. urens* (TH01) and from the stem bark of *F. curtipes* (TH06). Results represent the mean \pm SEM of three experiments, each performed in triplicate.

Considering the overall selectivity of the studied samples for α -glucosidase, the mechanism of inhibition elicited by the extracts was detailed. For this propose, α -glucosidase activity in the absence and presence of three different concentrations of each extract was evaluated as function of the substrate concentration (*p*-NPG, 1.667- 1666.667 μM). Data followed a Michaelis–Menten kinetics equation (**Figure 49**) and the calculated apparent kinetic parameters (K_m and V_{max}) are summarized in **Table 17**.

Apart from the extracts obtained from *C. urens* inflorescences (TH01) and from *F. curtipes* leaves (TH05), the remaining ones significantly decreased V_{max} and increased K_m , causing a mixed inhibition of α -glucosidase (**Table 17**). This means that the extract constituents can either bind to the enzyme or to the enzyme-substrate complex, blocking product formation. Relevantly, worth to mention that calculated α value, presented on the mixed inhibition models, allows to predict the degree to which the binding of inhibitor changes the affinity of the enzyme for substrate. As such, extracts TH06 and TH19, with calculated α values close to 1 (1.322 and 1.452, respectively) originated a mixed inhibition resembling the non-competitive mechanism displayed by TH01 and TH05 (**Table 17**, **Figure 49**). This specific type of inhibition results from the same affinity exhibited by the inhibitors for both the enzyme and the enzyme-substrate complex: the inhibitor dissociation constant from the substrate is equal to the inhibitor dissociation constant from

the substrate-enzyme complex. In this case, the dissociation constant is the same as the inhibition constant (k_i). As such, the k_i values calculated for TH01 and TH5 (1.380 and 146.4 $\mu\text{g}/\text{mL}$, respectively) (**Table 17**) are fairly related with the IC_{50} values (1.526 and 146.628 $\mu\text{g}/\text{mL}$, respectively) previously determined (**Table 5**). We have also studied the mode of inhibition of acarbose (25, 100 and 800 $\mu\text{g}/\text{mL}$) (data not shown) and, in agreement with previous reports (181), a competitive mechanism was observed, characterized by a significant K_m increase and a by a neglectable V_{max} alteration.

Table 17. Kinetic parameters for determining the type of α -glucosidase inhibition caused by the methanol extracts obtained from *C. urens* (TH01 and TH02), *F. curtipes* (TH05 and TH06), *C. tabularis* (TH07) and *G. gracillima* (TH19).^a

	V_{max}^b (mean \pm SD)	K_m (μM) (mean \pm SD)	r^2	$sy.x$	Inhibition type
α-Glucosidase activity	1086 \pm 17.5	167.8 \pm 8.3	0.9923	28.64	
TH01					
0.5 $\mu\text{g}/\text{mL}$	861.1 \pm 23.5**	161.1 \pm 13.6	0.9778	39.08	Non-competitive ($K_i = 1.380$)
1.0 $\mu\text{g}/\text{mL}$	722.1 \pm 22.3***	171.1 \pm 16.2	0.9731	36.18	
1.5 $\mu\text{g}/\text{mL}$	437.7 \pm 24.2****	194.7 \pm 32.1	0.9281	37.01	
TH02					
15 $\mu\text{g}/\text{mL}$	812.6 \pm 8.2****	165.5 \pm 5.1	0.9969	13.44	Mixed ($\alpha = 3.833$)
125 $\mu\text{g}/\text{mL}$	605.4 \pm 12.1****	335.5 \pm 17.9**	0.9939	13.65	
1000 $\mu\text{g}/\text{mL}$	181.5 \pm 12.6****	1260 \pm 160.6****	0.9878	4.04	
TH05					
50 $\mu\text{g}/\text{mL}$	1060 \pm 22.1	198.7 \pm 12.3	0.9883	33.43	Non-competitive ($K_i = 146.4$)
150 $\mu\text{g}/\text{mL}$	610.3 \pm 22.5****	206.1 \pm 22.4	0.9673	33.53	
500 $\mu\text{g}/\text{mL}$	101.3 \pm 10.7****	203.2 \pm 63.4	0.7985	16.01	
TH06					
5 $\mu\text{g}/\text{mL}$	870.2 \pm 26.8**	258.1 \pm 22.4	0.9811	35.48	Mixed ($\alpha = 1.322$)
10 $\mu\text{g}/\text{mL}$	605.9 \pm 24.0****	294.2 \pm 31.9	0.974	29.41	
20 $\mu\text{g}/\text{mL}$	31.2 \pm 2.3****	547.9 \pm 94.9***	0.9519	1.78	
TH07					
5 $\mu\text{g}/\text{mL}$	881.3 \pm 14.07**	328.9 \pm 14.06	0.996	16.1	Mixed ($\alpha = 8.511$)
20 $\mu\text{g}/\text{mL}$	680.4 \pm 17.03****	705.2 \pm 38.8**	0.9961	10.5	
40 $\mu\text{g}/\text{mL}$	509.3 \pm 24.9****	1529 \pm 129****	0.9955	6.2	
TH19					
2.5 $\mu\text{g}/\text{mL}$	704.8 \pm 25.85**	147.9 \pm 17.35	0.9571	44.2	Mixed ($\alpha = 1.452$)
5 $\mu\text{g}/\text{mL}$	463.6 \pm 45.56***	247.5 \pm 69.92**	0.8364	61.5	
15 $\mu\text{g}/\text{mL}$	348.5 \pm 35.04***	714.4 \pm 157.4****	0.9626	17.3	

^a Results represent the mean \pm SD of three experiments, performed in triplicate. Significant differences at ** $p < 0.01$, *** $p < 0.001$, and **** $p < 0.0001$. K_i , inhibition constant; K_m , Michaelis constant; r^2 , coefficient of determination; $Sy.x$, standard deviation of the residuals, V_{max} , maximum velocity, α , extra parameter (determines the degree to which the binding of inhibitor changes the affinity of the enzyme for substrate).

^b nmol/min/mg protein.

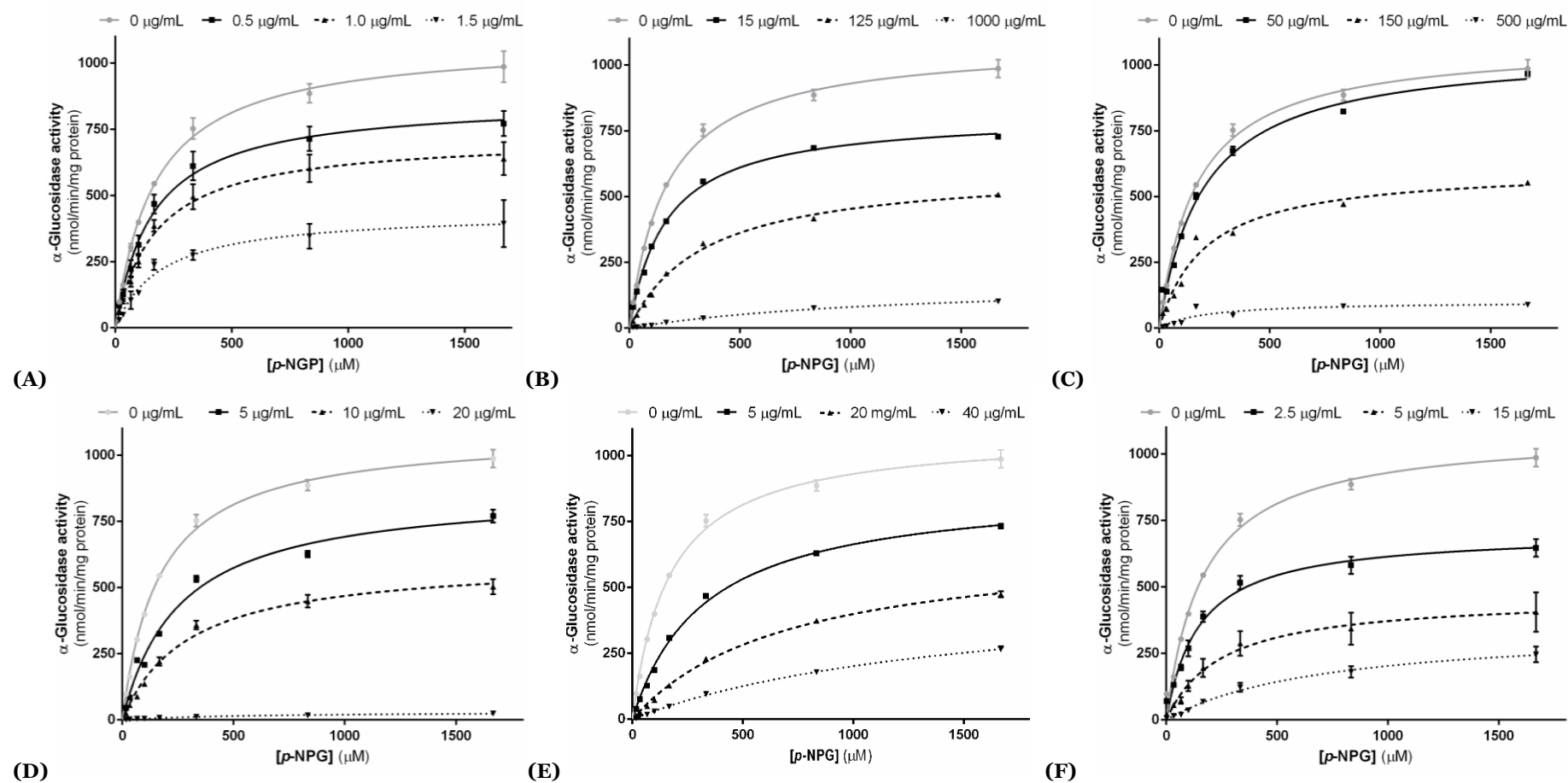


Figure 49. Michaelis-Menten kinetics of α -glucosidase activity recorded in the absence and presence of increasing concentrations of the methanol extracts obtained from the inflorescences (A) and fruits (B) of *C. urens*, from the leaves (C) and stem bark (C) of *F. curtipes*, from the leaves of *C. tabularis* (E) and from the flowers of *G. gracillima* (F). Results represent the mean \pm SEM of three experiments, performed in triplicate.

The recorded inhibitory mechanisms are commonly elicited by medicinal plants extracts, due to the presence of structurally distinct bioactives, that might bind with different affinities to the enzyme and/or to the enzyme-substrate complex (205). Relevantly, this might constitute an advantage relatively to the commercial drug, once on this type of inhibition the reaction V_{\max} decreases regardless of the substrate addition. As such, the inhibition of carbohydrates hydrolysis caused by the extracts is not compromised by the concentration of carbohydrates intake, which does not happen with acarbose (competitive inhibitor). With the mainstream therapy, the inhibition is conditioned by the substrate concentration, meaning that high carbohydrates intake can overcome the drug effect. Contrary, with the extracts under study, α -glucosidase inhibition is not limited by the substrate concentration, which means that higher carbohydrates intake will not originate a high postprandial hyperglycemia.

As previously discussed, the extracts obtained from the inflorescences of *C. urens* (TH01) and from the flowers of *G. gracillima* (TH19) displayed a pronounced yeast α -glucosidase inhibition, being significantly more effective than acarbose. However, the predictive *in vivo* value of the enzymes used on *in vitro* screening assays can easily vary according to their biological origin (*e.g.* yeast, human, rat) and obtaining processes (206). Thus, the inhibitory activity of these extracts was also investigated on the human α -glucosidase system. To this end, glucosidase-enriched cell supernatants, obtained from homogenates of human intestinal Caco-2 cells, were used. This cell line expresses most morphological and functional characteristics of human intestinal epithelium, including the dimeric intestinal enzyme sucrase-isomaltase system in the apical membrane (176).

To discharge acute cytotoxicity, the effects of the extracts on Caco-cells viability were checked, through the MTT assay. As evidenced on **Figure 50**, at concentrations below 250 $\mu\text{g}/\text{mL}$, no relevant alterations were noticed on the viability. Posteriorly, the capacity of the extracts to inhibit the human α -glucosidase enzymatic system was checked at concentrations ranging from 12.5 to 200 $\mu\text{g}/\text{mL}$ (TH01) and 3.9-62.5 $\mu\text{g}/\text{mL}$ (TH19). Again, both extracts were able to inhibit this enzymatic system in a concentration-dependent manner, being considerably more active than the reference drug acarbose, which required a concentration of 400 $\mu\text{g}/\text{mL}$ to cause $18.383 \pm 1.866\%$ inhibition of the enzyme. Moreover, contrarily to what was observed against yeast α -glucosidase, the extract obtained from *G. gracillima* (TH19) ($\text{IC}_{50} = 38.431$) was here significantly ($p < 0.01$) more active than the one obtained from the inflorescences of *C. urens* (TH01) ($\text{IC}_{50} = 64.788$) (**Figure 50B**). As formerly substantiated by others, the discrepancy on the enzymatic inhibitory activity detected in these two models certainly results from structural and biochemical differences between yeast α -glucosidase and the dimeric intestinal enzyme sucrase-isomaltase system

(generically designated as human α -glucosidases) (206). Nonetheless, all data gathered here evidence that under the same experimental conditions, both extracts (TH01 and TH19) are substantially more effective in inhibiting α -glucosidase than the conventional drug and, therefore, might be considered as novel therapeutic approach to manage postprandial hyperglycaemia. However, further *in vivo* studies, namely in high-maltose loaded rats, should be conducted to confirm these findings and to settle lethal and effective doses, before proceeding to small-scaled clinical trials.

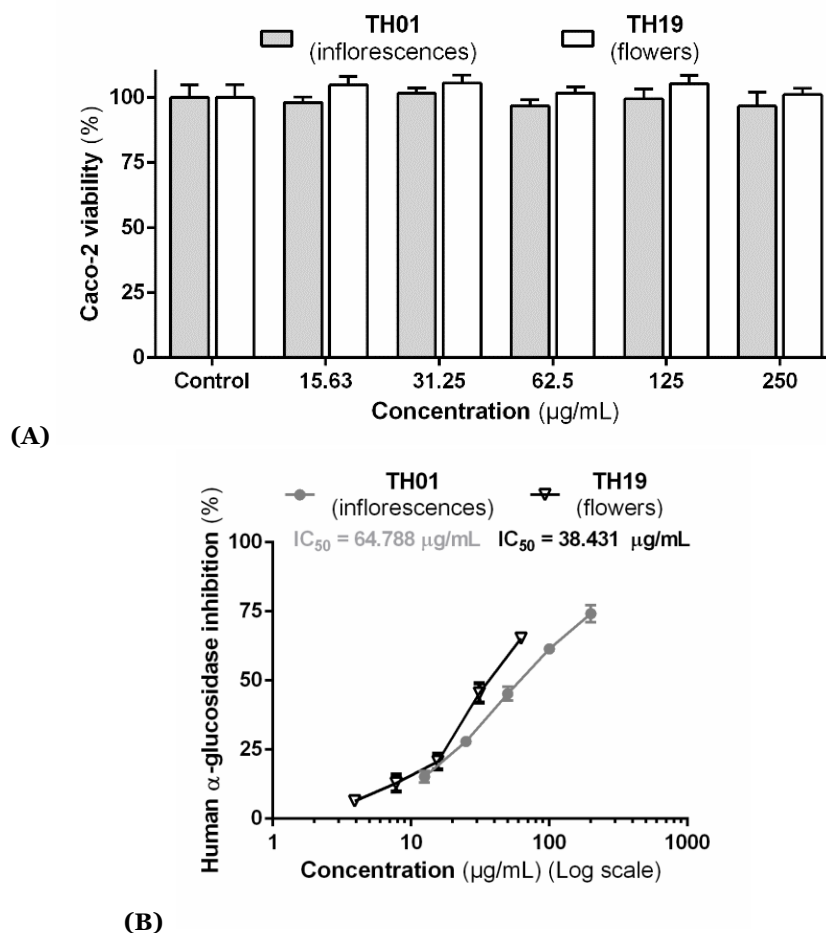


Figure 50. Effects of the methanol extracts obtained from the inflorescences of *C. urens* (TH01) and from the flowers of *G. gracillima* (TH19) on Caco-2 cells viability (A) and human α -glucosidase activity (B). Results represent the mean \pm SEM of at least three experiments, each performed in triplicate.

Futhermore, data obtained here is particularly relevant to support the alleged “glycaemic safety” of *C. urens*-derived food products, broadly consumed all over Asian countries (136,207). While we cannot directly extrapolate our outcomes for the processed kitul-based products, our results provide preliminary evidence on the antidiabetic properties of kitul inflorescences, calling for further studies on the processed aliments commercialized.

3.3.1.1. Inhibition of carbohydrates absorption enzymes vs phenolic content

A significant ($p < 0.01$) negative correlation between the phenolic content of the samples and the estimated IC_{50} values for yeast α -glucosidase inhibition was found (Pearson correlation; $r = -0.6934$; $p = 0.0014$) (**Figure 51**). This indicates that the observed activity might be related to the concentration of polyphenolic constituents. In fact, if we exclude the extract obtained from the stem bark of *F. curtipes* (TH06, IC_{50} value of $9.261 \mu\text{g/mL}$, **Table 5**), this correlation gets even stronger (Pearson correlation; $r = -0.9379$; $p < 0.0001$), suggesting that, for the remaining species, the inhibition of yeast α -glucosidase is even more dependent of the concentration of phenolics. According to this model, the inhibition caused by *F. curtipes* stem bark extract appears to be related with the presence of other non-phenolic components. However, the qualitative composition of the extract cannot be excluded.

Phenolic compounds, particularly flavonoids (181), hydroxycinnamic acids (208,209) and flavan-3-ols derivatives (210), are reported for their significant α -glucosidase inhibitory effects. In reality the noteworthy yeast α -glucosidase inhibitory effects with hydroxycinnamic-enriched extracts were previously reported (208,209). Therefore, considering the amounts of these metabolites at *C. urens* extracts (TH01 = $35\,538.9 \pm 1\,610.82 \text{ mg/kg}$ of dry extract; TH02 = $11\,091.57 \pm 4\,82.21 \text{ mg/kg}$ of dry extract, **Table 7**), and also based on the recorded IC_{50} values (TH01 = $1.526 \mu\text{g/mL}$; TH02 = $108.089 \mu\text{g/mL}$, **Table 7**) and on the shapes of the concentration-response graph (that vary according to the concentrations of phenolics on each sample) (**Figure 32A**), it is plausible to assume that these constituents contribute, at least in part, for the activity. Furthermore, flavonoids have shown to inhibit α -glucosidase and some crucial structural features were evidenced by structure activity relationship (SAR) studies: the 2,3-insaturation at the C ring and the hydroxylation at C5 in the A ring and at C4' in the B ring (181). Most of the flavonoids present in the other extracts, comply with these structural characteristics, and therefore may also have a role on the recorded inhibition. Besides, the low molecular weight proanthocyanidins, detected on the extracts obtained from the leaves of *C. tabularis* (total of $29\,796.41 \pm 1\,441.45 \text{ mg/kg}$ of dry extract, **Table 13**) and on the stem bark of *F. curtipes* (total of $4487.00 \pm 396.49 \text{ mg/kg}$ of dry extract, **Table 10**), are also known as α -glucosidase inhibitors (210). Hence, these constituents might also account as well for the observed biologic effects.

Also, for α -amylase inhibition a significant ($p < 0.01$) negative correlation (Pearson correlation; $r = -0.9990$; $p < 0.0001$) between the phenolic content and the calculated IC_{50}

values was observed. In this sense, the extract with higher concentration of phenolics (TH01 = $35\,538.9 \pm 1\,610.82$ mg/kg of dry extract *vs* TH06 = $5\,374.15 \pm 436.61$ mg/kg of dry extract, **Table 7** and **10**) exhibited also stronger inhibitory activity towards α -amylase (IC_{50} value of $44.748 \mu\text{g/mL}$ *vs* $109.802 \mu\text{g/mL}$), suggesting that the phenolic amounts are directly related with the recorded activity. However, in this case, such relation ought not to be directly draw, once other extracts also rich in phenolic constituents, namely TH07 ($41\,899.95 \pm 1\,768.87$ mg/kg of dry extract, **Table 13**) and TH19 ($45\,889.66 \pm 1816.43$ mg/kg of dry extract, **Table 16**), did not display noteworthy inhibitory effects on α -amylase activity at the highest tested concentration.

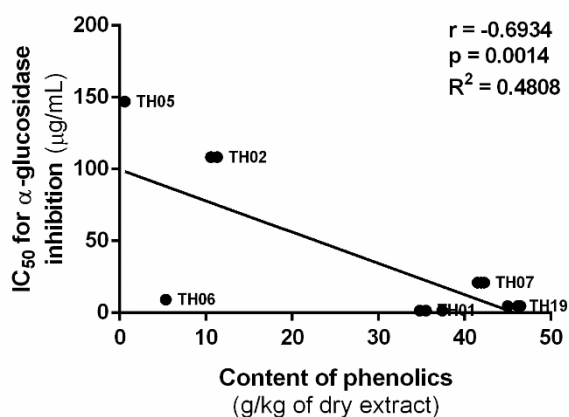


Figure 51. Pearson correlation between the content of phenolic compounds (g/kg of dry extract) of the extracts and the estimated IC_{50} values determined for the inhibition of α -glucosidase ($\mu\text{g/mL}$).

3.3.2. Inhibition of lipids absorption enzyme

As detailed in the introductory section, obesity is a trigger factor for diabetes development and progression (1,4). Thus, prevention and modulation of weight gain have also a pivotal role not only on the prevention of the disease, but also on its attenuation (4). Pancreatic lipase is the key enzyme involved on the sequential hydrolysis of complex triglycerides, allowing an easy and fast absorption of low molecular weight free fatty acids (211). So, selective inhibition of this enzyme can delay lipid digestion and consequently reduce the blood levels of free fatty acids and triglycerides, improving lipidemic parameters, including very low-density lipoprotein and low-density lipoprotein plasmatic levels (211). As such, the current work also included the assessment of the inhibitory capacity of methanol extracts upon pancreatic lipase activity.

Only the extracts obtained from the inflorescences of *C. urens* (TH01) and from the flowers of *G. gracillima* (TH19) inhibited pancreatic lipase activity in a concentration-dependent manner (**Figure 52**). However, inhibition of this enzyme was substantially weaker than the one recorded for the carbohydrates hydrolysing enzymes (**Figure 32** and **Figure 48**).

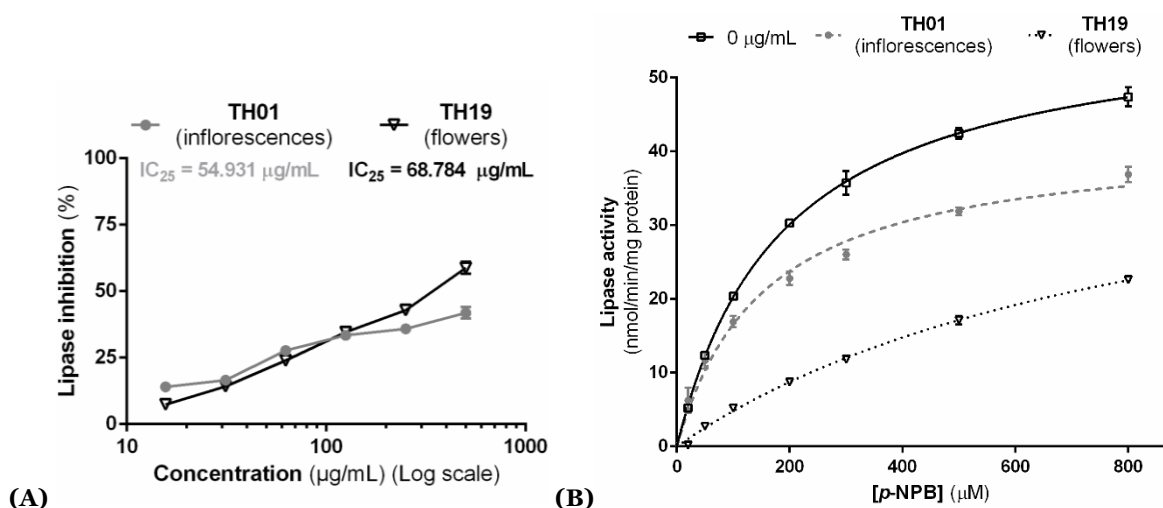


Figure 52. (A) Pancreatic lipase inhibition caused by the methanol extracts obtained from the inflorescences of *C. urens* (TH01) and from the flowers of *G. gracillima* (TH19). (B) Michaelis-Menten kinetics of pancreatic lipase activity recorded in the absence and presence of the methanol extracts obtained from the inflorescences of *C. urens* (TH01) and from the flowers of *G. gracillima* (TH19). Results represent the mean \pm SEM of three experiments, each performed in triplicate.

As evidenced on **Figure 52A**, at concentrations below 125 μg/mL the extract obtained from the inflorescences of *C. urens* (TH01) was more potent than the one obtained from *G. gracillima* flowers (TH19). Nevertheless, at higher concentrations, the inhibition caused by TH19 overcame the inhibition caused by TH01. Still, TH01 and TH19 treatment only originated a maximum inhibition of 43.40 ± 2.72 % and 58.78 ± 3.87 %, respectively. Hence, both extracts were considerably less potent than the therapeutic drug orlistat ($IC_{50} = 0.407$ μg/mL). Nevertheless, so far this is the only study addressing the pancreatic lipase inhibitory activity of both plant materials.

In virtue of the low inhibitory effects here recorded, the kinetic study of pancreatic lipase inhibition was performed only at 500 μg/mL. The pancreatic lipase activity was recorded in function of the substrate concentration (*p*-NPB, 20–800 μM) and fitted into a Michaelis–Menten kinetics equation (**Figure 52B**) to determine the kinetic parameters (K_m and V_{max}) (**Table 18**). Again, the inhibition recorded with *C. urens* methanol extract (TH01) was lower than the one caused by *G. gracillima* extract (TH19). The significant ($p < 0.001$) decrease of the reaction V_{max} originated by 500 μg/mL of *C. urens* inflorescences extract

(TH01), with no significant alteration on K_m , evidenced that the extract exerts a mixed-type pancreatic lipase inhibitory effect. Moreover, we can infer that this inhibition is close to uncompetitive ($\alpha = 0.3504$), which means that the components of *C. urens* extract bind preferentially to the enzyme-substrate complex. On the other hand, the extract obtained from *G. gracillima* flowers (TH19) (**Table 18**) exhibited a competitive-like inhibitory activity (K_m increased and no variation at the V_{max} was detected). In this type of inhibition, the extract compete with the substrate on the binding site of the active pocket of pancreatic lipase.

Table 18. Kinetic parameters for determining the inhibition type of pancreatic lipase caused by the methanol extracts obtained from the inflorescences of *C. urens* (TH01) and from the flowers of *G. gracillima* (TH19).^a

	V_{max}^b (mean \pm SD)	K_m (μ M) (mean \pm SD)	r^2	$sy.x$	Inhibition type
Pancreatic lipase activity	58.52 \pm 1.3	188.5 \pm 11.0	0.9931	1.274	
TH01					Mixed
500 μ g/mL	42.12 \pm 1.7 ^{***}	154.2 \pm 18.23 ^{**}	0.9653	2.001	($\alpha = 0.3504$)
TH19					Competitive
500 μ g/mL	47.6 \pm 2.9	888.0 \pm 84.4 ^{****}	0.9944	0.5828	

^a Results represent the mean \pm SD of three experiments, performed in triplicate. Significant differences at ^{***} $p < 0.001$, and ^{****} $p < 0.0001$. K_m , Michaelis constant; r^2 , coefficient of determination; $Sy.x$, standard deviation of the residuals; V_{max} , maximum velocity; α , extra parameter (determines the degree to which the binding of inhibitor changes the affinity of the enzyme for substrate).

^b nmol/min/mg protein.

To our knowledge, this is the first time that *C. urens* and *G. gracillima* have been investigated for pancreatic lipase inhibition. Hence, beyond of significantly inhibiting carbohydrates hydrolysing enzymes, these plant materials appear also to have some potential to mitigate, to certain extent, lipids absorption.

3.3.2.1. Inhibition of lipids absorption enzyme vs phenolic content

Contrarily to what was observed with α -glucosidase, for pancreatic lipase there is no correlation between the phenolic content of the extracts and the noticed inhibitory activity. In fact, as above outlined, the lipase inhibitory activity displayed by the two active extracts varied as a function of the concentrations tested (**Figure 52A**). Moreover, as observed for α -amylase, the extract TH07, with a significant phenolic content (41 899.95 \pm 1 768.87 mg/kg of dry extract, **Table 13**) did not express noteworthy pancreatic lipase inhibitory effects. Hence, it is plausible to assume that the recorded activity might not be related with the samples phenolics profile, at least in terms of their content.

Still, phenolic compounds inhibitory effects of on lipase activity are found in literature, particularly for flavonoids and their glycosylated derivatives (212). In this regard, studies evidence that glycosylation increases the inhibitory activity of flavonoids due to polarity improvement, allowing hydrogen bonding formation and consequently decreasing the necessary hydrophobic environment for triacylglyceride hydrolysis near the catalytic site of the enzyme (213,214). In fact, the extract prepared from *G. gracillima*, in comparison with the remaining, is particularly rich in glycosylated flavonoids, namely in kaempferol derivatives (**Table 16**), that might account, at least partially, for the observed antilipase activity. Also, the hydroxycinnamic acids of *C. urens*, namely the caffeoylquinic acid derivatives (**Table 7**), are known to inhibit pancreatic lipase activity, and, therefore, can also have a role on the observed effects (215). However, based on the above-described absence of correlation with the phenolic content, the binding of other constituents of the extracts to the enzyme and/or to the enzyme-substrate complex arises here as a probable hypothesis.

3.3.3. Aldose reductase inhibition

The polyol pathway is involved in the cellular toxicity of diabetic hyperglycaemia, being one of the main causes of diabetes-related complications. Aldose reductase overactivity is responsible for the accumulation of cytosolic sorbitol, compromising cell osmotic balance and leading to the destruction of microvasculature, mainly in the retina, kidney and nerves (17,216). While commercially available aldose reductase inhibitors are scarce, over the past decades, research and therapeutic approaches based on aldose reductase inhibition have been attempted, several patent applications being submitted (216).

Within this frame of reference, the capacity of the extracts to inhibit aldose reductase activity was investigated in a cell-free system. All the extracts caused a concentration-dependent aldose reductase inhibition (**Figure 53**). The extract prepared from the leaves of *C. tabularis* (TH07), followed by the extracts obtained from the inflorescences of *C. urens* (TH01) and from the flowers of *G. gracillima* (TH19) were the most potent (IC₅₀ values of 23.556, 55.689, and 62.544 µg/mL, respectively) (**Figure 53**). All these extracts displayed an aldose reductase inhibitory activity significantly ($p < 0.0001$) higher than the positive control rutin (IC₅₀ = 150.368 µg/mL).

To the best of our knowledge, the inhibitory activity of *C. urens*, *F. curtipes*, *C. tabularis* and *G. gracillima* towards aldose reductase was assessed herein for the first time. As above-

stated, the inhibition of this enzyme appears to have positive outcomes on some diabetic complications, as neuropathy, cataracts, nephropathy and retinopathy (217).

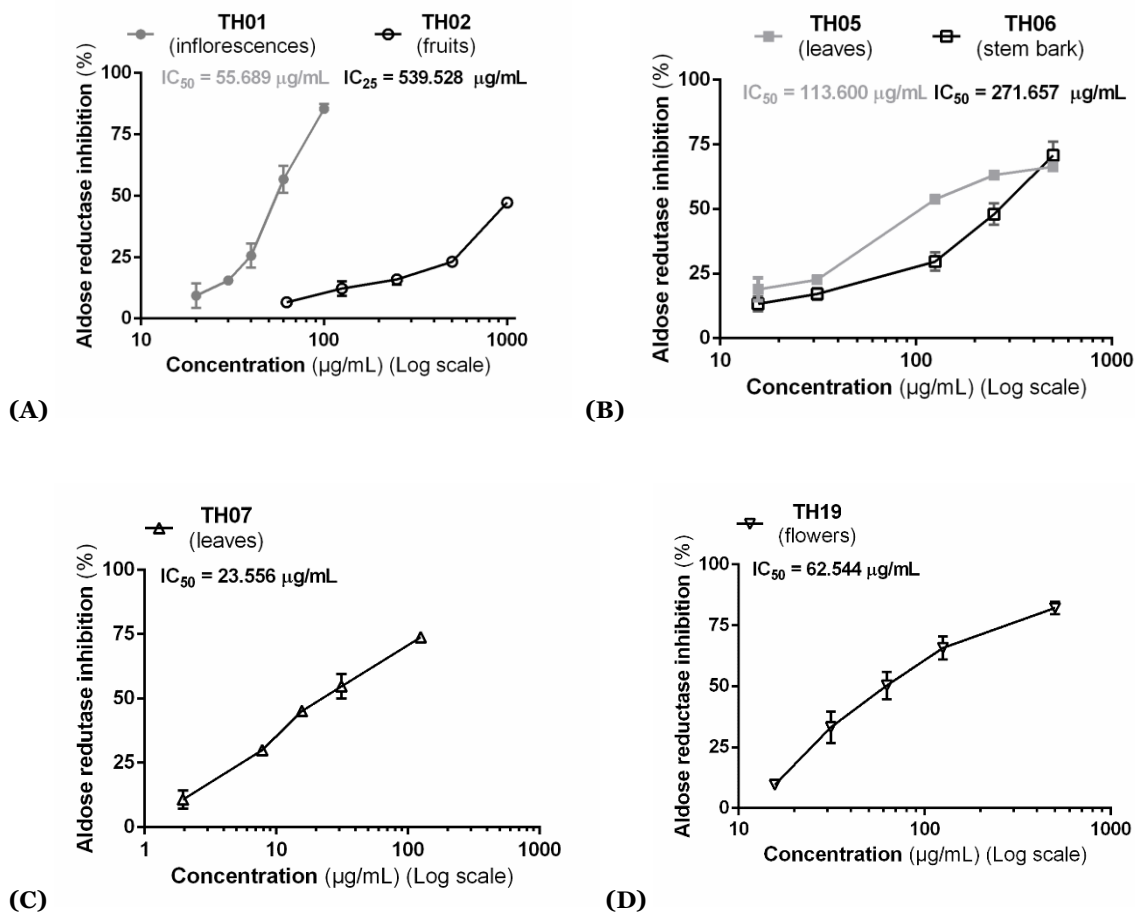


Figure 53. Aldose reductase inhibition caused by the methanol extracts obtained from the inflorescences and fruits of *C. urens* (A), from the stem bark and leaves of *F. curtipes* (B), from the leaves of *C. tabularis* (C) and from the flowers of *G. gracillima* (D). Results represent the mean \pm SEM of three experiments, each performed in triplicate.

3.3.3.1. Aldose reductase inhibition vs phenolic content

A negative correlation was observed between the total concentration of phenolics in the extracts and the IC_{50} values obtained for aldose reductase inhibition (Pearson correlation; $r = -0.7490$; $p < 0.0013$) (Figure 54). In fact, the extracts with greater aldose reductase inhibitory activity (TH01, TH07 and TH19) were the ones that exhibited higher phenolic compounds amounts ($35\,538.9 \pm 1\,610.82$, $41\,899.95 \pm 1\,768.87$ and $45\,889.66 \pm 1816.43$ mg/kg of dry extract, correspondingly; Tables 7, 13 and 16).

Indeed, hydroxycinnamic acids, constituting the total phenolic fraction *C. urens* extracts ($35\,538.9 \pm 1\,610.82$ and $11\,091.57 \pm 4\,82.21$ mg/kg of dry extract; **Table 7**) and also occurring on TH06 (268.81 ± 11.62 mg/kg of dry extract, **Table 10**), meet the structural requirements for aldose reductase inhibition, including the acidic group, that forms an ionic interaction in the binding pocket of the active site of the enzyme, and the aromatic moiety, which is placed on the lipophilic pocket (218,219). The same applies to the flavonoids and, in less extent, to the flavan-3-ols derivatives detected in the other extracts. In agreement, a previous study also evidenced a negative correlation ($r = -0.761$) between flavonoids content and the aldose reductase inhibitory activity of Lauraceae leaf extracts (217). Yet, authors claimed that the inhibitory activities of flavan-3-ols were weaker than flavonol-type compounds (217). In fact, as assessed by us, while no significant relation (Pearson correlation; $r = -0.4140$; $p = 0.1809$) between flavan-3-ols derivatives concentrations of the samples and the estimated IC_{50} values for aldose reductase inhibition has been detected, a negative correlation (Pearson correlation; $r = -0.7490$; $p = 0.0130$) between the amounts of flavonoids and the recorded activity was observed. As *C. tabularis* and *G. gracillima* extracts have considerable amounts of flavonoids ($12\,103.55 \pm 327.42$ and $34\,856.35 \pm 1479.11$ mg/kg of dry extract, respectively; **Tables 13** and **16**), these metabolites might also account for the recorded inhibitory activity. Furthermore, previous SAR studies demonstrated that di and triglycosylated kaempferol derivatives (corresponding to *ca.* 75 % of the phenolic content of the extract obtained from *G. gracillima* flowers) exhibited stronger inhibitory activity than monoglycosylated flavonols, which, in turn, had higher activity than the corresponding aglycone (220). Therefore, considering the abundance of tri- and diglycosylated derivatives of kaempferol in the extract obtained from *G. gracillima* (**Table 16**), it is plausible to assume that the significant inhibitory activity herein observed might outcome, at least in part, from the presence of these derivatives.

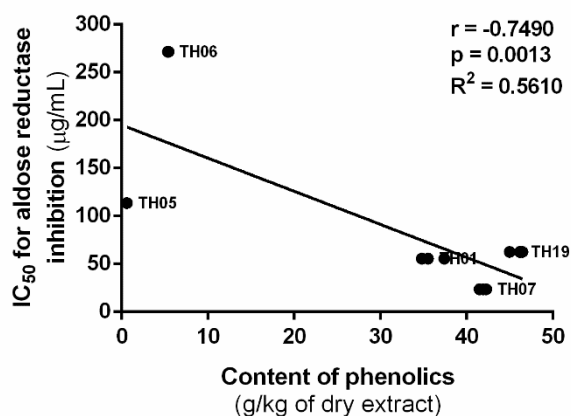


Figure 54. Pearson correlation between the content of phenolic compounds (g/kg of dry extract) of the extracts and the estimated IC_{50} value determined for the inhibition of aldose reductase ($\mu\text{g/mL}$).

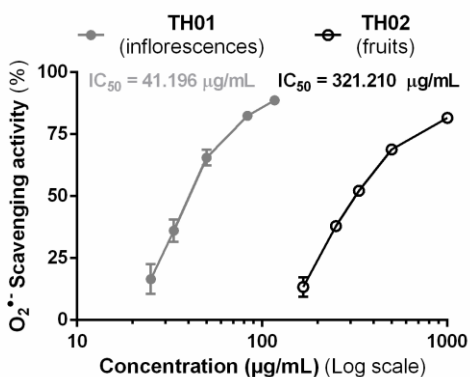
Notwithstanding the previously noted correlation, and as it can be perceived in **Figure 53A**, different concentration-response curve shapes were obtained with fruits and inflorescences extracts of *C. urens* (TH01 and TH02). Those extracts have a similar qualitative phenolic footprint that does not reflect the inhibition pattern recorded, hence suggesting the contribution of other non-phenolic constituents for aldose reductase inhibition. In the same way, a similar behaviour was also recorded with the extracts obtained from *F. curtipes* (TH05 and TH06, **Figure 53B**). Therefore, and aside the partial contribution of the phenolic constituents, it is plausible to assume that the aldose reductase inhibitory activity here observed might also outcome from the presence of other bioactives from distinct structural origin.

3.4. Anti-radical activity

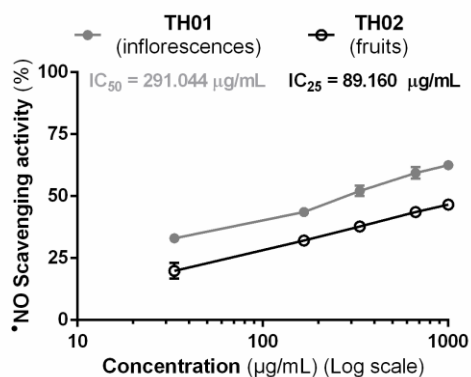
3.4.1. Radical scavenging effects

As outlined in the introductory section, the intimate link between the development of diabetes and the overproduction of radical species is currently deep-seated and well-sustained, free radical scavengers being acknowledged to delay the development and progression of diabetes and associated complications (221). Therefore, the radical scavenging properties of the extracts were assessed, towards nitrogen and oxygen reactive species, correspondingly $\cdot\text{NO}$ and $\text{O}_2\cdot^-$.

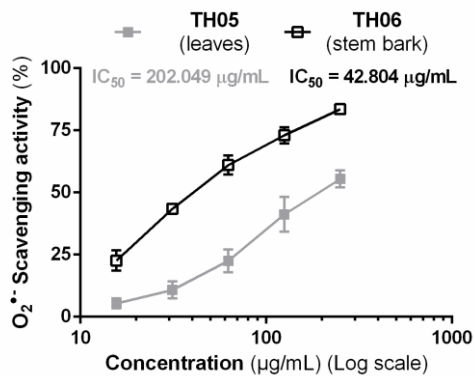
$\text{O}_2\cdot^-$, directly resulting from several cellular processes, including glucose oxidation, acts as a precursor for the generation of other ROS, namely the extremely reactive hydroxyl radical (221). All the extracts were able to scavenge $\text{O}_2\cdot^-$ radicals in a concentration-dependent manner (**Figure 55A**). Higher antiradical effects were observed with the extract obtained from leaves of *C. tabularis* (TH07) ($\text{IC}_{50} = 33.793 \mu\text{g/mL}$), followed by the extracts obtained from the inflorescences of *C. urens* (TH01) ($\text{IC}_{50} = 41.196 \mu\text{g/mL}$) and from the stem bark of *F. curtipes* (TH06) ($\text{IC}_{50} = 42.804 \mu\text{g/mL}$). Still, *G. gracillima* flowers extract (TH19) also displayed an important $\text{O}_2\cdot^-$ scavenging activity ($\text{IC}_{50} = 79.278 \mu\text{g/mL}$) (**Figure 55A**). On the other hand, the extracts prepared from the fruits of *C. urens* and from the leaves of *F. curtipes* exhibited a weak $\text{O}_2\cdot^-$ scavenging capacity (IC_{50} values of $321.210 \mu\text{g/mL}$ and $214.674 \mu\text{g/mL}$, respectively), being significantly ($p < 0.0001$) less active than the positive control quercetin ($\text{IC}_{50} = 24.621 \mu\text{g/mL}$) (**Figure 55A**). $\text{O}_2\cdot^-$ can directly interact with $\cdot\text{NO}$ leading to the formation of reactive peroxynitrite anions, which, in turn, can



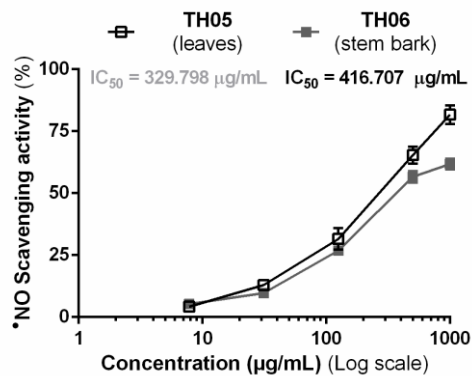
(A1)



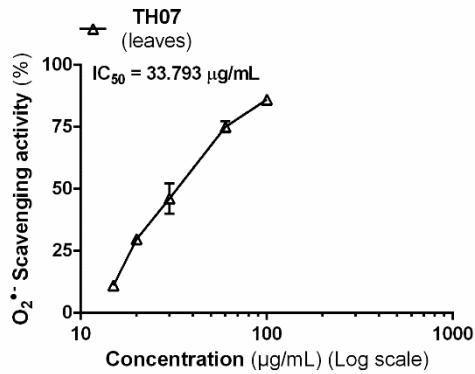
(B1)



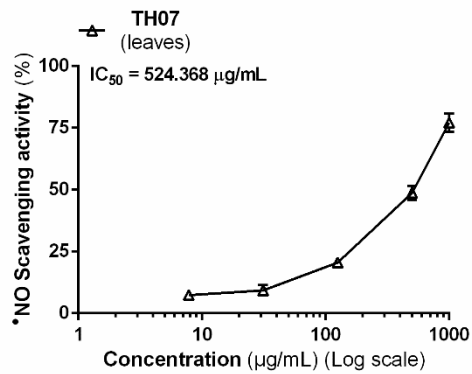
(A2)



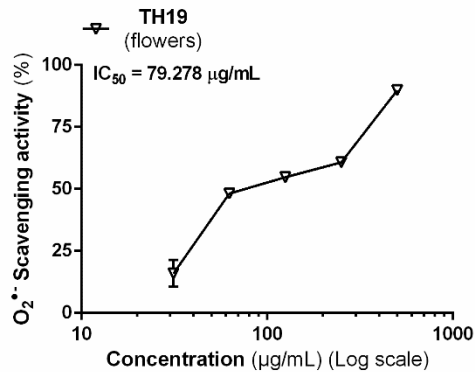
(B2)



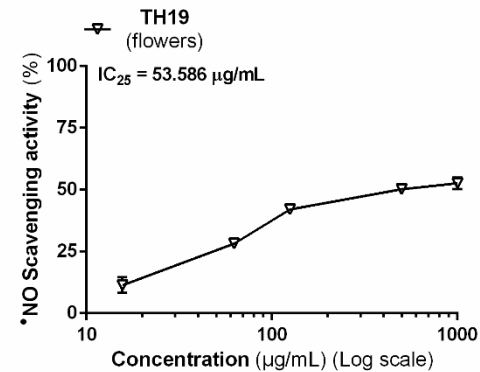
(A3)



(B3)



(A4)



(B4)

Figure 55. $O_2\cdot^-$ (A) and $\cdot NO$ (B) scavenging activity displayed by the methanol extracts obtained from the inflorescences and fruits of *C. urens* (A1 and B1), from the stem bark and leaves of *F. curtipes* (A2 and B2), from the leaves of *C. tabularis* (A3 and B3) and from the flowers of *G. gracillima* (A4 and B4). Results represent the mean \pm SEM of three experiments, each performed in triplicate.

damage lipids, proteins or DNA, causing changes in protein expression (221). Concerning the ability to scavenge $\cdot NO$ (**Figure 55B**), the extracts obtained from the inflorescences of *C. urens* (TH01) and from the leaves of *F. curtipes* (TH04) and *C. tabularis* (TH07) were the most effective (IC_{50} values of 291.044, 329.798 and 524.369 $\mu g/mL$, respectively), exhibiting 62.55 ± 1.64 % (TH01), 81.68 ± 6.59 % (TH05) and 77.09 ± 6.27 % (TH07) scavenging activity at the highest tested concentration (1 000 $\mu g/mL$). The remaining extracts barely reached 60% of the $\cdot NO$ scavenging activity (**Figure 55B**).

As free radical-mediated peroxidation of lipids is also known to be increased in diabetic and obese patients (15), the capacity of the extracts to mitigate lipid peroxidation was also investigated. All the extracts, except the one prepared from *C. urens* fruits (TH02), were capable of reducing linolenic acid peroxidation in a concentration-dependent manner (**Figure 56**). As observed for $O_2\cdot^-$ scavenging, the extract obtained from *C. tabularis* leaves (TH07) featured as the most potent ($IC_{50} = 165.597$ $\mu g/mL$), followed by the extract from the inflorescences of *C. urens* (TH01, $IC_{50} = 228.534$ $\mu g/mL$) (**Figure 56A and C**). Those extracts prove to be more effective than BHT ($IC_{50} = 295.29$ $\mu g/mL$), used herein as a positive control. Both extracts obtained from *F. curtipes* (TH05 and TH06, **Figure 56B**) exhibited similar antiradical effects, being however the extract obtained from the stem bark (TH06) more active at the highest tested concentration (1 000 $\mu g/mL$).

Even though literature already evidenced the antioxidant properties of the leaves (141) and fruits (99, 108) of *C. urens*, this is the first time that the inflorescences of the palm tree are investigated on their antiradical effects. Analogously, the scavenging properties of *C. tabularis* have been previously evidenced by others (158–160). In agreement with our findings, Kaur and colleagues verified that a methanol extract obtained from *C. tabularis* leaves inhibited 91.52 % of lipid peroxidation at 100 $\mu g/mL$ (158). Moreover, a 80% methanol extract obtained from the leaves displayed also a significant scavenging activity against the radicals DPPH \cdot (92.91% at 180 $\mu g/mL$) (159) and $O_2\cdot^-$ (61.25% at 100 $\mu g/mL$) (160). Still, for the remaining plant species, this is the first time that radical scavenging effects are outlined.

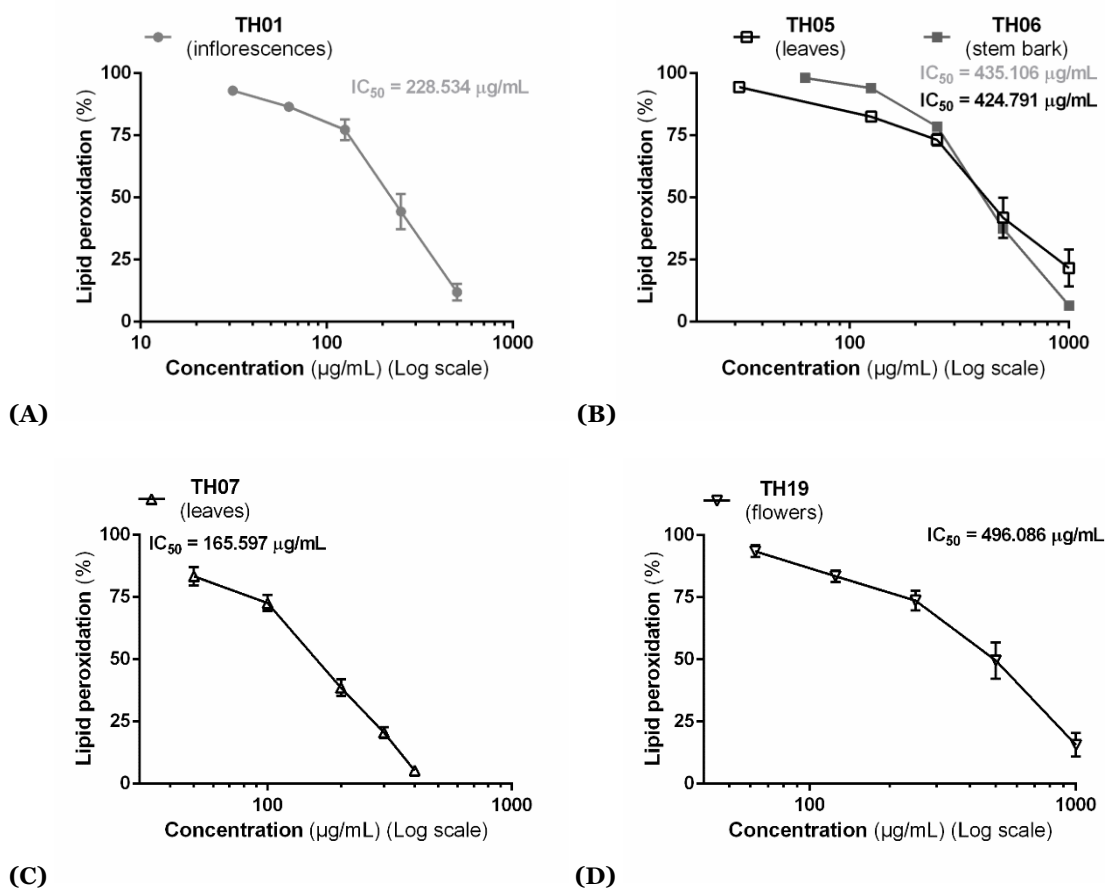


Figure 56. Inhibition of lipid peroxidation caused by the methanol extracts obtained from the inflorescences of *C. urens* (A), from the stem bark and leaves of *F. curtipes* (B), from the leaves of *C. tabularis* (C) and from the flowers of *G. gracillima* (D). Results represent the mean \pm SEM of three experiments, each performed in triplicate.

3.4.1.1. Antiradical activity vs phenolic content

The DPPH \cdot and O $_2\cdot^-$ scavenging activities were negatively correlated (Pearson correlation; $r = -0.6777$ and $r = -0.5571$, $p = 0.0020$ and $p = 0.0176$, correspondingly) (**Figure 57**) with the phenolic content of the samples, suggesting that the recorded scavenging effects are also mediated, to some extent, by the phenolic constituents. In fact, polyphenols, bearing privileged structural scaffolds, act as potent natural antioxidants. These metabolites can transfer a hydrogen atom from hydroxyl groups, originating a phenoxyl radical, that is quickly stabilized by resonance (222). Particularly concerning flavan-3-ols oligomers, occurring in high amounts in the extracts obtained from the stem bark of *F. curtipes* and in *C. tabularis* leaf extract ($4\,487.00 \pm 396.49$ and $29\,796.41 \pm 1441.44$ mg/kg dry extract, respectively, **Table 10** and **13**), studies evidence a positive correlation between their content and the antiradical activity (223,224). In addition, flavonoids and hydroxycinnamic

acids, present in the other samples, are acknowledged by their radical scavenging properties (225). The double bond at C2-C3 in conjugation with a 4-oxo function in the C-ring, observed in flavonols, found in TH07 ($12\ 103.55 \pm 327.42$ mg/kg of dry extract, **Table 13**) and TH19 ($61\ 811.96 \pm 1\ 932.74$ mg/kg of dry extract, **Table 16**), enhances the flavonoid phenoxyl radical stabilization and, consequently, increases the radical scavenging activity (225). Besides, the catechol moiety in B-ring, also enhances the antiradical effect, once it confers higher stability to the resulting phenolate radical (225).

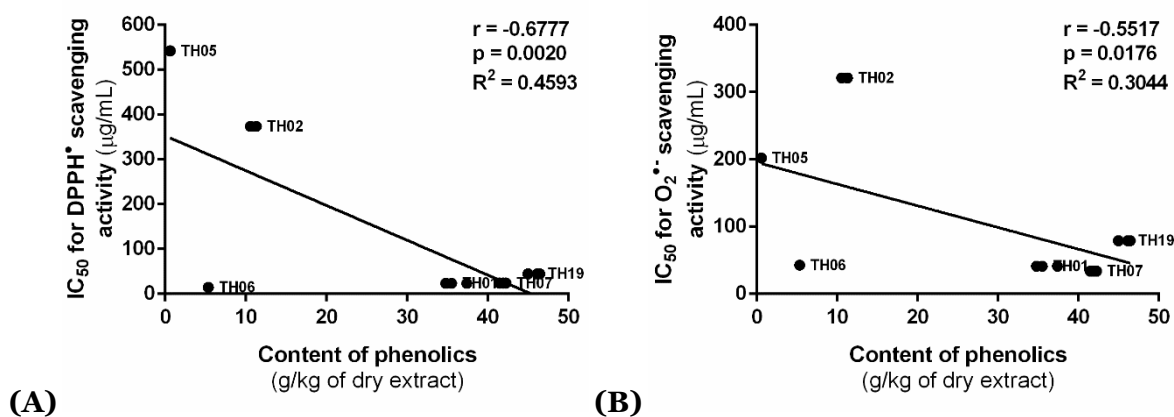


Figure 57. Pearson correlation between the content of phenolic compounds (g/kg of dry extract) of the extracts and the estimated IC₅₀ value determined for the DPPH• (A) and O₂•⁻ (B) scavenging activities (µg/mL).

Even though no significant correlation (Pearson correlation; $r = 0.4830$, $p = 0.0682$) was observed between •NO scavenging activity and the concentrations of phenolics in the extracts, a phenolic content-dependent activity was observed upon exposure to the extracts obtained from *C. urens* inflorescences (**Figure 55B1**). The extract prepared from the inflorescences, with *ca.* 3-times higher hydroxycinnamic acids derivatives concentrations (**Table 7**), was significantly more active than the one obtained from the fruits; in addition, as already happened in regards to O₂•⁻, both extracts exhibited also a parallel concentration-response behaviour for •NO, suggesting that dissimilarities on the activity result from differences on the phenolics quantitative profiles. Congruently, also Sambanthamurthi et al. detected a potent free radical scavenging activity with a 3-*O*, 4-*O* and 5-*O*-caffeoylshikimic acids-rich extract (226). Therefore, based on such literature reports, it is plausible to assume that those compounds, along with the other caffeoylquinic acid derivatives also reported by their antiradical properties (227), contribute for *C. urens* antiradical effects.

Particularly concerning lipid peroxidation, the lack of a significant correlation (Pearson correlation; $r = -0.4021$, $p = 0.1373$) between the phenolics concentration at the samples and

the estimated IC₅₀ values, suggests that the observed reduction is not related with the quantitative polyphenolic fingerprint of the extracts. In this case, the type of phenolics present in the extracts, the other non-phenolic constituents and the overall interactions among all, might have also an impact on the recorded activity.

3.4.2. Modulation of reactive species in pancreatic cells

Hyperglycemia-induced ROS production (resulting from both glucose autoxidation and protein glycation) is one of the major physiopathological events underlying diabetes development, strongly contributing for pancreatic β -cells dysfunction (228). In comparison with other tissues, pancreatic cells express less antioxidant enzymatic systems and produce high levels of endogenous ROS, being, therefore, highly susceptible to oxidative stress-induced damage (26).

Considering the above-reported antidiabetic properties, and also bearing in mind the recorded antiradical effects, the extracts obtained from the inflorescences of *C. urens* and from the flowers of *G. gracillima* were selected as the most promising ones. Hence, the effects of those extracts on the levels of intracellular reactive species were investigated in glucose-stimulated pancreatic RIN-5F cells. Moreover, it is worth to remember that, due to the available residual amounts of the former methanol extracts, from this point, the second extracts prepared from the later collection of *C. urens* inflorescences and *G. gracillima* flowers were utilized (TH21 and TH22, respectively).

RIN-5F cells are broadly used to study pancreatic islet biology, as well as the mechanisms underlying β -cells disfunction (229,230), thus being selected to assess the protective effects of the extracts (TH21 and TH22) on hyperglycaemia-induced reactive species formation. Cells were treated under two distinct conditions: normal glucose (11 mM) and high glucose (33 mM), to mimic a minor state of glucotoxicity, where the production of intracellular reactive species is enhanced, but with no significant cell mass loss (230). The extracts working concentrations were selected considering the interference with the mitochondrial activity of RIN-5F cells, which was assessed by the MTT assay. As evidenced in **Figure 58A** and **B**, both extracts caused a significant reduction ($p < 0.0001$ and $p < 0.01$) of RIN-5F cells mitochondrial activity at 500 $\mu\text{g}/\text{mL}$, under normal (11 mM) and glucotoxic conditions (33 mM). Therefore, 250 $\mu\text{g}/\text{mL}$ was selected as the highest working concentration.

As shown in **Figure 58B**, glucose treatment (glucotoxic conditions, 33 mM) significantly ($p < 0.05$ and $p < 0.01$) enhanced basal (normal glucose conditions, 11 mM)

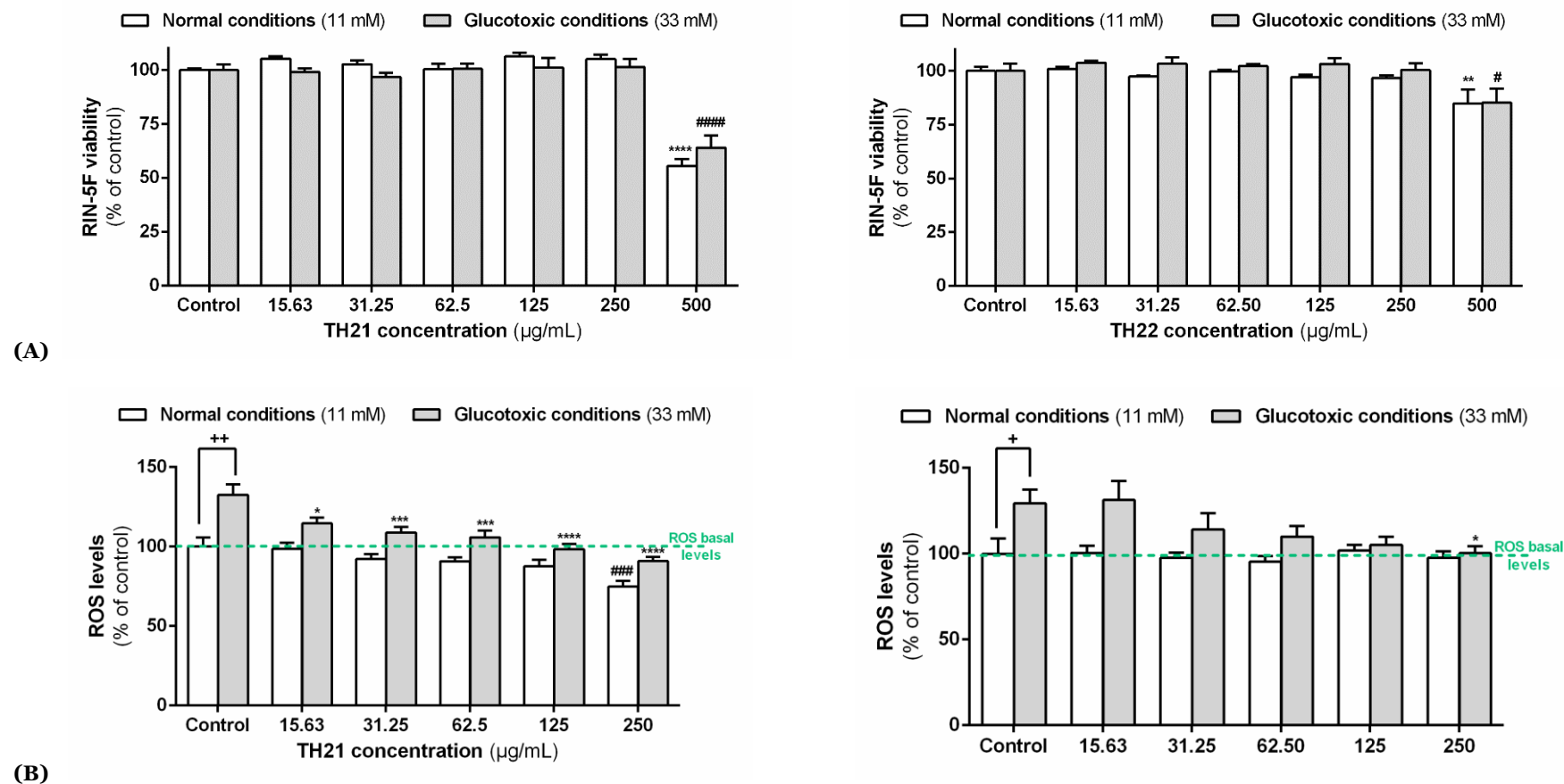


Figure 58. Effects of the methanol extracts obtained from *C. urens* inflorescences (TH21) and from *G. gracillima* flowers (TH22) on RIN-5F cells' viability (A) and on intracellular species levels (B) under normal glucose conditions (11 mM glucose) and under glucotoxic conditions (33 mM glucose). Results represent the mean \pm SEM of at least three independent experiments, performed in triplicate. Statistical significance: + $p < 0.05$ and + $p < 0.01$ significant differences between untreated cells under normal glucose conditions (11 mM) and glucotoxic conditions (33 mM glucose); * $p < 0.05$, *** $p < 0.001$, **** $p < 0.0001$ and **** $p < 0.0001$ significant differences between treatment and the control (untreated cells) at glucotoxic conditions (33 mM); # $p < 0.05$, ### $p < 0.001$ and #### $p < 0.001$ significant differences between treatment and the control (untreated cells) at normal conditions (11 mM glucose).

production of intracellular reactive species in pancreatic RIN-5F cells. Reactive species overproduction was reverted by the benchmark antioxidant NAC (20 mM), which originated an intracellular radical species falloff of 28.57 ± 11.43 % under normal glucose conditions and significantly damped glucose-induced reactive species down to basal levels, under glucotoxic conditions. *C. urens* (TH21) treatment significantly decreased glucose-induced overproduction of intracellular reactive species at concentrations ranging from 15.63 to 250 $\mu\text{g/mL}$, being significantly ($p < 0.0001$) more effective at the highest tested concentration (250 $\mu\text{g/mL}$) (**Figure 58B**). In fact, intracellular reactive species levels decayed to values under the basal, after treatment with 250 $\mu\text{g/mL}$ of *C. urens* extract (TH21) in cells cultured under both normal and glucotoxic conditions (**Figure 58B**). On the other hand, *G. gracillima* extract caused no variation on intracellular reactive species levels, except at the highest tested concentration (250 $\mu\text{g/mL}$), with which ROS levels of glucose-stimulated cells significantly ($p < 0.05$) decayed down to basal levels (**Figure 58B**).

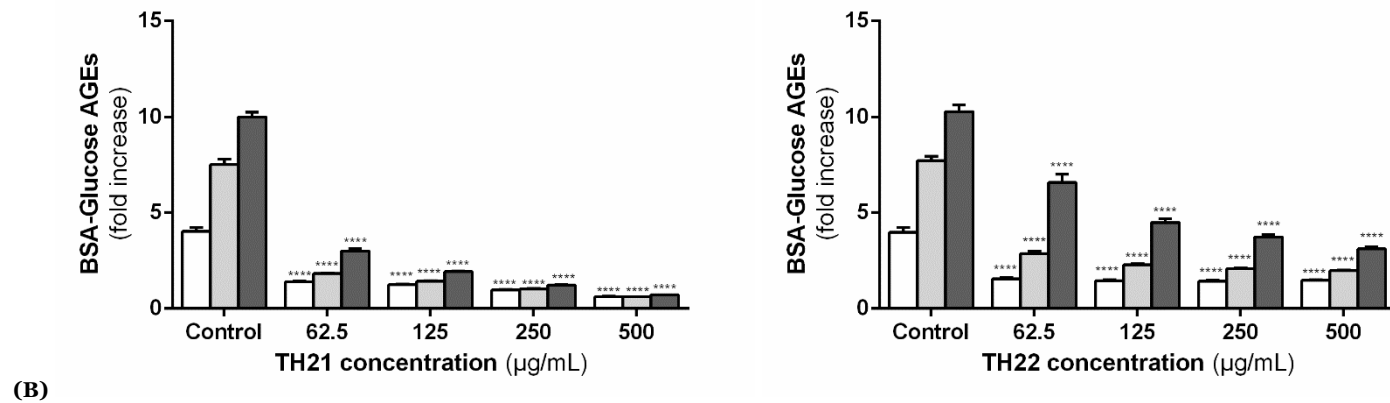
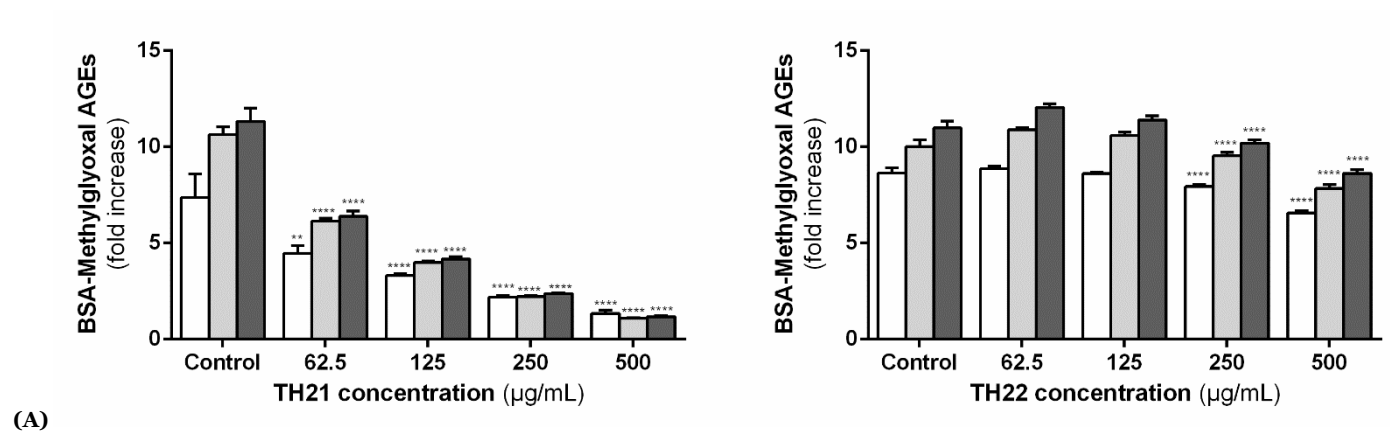
Relevantly, data gathered here is in line with the antiradical activities previously evidenced by each of these plant materials (**Figure 34** and **Figure 55**). Moreover, the extract obtained from the inflorescences of *C. urens* (TH21) ($217\,492.22 \pm 6\,276.79$ mg/kg of dry extract, **Table 7**) is more than twice richer in phenolic constituents than the one obtained from *G. gracillima* flowers (TH22) ($71\,413.55 \pm 2177.13$ mg/kg of dry extract, **Table 16**), which supports the previous evidenced negative association between the polyphenolic quantitative profile of the samples and the antiradical effect (**Figure 57**).

3.4.3. Modulation AGEs formation

AGEs formation and the polyol pathway are overactivated during chronic exposure to hyperglycaemia (17,20). The hyperactivity of these two pathways contributes for the intracellular accumulation of ROS in various tissues, including the heart, vasculature, neurons, eyes and kidneys (17,20). Besides, AGEs can activate intracellular signalling pathways, leading to the generation of pro-inflammatory cytokines and contributing to the development and progression of diabetes (**Figure 3**) (17,20). In fact, glycated haemoglobin (HbA1c), commonly measured in diabetic patients, is an AGE that results from the glycation of blood haemoglobin (231). HbA1c levels estimation delivers a long-term overview of blood glucose levels, constituting a diabetes diagnostic criterion and a monitoring parameter of the disease (231).

The inhibitory effects of the extracts obtained from *C. urens* inflorescences (TH21) and from *G. gracillima* flowers (TH22) upon protein glycation were investigated in a cell-free model. To deliver a specific indication on the inhibited glycation stage, selected glycation inducers were fructose and glucose (initial stage) and methylglyoxal (intermediate stage). Also, to have a temporal overview of the inhibitory effects, BSA-AGEs formation was monitored through time (3, 7 and 14 days after the beginning of the experience). In this model, and according to literature reports (178,232), after 14 days, fructose was the inducer that originated a higher glycation of BSA (ca. 25-fold increase) (**Figure 59**) (178).

Data obtained evidence that the two extracts were able to stop the glycation process at different stages, reducing the formation of both early (BSA-glucose AGEs and BSA-fructose AGEs) and middle (BSA-methylglyoxal AGEs) glycation products (**Figure 59**). Additionally, it can be also perceived that the inhibitory effects endured in time, being noted until day 14 (**Figure 59**). Worth note that the inhibition of BSA-methylglyoxal adducts was lower, when comparing with the other inducers. In fact, after 14 days, the reduction of AGEs deriving from methylglyoxal was only significant ($p < 0.0001$) at concentrations above 125 $\mu\text{g/mL}$ for *G. gracillima* (TH22) (**Figure 59A**). However, in the presence of *C. urens* extract (TH21), this reduction was significant at the full concentration range, a 90% inhibition of AGEs formation being recorded with the highest concentration (**Figure 59A**). Regarding the two other inducers (fructose and glucose), *C. urens* extract was again more active (**Figure 59B** and **C**). At all tested concentrations both extracts significantly ($p < 0.0001$) reduced BSA glycation induced by glucose during 14 days, a 69 % and 92% inhibition of AGEs formation being recorded with 500 $\mu\text{g/mL}$ of *G. gracillima* (TH22) and *C. urens* (TH21), respectively (**Figure 59B**). Moreover, both extracts also significantly ($p < 0.0001$) reduced AGEs formation when fructose was the inducer (**Figure 59C**), being this effect particularly evident at the highest tested concentration (500 $\mu\text{g/mL}$). Again, the extract obtained from *C. urens* inflorescences (TH22) was more effective, causing a 21-fold decrease of fructose-derived AGEs at the lowest concentration (62.5 $\mu\text{g/mL}$).



(Continued on the next page)

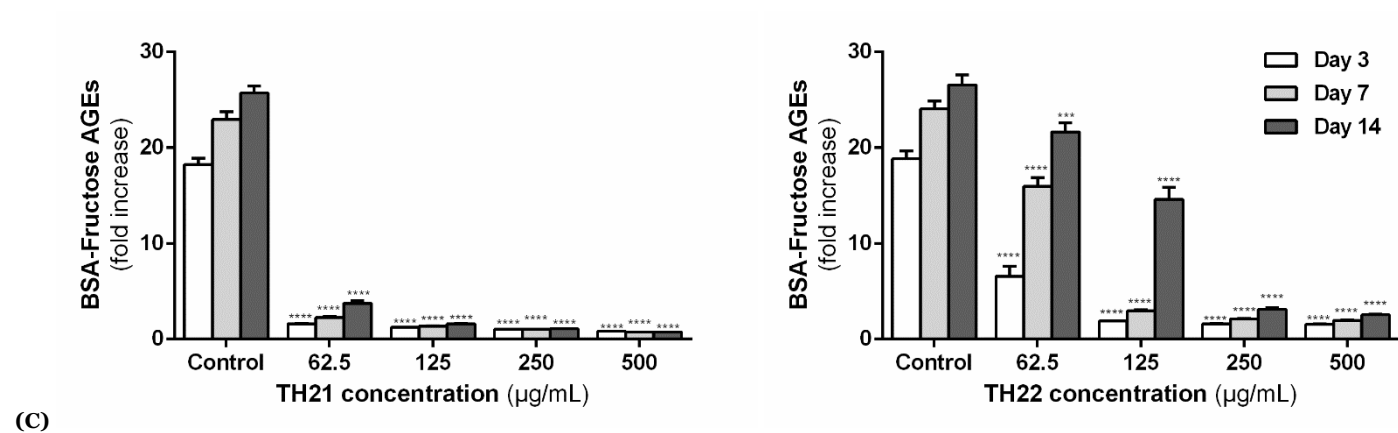


Figure 59. Inhibitory effects of *C. urens* (TH21) and *G. gracillima* methanol extracts on BSA glycation induced by methylglyoxal (A), glucose (B) and fructose (C), after 3, 7 and 14 days. Results represent mean \pm SEM of three independent experiments, each performed in triplicate. Statistical significance: ** $p < 0.01$, *** $p < 0.001$ and **** $p < 0.0001$ compared to the respective control (day 3, day 7 or day 14 with no extract treatment) (ANOVA, Tukey's multiple comparison test).

3.4.3.1. Antigliycative effects vs phenolic content

The recorded antiglycative effects appeared to be related with the phenolic content of the samples, once the inflorescences extract (with *ca.* 3 times more phenolics, **Table 7** and **16**), was the most effective on stopping the glycation caused by the three inductors. Pearson correlations corroborate these findings, a positive correlation being observed between the samples phenolic content and the glycation inhibition after 14 days when induced by fructose ($r=0.9940$, $p < 0.0001$), methylglyoxal ($r=0.9684$, $p = 0.0015$), and glucose ($r=0.9653$, $p = 0.0018$) (**Figure 60**).

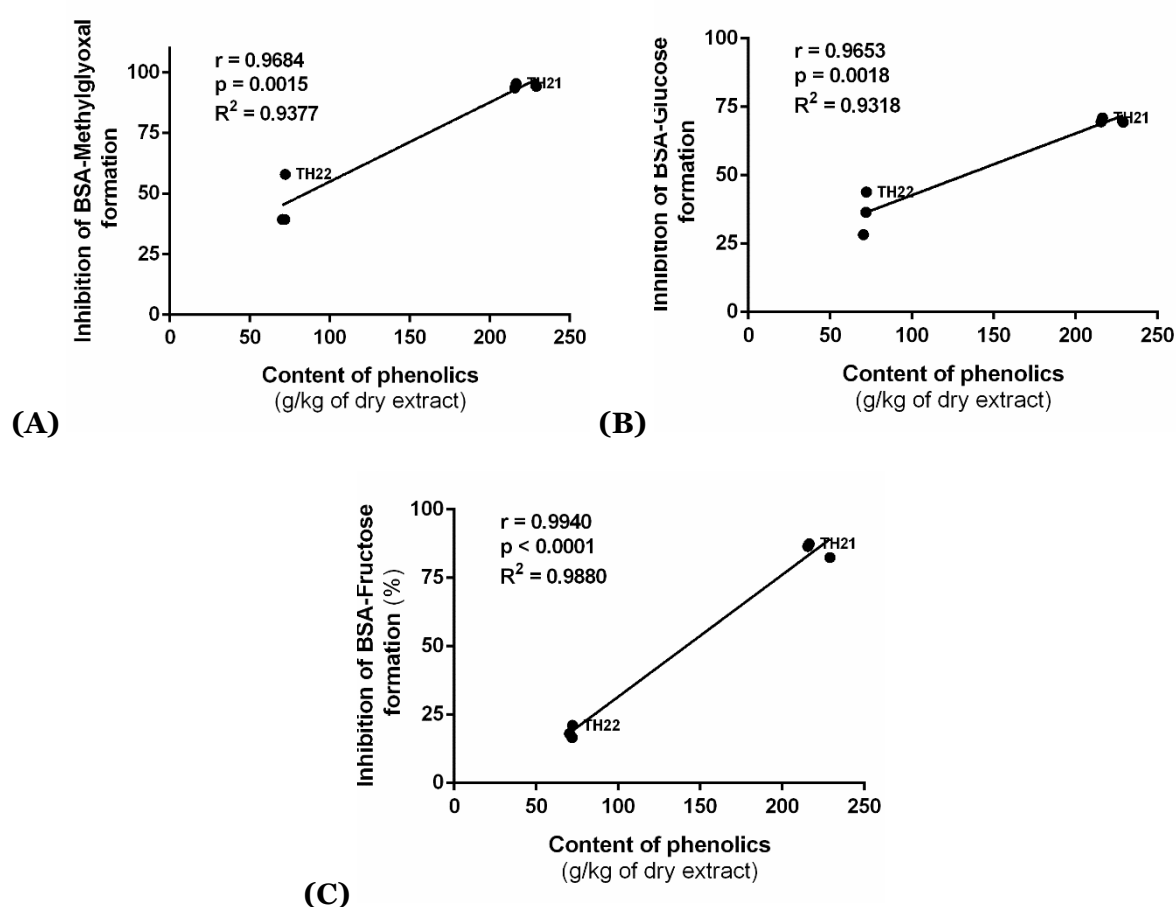


Figure 60. Pearson correlation between the content of phenolic compounds (g/kg of dry extract) of the extracts and the inhibition of BSA-methylglyoxal (A), BSA-glucose (B) and BSA-fructose (C) formation.

At this point, considering the phenolic composition of the two extracts and also based on literature evidence, it is plausible to assume that the recorded antiglycative effects might result, at least partially, from the samples polyphenolic richness (233,234). In fact, flavonoids and phenolic acids, present in considerable amounts in the two extracts, are

recognized by their inhibitory effects on the formation of AGEs (233,234). Spínola and colleagues also found a strong correlation between AGEs inhibition and the total phenolic content of several samples of *Vaccinium* species, hydroxycinnamic acids and flavonols being highlighted as the main players (233). Moreover, authors also claimed that the contribution of the hydroxycinnamic acids derivatives was higher, when compared to flavonoids (233). These findings were further corroborated by another group, that evidenced that phenolic acids were particularly effective at inhibiting AGEs formation, when comparing with other metabolites, as flavonoids and ellagitannins (234). Considering that the extract obtained from *C. urens* inflorescences (TH21) has a richer content of phenolics ($217\ 492.22 \pm 6\ 276.79$ mg/kg of dry extract, **Table 7**), particularly in hydroxycinnamic acid derivatives, this might justify, at least in part, the greater antiglycative properties recorded for this species. Still worth mentioning that, despite of less evident than phenolic acids, also ellagic acid and other ellagitannins and flavonoids, detected in *G. gracillima* (TH22) flowers, are also reported to display antiglycative effects (234). Thus, these constituents might also account, in some extent, for the observed activity (**Figure 59**).

3.5. Anti-inflammatory-like activity

3.5.1. Modulation of the arachidonic acid pathway

Studies on 5-LOX inhibition are often performed to screen the anti-inflammatory potential of a given matrix (168). 5-LOX inhibitors can modulate the arachidonic acid pathway, mitigating the production of pro-inflammatory leukotrienes (LTB). Furthermore, the 5-LOX pathway is also known to be implicated in adipose tissue inflammation, being the plasma concentration of LTB₄ correlated with insulin resistance (235,236). Hence, considering the 5-LOX inhibitory effects recorded by the extracts on the initial screening, the underlying inhibitory mechanism was detailed for the most active extracts, namely, the extracts prepared from the stem bark of *F. curtipes* (TH06) and from the leaves of *C. tabularis* (TH07) (IC₅₀ values of 10.750 and 13.118 µg/mL, respectively, **Table 5**). Additionally, taking into account the relevant antidiabetic and antiradical effects displayed by *C. urens* inflorescences (TH01), the 5-LOX inhibitory mechanism was also detailed. 5-LOX activity was assessed in the absence and presence of two different concentrations of each extract as function of the substrate concentration (linolenic acid, 1-600 µM). Data followed a Michaelis–Menten kinetics equation (**Figure 61**) and the apparent kinetic parameters (K_m and V_{max}) were calculated and are summarized in **Table 19**.

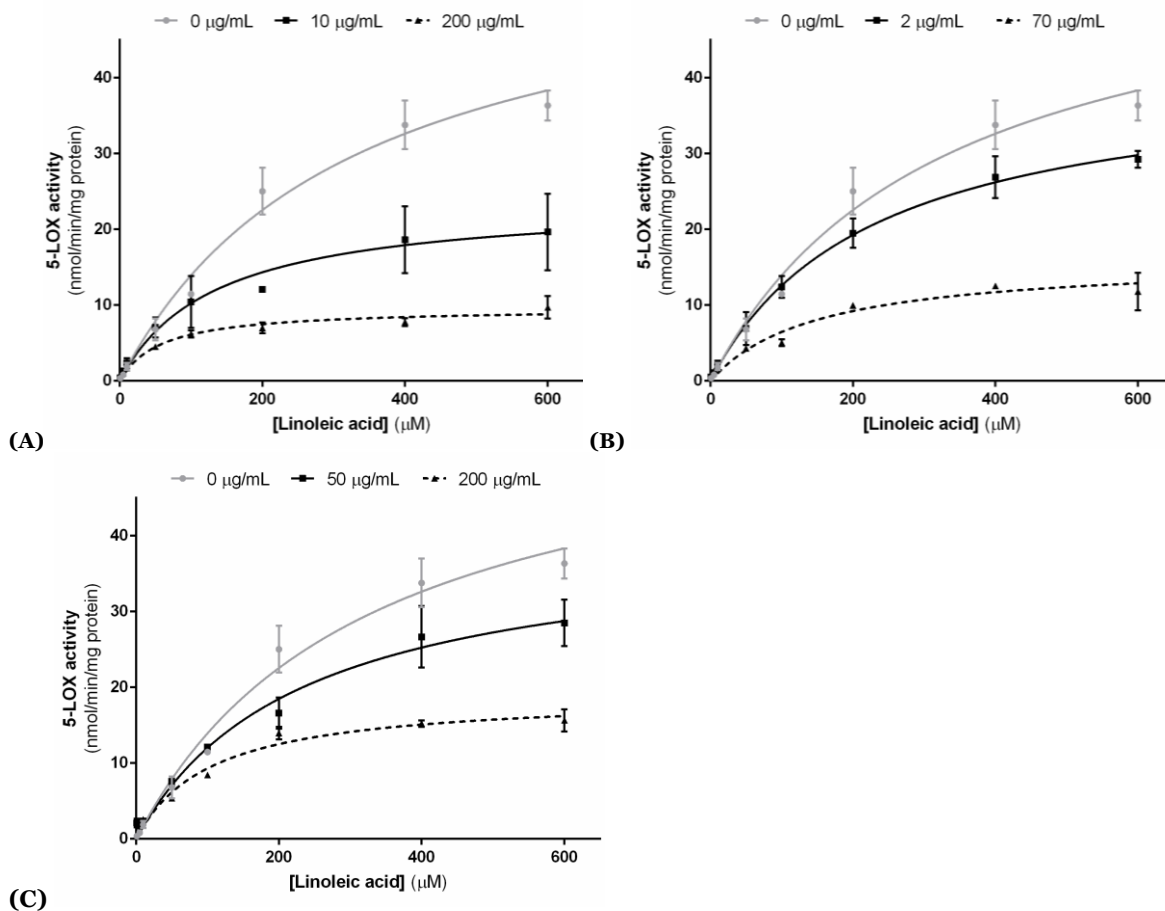


Figure 61. Michaelis-Menten kinetics of 5-LOX activity in the absence and presence of increasing concentrations of the methanol extracts obtained from the stem bark of *F. curtipes* (A), from the leaves of *C. tabularis* (B) and from the inflorescences of *C. urens* (C). Results represent the mean \pm SEM of three experiments, each performed in triplicate.

At all tested concentrations, extracts caused a significant decrease of the reaction V_{\max} , extracts obtained from *F. curtipes* (TH06) and *C. urens* (TH21) being also capable of reducing K_m (**Table 19, Figure 61**). This means that the inhibition caused by the extracts occurs through an uncompetitive mechanism, where the extract components can only bind to the enzyme-substrate complex, avoiding therefore the formation of the product. In such case, the inhibitor dissociation constant from the substrate is too high and the inhibitor dissociation constant from the substrate-enzyme complex is very low. The product of these two constants results in the inhibition constant (αk_i) (10.51 $\mu\text{g/mL}$ and 94.21 $\mu\text{g/mL}$, **Table 19**), being its value in agreement with the previously determined IC_{50} values (10.750 $\mu\text{g/mL}$ for *F. curtipes* and 164.419 $\mu\text{g/mL}$ for *C. urens*, **Table 5**). On the other hand,

Table 19. Kinetic parameters for the inhibition of 5-LOX activity caused by the extracts obtained from *F. curtipes* stem bark (TH06), *C. tabularis* leaves (TH07) and *C. urens* inflorescences (TH21).^a

	V_{max}^b (mean \pm SD)	K_m (μ M) (mean \pm SD)	r^2	$sy.x$	Inhibition type
5-LOX activity	58.97 \pm 5.1	322.9 \pm 55.9	0.9765	2.189	
TH06					
10 μ g/mL	23.9 \pm 2.4**	133.0 \pm 38.9**	0.8986	2.506	Uncompetitive ($\alpha_k = 10.51$)
200 μ g/mL	9.6 \pm 0.4***	57.2 \pm 10.3**	0.9499	0.7555	
TH07					
2 μ g/mL	41.0 \pm 2.1*	225.3 \pm 27.1	0.9848	1.411	Mixed ($\alpha = 0.241$)
70 μ g/mL	16.1 \pm 1.2**	148.0 \pm 29.6*	0.9483	1.068	
TH21					
50 μ g/mL	39.83 \pm 2.9*	230.9 \pm 2.9*	0.9686	1.892	Uncompetitive ($\alpha_k = 94.21$)
200 μ g/mL	19.0 \pm 1.1**	103.9 \pm 18.2**	0.9512	1.304	

^a Results represent the mean \pm SD of three experiments, each performed in triplicate. Significant differences at * $p < 0.05$, ** $p < 0.01$ and *** $p < 0.001$. V_{max} , maximum velocity; K_m , Michaelis constant; r^2 , coefficient of determination; $Sy.x$, standard deviation of the residuals, α , extra parameter (determines the degree to which the binding of inhibitor changes the affinity of the enzyme for substrate); α_k , inhibition constant.

^b nmol/min/mg protein.

the inhibition caused by *C. tabularis* (TH07) extract, characterized by a significant ($p < 0.001$) decay on the reaction V_{max} and by a neglectable effect on the K_m at the lowest tested concentration, suggests again a mixed inhibition. However, according to the recorded α value (0.241, **Table 19**), the inhibitor dissociation constant from the substrate-enzyme complex appears to be lower than the inhibitor dissociation constant from the enzyme. Hence, the inhibitor preferentially binds to the enzyme-substrate complex, blocking the product formation and, therefore, halting the arachidonic acid pathway. As far as we are aware, this is the first time that the 5-LOX inhibitory activity and the underlying inhibitory mechanism are disclosed for the studied species.

3.5.2. Modulation of macrophages activation

Inflammation plays an important role in diabetes pathogenesis, contributing not only to the development of insulin resistance, but also to the dysfunction of pancreatic cells and for the progression of the complications (13). Hyperglycaemia triggers a pro-inflammatory response in residing macrophages, mostly in adipose tissue, pancreatic islets and endothelial cells (13,237). The activation and secretion of multiple pro-inflammatory cytokines can ultimately lead to the apoptosis of pancreatic cells, thus contributing to β -cell

dysfunction and to insulin resistance development (13,237). Modulation of this pro-inflammatory cascades might mitigate the progression of the disease and delay the development of severe complications. As such, we considered pertinent to detail the anti-inflammatory effects elicited by the selected extracts on macrophages. To achieve this goal, LPS-challenged RAW 264.7 murine macrophages were utilized. LPS stimulation triggers pro-inflammatory cytokines (IL-1 β , IL-6 and TNF- α) release and pro-inflammatory proteins (iNOS) overexpression, mimicking both acute and chronic inflammatory processes (238,239). Furthermore, iNOS overexpression will increase L-citrulline and NO production, exacerbating the inflammatory response (238). Downregulation of these well-known inflammatory mediators attenuates inflammatory cascades and might delay the progression of the disease.

Initially, to ensure that the observed effects are not derived from cell death, interference of each extract with the mitochondrial activity of LPS-untreated RAW 264.7 macrophages was assessed, by the MTT reduction assay (**Figure 23**). Solely the extracts obtained from *F. curtipes* and *C. tabularis* leaves (TH07) cause significant alterations in the mitochondrial activity of RAW 264.7 macrophages, at 1 000 and 500 $\mu\text{g/mL}$, respectively (**Figure 62**). Therefore, 250 $\mu\text{g/mL}$ was settled as the maximum working concentration for *C. tabularis* leaves (TH07), while for the remaining extracts higher non-toxic doses were used (**Figure 62**). The cytotoxic effects of the selected working concentrations were posteriorly rechecked in the inflammatory model (LPS-stimulated RAW 264.7 macrophages) and, as evidenced on **Figure 63**, no significant alteration on the mitochondrial activity of the cells was again recorded. Hence, we can certainly ensure that the biologic effects discussed next, did not result from cell death, rather from a direct anti-inflammatory effect.

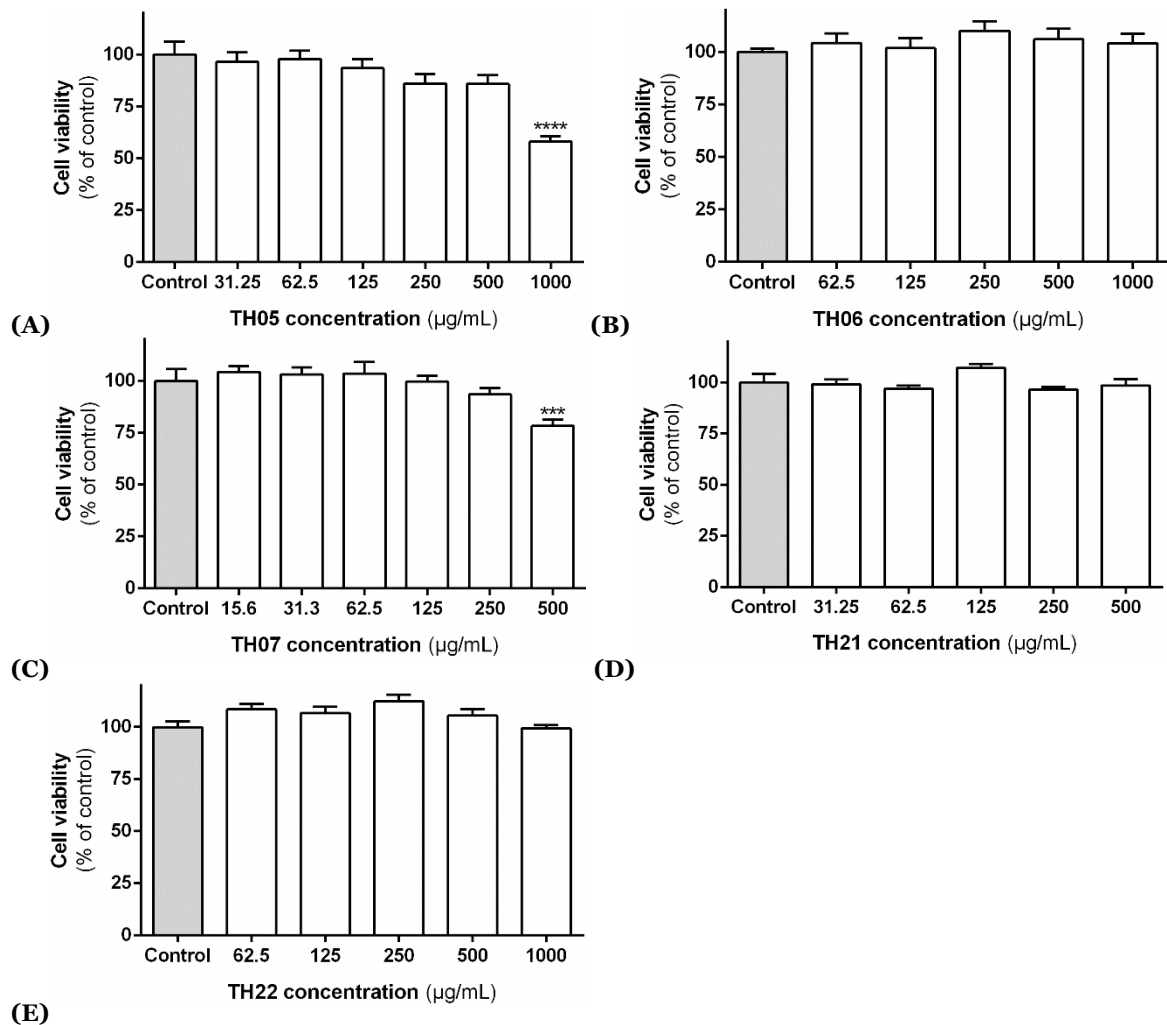


Figure 62. Effects of the methanol extracts obtained from the leaves (TH05, A) and stem bark (TH06, B) of *F. curtipes*, from the leaves of *C. tabularis* (TH07, C), from the inflorescences of *C. urens* (TH20, D) and from the flowers of *G. gracillima* (TH21, E) on the mitochondrial activity of RAW 264.7. Cells were treated for 24 h with the extracts. Results represent the mean \pm SEM of at least three independent experiments, each performed in triplicate. Statistical significance: *** $p < 0.001$ and **** $p < 0.0001$ significantly different from the control (untreated macrophages).

As mentioned above, the stimulation of macrophages with LPS induces the overexpression of the pro-inflammatory protein iNOS, consequently increasing L-citrulline and NO cellular levels (238). Considering NO relevance on both acute and chronic inflammatory processes, the levels of this pro-inflammatory biomarker were determined in the cell medium, following LPS and extracts co-treatment. As evidenced in **Figure 63**, all the extracts, except the one obtained from the stem bark of *F. curtipes* (TH06, **Figure 63**)

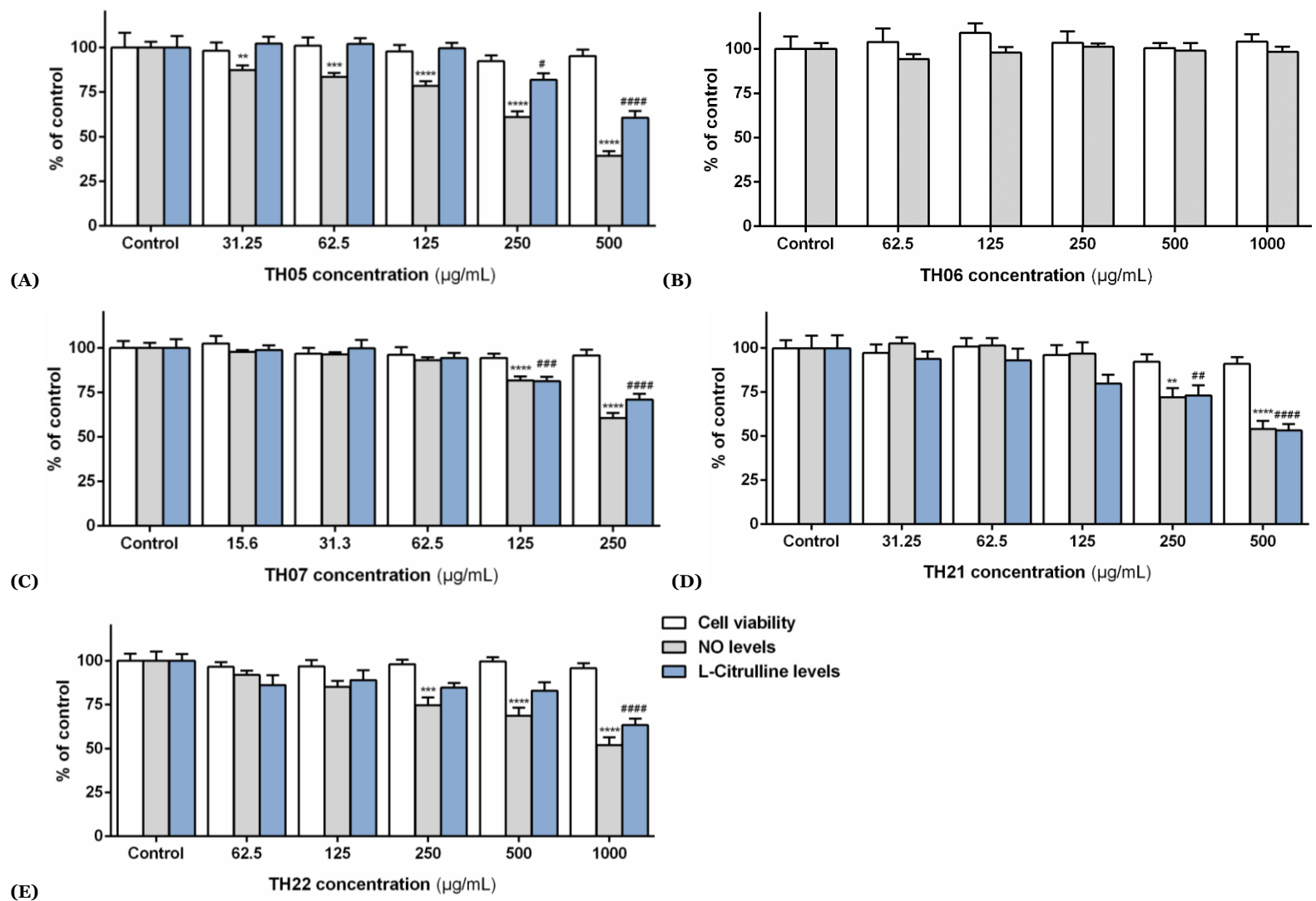


Figure 63. Effects of the methanol extracts obtained from the leaves (TH05, A) and stem bark (TH06, B) of *F. curtipes*, from the leaves of *C. tabularis* (TH07, C), from the inflorescences of *C. urens* (TH20, D) and from the flowers of *G. gracillima* (TH21, E) on the mitochondrial activity, NO levels and L-citrulline levels in LPS-stimulated RAW 264.7. Cells were pre-treated for 2 h with the extract, followed by 22 h co-treatment with LPS (1 µg/mL). Results represent the mean ± SEM of at least three independent experiments, each performed in triplicate. Statistical significance: ** $p < 0.01$, *** $p < 0.001$ and **** $p < 0.0001$ NO levels significantly different from the control (LPS-stimulated untreated macrophages); # $p < 0.05$, ### $p < 0.001$ and #### $p < 0.0001$ L-citrulline levels significantly different from the control (LPS-stimulated untreated macrophages).

were capable to reduce NO levels in stimulated macrophages. Relevantly, the extract obtained from the leaves of *F. curtipes* appeared to be the more effective, originating a concentration-dependent NO reduction, significant at all tested concentrations ($IC_{25} = 155.059$ µg/mL) (**Figure 63A**). Also, treatment of LPS-stimulated macrophages with the extracts TH07, TH21 and TH22 at 250 µg/mL reduced NO levels to 60.70 ± 9.86 %, 72.02 ± 16.04 % and 74.65 ± 15.35 %, respectively (comparing with the control, untreated macrophages following LPS-stimulation) (**Figure 63**). The estimated IC_{25} values found for the extracts on NO levels are outlined in **Table 20**.

Table 20. Estimated IC_{25} values for the methanol extracts on NO and L-citrulline levels in LPS-stimulated RAW 264.7 macrophages.

Sample ^a	NO reduction	L- Citrulline reduction
	IC_{25} (µg/ml)	IC_{25} (µg/ml)
TH05	155.059	365.919
TH07	167.026	156.972
TH21	211.619	237.417
TH22	313.754	718.697

^a Methanolic extract obtained from the leaves of *F. curtipes* (TH05), from the leaves of *C. tabularis* (TH06), from the inflorescences of *C. urens* (TH21), from the flowers of *G. gracillima* (TH22).

NO reduction can result either from direct radical scavenging effects and/or from the ability to inhibit the activity and/or gene expression of iNOS (238). Thus, to enlighten the mechanism underling the observed NO decay, L-citrulline levels in the cell medium of LPS-challenged RAW 264.7 macrophages were also determined (for all the extracts that caused a significant NO reduction). The iNOS commercial inhibitor L-NAME was used here as positive control, and when tested at 25 µM, reduced NO levels to 74.11 ± 10.09 % and L-citrulline levels to 80.11 ± 11.49 %.

As indicated in **Figure 63**, after 24 h of treatment, all samples exhibited a significant reduction on L-citrulline levels, all matching the concentrations causing a significant reduction of NO levels. This indicates that the extracts investigated have the ability to modulate iNOS, at least up until concentrations where L-citrulline reduction was

significant. Moreover, for TH07 and TH21, the IC₂₅ values calculated for NO (167.026 and 211.619 µg/mL, respectively; **Table 20**) and L-citrulline reduction (156.972 and 237.417µg/mL, respectively; **Table 20**) are interconnected, suggesting that iNOS inhibition is the main mechanism underlying the NO decrease. However, with extracts TH05 and TH022, the estimated IC₂₅ values for L-citrulline reduction (365.919 and 718.697 µg/mL, respectively; **Table 20**) were considerably higher than the one calculated for NO reduction (155.059 and 313.754 µg/mL, respectively; **Table 20**), pointing to NO scavenging additional effects. This is also evident in **Figure 63**, where significant NO reductions were observed at concentrations where no L-citrulline alteration was detected. As such, the NO falloff noted with the leaves of *F. curtipes* (TH07) (**Figure 63A**), at the concentrations range 31.5-250 µg/ml, outcomes from the ability of the extract components to scavenge NO directly, while at higher concentrations, it results from the inhibition of iNOS. The same applies to the extract obtained from the flowers of *G. gracillima* (TH22) at 250 µg/ml (**Figure 63E**).

In addition to NO production, LPS-stimulated macrophages also secrete considerable amounts of pro-inflammatory cytokines, including TNF-α and IL-6, which further exacerbate the inflammatory response (238). Hence, the capacity to downregulate the expression of these pro-inflammatory mediators was evaluated, in the same experimental model. IL-6 and TNF-α were determined in the cell medium by ELISA, their relative amounts being expressed as percentage of control (untreated cells following LPS stimulation). The benchmark drug dexamethasone, when tested at 100 µM, reduced IL-6 levels down to 20.30 ± 4.57 % and TNF-α levels to 76.90 ± 15.31%.

As evidenced in **Figure 64A**, *F. curtipes* leaf extract showed a significant inhibition of IL-6 levels at 250 ($p < 0.05$) and 500 µg/mL ($p < 0.0001$), with no relevant alterations of TNF-α. In the same way, the extract obtained from the leaves of *C. tabularis* (TH07) was also only capable of reducing ($p < 0.001$) IL-6 levels at 125 and 250 µg/mL (**Figure 64B**). In fact, these findings are in agreement with those documented by Patel and colleagues, who evidenced that a methanol extract prepared from another collection of *C. tabularis* leaves (TH07) was capable of damping both NO and IL-1β levels, with neglectable interference on TNF-α expression (157). Overall, data gathered from the cellular assays indicate that both *F. curtipes* and *C. tabularis* extracts can attenuate the inflammatory response in activated macrophages, reducing IL-6 overexpression and inhibiting iNOS (expression and/or activity), possibly hampering macrophages infiltration in the pancreas and/or peripheral tissues. However, despite of also eliciting a noteworthy IL-6 falloff, the extracts obtained from *C. urens* inflorescences (TH21) and *G. gracillima* flowers (TH22) also caused a significant ($p < 0.01$) enhancement on TNF-α expression, at the highest tested concentration

(Figure 64C and D). This indicates that while some components of the extract exert anti-inflammatory effects, others might trigger pro-inflammatory processes, thus compromising the application of these extracts as anti-inflammatory agents.

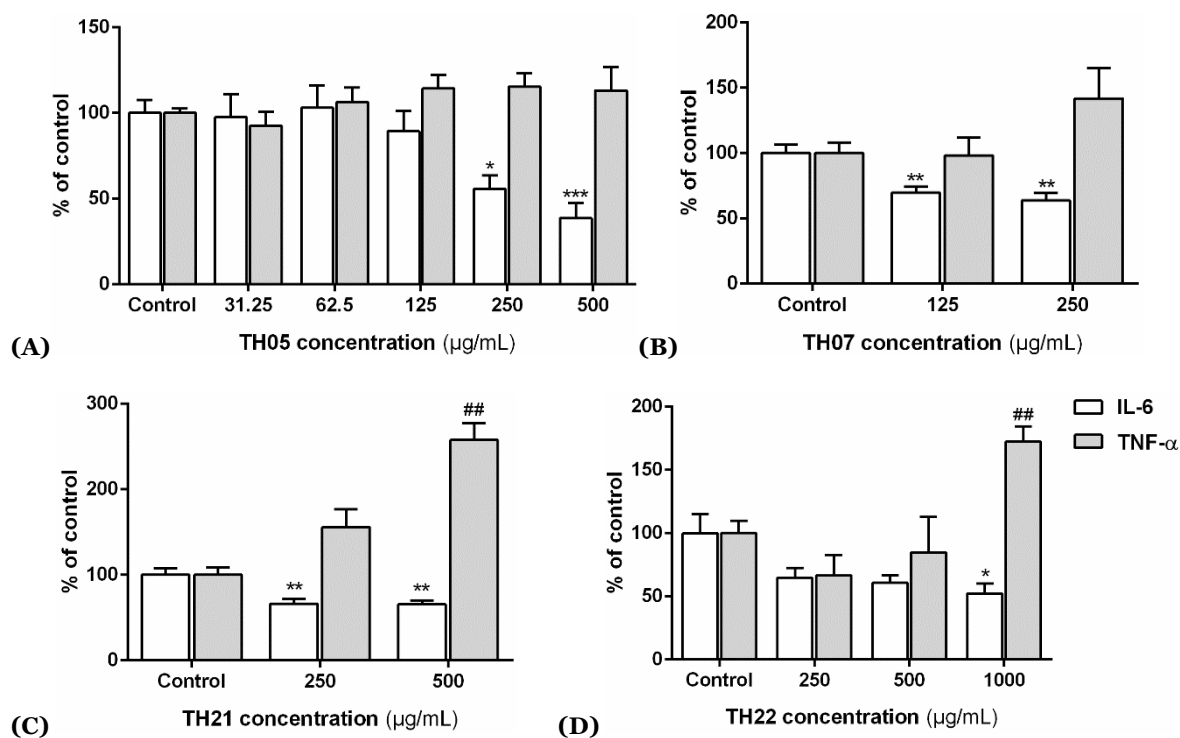


Figure 64. Effects of the treatment with the methanol extracts obtained from the leaves of *F. curtipes* (A), from the leaves of *C. tabularis* leaves (B), from the inflorescences of *C. urens* (C) and from the flowers of *G. gracillima* (D) on IL-6 and TNF- α levels in LPS-stimulated RAW 264.7 macrophages. Cells were pre-treated for 2 h with the extract, followed by 22 h co-treatment with LPS (1 $\mu\text{g}/\text{mL}$). Results represent the mean \pm SEM of at least three independent experiments, each performed in duplicate. Statistical significance: * $p < 0.05$, ** $p < 0.01$ and *** $p < 0.001$ IL-6 levels significantly different from the control (LPS-stimulated untreated macrophages); ## $p < 0.01$ TNF- α levels significantly different from the control (LPS-stimulated untreated macrophages).

3.5.2.1. Anti-inflammatory effects vs phenolic content

No significant correlation (Pearson correlation, $r = -0.0501$, $p = 0.8435$) was found between the concentrations of phenolics present on the extracts and the IC_{50} values estimated for 5-LOX inhibition. However, considering the more active extracts, a negative correlation (Pearson correlation, $r = -0.6231$, $p = 0.0057$) was noticed between the flavan-3-ols oligomers content and the IC_{50} values calculated for 5-LOX inhibition (Figure 65). The 5-LOX inhibitory activity of epicatechin and related oligomers was also evidenced by other studies strongly indicating that low-molecular weight procyanidins, as dimers and

trimers, are particularly effective on inhibiting 5-LOX activity (240). Given the substantial abundance of flavon-3-ols dimers and trimers on *F. curtipes* and *C. tabularis* extracts and also having in consideration the negative correlation above-stated, it is plausible to assume the contribution of these metabolites on the recorded anti-inflammatory properties.

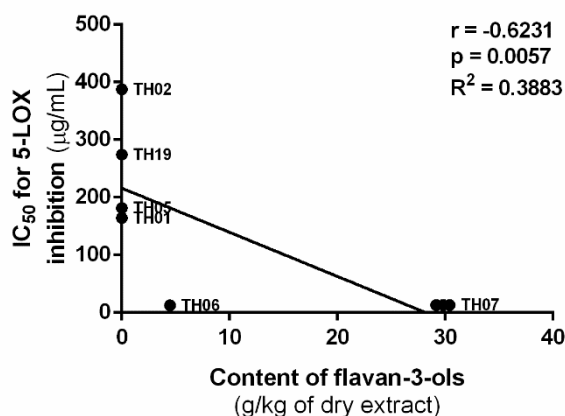


Figure 65. Pearson correlation between the content of flavan-3-ols (g/kg of dry extract) of the extracts and the estimated IC₅₀ value determined for the 5-LOX inhibition (µg/mL).

In the same-way, no relevant association between the inflammatory biomarkers decrease at the cellular model and the samples polyphenolic content could be extrapolated, suggesting that the denoted anti-inflammatory effects are not restrictively related with the phenolic content. Nevertheless, there is extensive literature reports on the anti-inflammatory properties of many polyphenols detected in our samples and/or of their metabolites (168,241–243). Thus, the qualitative composition of the extracts cannot be excluded, even though other non-phenolic constituents might also be playing a role on the herein observed activities. In this sense, the further fractioning of the extracts, should be made to understand if there is, effectively, any partial contribution of the phenolic compounds for the anti-inflammatory properties recorded.

CHAPTER IV

CONCLUSIONS

4. Conclusions

The work developed under the scope of this thesis allowed to bring out the following conclusions:

First of all, the current work broadened the knowledge of previously under-studied plant materials with ethnomedicinal value in TTM, highlighting the pharmacologic relevance of *C. urens*, *F. curtipes*, *C. tabularis* and *G. gracillima*.

Data on the phenolic composition provides evidence of the chemical richness of uninvestigated plants, valuing the species as important sources of structurally diverse phenolic compounds. Therefore, *C. urens* is here highlighted as source of hydroxycinnamic acid derivatives, known for their antidiabetic ability and therapeutic utility, while the remaining species are characterized by the occurrence of tannins and flavonoids, with also therapeutic value on diabetes amelioration.

F. curtipes and *C. tabularis* are here valorized on their anti-inflammatory properties, attenuating the inflammatory pathways induced by LPS in RAW 264.7 macrophages and also inhibiting 5-LOX activity. Both extracts were capable of reducing NO and L-citrulline levels in inflammatory cells through inhibition of iNOS (activity and/or expression). These natural anti-inflammatory extracts might halt macrophages infiltration in the pancreas and/or peripheral tissues and can be also considered in the treatment of other pathologies with inflammatory background.

The lack of correlation between the phenolic content of the samples and the observed anti-inflammatory properties suggests that the recorded effects can outcome from the presence of other non-phenolic constituents and/or from the synergic interactions of the phytoconstituents of the extract. However, particularly considering 5-LOX, the flavan-3-ols content appears to have a role on the inhibition of the activity of the enzyme. The positive correlations observed between both α -glucosidase and aldose reductase inhibitory activity and the content of phenolic compounds present in the samples suggest that these metabolites are, at least partially, responsible for the inhibitory effects displayed by the extracts. Also, the phenolic compounds appear to contribute to the scavenging activities recorded, particularly towards $O_2^{\cdot-}$ and DPPH $^{\cdot}$ radicals.

C. urens inflorescences and *G. gracillima* flowers are distinguished by their antidiabetic properties, and particularly on the alleviation of oxidative stress and on the mitigation of postprandial hyperglycaemia. Relevantly, the two plant materials are widely distributed and easily accessible, enabling large-scale cultivation and utilization. Particular emphasis must be given to *C. urens*, once several food products prepared from its inflorescences are

regularly consumed in Asian countries, calling for urgent studies on the antidiabetic-like effects of the already kitul-based commercialized saps and jaggeries.

Besides of extending the knowledge of common plant species from TTM, the outcomes of the current dissertation evidence the multi-target capacity of several uninvestigated plant materials, which might inspire food industries and/or pharmaceutical companies to produce new functional products/foods.

4.1. Future perspectives

The current work delivers new prospects on the application of the plant materials studied, preliminary disclosing their phytochemical profile, biologic properties and possible therapeutic applications on diabetes and associated inflammation. Still, further studies should be conducted from here on to fully understand the potential clinical application of these natural approaches, namely:

- Purification of the extracts through liquid-liquid partitioning and/or solid phase extraction, particularly the ones obtained from the inflorescences of *C. urens* and the flowers of *G. gracillima*, and reassessment of the purified fraction in LPS-stimulated RAW macrophages to see if the pro-inflammatory effects on TNF- α levels are overcome;
- Assessing the hypoglycaemic effects of *C. urens* inflorescences and *G. gracillima* flowers extracts on maltose-loaded rats, in order to check if post-prandial hyperglycaemia inhibition also occurs *in vivo*;
- Assessing the effects of *C. urens* inflorescences, *G. gracillima* flowers, *F. curtipes* leaves and stem bark and *C. tabularis* leaves treatment on diabetic (HbA_{1c}, fasting blood glucose, plasmatic insulin, expression of GLUT-4 and IRS-1), lipidemic (TG, cHDL, CT and cLDL) inflammatory (TNF- α , INF- γ , IL-6 and IL-1 β) and oxidative biomarkers (GSH) levels in high-fat diet and streptozotocin-induced diabetic rats (experimental model of type 2 diabetes);
- Preliminary studies, as the ones delivered here, on the antidiabetic-like potential of Kitul (*C. urens*) processed foods, namely flours and syrups that are prepared from the tree inflorescences and indiscriminately consumed in Asia by diabetic patients.

- Fractioning of the extracts and assessment of the activities displayed by the resulting fractions. At this stage fractions of non-phenolic compounds should also be obtained, to study the interference of other non-phenolic constituents on the recorded activities, particularly in the cases where the activity registered was not related with the samples phenolic content. After this, and when justifiable, the bioactive constituent's isolation (phenolics and/or non-phenolics) would also be of interest.

CHAPTER V
REFERENCES

5. References

1. International Diabetes Federation. IDF Diabetes Atlas, 10th edn. Brussels, Belgium: International Diabetes Federation, 2021.
2. Saeedi P, Petersohn I, Salpea P, Malanda B, Karuranga S, Unwin N, et al. Global and regional diabetes prevalence estimates for 2019 and projections for 2030 and 2045 : Results from the International Diabetes Federation Diabetes Atlas, 9 th edition. *Diabetes Res Clin Pract* 2019 Nov; 157 (107843): 1-10.
3. Alkhatib A, Tsang C, Tiss A, Bahorun T, Arefanian H, Barake R, et al. Functional foods and lifestyle approaches for diabetes prevention and management. *Nutrients* 2017 Dec; 9 (1310): 1-18.
4. Moini J. Pathophysiology of diabetes. In: Broderick TK, editor. *Epidemiology of Diabetes*. Elsevier; 2019. p. 25-43.
5. American Diabetes Association. Classification and diagnosis of diabetes: standards of medical care in diabetes 2021. *Diabetes Care* 2021 Jan;44(Suppl 1):15-33.
6. D'Adamo E, Caprio S. Type 2 diabetes in youth: epidemiology and pathophysiology. *Diabetes Care* 2011 May;34(Suppl 2):S161-165.
7. Fang X, Zuo J, Zhou J, Cai J, Chen C, Xiang E, et al. Childhood obesity leads to adult type 2 diabetes and coronary artery diseases: A 2-sample mendelian randomization study. *Medicine* 2019 Aug;98(32):1-8.
8. Ganesan K, Rana MBM, Sultan S. Oral Hypoglycemic Medications. [Updated 2022 May 8]. In: StatPearls. Treasure Island (FL): StatPearls Publishing; 2022 Jan. Available in: <https://www.ncbi.nlm.nih.gov/books/NBK482386/> [accessed in 18/11/2021].
9. Deshpande AD, Harris-Hayes M, Schootman M. Epidemiology of diabetes and diabetes-related complications. *Phys Ther* 2008 Nov;88(11):1254–64.
10. Galicia-Garcia U, Benito-Vicente A, Jebari S, Larrea-Sebal A, Siddiqi H, Uribe KB, et al. Pathophysiology of type 2 diabetes mellitus. *Int J Mol Sci* 2020 Aug;21(17):1-34.
11. Wilcox G. Insulin and insulin resistance. *Clin Biochem Rev* 2005 May;26(2):19-39.

12. Ampofo AG, Boateng EB. Beyond 2020: modelling obesity and diabetes prevalence. *Diabetes Res Clin Pract* 2020 Sep;167(108362):1-16.
13. Zand H, Morshedzadeh N, Naghashian F. Signaling pathways linking inflammation to insulin resistance. *Diabetes Metab Syndr* 2017 Nov;11(Suppl 1):S307-9.
14. Shoelson SE, Lee J, Goldfine AB. Inflammation and insulin resistance. *Rev Ser* 2006 Jul;116(7):1793-801.
15. Tangvarasittichai S. Oxidative stress, insulin resistance, dyslipidemia and type 2 diabetes mellitus. *World J Diabetes* 2015 Apr;6(3):456-80.
16. Holohan C, Szegezdi E, Ritter T, O'Brien T, Samali A. Cytokine-induced beta-cell apoptosis is NO-dependent, mitochondria-mediated and inhibited by BCL-XL. *J Cell Mol Med* 2008 Apr;12(2):591-606.
17. Tang WH, Martin KA, Hwa J. Aldose reductase, oxidative stress, and diabetic mellitus. *Front Pharmacol* 2012 May;3(87):1-8.
18. Singh M, Kapoor A, Bhatnagar A. Physiological and pathological roles of aldose reductase. *Metabolites* 2021 Sep;11(10):1-29.
19. Eguchi N, Vaziri ND, Dafoe DC, Ichii H. The role of oxidative stress in pancreatic β cell dysfunction in diabetes. *Int J Mol Sci* 2021 Apr; 22(4):1-18.
20. Singh VP, Bali A, Singh N, Jaggi AS. Advanced glycation end products and diabetic complications. *Korean J Physiol Pharmacol* 2014 Feb;18(1):1-14.
21. Chawla A, Chawla R, Jaggi S. Microvascular and macrovascular complications in diabetes mellitus: Distinct or continuum? *Indian J Endocrinol Metab* 2016 Aug;20(4):546-51.
22. Cade WT. Diabetes-related microvascular and macrovascular diseases in the physical therapy setting. *Phys Ther* 2008 Nov;88(11):1322-35.
23. Bommer C, Sagalova V, Heesemann E, Manne-Goehler J, Atun R, Bärnighausen T, et al. Global economic burden of diabetes in adults: projections from 2015 to 2030. *Diabetes Care* 2018 May;41(5):963-970.
24. Davies MJ, D'Alessio DA, Fradkin J, Kernan WN, Mathieu C, Mingrone G, et al.

- Management of hyperglycemia in type 2 diabetes, 2018. A consensus report by the American Diabetes Association (ADA) and the European Association for the Study of Diabetes (EASD). *Diabetes Care* 2018 Dec;41(12):2669-2701.
25. Direção Geral da Saúde (DGS). Norma: Abordagem terapêutica farmacológica na diabetes mellitus tipo 2 no adulto. 2015:1-28.
 26. Andrade C, Gomes NGM, Duangsrissai S, Andrade PB, Pereira DM, Valentão P. Medicinal plants utilized in Thai Traditional Medicine for diabetes treatment: Ethnobotanical surveys, scientific evidence and phytochemicals. *J Ethnopharmacol* 2020 Dec;263(113177):1-54.
 27. Chaudhury A, Duvoor C, Reddy Dendi VS, Kraleti S, Chada A, Ravilla R, et al. Clinical review of antidiabetic drugs: implications for type 2 diabetes mellitus management. *Frontiers in Endocrinology* 2017 Jan;8(6):1-12.
 28. Sirtori CR, Pasik C. Re-evaluation of a biguanide, metformin: mechanism of action and tolerability. *Pharmacol Res* 1994 Nov;30(3):187-228.
 29. Sola D, Rossi L, Schianca GPC, Maffioli P, Bigliocca M, Mella R, et al. Sulfonylureas and their use in clinical practice. *Arch Med Sci* 2015 Aug;11(4):840-8.
 30. Hauner H. The mode of action of thiazolidinediones. *Diabetes Metab Res Rev* 2002 Apr;18(Suppl 2):S10-5.
 31. Shaefer CFJ, Kushner P, Aguilar R. User's guide to mechanism of action and clinical use of GLP-1 receptor agonists. *Postgrad Med* 2015 Sep;127(8):818-26.
 32. Vella A. Mechanism of action of DPP-4 inhibitors - new insights. *J Clin Endocrinol Metab* 2012 Aug;97(8):2626-8.
 33. Bischoff H. The mechanism of alpha-glucosidase inhibition in the management of diabetes. *Clin Investig Med* 1995 Aug;18(4):303-11.
 34. Hsia DS, Grove O, Cefalu WT. An update on sodium-glucose co-transporter-2 inhibitors for the treatment of diabetes mellitus. *Curr Opin Endocrinol Diabetes Obes* 2017 Feb;24(1):73-9.
 35. Nasri H, Rafieian-Kopaei M. Metformin: Current knowledge. *J Res Med Sci Off J Isfahan Univ Med Sci* 2014 Jul;19(7):658-64.

36. Rizos C V, Elisaf MS, Mikhailidis DP, Liberopoulos EN. How safe is the use of thiazolidinediones in clinical practice? *Expert Opin Drug Saf.* 2009 Jan;8(1):15-32.
37. He K, Shi J-C, Mao X-M. Safety and efficacy of acarbose in the treatment of diabetes in Chinese patients. *Ther Clin Risk Manag* 2014 Jun;30(10):505-11.
38. Blind E, Janssen H, Dunder K, de Graeff PA. The European Medicines Agency's approval of new medicines for type 2 diabetes. *Diabetes Obes Metab* 2018 Sep;20(9):2059-63.
39. Newman DJ, Cragg GM. Natural products as sources of new drugs over the nearly four decades from 01/1981 to 09/2019. *J Nat Prod* 2020 Mar;83(3):770-803.
40. Bailey CJ. Metformin: historical overview. *Diabetologia* 2017 Sep;60(9):1566-1576.
41. Wehmeier UF. The biosynthesis and metabolism of acarbose in *Actinoplanes* sp. SE 50/110: a progress report. *Biocatal Biotransformation* 2003 Oct;21(4-5):279-84.
42. Perry RJ, Shulman GI. Sodium-glucose cotransporter-2 inhibitors: understanding the mechanisms for therapeutic promise and persisting risks. *J Biol Chem* 2020 Oct; 295(42):14379-90.
43. Sinha RP, Häder D-P. Chapter 1 - Introduction. In: Rajeshwar Sinha, h.c. Donat-P. Häder, editors. *Natural Bioactive Compounds*. Academic Press;2021.p.1-17.
44. Pereira DM, Andrade C, Valentão P, Andrade PB. Natural products as enzyme inhibitors. In: Paula B. Andrade, Patrícia Valentão, David M. Pereira, editors. *Natural products targeting clinically relevant enzymes*. Wiley;2017.p.1-18.
45. Lautié E, Russo O, Ducrot P, Boutin JA. Unraveling plant natural chemical diversity for drug discovery purposes. *Front Pharmacol* 2020 Apr;11(397):1-37.
46. Wang S, Alseekh S, Fernie AR, Luo J. The structure and function of major plant metabolite modifications. *Mol Plant* 2019 Jul;12(7):899-919.
47. Pang Z, Chen J, Wang T, Gao C, Li Z, Guo L, et al. Linking plant secondary metabolites and plant microbiomes: a review. *Front Plant Sci* 2021 Mar;12:(621276):1-22.
48. Bruneton J. *Pharmacognosie, phytochimie, plantes médicinales*. 3rd ed. Paris: TEC

- & DOC;1999.
49. Alvarez MA. Plant secondary metabolism chapter. In: Alvarez MA, editor. *Plant Biotechnology for Health*. Springer International Publishing; 2014.p.15–31.
 50. Tungmunnithum D, Thongboonyou A, Pholboon A, Yangsabai A. Flavonoids and other phenolic compounds from medicinal plants for pharmaceutical and medical aspects: an overview. *Medicines* 2018 Aug;5(3):1-64.
 51. Vinayagam R, Jayachandran M, Xu B. Antidiabetic effects of simple phenolic acids: a comprehensive review. *Phytother Res* 2016 Feb;30(2):184-99.
 52. Yeh W-J, Hsia S-M, Lee W-H, Wu C-H. Polyphenols with antiglycation activity and mechanisms of action: a review of recent findings. *J Food Drug Anal* 2017 Jan;25(1):84-92.
 53. Cosme P, Rodríguez AB, Espino J, Garrido M. Plant phenolics: bioavailability as a key determinant of their potential health-promoting applications. *Antioxidants*. 2020 Dec;9(12):1-20.
 54. Šamec D, Karalija E, Šola I, Vujčić Bok V, Salopek-Sondi B. The role of polyphenols in abiotic stress response: the influence of molecular structure. *Plants* 2021 Jan;10(118):1-24.
 55. Hussein RA, El-Anssary AA. Plants secondary metabolites: the key drivers of the pharmacological actions of medicinal plants. In: Philip F, editor. *Herbal Medicine*. IntechOpen; 2018.
 56. Lattanzio V. Phenolic compounds: introduction. In: K.G. Ramawat, J.M. Mérillon, editors. *Natural products*. Springer;2013.p.1543-79.
 57. Quideau S, Deffieux D, Douat-Casassus C, Pouységu L. Plant polyphenols: chemical properties, biological activities, and synthesis. *Angew Chem Int Ed Engl* 2011 Jan;50(3):586-621.
 58. Cunha APDA, Gulbenkian FC, Graça JAB. *Farmacognosia e fitoquímica*. Lisboa: Fundação Calouste Gulbenkian; 2005.
 59. Martini D, Bernardi S, Del Bo' C, Liberona NH, Zamora-Ros R, Tucci M, et al. Estimated intakes of nutrients and polyphenols in participants completing the maple

- randomised controlled trial and its relevance for the future development of dietary guidelines for the older subjects. *Nutrients* 2020 Aug;12(8):1-17.
60. Kumar N, Goel N. Phenolic acids: natural versatile molecules with promising therapeutic applications. *Biotechnol reports* 2019 Dec;24(e00370):1-10.
61. Vinholes J, Silva B, Silva L. Hydroxycinnamic acids (HCAS): Structure, biological properties and health effects. In: Leon V. Berhardt, editors. *Advances in Medicine and Biology*. Nova Science Publishers; 2015.p.105-130.
62. Herrmann K. Occurrence and content of hydroxycinnamic and hydroxybenzoic acid compounds in foods. *Crit Rev Food Sci Nutr* 1989;28(4):315-47.
63. Panche AN, Diwan AD, Chandra SR. Flavonoids: an overview. *J Nutr Sci* 2016 Dec;5(e47):1-15.
64. Vasilopoulou E, Georga K, Joergensen M, Naska A, Trichopoulou A. The antioxidant properties of Greek foods and the flavonoid content of the mediterranean menu. *Curr Med Chem - Immunol Endocr Metab Agents* 2005 Feb;1(5):33-45.
65. Vogiatzoglou A, Mulligan AA, Lentjes MAH, Luben RN, Spencer JPE, Schroeter H, et al. Flavonoid intake in European adults (18 to 64 years). *PLoS One* 2015 May;10(5):e0128132.
66. Chun OK, Chung SJ, Song WO. Estimated dietary flavonoid intake and major food sources of U.S. adults. *J Nutr* 2007 May;137(5):1244-52.
67. Corradini E, Foglia P, Giansanti P, Gubbiotti R, Samperi R, Lagana A. Flavonoids: chemical properties and analytical methodologies of identification and quantitation in foods and plants. *Nat Prod Res* 2011 Mar;25(5):469-95.
68. Sieniawska E, Baj T. Chapter 10 - Tannins. In: Simone Badal McCreath, editors. *Pharmacognosy: Fundamentals, Applications and Strategies*. Boston: Academic Press; 2017.p.199-232.
69. Dai J, Mumper RJ. Plant phenolics: extraction, analysis and their antioxidant and anticancer properties. *Molecules* 2010 Oct;15(10):7313-52.
70. Thamkaew G, Sjöholm I, Galindo FG. A review of drying methods for improving the quality of dried herbs. *Crit Rev Food Sci Nutr* 2021 May;61(11):1763-86.

71. Babbar N, Oberoi HS, Sandhu SK, Bhargav VK. Influence of different solvents in extraction of phenolic compounds from vegetable residues and their evaluation as natural sources of antioxidants. *J Food Sci Technol* 2014 Oct;51(10):2568-75.
72. Alara OR, Abdurahman NH, Ukaegbu CI. Extraction of phenolic compounds: a review. *Curr Res Food Sci* 2021 Apr;2(4):200-214.
73. Köseoğlu Yılmaz P, Kolak U. SPE-HPLC determination of chlorogenic and phenolic acids in coffee. *J Chromatogr Sci* 2017 Aug;55(7):712-8.
74. Khoo HE, Azlan A, Ismail A, Abas F. Antioxidative properties of defatted dabai pulp and peel prepared by solid phase extraction. *Molecules* 2012 Aug;17(8):9754-73.
75. Aleixandre-Tudo ose L, Toit W du. The Role of UV-visible spectroscopy for phenolic compounds quantification in winemaking. In: Solís-Oviedo RL, Pech-Canul Á de la C, editors. *Frontiers and New Trends in the Science of Fermented Food and Beverages*. IntechOpen;2018.p.1-21.
76. Stalikas CD. Extraction, separation, and detection methods for phenolic acids and flavonoids. *J Sep Sci* 2007 Dec;30(18):3268–95.
77. Lamuela-Raventós RM, Vallverdú-Queralt A, Jáuregui O, Martínez-Huélamo M, Quifer-Rada P. Chapter 14 - Improved characterization of polyphenols using liquid chromatography. In: Watson RRBT-P in P, editor. *Polyphenols in Plants*. San Diego: Academic Press; 2014.p.261-92.
78. Robbins RJ. Phenolic acids in foods: an overview of analytical methodology. *J Agric Food Chem* 2003 Apr;51:2866-87.
79. Oliveira A. *Ficus carica* L.: Estudo fitoquímico, biológico e molecular [dissertation]. Porto: Faculdade de Farmácia da Universidade do Porto; 2012.
80. Mabry TJ, Markham KR, Thomas MB. The ultraviolet spectra of flavones and flavonols. In: *The Systematic Identification of Flavonoids*. Springer, Berlin, Heidelberg; 1970.p.41-164.
81. Harnly JM, Bhagwat S, Lin L-Z. Profiling methods for the determination of phenolic compounds in foods and dietary supplements. *Anal Bioanal Chem* 2007 Sep;389(1):47-61.

82. Stobiecki M. Application of mass spectrometry for identification and structural studies of flavonoid glycosides. *Phytochemistry* 2000 Jun;54(3):237-56.
83. De Rijke E, Zappey H, Ariese F, Gooijer C, Brinkman UAT. Liquid chromatography with atmospheric pressure chemical ionization and electrospray ionization mass spectrometry of flavonoids with triple-quadrupole and ion-trap instruments. *J Chromatogr A* 2003 Jan;984(1):45-58.
84. Cuyckens F, Claeys M. Mass spectrometry in the structural analysis of flavonoids. *J Mass Spectrom* 2004 Jan;39(1):1-15.
85. Khoddami A, Wilkes MA, Roberts TH. Techniques for analysis of plant phenolic compounds. *Molecules* 2013 Feb;18(2):2328-75.
86. Lin D, Xiao M, Zhao J, Li Z, Xing B, Li X, et al. An overview of plant phenolic compounds and their importance in human nutrition and management of type 2 diabetes. *Molecules* 2016 Oct;21(10):1-19.
87. Cory H, Passarelli S, Szeto J, Tamez M, Mattei J. The role of polyphenols in human health and food systems: a mini-review. *Frontiers in Nutrition* 2018 Sep; 5:(87):1-9.
88. González-Burgos E, Gómez-Serranillos MP. Effect of phenolic compounds on human health. *Nutrients* 2021 Nov;13(11):1-2.
89. Shahidi F, Ambigaipalan P. Phenolics and polyphenolics in foods, beverages and spices: antioxidant activity and health effects - a review. *J Funct Foods* 2015 Oct;18(B):820-97.
90. Kim YA, Keogh JB, Clifton PM. Polyphenols and glycemic control. *Nutrients*. 2016 Jan;8(1):1-27.
91. De Paulo Farias D, de Araújo FF, Neri-Numa IA, Pastore GM. Antidiabetic potential of dietary polyphenols: a mechanistic review. *Food Res Int [Internet]*. 2021 Jul;145(110383):1-16.
92. Hanhineva K, Törrönen R, Bondia-Pons I, Pekkinen J, Kolehmainen M, Mykkänen H, et al. Impact of dietary polyphenols on carbohydrate metabolism. *Int J Mol Sci* 2010 Mar;11(4):1365-402.
93. Tan Y, Chang SKC. Digestive enzyme inhibition activity of the phenolic substances in

- selected fruits, vegetables and tea as compared to black legumes. *J Funct Foods* 2017 Nov;38:644-55.
94. Domínguez Avila JA, Rodrigo García J, González Aguilar GA, de la Rosa LA. The antidiabetic mechanisms of polyphenols related to increased glucagon-like peptide-1 (GLP1) and insulin signaling. *Molecules* 2017 May;22(6):903.
 95. Nagamine R, Ueno S, Tsubata M, Yamaguchi K, Takagaki K, Hira T, et al. Dietary sweet potato (*Ipomoea batatas* L.) leaf extract attenuates hyperglycaemia by enhancing the secretion of glucagon-like peptide-1 (GLP-1). *Food Funct* 2014 Sep;5(9):2309-16.
 96. Fujii Y, Osaki N, Hase T, Shimotoyodome A. Ingestion of coffee polyphenols increases postprandial release of the active glucagon-like peptide-1 (GLP-1(7-36)) amide in C57BL/6J mice. *J Nutr Sci* 2015 Mar;4:e9.
 97. Nagano T, Hayashibara K, Ueda-Wakagi M, Yamashita Y, Ashida H. Black tea polyphenols promotes GLUT4 translocation through both PI3K-and AMPK-dependent pathways in skeletal muscle cells. *Food Sci Technol Res* 2015 Feb;21(3):489-94.
 98. Bouknana S, Bouhrim M, Ouassou H, Bnouham M. Review of medicinal plants and their compounds for aldose reductase inhibitory activity. *Lett Drug Des Discov.* 2017 Oct;15(7).
 99. Kuryłowicz A. The role of isoflavones in type 2 diabetes prevention and treatment - a narrative review. *Int J Mol Sci* 2021 Dec;22(1):1-36.
 100. Isono Y, Watanabe H, Kumada M, Takara T, Iio S-I. Black tea decreases postprandial blood glucose levels in healthy humans and contains high-molecular-weight polyphenols that inhibit α -glucosidase and α -amylase *in vitro*: A randomized, double blind, placebo-controlled, crossover trial. *Funct Foods Heal Dis* 2021;11(5):222-37.
 101. Lee AH, Tan L 'b, Hiramatsu N, Ishisaka A, Alfonso H, Tanaka A, et al. Plasma concentrations of coffee polyphenols and plasma biomarkers of diabetes risk in healthy Japanese women. *Nutr Diabetes* 2016 Jun;6(6):e212.
 102. Zhang F-L, Gao H-Q, Wu J-M, Ma Y-B, You B-A, Li B-Y, et al. Grape seed proanthocyanidin extracts inhibit vascular cell adhesion molecule expression induced by advanced glycation end products through activation of peroxisome

- proliferators-activated receptor gamma. *J Cardiovasc Pharmacol* 2006 May;49(2):47-53.
103. Pereira ASP, Banegas-Luna AJ, Peña-García J, Pérez-Sánchez H, Apostolides Z. Evaluation of the anti-diabetic activity of some common herbs and spices: providing new insights with inverse virtual screening. *Molecules* 2019 Nov;24(22):1-42.
104. AL-Ishaq RK, Abotaleb M, Kubatka P, Kajo K, Büsselberg D. Flavonoids and their anti-diabetic effects: cellular mechanisms and effects to improve blood sugar levels. *Biomolecules* 2019 Sep;9(430):1-35.
105. Ekor M. The growing use of herbal medicines: issues relating to adverse reactions and challenges in monitoring safety. *Front Pharmacol* 2014 Jan;4(177).
106. Njateng GSS, Du Z, Gatsing D, Mouokey RS, Liu Y, Zang HX, et al. Antibacterial and antioxidant properties of crude extract, fractions and compounds from the stem bark of *Polyscias fulva* Hiern (Araliaceae). *BMC Complement Altern Med* 2017 Feb;17(1):1-8.
107. Zahoor M, Shafiq S, Ullah H, Sadiq A, Ullah F. Isolation of quercetin and mandelic acid from *Aesculus indica* fruit and their biological activities. *BMC Biochem* 2018 Dec 1;19(5):1-14.
108. Zhou J, Yang Q, Zhu X, Lin T, Hao D, Xu J. Antioxidant activities of *Clerodendrum cyrtophyllum* Turcz leaf extracts and their major components. *PLoS One* 2020 Jun; 15(6):e0234435.
109. Rasoanaivo P, Wright CW, Willcox ML, Gilbert B. Whole plant extracts versus single compounds for the treatment of malaria: synergy and positive interactions. *Malar J* 2011 Mar;10(Suppl 1):1-12.
110. Che C, Wang ZJ, Sing M, Chow S, Wai C, Lam K. Herb-herb combination for therapeutic enhancement and advancement: theory, practice and future perspectives. *Molecules* 2013 May;18(5):5125-4.
111. Choudhury H, Pandey M, Hua CK, Mun CS, Jing JK, Kong L, et al. An update on natural compounds in the remedy of diabetes mellitus: a systematic review. *J Tradit Complement Med* 2017 Nov;8(3):361-376.

112. Phumthum M, Srithi K, Inta A, Junsongduang A, Tangjitman K, Pongamornkul W, et al. Ethnomedicinal plant diversity in Thailand. *J Ethnopharmacol* 2018 Mar;25(214):90-98.
113. Kwankhao P, Administration PDP. The current situation of the herbal medicinal product system in Thailand. *J Heal Sci* 2020 Feb;29(2563):S82–95.
114. Chotchoungchatchai S, Saralamp P, Jenjittikul T, Pornsiripongse S, Prathanturarug S. Medicinal plants used with Thai Traditional Medicine in modern healthcare services: a case study in Kabchoeng Hospital, Surin Province, Thailand. *J Ethnopharmacol* 2012 May;141(1):193-205.
115. Manosroi J, Moses ZZ, Manosroi W, Manosroi A. Hypoglycemic activity of Thai medicinal plants selected from the Thai/Lanna Medicinal Recipe Database MANOSROI II. *J Ethnopharmacol* 2011 Oct;138(1):92-8.
116. Del Casino VJ. (Re)placing health and health care: mapping the competing discourses and practices of ‘traditional’ and ‘modern’ Thai medicine. *Health Place* 2004 Mar;10(1):59-73.
117. Andrade C, Gomes NGM, Duangsrisai S, Andrade PB, Pereira DM, Valentão P. Medicinal plants utilized in Thai Traditional Medicine for diabetes treatment: Ethnobotanical surveys, scientific evidence and phytochemicals. *J Ethnopharmacol* 2020 Dec;263(113177):1-54.
118. Phumthum M, Balslev H, Barfod AS. Important medicinal plant families in Thailand. *Front Pharmacol* 2019 Sep;10(1125):1-14.
119. Phumthum M, Balslev H. Anti-infectious plants of the Thai karen. *Antibiotics*. 2020 Jun;9(298):1-11.
120. Anderson EF. Plants and people of the golden triangle: ethnobotany of the hill tribes of northern Thailand. *Nord J Bot* 1994;14:530-530.
121. Chotchoungchatchai S, Saralamp P, Jenjittikul T, Pornsiripongse S. Medicinal plants used with Thai Traditional Medicine in modern healthcare services : a case study in Kabchoeng Hospital, Surin Province, Thailand. *J Ethnopharmacol* 2012 May;141(1): 193-205.

122. Boonudomkit P, Temsiririrkkul R, Kermanee P, Traiperm P, Bongcheewin B. Wood anatomical study of Thai traditional Chan Khao crude drug. *Thai J Bot* 2019;11 (1):25-39.
123. Neamsuvan O, Komonhiran P, Boonming K. Medicinal plants used for hypertension treatment by folk healers in Songkhla province, Thailand. *J Ethnopharmacol* 2018 Mar;214:58-70.
124. Srithi K. Comparative ethnobotany in Nan province, Thailand [dissertation]. Chiang Mai: Biology. Chiang Mai University;2012.
125. Rattanapotanan N. Plant diversity and utilization of medicinal plants by traditional healers. *Naresuan Univ J Sci Technol* 2019 Mar;27(1):55-64.
126. Maisuthisakul P. Phenolic constituents and antioxidant properties of some Thai plants. In: Rao V, editor. *Phytochemicals - a global perspective of their role in nutrition and health*. IntechOpen;2012.p.187-212.
127. Balaji S, Ganesan KK. Acute and subacute toxicity evaluation of hydroalcoholic extract of *Caryota urens* leaves in Wistar rats. *J Appl Pharm Sci* 2020 Apr;10 (04):121-8.
128. Hall W. The Kitul palm: ethnobotany of *Caryota urens* L. in highland Sri Lanka. *Journal Ethnobiol* 1995 Aug;15(2):161-76.
129. Ma C, Dunshea FR, Suleria HAR. LC-ESI-QTOF/MS characterization of phenolic compounds in palm fruits (jelly and fishtail palm) and their potential antioxidant activities. *Antioxidants* 2019 Oct;8(483):1-20.
130. Prakash K, Chaudhury R, M R R, Singh B, Malik S. Contrasting seed biology of two ornamental palms: pygmy date palm (*Phoenix roebelenii* O'Brien) and fishtail palm (*Caryota urens* L.) and implications for their long-term conservation. *Indian J Tradit Knowl* 2019 Jul;18(3):477-84.
131. Sujitha B, Kripa KG. Comparative evaluation of antioxidant activity and liquid chromatography - mass spectrometry - based phytochemical profiling of various biological parts of *Caryota urens*. *Pharmacogn Mag* 2019 Jan;14(59):665-2.
132. Azam FMS, Biswas A, Mannan A, Afsana NA, Jahan R, Rahmatullah M. Are famine

- food plants also ethnomedicinal plants? An ethnomedicinal appraisal of famine food plants of two districts of Bangladesh. *Evidence-based Complement Altern Med* 2014 Feb; 2014(741712):1-28.
133. Srivastav AK, Singh R, Manimegalai S, Rajeswari VD. Identification of flavonoids in methanolic extract of *Caryota urens* (fish tail palm): a phytochemical screening involving structure analysis by FTIR spectroscopy. *Res J Phytochem* 2015 Mar;9(3):127-36.
134. Buragohain J. Folk medicinal plants used in gynecological disorders in Tinsukia district, Assam, India. *Fitoterapia* 2008 Jul;79(5):388-92.
135. Vantomme P, Markkula A, Robin NL. Non-Wood Forest Products in 15 Countries Of Tropical Asia: An Overview. 2002.
136. Seneviratne MAP., Dissanayake DMDKS. A study on the practice of adulteration of Kitul (*Caryota urens*) sap products in Sri Lanka. *Sri Lanka J Soc Sci* 2016 Dec; 39(2):69-73.
137. Sudheesh C, Sunooj K, George J, Kumar S, Sajeevkumar V. Physico-chemical, morphological, pasting and thermal properties of stem flour and starch isolated from kithul palm (*Caryota urens*) grown in valley of Western Ghats of India. *J Food Meas Charact* 2019 Jun;13(2):1020-20.
138. Senavirathna RMISK, Ekanayake S, Jansz ER. Traditional and novel foods from indigenous flours: nutritional quality, glycemic response, and potential use in food industry. *Starch* 2016 Sep;68(9):999-1007.
139. Arul D, Sivasudha T, Rameshkumar A. Free radicals and antioxidants chemical constituents, in vitro antioxidant and antimicrobial potential of *Caryota urens* L . *Free Radicals Antioxidants* 2013 Apr;8(3):6-1.
140. Uddin S, Hasan F, Mamun A Al, Hossain S, Islam T, Asaduzzaman. *In vitro* estimation of antioxidant activity of *Caryota urens* fruits. *Indo Am J Pharmeceutical Sci* 2015 Jan;2(11):2349-775.
141. Azam S, Mahmud K, Naquib H, Hossain SM, Alam MN, Uddin J, et al. *In vitro* anti-oxidant and anti-microbial potentiality investigation of different fractions of *Caryota urens* leaves. *Biomedicines* 2016 Jul;4(17):1-10.

142. Balaji S, Kavasseri Ganesan K. Inhibition of inducible nitric oxide production by *Caryota urens* and its active constituents umbelliferone and rutin. *J Ayurveda Integr Med* 2021 Jun;12(2):369-72.
143. El-Akad RH, Abou Zeid AH, El-Rafie HM, Kandil ZAA, Farag MA. Comparative metabolites profiling of *Caryota mitis* & *Caryota urens* via UPLC/MS and isolation of two novel in silico chemopreventive flavonoids. *J Food Biochem* 2021 Apr;45 (4):1-14.
144. Wang ZJ, Zhang FP, Peng YQ, Bai LF, Yang DR. Comparison of reproductive strategies in two externally ovipositing non-pollinating fig wasps. *Symbiosis*. 2010 Sep;51(2):181-6.
145. Zhang FP, Peng YQ, Compton SG, Yang DR. Floral characteristics of *Ficus curtipes* and the oviposition behavior of its pollinator Fig wasp. *Ann Entomol Soc Am*. 2009 May;102(3):556-9.
146. Zhang D, Zeng W, Huang J, Zeng Y, Peng Y, Ye W, et al. *Ficophagus curtipes* n. sp. (Nematoda: Aphelenchoididae), an associate of *Ficus curtipes* in China. *Nematology*. 2019 Jan;21(10):1091-101.
147. Gu D, Yang D, Compton SG, Peng Y. Age at pollination modifies relative male and female reproductive success in a monoecious fig tree. *Symbiosis* 2012 Jun;57(2):73-81.
148. Philip E, Paavilainen HM, Pawlus AD, Newman RA. *Ficus* spp. (fig): ethnobotany and potential as anticancer and anti-inflammatory agents. *J Ethnopharmacol* 2008 Sep;119(2):195-213.
149. Taxon Details: *Gustavia gracillima* Miers. The new york botanical garden. Available in: <http://sweetgum.nybg.org/science/projects/lp/taxon-details/?irn=111966> [accessed in 10/10/2021].
150. Lopez-gallego C, Morales PA. The IUCN Red List of Threatened Species. Vol. 2. 2020.
151. Stewart AB, Sritongchuay T, Teartisup P, Kaewsomboon S, Bumrungsri S. Habitat and landscape factors influence pollinators in a tropical megacity, Bangkok, Thailand. *PeerJ* 2018 Jul;6:e5335.

152. Watanabe D, Kerakawati R, Morita T, Nakamura T, Ueno K, Kumamoto T, et al. Isolation of β -Sitosterol and digalactopyranosyl-diacylglyceride from *Citrus hystrix*, a thai traditional herb, as pancreatic lipase inhibitors. *Heterocycles* 2009 Jun;78(6):1497-1505.
153. Kaur R, Arora S. Chemical constituents and biological activities of *Chukrasia tabularis* A. Juss . A review. *J Med Plants Res* 2009 May;3(4):196-216.
154. Peng J, Kong F, Liu Z, Wang P, Gai C, Jiang B, et al. Two new phragmalin-type limonoids from stems of *Chukrasia tabularis*. *Phytochem Lett* 2016 Jul;18(7):629-36.
155. Nakatani M, Abdelgaleil SAM, Saad MMG, Huang RC, Doe M, Iwagawa T. Phragmalin limonoids from *Chukrasia tabularis*. *Phytochemistry* 2013;65(20):2833-41.
156. Nagalakshmi MAH, Thangadurai D, Rao M, Pullaiah T. Phytochemical and antimicrobial study of *Chukrasia tabularis* leaves. *Fitoterapia* 2001 Jan;72(1):62-4.
157. Patel NK, Pulipaka S, Dubey SP, Bhutani KK. Pro-inflammatory cytokines and nitric oxide inhibitory constituents from *Cassia occidentalis* roots. *Nat Prod Commun* 2014 May;9(5):661-4.
158. Kaur R, Thind TS, Singh B, Arora S. Inhibition of lipid peroxidation by extracts/subfractions of Chickcrassy (*Chukrasia tabularis* A. Juss.). *Naturwissenschaften* 2009 Jan;96(1):129-33.
159. Kaur R, Arora S, Singh B. Antioxidant activity of the phenol rich fractions of leaves of *Chukrasia tabularis* A. Juss. *Bioresour Technol* 2008 Nov;99(16):7692-8.
160. Kaur R, Sharma U, Singh B, Arora S. Antimutagenic and antioxidant characteristics of *Chukrasia tabularis* A Juss Extracts. *Int J Toxicol* 2011 Feb;30(1):21-34.
161. Peng J, Wang J, Mei W, Kong F, Liu Z, Wang P, et al. Two new phragmalin-type limonoids from *Chukrasia tabularis* and their α -glucosidase inhibitory activity. *J Asian Nat Prod Res* 2016 Jul;18(7):629-36.
162. Zhang F, Zhang C, Tao X, Wang J, Chen W, Yue J. Phragmalin-type limonoids with NF-kB inhibition from *Chukrasia tabularis* var. *velutina*. *Bioorg Med Chem Lett* 2014 Aug;24(16):3781-96.

163. Li Y, Luo J, Li H, Kong L. Two new phragmalin-type limonoids from *Chukrasia tabularis* var. *velutina*. *Molecules* 2013 Dec;18(1):373-380.
164. Zhang C, Fan C, Zhang L, Yang S, Wu Y, Lu Y, et al. Chuktabrins A and B, two novel limonoids from the twigs and leaves of *Chukrasia tabularis*. *Org Lett* 2008 Apr; 10(15):3183-6.
165. Luo J, Li Y, Wang J, Lu J, Wang X, Luo J, et al. Twelve novel and diverse 16-norphragmalin-type limonoids from *Chukrasia tabularis* var. *velutina*. *Chem Pharm Bull* 2012 Feb;60(2):195-204.
166. Purushotaman KK, Sarada A, Saraswathi G, Connolly JD. 5,7-dihydroxy-6,2',4',5'-tetramethoxyflavone from *Chukrasia tabularis*. *Phytochemistry* 1977;16:398-9.
167. Vinholes J, Grosso C, Andrade PB, Gil-Izquierdo A, Valentão P, Pinho PG De, et al. *In vitro* studies to assess the antidiabetic, anti-cholinesterase and antioxidant potential of *Spergularia rubra*. *Food Chem* 2011 Nov;129(2):454-462.
168. Ribeiro D, Freitas M, Tomé SM, Silva AMS, Porto G, Cabrita EJ, et al. Inhibition of LOX by flavonoids: a structure-activity relationship study. *Eur J Med Chem* 2014 Dec;72:137-45.
169. Pereira RB, Taveira M, Valentão P, Sousa C, Andrade PB. Fatty acids from edible sea hares: anti-inflammatory capacity in LPS-stimulated RAW 264.7 involves iNOS modulation. *RSC Adv* 2015 Dec;5(12):8981-7.
170. Oliveira AP, Silva LR, Ferreres F, De Pinho PG, Valentão P, Silva BM, et al. Chemical assessment and *in vitro* antioxidant capacity of *Ficus carica* latex. *J Agric Food Chem* 2010 Feb;58(6):3393-8.
171. Garcia CJ, García-Villalba R, Garrido Y, Gil MI, Tomás-Barberán FA. Untargeted metabolomics approach using UPLC-ESI-QTOF-MS to explore the metabolome of fresh-cut iceberg lettuce. *Metabolomics* 2016 Jul;12:138-150.
172. Figueiredo-González M, Grosso C, Valentão P, Andrade PB. α -Glucosidase and α -amylase inhibitors from *Myrcia* spp.: a stronger alternative to acarbose? *J Pharm Biomed Anal* 2016 Jan;118:322-327.
173. Suryanarayana P, Kumar PA, Saraswat M, Petrash JM, Reddy GB. Inhibition of

- aldose reductase by tannoid principles of *Embllica officinalis*: implications for the prevention of sugar cataract. *Mol Vis* 2004 Mar;10:148-54.
174. Catarino MD, Silva AMS, Mateus N, Cardoso SM. Optimization of phlorotannins extraction from *Fucus vesiculosus* and evaluation of their potential to prevent metabolic disorders. *Mar Drugs* 2019 Mar;17(3):1-23.
175. Stockert JC, Blázquez-Castro A, Cañete M, Horobin RW, Villanueva Á. MTT assay for cell viability: Intracellular localization of the formazan product is in lipid droplets. *Acta Histochem* 2012 Dec;114(8):785-96.
176. Cheng M-W, Chegeni M, Kim K-H, Zhang G, Benmoussa M, Quezada-Calvillo R, et al. Different sucrose-isomaltase response of Caco-2 cells to glucose and maltose suggests dietary maltose sensing. *J Clin Biochem Nutr* 2014 Jan;54(1):55-60.
177. Ferreres F, Lopes G, Gil-Izquierdo A, Andrade PB, Sousa C, Mouga T, et al. Phlorotannin extracts from *Fucales* characterized by HPLC-DAD-ESI-MSn: approaches to hyaluronidase inhibitory capacity and antioxidant properties. *Mar Drugs* 2012 Dec;10(12):2766-81.
178. Barbosa M, Valentão P, Ferreres F, Gil-izquierdo Á, Andrade PB. *In vitro* multifunctionality of phlorotannin extracts from edible *Fucus* species on targets underpinning neurodegeneration. *Food Chem* 2020 Dec;333(127456):1-10.
179. Subash-Babu P, Ignacimuthu S, Alshatwi AA. Nymphayol increases glucose-stimulated insulin secretion by RIN-5F cells and GLUT4-mediated insulin sensitization in type 2 diabetic rat liver. *Chem Biol Interact* 2015 Jan;226:72-81.
180. Pereira RB, Pereira DM, Jiménez C, Rodríguez J, Nieto RM, Videira RA, et al. Anti-inflammatory effects of 5 α ,8 α -epidioxycholest-6-en-3 β -ol, a steroidal endoperoxide isolated from *Aplysia depilans*, based on bioguided fractionation and NMR analysis. *Mar Drugs* 2019 Jun;17(6):330-45.
181. Proença C, Freitas M, Ribeiro D, Oliveira EFT, Sousa JLC, Tomé SM, et al. α -Glucosidase inhibition by flavonoids: an *in vitro* and *in silico* structure-activity relationship study. *J Enzyme Inhib Med Chem* 2017 Dec;32(1):1216-1228.
182. Vrchovská V, Sousa C, Valentão P, Ferreres F, Pereira JA, Seabra RM, et al. Antioxidative properties of tronchuda cabbage (*Brassica oleracea* L. var. costata DC) external leaves against DPPH, superoxide radical, hydroxyl radical and hypochlorous

- acid. Food Chem 2006 Mar;98 (3)416-25.
183. Rathinavel T, Nasir M, Kumarasamy S. Lupeol from *Crateva adansonii* DC exhibits promising enzymes inhibition: play a crucial role in inflammation and diabetes. South African J Bot 2021 Dec;143:449-456.
184. Rathinavel T, Nasir M, Kumarasamy S. Lupeol from *Crateva adansonii* DC exhibits promising enzymes inhibition: play a crucial role in inflammation and diabetes. South African J Bot 2021 Dec;143:449-456.
185. Arsakit K, Thongchuai B, Sedlak S, Surapinit S. Assessment of the anti-diabetic potential of the *Cratoxylum formosum* subsp. *formosum* extracts via carbohydrate hydrolyzing enzymes inhibitory activities. J Herbmed Pharmacol 2020 May;9(3):286-92.
186. Kukongviriyapan U, Luangaram S, Leekhaosoong K, Kukongviriyapan V, Preeprame S. Antioxidant and vascular protective activities of *Cratoxylum formosum*, *Syzygium gratum* and *Limnophila aromatica*. Biol Pharm Bull 2007 Apr;30(4):661-6.
187. Boonnak N, Chantrapromma S. Inhibition of nitric oxide production in lipopolysaccharide-activated RAW 264.7 macrophages by isolated xanthenes from the roots of *Cratoxylum formosum* ssp . *pruniflorum*. Arch Pharm Res 2014 Oct;37(10):1329-35.
188. Ramanathan S, Sivakumar T, Sundaram R, Sivakumar P, Nethaji R, Gupta M, et al. Antimicrobial and antioxidant activities of *Careya arborea* Roxb. Stem Bark. Iran J Pharmacol Ther 2006 Jul;5(1):35-41.
189. Rahman MT, Khan OF, Saha S, Alimuzzaman M. Antidiarrhoeal activity of the bark extract of *Careya arborea* Roxb. Fitoterapia 2003 Feb; 74 (1-2): 116-8.
190. Mai TT, Thu NN, Tien PG, Chuyen N Van. Alpha-glucosidase inhibitory and antioxidant activities of Vietnamese edible plants and their relationships with polyphenol contents. J Nutr Sci Vitaminol (Tokyo) 2007 Jun;53(3):267-76.
191. Shailaja W, Balaji W, Madhav M. Phytochemical and *in-vitro* antioxidant activity of *Careya arborea* Roxb. leaves successive extracts. J Drug Deliv Ther 2019 Mar; 9(2s):53-6.

192. Mruthunjaya K, Hukkeri VI. Antioxidant and free radical scavenging potential of *Justicia gendarussa* Burm. leaves *in vitro*. *Nat Prod Sci* 2007 Sep; 13 (3): 199-206.
193. Soun-udom M, Choowongkomon K, Vajrodaya S, Ratanabunyong S, Suksungworn R, Srisombat N, et al. Antioxidant and anti-HIV properties and isolation of bioactive compound of *Hymenodictyon orixense* (Roxb.) Mabb. *Agric Nat Resour* 2019 Dec;53:621-8.
194. Clifford MN, Johnston KL, Knight S, Kuhnert N. Hierarchical scheme for LC-MSⁿ identification of chlorogenic acids. *J Agric Food Chem* 2003 Apr;51(10):2900-11.
195. Saldanha LL, Allard P, Afzan A, Melo FP de SR de, Marcourt L, Queiroz EF, et al. Metabolomics of *Myrcia bella* populations in brazilian savanna reveals strong influence of environmental factors on its specialized metabolism. *Molecules* 2020 Jun;25(2954):1-20.
196. Mandim F, Petropoulos SA, Pinela J, Dias MI, Giannoulis KD, Kostić M, et al. Chemical composition and biological activity of cardoon (*Cynara cardunculus* L. var. *altilis*) seeds harvested at different maturity stages. *Food Chem* 2022; Aug;369:1–10.
197. Chepel V, Lisun V, Skrypnyk L. Changes in the content of some groups of phenolic compounds and biological activity of extracts of various parts of heather (*Calluna vulgaris* (L.) hull) at different growth stages. *Plants* 2020 Jul;9(8):1-19.
198. Ferreres F, Silva MB, Andrade PB, Seabra RM, Ferreira MA. Approach to the study of C-glycosyl flavones by ion trap HPLC-PAD-ESI/MS/MS: application to seeds of quince (*Cydonia oblonga*). *Phytochem Anal* 2003 Dec;14(6):352-9.
199. Ferreres F, Gil-izquierdo A, Andrade PB, Valent P, Tom FA. Characterization of C - glycosyl flavones O-glycosylated by liquid chromatography - tandem mass spectrometry. *Rapid Commun Mass Spectrom* 2005;19(21):3143-58.
200. Kim HJ, Woo E-R, Park H. A novel lignan and flavonoids from *Polygonum aviculare*. *J Nat Prod* 1994 May;57(5):581-6.
201. J. Steynberg P, P. Steynberg J, Vincent Brandt E, Ferreira D, W. Hemingway R. Oligomeric flavanoids. Part 26. Structure and synthesis of the first profisetinidins with epifisetinidol constituent units. *J Chem Soc Perkin Trans* 1997;(13):1943-50.
202. Chatterjee A, Banerjee B, Ganguly SN, Sircar SM. Triterpenes and coumarins from

- Chukrasia tabularis*. Phytochemistry. 1974;13:2012-3.
203. Garcia-Villalba R, Espin JC, Aaby K, Alasalvar C, Heinonen M, Jacobs G, et al. Validated method for the characterization and quantification of extractable and nonextractable ellagitannins after acid hydrolysis in pomegranate fruits, juices and extracts. *J Agric Food Chem* 2015 Jul; 63(29):6555-66.
204. Souza A, Rocha A, Pinheiro M, Andrade C, Galotta AL, Santos M. Constituintes químicos de *Gustavia augusta* L. (Lecythidaceae). *Quim Nova* 2001 Aug;24(4):439-42.
205. Zhang H, Wang G, Beta T, Dong J. Inhibitory properties of aqueous ethanol extracts of propolis on alpha-glucosidase. *Evidence-based Complement Altern Med* 2015 Feb; 2015(587383):1-17.
206. Jockovic N, Fischer W, Brandsch M, Brandt W, Drager B. Inhibition of human intestinal alpha-glucosidases by calystegines. *J Agric Food Chem* 2013 Jun;61(23): 5550-7.
207. Ranasinghe, P., Premakumara, G. A. S., Wijayarathna, D. & Ratnsooriya WD. Anti-diabetic properties of *Caryota urens* (Kithul palm) sap and treacle. International Conference on Chemistry - Technology and Innovation for greater safety and Economic. Transasia Hotel, Colombo, Chemtech; 2007.
208. Xu D, Wang Q, Zhang W, Hu B, Zhou L, Zeng X, et al. Inhibitory activities of caffeoylquinic acid derivatives from *Ilex kudingcha* C.J. Tseng on α -glucosidase from *Saccharomyces cerevisiae*. *J Agric Food Chem* 2015 Mar;63(14):3694-703.
209. Kajszczyk D, Kowalska-baron A, Pods A. Glycoside hydrolases and non-enzymatic glycation inhibitory potential of *Viburnum opulus* L . fruit - *in vitro* studies. *Antioxidants* 2021 Jun;10(989):1-18.
210. Hsu C, Lin G, Lin H, Chang S. Characteristics of proanthocyanidins in leaves of *Chamaecyparis obtusa* var. formosana as strong α -glucosidase inhibitors. *J Sci Food Agric* 2018 Aug;98(10):3806-3814.
211. Rajan L, Palaniswamy D, Mohankumar SK. Targeting obesity with plant-derived pancreatic lipase inhibitors: a comprehensive review. *Pharmacol Res* 2020 May;115(104681):1-34.

-
212. Tan Y, Chang SKC, Zhang Y. Comparison of α -amylase, α -glucosidase and lipase inhibitory activity of the phenolic substances in two black legumes of different genera. *Food Chem* 2017 Jan;214:259-68.
213. Li YQ, Yang P, Gao F, Zhang ZW, Wu B. Probing the interaction between 3 flavonoids and pancreatic lipase by methods of fluorescence spectroscopy and enzymatic kinetics. *Eur Food Res Technol* 2011 May;233(1):63-9.
214. Habtemariam S. Antihyperlipidemic components of *Cassia auriculata* aerial parts: identification through *in vitro* studies. *Phyther Res* 2013 Jan;27(1):152-5.
215. Hu B, Cui F, Yin F, Zeng X, Sun Y, Li Y. Caffeoylquinic acids competitively inhibit pancreatic lipase through binding to the catalytic triad. *Int J Biol Macromol* 2015 Sep;80:529-35.
216. Quattrini L, La Motta C. Aldose reductase inhibitors: 2013-present. *Expert Opin Ther Pat* 2019 Mar;29(3):199-213.
217. Spínola V, Castilho PC. Assessing the *in vitro* inhibitory effects on key enzymes linked to type-2 diabetes and obesity and protein glycation by phenolic compounds of *Lauraceae* plant species endemic to the laurisilva forest. *Molecules* 2021 Mar;26(2023):1-11.
218. Ah H, Islam MDN, Soo Y, Eun S, Kyung Y, Ju J, et al. Extraction and identification of three major aldose reductase inhibitors from *Artemisia montana*. *Food Chem Toxicol* 2011 Feb;49(2):376-84.
219. Ferreres F, Andrade C, Gomes NGM, Andrade PB, Gil-izquierdo A, Pereira DM, et al. Valorisation of kitul, an overlooked food plant: Phenolic profiling of fruits and inflorescences and assessment of their effects on diabetes-related targets. *Food Chem* 2021 Apr;342(128323):1-9.
220. Lim SS, Jung YJ, Hyun SK, Lee YS, Choi JS. Rat lens aldose reductase inhibitory constituents of *Nelumbo nucifera* Stamens. *Phytother Res* 2006 Oct;20(10):825-30.
221. Panigrahy SK, Bhatt R, Kumar A. Reactive oxygen species: Sources, consequences and targeted therapy in type-II diabetes. *J Drug Target* 2017 Feb;25(2):93-101.
222. D'Amelia V, Aversano R, Chiaiese P, Carputo D. The antioxidant properties of plant flavonoids: their exploitation by molecular plant breeding. *Phytochem Rev* 2018 Apr;

- 17(3):611-25.
223. Bakkalbaşı E, Yemiş O, Aslanova D, Artık N. Major flavan-3-ol composition and antioxidant activity of seeds from different grape cultivars grown in Turkey. *Eur Food Res Technol* 2005 Aug;221(6) 792-7.
224. Monagas M, Garrido I, Lebrón-Aguilar R, Gómez-Cordovés MC, Rybarczyk A, Amarowicz R, et al. Comparative flavan-3-ol profile and antioxidant capacity of roasted peanut, hazelnut, and almond skins. *J Agric Food Chem* 2009 Nov;57(22):10590-9.
225. Amić D, Davidović-Amić D, Beslo D, Rastija V, Lucić B, Trinajstić N. SAR and QSAR of the antioxidant activity of flavonoids. *Curr Med Chem* 2007;14(7):827-45.
226. Sambanthamurthi R, Tan Y, Sundram K, Abeywardena M, Sambandan TG, Rha C, et al. Oil palm vegetation liquor: A new source of phenolic bioactives. *Br J Nutr* 2011 Jun;106(11):1655-63.
227. Cao X, Yang L, Xue Q, Yao F, Sun J, Yang F, et al. Antioxidant evaluation-guided chemical profiling and structure-activity analysis of leaf extracts from five trees in *Broussonetia* and *Morus* (Moraceae). *Sci Rep* 2020 Mar;10(1):1-14.
228. Nowotny K, Jung T, Höhn A, Weber D, Grune T. Advanced glycation end products and oxidative stress in type 2 diabetes mellitus. *Biomolecules* 2015 Mar;5(1):194-222.
229. Ahmed QU, Sarian MN, So'ad SZM, Latip J, Ichwan SJA, Hussein NN, et al. Methylation and acetylation enhanced the antidiabetic activity of some selected flavonoids: *In vitro*, molecular modelling and structure activity relationship-based study. *Biomolecules* 2018 Nov;8(4):1-22.
230. Alshatwi AA, Subash-Babu P. Aloe-emodin protects RIN-5F (pancreatic β -cell) cell from glucotoxicity via regulation of pro-inflammatory cytokine and downregulation of Bax and caspase 3. *Biomol Ther* 2016 Jan;24(1):49-56.
231. Wolffenbittel BH, Giordano D, Founds HW, Bucala R. Long-term assessment of glucose control by haemoglobin-AGE measurement. *Lancet* 1996 Feb;347(9000): 513-5.
232. Bernardo J, Malheiro I, Videira RA, Valentão P, Santos AC, Veiga F, et al. *Trichilia*

- catigua* and *Turnera diffusa* extracts: *in vitro* inhibition of tyrosinase, antiglycation activity and effects on enzymes and pathways engaged in the neuroinflammatory process. *J Ethnopharmacol* 2021 May;271(113865):1-8.
233. Spínola V, Castilho PC. Assessing the *in vitro* inhibitory effects on key enzymes linked to type-2 diabetes and obesity and protein glycation by phenolic compounds of *Lauraceae* plant species endemic to the laurisilva forest. *Molecules* 2021 Mar;26(2023):1-11.
234. Piwowar A, Rorbach-Dolata A, Fecka I. The antiglycoxidative ability of selected phenolic compounds - an *in vitro* study. *Molecules*. 2019 Aug;24(15):2689-710.
235. Hosooka T, Hosokawa Y, Matsugi K, Shinohara M, Senga Y, Tamori Y, et al. The PDK1-FoxO1 signaling in adipocytes controls systemic insulin sensitivity through the 5-lipoxygenase-leukotriene B4 axis. *Proc Natl Acad Sci U S A* 2020 May;117 (2): 11674-84.
236. Hosooka T, Hosokawa Y, Matsugi K, Shinohara M, Senga Y, Tamori Y, et al. The PDK1-FoxO1 signaling in adipocytes controls systemic insulin sensitivity through the 5-lipoxygenase-leukotriene B4 axis. *Proc Natl Acad Sci U S A* 2020 May;117 (2): 11674-84.
237. Shoelson SE, Lee J, Goldfine AB. Review series inflammation and insulin resistance. *FEBS Lett* 2008 Jan;582(1):97-105.
238. Andrade C, Ferreres F, Gomes NGM, Duangrisai S, Srisombat N, Vajrodaya S, et al. Phenolic profiling and biological potential of *Ficus curtipes* Corner leaves and stem Bark: 5-lipoxygenase inhibition and interference with NO Levels in LPS-stimulated RAW 264.7 macrophages. *Biomolecules*. 2019 Aug;9(400):1-17.
239. Tursun X, Zhao Y, Alat Z, Xin X, Tursun A, Abdulla R, et al. Anti-inflammatory Effect of *Rosa rugosa* flower extract in lipopolysaccharide-stimulated RAW 264.7 macrophages. *Biomol Ther (Seoul)* 2016 Mar;24(2):184-90.
240. Schewe T, Ku H. Biochemical and molecular actions of nutrients flavonoids of cocoa inhibit recombinant human 5-lipoxygenase. *Biochem Mol Actions Nutr* 2002 Jul; 132(7):1825-9.
241. Hwang SJ, Kim Y-W, Park Y, Lee H-J, Kim K-W. Anti-inflammatory effects of chlorogenic acid in lipopolysaccharide-stimulated RAW 264.7 cells. *Inflamm Res*.

2014 Jan;63(1):81-90.

242. Hämäläinen M, Nieminen R, Vuorela P, Heinonen M, Moilanen E. Anti-inflammatory effects of flavonoids: genistein, kaempferol, quercetin, and daidzein inhibit STAT-1 and NF-kappaB activations, whereas flavone, isorhamnetin, naringenin, and pelargonidin inhibit only NF-kB activation along with their inhibitory effect on iNOS expression and NO production in activated macrophages. *Mediators Inflamm* 2007 Aug;45673:1-10.
243. Zhang YY, Thakur K, Wei CK, Wang H, Zhang JG, Wei ZJ. Evaluation of inhibitory activity of natural plant polyphenols on Soybean lipoxygenase by UFLC-mass spectrometry. *South African J Bot* 2019 Jan;120:179-85.